



The University of
Nottingham

UNITED KINGDOM • CHINA • MALAYSIA

Innovative Heat Pipe-Based Photovoltaic/Thermoelectric (PV/TEG) Generation System

Adham Makki

B.Eng., MSc

**Thesis submitted to the University of Nottingham for the
degree of Doctor of Philosophy**

© University of Nottingham, 2017. All rights reserved. No part of this publication may be reproduced without the written permission of the copyright holder

June, 2017

To my Beloved Parents

Mr. & Mrs Hossam and Eman Makki

To my siblings

Haytham and Hadeel Makki

ACKNOWLEDGEMENT

The completion of this work would not have been possible without the support of many individuals and institutions to whom I am eternally grateful to. I would like to take this opportunity to thank Dr. Siddig for his continuous support, scientific insights as well as the invaluable guidance through this journey. I remain truly grateful for all the effort and investment in my journey to completion. I would also like to thank my internal assessor Dr. Shenyi Wu for his constructive feedback and criticism that only resulted in improved work. I would also like to thank the laboratory technicians for their helping hands and support.

I would express my gratitude to my parents and siblings, whose support and constant encouragement facilitated this journey. My deepest appreciation for their love, understanding, and inspiration. Without their blessings and encouragement, I would not have been able to complete this work.

Finally, I would like to express my sincere appreciation to my friends whom have been my family while I am away from home.

DECLARATION

The material contained within this research has not previously been submitted for a degree at the University of Nottingham or any other university. The research reported within this thesis has been conducted by the author unless indicated otherwise. This work has been documented in part in the following publications in peer reviewed journals and international conferences.

List of Publications:

- Makki, A., Omer, S. and Sabir, H. (2015) '*Advancements in hybrid photovoltaic systems for enhanced solar cells performance*', Renewable and Sustainable Energy Reviews, 41, pp. 658–684. doi: 10.1016/j.rser.2014.08.069.
- Makki, A., Omer, S., Su, Y. and Sabir, H. (2016) '*Numerical investigation of heat pipe-based photovoltaic–thermoelectric generator (HP-PV/TEG) hybrid system*', Energy Conversion and Management, 112, pp. 274–287. doi: 10.1016/j.enconman.2015.12.069.
- Makki, Omar, Su and Riffat (2015) '*Performance analysis of heat pipe-based photovoltaic-thermoelectric generator hybrid system*', Nottingham: 14th International Conference on Sustainable Energy Technologies.

Table of Contents

| | |
|--|-------|
| ACKNOWLEDGEMENT | I |
| DECLARATION | II |
| Table of Contents | III |
| Table of Figures | VIII |
| List of Tables | XVI |
| NOMENCLATURE | XVII |
| ABSTRACT | XVIII |
| Chapter 1 Introduction | 1 |
| 1.1 The Ultimate Energy Source | 3 |
| 1.2 Solar Energy Utilisation | 5 |
| 1.3 Aim & Objectives | 8 |
| 1.3.1 Aim | 8 |
| 1.3.2 Objectives..... | 8 |
| 1.4 Novelty and Contributions | 10 |
| 1.4.1 Novelty..... | 10 |
| 1.4.2 Contributions | 12 |
| 1.5 Thesis Outline | 13 |
| Chapter 2 Thermal Management of Solar Photovoltaics | 18 |
| 2.1 Temperature Influence on Photovoltaic Cells | 20 |
| 2.2 Thermal Management of PV Cells | 25 |
| 2.3 Waste Heat Recovery | 29 |
| 2.4 Technologies Considered | 31 |
| 2.4.1 Photovoltaic (PV) Cells | 33 |
| 2.4.1.1 Efficiency..... | 34 |

Table of Contents

| | | |
|---|--|------------|
| 2.4.1.2 | I-V Characteristic Curves:..... | 35 |
| 2.4.2 | Thermoelectric Generators (TEGs)..... | 36 |
| 2.4.2.1 | Theory of Thermoelectric Conversion: | 38 |
| 2.4.2.2 | Thermoelectric Modules..... | 40 |
| 2.4.3 | Heat Pipes | 41 |
| 2.4.3.1 | Heat Pipes Structure and Operation..... | 42 |
| 2.4.3.2 | Heat Transport Limitations of Heat Pipes..... | 42 |
| 2.4.3.3 | Wick Structure of Heat Pipes | 44 |
| 2.4.3.4 | Working Fluid..... | 45 |
| Chapter 3 Advancements in Hybrid Photovoltaic Collectors | | 47 |
| 3.1 | Hybrid PV-Thermal Collectors | 48 |
| 3.1.1 | Air-based PVT Collectors | 49 |
| 3.1.2 | Liquid-based PVT collectors | 66 |
| 3.1.2.1 | Water-based PVT collectors..... | 67 |
| 3.1.2.2 | Refrigerant-based PVT collectors..... | 77 |
| 3.1.3 | Heat pipe-based PVT collectors | 83 |
| 3.1.4 | PCM-based PVT collectors..... | 92 |
| 3.1.5 | Thermoelectric (PV-TE) Systems | 105 |
| 3.2 | Discussion | 119 |
| 3.3 | Conclusions | 121 |
| Chapter 4 Proposed System Design and | | |
| Research Methodology..... | | 127 |
| 4.1 | Proposed System Design and Operation Principle..... | 128 |
| 4.1.1 | Proposed System Design | 128 |
| 4.1.2 | Operation Principle | 132 |
| 4.2 | Research Methodology | 136 |
| 4.2.1 | Computer Modelling..... | 137 |

Table of Contents

| | | |
|--|--|------------|
| 4.2.1.1 | Heat Transfer | 140 |
| 4.2.1.2 | Problem Solving Technique..... | 142 |
| 4.2.1.3 | System Equations | 143 |
| 4.2.1.4 | Numerical Solution (Finite Difference Approximation) | 147 |
| 4.2.2 | Experimental Investigation..... | 150 |
| Chapter 5 Energy Balance Equations..... | | 151 |
| 5.1 Heat pipe-based PV collector | | 153 |
| 5.1.1 | Energy balance of the front glazing | 153 |
| 5.1.2 | Energy balance of PV layer | 155 |
| 5.1.3 | Energy balance of the aluminum base panel..... | 159 |
| 5.1.4 | Energy balance of the heat pipe | 161 |
| 5.2 Thermoelectric Generator - Fan Heat Sink Assembly | | 168 |
| 5.2.1 | Energy balance of thermoelectric generator (TEG) | 168 |
| 5.2.2 | Fan-Heat sink assembly | 174 |
| 5.3 Discretising energy balance equations..... | | 176 |
| 5.4 Solution Routine (Flow Chart) | | 180 |
| Chapter 6 Computer Model Results and Discussion..... | | 183 |
| 6.1 Temperature response..... | | 184 |
| 6.1.1 | Steady State Response | 184 |
| 6.1.2 | Transient Response | 191 |
| 6.2 Low Temperature Thermal Waste Recovery | | 193 |
| 6.2.1 | Thermal energy absorbed by Thermoelectric generators | 193 |
| 6.3 Electrical Performance..... | | 195 |
| 6.3.1 | Steady State Response | 195 |
| 6.3.2 | Transient Response..... | 197 |
| 6.4 Thermoelectric Generator Electrical Performance..... | | 199 |
| 6.5 Conversion Efficiency | | 201 |

Table of Contents

| | | |
|--|--|------------|
| 6.5.1 | PV Cells Conversion Efficiency..... | 201 |
| 6.5.2 | Integrated PV-TEG Collector Efficiency..... | 203 |
| Chapter 7 Experimental Study..... | | 206 |
| 7.1 | Testing of Solar Simulator Intensity and Uniformity | 207 |
| 7.1.1 | Solar Simulator Construction..... | 208 |
| 7.1.2 | Measurements of Light Intensity and Uniformity | 210 |
| 7.2 | Testing of Heat Pipe-based PV/Thermoelectric Collector..... | 214 |
| 7.2.1 | Fabrication of the Prototype Collector..... | 215 |
| 7.2.1.1 | Materials and Instruments | 215 |
| 7.2.1.2 | Heat Pipe-based PV Collector Fabrication | 223 |
| 7.2.1.3 | Waste Heat Recovery Assembly Fabrication | 225 |
| 7.2.1.4 | Performance Measurements..... | 228 |
| Chapter 8 | | |
| Experimental Results and Computer Model Validation..... | | 234 |
| 8.1 | Experimental Results..... | 235 |
| 8.1.1 | Solar Simulator Testing Results | 235 |
| 8.1.2 | Temperature Response..... | 238 |
| 8.1.3 | Electrical Performance..... | 241 |
| 8.1.4 | TEG Thermal Performance..... | 245 |
| 8.2 | Computer Model Validation..... | 248 |
| 8.2.1 | Photovoltaic Electrical Characteristics | 248 |
| 8.2.1.1 | Validation Against Manufacturer’s Datasheet..... | 249 |
| 8.2.1.2 | Validation Against Experimental Test..... | 251 |
| 8.2.2 | Thermoelectric Electrical Characteristics | 254 |
| 8.2.2.2 | Validation of TEG Against Experimental Test of Single Module | 254 |
| 8.2.3 | Heat Pipe Performance Validation..... | 260 |
| 8.3 | System Optimization | 264 |
| 8.3.1 | Influence of Pipes Number Attached on System Performance | 264 |

Table of Contents

8.3.1.1 Temperature Response..... 265

8.3.1.2 Electrical Performance..... 267

Chapter 9 Conclusion and Future Work..... 269

9.1 Summary 270

9.2 Research Findings..... 273

9.3 Limitations 276

9.4 Recommendation for Future Work..... 278

References..... 280

Appendix..... 298

Table of Figures

| | |
|---|----|
| Fig. 1.1 Estimated energy consumption per person per day over the ages (Cook, 1971)..... | 2 |
| Fig. 1. 2 United Nations prediction of world's population (George, 2011)..... | 3 |
| Fig. 1. 3 The ultimate energy source (European Centre for Medium-Range Weather Forecasts) | 4 |
| Fig. 2. 1 Fraction of terrestrial sunlight absorbed by crystalline silicon device (Kulish and Object, 2016)21 | |
| Fig. 2. 2 Open-circuit voltage variation against temperature - 40-80°C (Huang et al., 2011) | 23 |
| Fig. 2. 3 Slight increase in short circuit current observed with increasing temperature (Michael, 2009)..... | 24 |
| Fig. 2. 4 Linear drop in maximum power output of PV module with temperature increase (Radziemska, 2003) | 24 |
| Fig. 3. 1 PV Electricity Generation Process | 34 |
| Fig. 3. 2 I-V and P-V characteristic curves of PV cell under various operating conditions..... | 35 |
| Fig. 3. 3 Waste heat recovery in vehicle (left) and TEG devices powering communications and cathodic protection of gas pipeline, India (right) | 37 |
| Fig. 3. 4 Schematic of basic thermocouple (Lee, 2010). | 38 |
| Fig. 3. 5 Current flow through dissimilar materials (Lee, 2010)..... | 39 |
| Fig. 3. 6 Thermocouple in thermoelectric module (California Inst. of Tech., 2013) | 40 |
| Fig. 3. 7 Cutaway view of heat pipe (Lee, 2010) | 41 |
| Fig. 3. 8 Schematic of limits on heat pipe performance (Lee, 2010) | 43 |
| Fig. 3. 9 Wick section structures of heat pipes (Lee, 2010) | 44 |
| Fig. 3. 1 Classification of PVT modules based on heat extraction mechanism | 50 |
| Fig. 3. 2 Different designs of air-based PVT collectors (Zhang et al., 2012)..... | 51 |
| Fig. 3. 3 (a) Glass-to-glass module with duct, (b) Glass-to-temlar module with duct Dubey et al. (2009) | 52 |
| Fig. 3. 4 Electrical efficiency of PV cells for collectors investigated in Dubey et al. (2009) | 52 |
| Fig. 3. 5 Air-based PVT collectors with thin metal sheet and finned metal sheet Tonui and Tripanagnostopoulos (2008)..... | 54 |

Table of Figures

| | |
|--|----|
| Fig. 3. 6 PV surface temperature as function of air duct depth Tonui and Tripanagnostopoulos (2008) | 54 |
| Fig. 3. 7 Electrical efficiency variation with mass flow rate (Solanki, Dubey, and Tiwari, 2009) | 55 |
| Fig. 3. 8 Variation of electrical efficiency and cell temperature (Solanki, Dubey, and Tiwari, 2009) | 56 |
| Fig. 3. 9 Air-based PVT with open loop single pass duct Bambrook and Sproul (2012) | 57 |
| Fig. 3. 10 Ventilated PV façade system (a) summer, (b) winter Yun et al. (2007) | 60 |
| Fig. 3. 11 PV efficiency and module temperature of ventilated PV façade Yun et al. (2007) | 60 |
| Fig. 3. 12 Micro-channel solar cell thermal (MCSCCT) tile (Agrawal and Tiwari, 2011) | 62 |
| Fig. 3. 13 Exergy efficiency utilising micro-channel solar cell thermal tile with air cooling Agrawal and Tiwari (2011) | 63 |
| Fig. 3. 14 Series and parallel arrangement of ventilated micro-channel solar cell tiles (Agrawal and Tiwari, 2011) (Rajoria, Agrawal, and Tiwari, 2012) | 63 |
| Fig. 3. 15 PV modules with different heat exchanger designs (a) Honeycomb, (b) V-groove, (c) stainless steel wool (Othman, 2013) | 65 |
| Fig. 3. 16 Various configurations of water-based PVT collectors (Chow, 2010) | 69 |
| Fig. 3. 17 Sheet-and-tube PVT collector (Zondag et al., 2002) | 70 |
| Fig. 3. 18 Flat-box aluminium-alloy heat exchanger (Chow, He, and Ji, 2006) (He et al., 2006) | 72 |
| Fig. 3. 19 Wall-mounted water-based PVT collectors Ji et al. (2006) | 73 |
| Fig. 3. 20 (a) Direct flow design, (b) serpentine flow design, (c) parallel-serpentine flow design, (d) modified serpentine-parallel flow design, (e) oscillatory flow design, (f) spiral flow design, (g) web flow design (Ibrahim, 2009) | 75 |
| Fig. 3. 21 Schematic diagram of PV solar-assisted heat pump (Ji et al. 2009) | 79 |
| Fig. 3. 22 PV/evaporator heat pump system (Zhao et al. 2011) | 80 |
| Fig. 3. 23 PV/loop-heat-pipe (PV/LHP) heat pump solar system (Zhang et al., 2013) | 81 |
| Fig. 3. 24 PV cell operating temperature of low concentrating PVT integrated heat pump (LCPVT-HP) (Xu et al. 2011) | 82 |
| Fig. 3. 25 Schematic diagram of heat pipe (Zhang et al., 2012) | 84 |
| Fig. 3. 26 Heat pipe cooling of PV cells (Russell, 1982) | 85 |
| Fig. 3. 27 Cooling of low concentrator PV cell with heat pipe extruded fin Akbarzadeh and Wadowski (1996) | 86 |

Table of Figures

| | |
|---|-----|
| Fig. 3. 28 Cooling PV concentrator through copper/water heat pipe with aluminium fins (Anderson et al. 2008) | 87 |
| | |
| Fig. 3. 29 Micro heat pipe array cooling for conventional flat-plate PV module using (a) air, (b) water | 89 |
| Fig. 3. 30 Schematic drawing of a PV/PCM system (Huang et al. 2004) | 94 |
| Fig. 3. 31 V-trough stand-alone PV/PCM system (Maiti et al., 2011) | 95 |
| Fig. 3. 32 Surface temperatures at different levels of insolation and ambient temperature of 20°C | 97 |
| Fig. 3. 33 Surface Temperatures of PV/PCM systems with and without internal fins at a particular operating condition | 98 |
| Fig. 3. 34 Average measured surface temperature of finned PV/PCM systems (Huang, Eames, and Norton 2006) | 99 |
| | |
| Fig. 3. 35 Schematic diagram of PV/PCM system with triangular cell (Jun Huang, 2011) | 100 |
| Fig. 3. 36 Predicted surface temperature evolution using different combinations of PCMs within PV/PCM system (Jun Huang, 2011) | 101 |
| Fig. 3. 37 Temperature regulation with the ratio of fins spacing on PV/PCM system design (Huang et al. 2011) | 101 |
| | |
| Fig. 3. 38 Temperature difference from reference PV using four different PCMs (Hasan et al. 2010) | 103 |
| Fig. 3. 39 Output power data of different system configuration taken from (Maiti et al. 2011) | 104 |
| Fig. 3. 40 Operation modes of thermoelectric TE module (Nolas et al., 1999) | 107 |
| Fig. 3. 41 Cooling of PV cell through TE cooler (Najafi and Woodbury, 2013) | 108 |
| Fig. 3. 42 Incorporation of TE generators with PV cell (a) non-concentrated (b) concentrated (Vorobiev et al. 2006) | 112 |
| Fig. 3. 43 A scheme of hybrid PV/T system with TEGs: (1) solar cell, (2) cell's back electrode, (3) TEG, (4) heat extractor, (5) plane collector, (6) thermal tank (Chávez-Urbiola et al., 2012) | 112 |
| Fig. 3. 44 Scheme of hybrid system with TEG and concentrated solar radiation: (1) concentrating lens, (2) tracking system, (3) TEG, (4) heat extractor, (5) PV panel, (6) solar radiation | 113 |
| Fig. 3. 45 Calculated temperature dependence efficiency as function of the temperature difference: (1) PV cells, TEG with different ZT=2.4 curve (2) 0.7 curve (3), and 4 curve (4), total efficiency with different TEGs (ZT=4 curve (5), 0.7 curve (6), and 2.4 curve (7) . (Chávez-Urbiola et al., 2012) | 115 |

Table of Figures

| | |
|--|-----|
| Fig. 3. 46 Generated PV-TE power as a function of irradiance for four values of the figure of merit Z, and generated PV power as a function of irradiance at STC and module temperature (Sark, 2011) | 117 |
| Fig. 3. 47 Schematic of PE-TE hybrid module (Deng et al., 2013b)..... | 118 |
| Fig. 4. 1 (a) PV module with heat pipes attached at rear (b) Side section view for heat pipe-based PV/TEG collector with technologies incorporated..... | 129 |
| Fig. 4. 2 Heat recovery system utilizing heat pipes and thermoelectric generators of PV cooling | 131 |
| Fig. 4. 3 (a) Top view of collector proposed showing 5 heat pipes attached at rear. (b) TEG-fan heat sink assembly for waste heat recovery front view and layout | 131 |
| Fig. 4. 4 TEG-fan heat sink assembly..... | 132 |
| Fig. 4. 5 Operating principle; energy balance: (a) Heat pipe-base PV collector (b) TEG-fan heat sink assembly. | 133 |
| Fig. 4. 6 Optical transmittance and reflectance versus wavelength for the FTO/glass substrate (Tseng et al., 2011) | 134 |
| Fig. 4. 7 Research methodology adopted in this investigation..... | 137 |
| Fig. 4. 8 Computer modelling development process | 138 |
| Fig. 4. 9 Energy interaction on a surface..... | 141 |
| Fig. 4. 10 Computer modelling approach implemented..... | 142 |
| Fig. 4. 11 Schematic of energy flow within the integrated heat pipe PV/TEG collector..... | 145 |
| Fig. 4. 12 Schematic depicting energy interactions and layers from which the system is designed | 145 |
| Fig. 4. 13 Thermal resistance network of integrated heat pipe-based PV/TEG collector..... | 146 |
| Fig. 4. 14 Nodal temperatures (discrete points in time as well as space) | 147 |
| Fig. 5. 1 Energy interactions of front glazing at surface and layer underneath..... | 153 |
| Fig. 5. 2 Energy interactions at PV encapsulation layer | 156 |
| Fig. 5. 3 Illustration of PV cell encapsulation | 157 |
| Fig. 5. 4 Conduction to/from base panel layer from/to PV and heat pipe at middle node..... | 160 |
| Fig. 5. 5 Heat pipe thermal resistance network (Lee, 2010)..... | 162 |
| Fig. 5. 6 Thermo-physical properties of saturated water over range of operating temperatures (Cengel, 2007) | 167 |
| Fig. 5. 7 Thermoelectric generator schematic diagram | 169 |

Table of Figures

| | |
|--|-----|
| Fig. 5. 8 Condenser-TEG hot plate interface boundary with 3 differential elements..... | 170 |
| Fig. 5. 9 Fan-Heat sink assembly attached at the TEG cold plate | 175 |
| Fig. 5. 10 Correlation between collector and TEG cold plate temperatures | 176 |
| Fig. 5. 11 Heat pipe-based Photovoltaic collector thermal modelling flow chart | 181 |
| Fig. 5. 12 Thermoelectric generator computer model implementation flow chart | 182 |
| Fig. 6. 1 PV encapsulation temperature against radiation intensity for range of wind speeds..... | 185 |
| Fig. 6. 2 Steady state PV temperature response for ambient temperature range of 20-50 °C and Wind speed range of 0-5 m/s under light intensity of 1000 W/m ² | 189 |
| Fig. 6. 3 Influence of insulation on the temperature response of the integrated PV-TEG collector | 189 |
| Fig. 6. 4 PV cells temperature for varying operating temperature and (0 m/s) wind speed..... | 190 |
| Fig. 6. 5 Transient PV Temperature response for range of light intensities at operating temperature T _{amb} = 25 °C and wind speed = 0 m/s; a) 300 W/m ² , b) 400 W/m ² , c) 500 W/m ² , d) 600 W/m ² , e) 700 W/m ² , f) 800 W/m ² , g) 900 W/m ² , h) 1000 W/m ² | 193 |
| Fig. 6. 6 Thermal waste energy absorbed by TEG, a) 1060 W/m ² , b) 740 W/m ² | 194 |
| Fig. 6. 7 Thermal waste energy absorbed by thermoelectric generators for range of light intensities and operating temperatures at wind speed = 0 m/s..... | 195 |
| Fig. 6. 8 Conventional PV module power output for varying wind speed and light intensity. | 196 |
| Fig. 6. 9 Output power comparison between the three considered for radiation intensity level of 1000 W/m ² and wind speed of 0 m/s. | 196 |
| Fig. 6. 10 Transient PV Temperature response for range of light intensities at operating temperature T _{amb} = 25 °C and wind speed = 0 m/s; a) 300 W/m ² , b) 400 W/m ² , c) 500 W/m ² , d) 600 W/m ² , e) 700 W/m ² , f) 800 W/m ² , g) 900 W/m ² , h) 1000 W/m ² | 198 |
| Fig. 6. 11 Thermoelectric generator power output against the temperature difference across TEG plates intensities at operating temperature T _{amb} = 25 °C and wind speed = 0 m/s; a) 300 W/m ² , b) 400 W/m ² , c) 500 W/m ² , d) 600 W/m ² , e) 700 W/m ² , f) 800 W/m ² , g) 900 W/m ² , h) 1000 W/m ² | 200 |
| Fig. 6. 12 Steady State Electrical Conversion Efficiency Against Wind Speed..... | 201 |
| Fig. 6. 13 PV cells efficiency against the temperature difference across TEG plates intensities at operating temperature T _{amb} = 25 °C and wind speed = 0 m/s; a) 300 W/m ² , b) 400 W/m ² , c) 500 W/m ² , d) 600 W/m ² , e) 700 W/m ² , f) 800 W/m ² , g) 900 W/m ² , h) 1000 W/m ² | 202 |

Table of Figures

| | |
|---|-----|
| Fig. 6. 14 PV panel and TEG efficiencies as a function of irradiance | 203 |
| Fig. 6. 15 PV panel and TEG efficiencies against wind speed | 204 |
| Fig. 6. 16 PV panel and TEG efficiencies as a function of ambient temperature..... | 204 |
| Fig. 6. 17 Hybrid collector efficiency as a function of irradiance..... | 205 |
| Fig. 6. 18 Hybrid collector efficiencies as a function of wind speed..... | 205 |
| Fig. 6. 19 Hybrid collector efficiencies as a function of ambient temperature | 205 |
| Fig. 7. 1 a) Tungsten halogen lamp. b) Spectra from common sources of visible light | 209 |
| Fig. 7. 2 Spectrum distribution of Tungsten-Halogen lamps used for solar simulator | 209 |
| Fig. 7. 3 Solar simulator utilised for experimental performance characterization..... | 210 |
| Fig. 7. 4 a) Artificial light intensity and uniformity test. b) Screen with grids indicating points of measurement for radiation intensity and uniformity assessment..... | 211 |
| Fig. 7. 5 Schematic illustrating solar simulator displacement from PV module with respective recorded average light intensities..... | 214 |
| Fig. 7. 6 Thermoelectric generation module..... | 218 |
| Fig. 7. 7 Pyranometer for light intensity measurement..... | 219 |
| Fig. 7. 8 Wiring arrangement for current and voltage measurement of PV module..... | 220 |
| Fig. 7. 9 a) Solar module analyser ISO-TECH (ISM490) to characterize electrical performance of PV module. b) Wiring of PV module and solar module analyser | 221 |
| Fig. 7. 10 K-Type thermocouples for temperature measurements | 222 |
| Fig. 7. 11 Fabrication of heat pipe-based PV collector | 224 |
| Fig. 7. 12 Schematic illustrating components of waste heat recovery system | 226 |
| Fig. 7. 13 Aluminium heating block integration to condenser section of heat pipe..... | 226 |
| Fig. 7. 14 Actual TEG waste heat recovery assembly fabricated | 227 |
| Fig. 7. 15 Integration of TEG-fan-heat-sink waste heat recovery system with heat pipe-based PV collector . | 227 |
| Fig. 7. 16 Wiring of PV module and solar module analyser (ISM 490) for electrical characterization of PV panel | 229 |
| Fig. 7. 17 Locations of K-type thermocouples attached for temperature measurement..... | 230 |
| Fig. 7. 18 Experimental tests performed on waste heat recovery system. | 232 |
| Fig. 7. 19 Photo showing test of integrated collector under artificial light simulator..... | 232 |

Table of Figures

| | |
|--|-----|
| Fig. 7. 20 Photo showing tested collector and temperature sensors attached on surface as well as waste heat recovery assemblies at condenser section of heat pipe..... | 233 |
| Fig. 8. 1 Schematic illustrating solar simulator displacement from PV module with respective recorded average light intensities..... | 235 |
| Fig. 8. 2 Variation percentage of light intensities at evenly spaced points | 237 |
| Fig. 8. 3 Solar simulator light intensities and uniformity percentage for different displacement of light simulator | 237 |
| Fig. 8. 4 Temperature response of integrated PV-TEG with and without insulation relative to conventional PV module..... | 238 |
| Fig. 8. 5 Temperature distribution at the surface of tested collector | 239 |
| Fig. 8. 6 Recorded power output and estimated efficient of conventional PV module under varying light intensities..... | 242 |
| Fig. 8. 7 Electrical performance recorded of integrated PV-TEG collector | 243 |
| Fig. 8. 8 Comparison between experimental results of conventional PV module and integrated PV-TEG module without insulation..... | 244 |
| Fig. 8. 9 Power measured for the considered collectors under varying light intensity | 245 |
| Fig. 8. 10 Thermoelectric generator thermal performance | 246 |
| Fig. 8. 11 Open circuit voltage of TEG bank at light intensity of 1060 W/m^2 | 247 |
| Fig. 8. 12 Comparison of power output and conversion efficiency trends of conventional PV module | 252 |
| Fig. 8. 13 Temperature response of PV module under varying of light intensities | 253 |
| Fig. 8. 18 Experimental testing condition experienced during characterization of single TEG module | 255 |
| Fig. 8. 19 Simulation results applying conditions experienced during experimental test of a single TEG module | 256 |
| Fig. 8. 20 Comparison between theoretical predictions and experimental results for a single TEG module... | 257 |
| Fig. 8. 21 Comparison between simulated and recorded maximum power output of single TEG module..... | 258 |
| Fig. 8. 22 Comparison between simulated and recorded voltages and currents at maximum power point for single TEG module | 258 |
| Fig. 8. 23 Actual and averaged deviation of TEG module performance parameters..... | 259 |
| Fig. 8. 24 Evaporator section temperature comparison | 261 |

Table of Figures

Fig. 8. 25 Evaporator section temperature comparison 261

Fig. 8. 26 Transient response of the integrated collector power output, front glazing, and condenser section temperature for validation purpose 263

Fig. 8. 27 deviation of the output power for the range of incoming light intensities 263

Fig. 8. 28 Influence of number of heat pipes attached on the temperature response of the collectors 265

Fig. 8. 29 PV Temperature difference between integrated collector and conventional PV module at wind speed 0 and varying ambient temperature..... 266

Fig. 8. 30 Influence of number of heat pipes attached on the total power output..... 267

List of Tables

| | |
|---|-----|
| Table 2. 1 Temperature coefficients of various commercially available PV technologies..... | 24 |
| Table 3. 1 Most efficient solar PV panels available commercially (The Eco Experts, 2015) | 34 |
| Table 3. 2 Working fluid options for heat pipes and useful temperature range (Byon, 2016)..... | 46 |
| Table 3. 1 Efficiency of TEG-based concentrator systems for maximum irradiance (Chávez-Urbiola et al., 2012). | 115 |
| Table 3. 2 Performances of TEG, solar cell and hybrid PV-TEmodule (Deng et al., 2013b) | 119 |
| Table 3. 3 Advantages and disadvantages of different thermal management techniques (Makki, Omer, and Sabir, 2015) | 124 |
| Table 3. 4 Summary of some of the various systems reviewed..... | 125 |
| Table 5. 1 Estimation of effective heat capacity of PV encapsulation (Armstrong and Hurley, 2010) | 157 |
| Table 6. 1 Theoretical performance evaluation conditions applied | 184 |
| Table 6. 2 Temperature difference between PV-TEG and conventional PV collectors | 192 |
| Table 6. 3 Power output difference between PV-TEG and conventional PV collectors | 199 |
| Table 7. 1 List of components for experimental testing collector fabrication..... | 216 |
| Table 7. 2 PV Panel Specifications | 217 |
| Table 7. 3 Specification of thermoelectric generation modules employed..... | 218 |
| Table 7. 4 List of parameters measured | 228 |
| Table 8. 1 Deviation of collector temperature values at steady state..... | 241 |
| Table 8. 2 PV module characteristics reported in manufacturer’s datasheet | 248 |
| Table 8. 3 Conventional PV module validation parameters considered..... | 249 |
| Table 8. 4 Recorded results and influence of spectral mismatch on PV performance | 250 |
| Table 8. 5 Summary of PV module power output and temperature response validation | 253 |
| Table 8. 6 TEG module validation parameters considered..... | 254 |
| Table 9. 1 Performance improvements of the hybrid collector as function of heat pipe number attached ... | 275 |

NOMENCLATURE

| | | | |
|----------------------|---|-------------------|-------------------------|
| <i>A</i> | Area [m ²] | Subscripts | |
| <i>C_p</i> | Specific heat capacity [J/kg K] | <i>amb</i> | Ambient |
| <i>d</i> | Diameter [m] | <i>base</i> | Base panel |
| <i>E</i> | Electrical output [W] | <i>c</i> | Collector |
| <i>G</i> | Irradiance [W/m ²] | <i>cold</i> | Cold plate of TEG |
| <i>h</i> | Heat transfer coefficient [W/(m ² K)] | <i>con</i> | Condenser |
| <i>I</i> | Electric current [A] | <i>eva</i> | Evaporator |
| <i>k</i> | Thermal conductivity [W/(m. K)] | <i>EVA</i> | Ethylene vinyl acetate |
| <i>l</i> | length [m] | <i>g</i> | Front glazing |
| <i>R</i> | Thermal resistance [(m ² K)/W] | <i>hot</i> | Hot plate of TEG |
| <i>T</i> | Temperature [K] | <i>i</i> | Differential node "i" |
| <i>u</i> | Wind speed | <i>l</i> | liquid |
| <i>V</i> | Voltage [V] | <i>n</i> | n-element |
| <i>Z</i> | Figure of merit | <i>oc</i> | Open-circuit |
| | | <i>p</i> | Heat Pipe, p-element |
| Greek | | <i>PV</i> | PV cells |
| (<i>τα</i>) | Effective transmittance- absorption | <i>r</i> | Reference |
| <i>α</i> | Absorptivity, Seebeck coefficient [uV/K] | <i>rad</i> | Radiative |
| <i>β</i> | Temperature Coefficient | <i>ins</i> | Thermal insulation |
| <i>γ</i> | PV cell coverage ratio | <i>sc</i> | Short-circuit |
| <i>δ</i> | Thickness [m] | <i>TPT</i> | Tedlar-Polyester-Tellar |
| <i>ε</i> | Emissivity, electrical resistivity [uΩm] | <i>w</i> | Heat pipe wick |
| <i>η</i> | Efficiency [%] | | |
| <i>ρ</i> | Density [kg/m ³], reflectance | | |
| <i>σ</i> | Stefan-Boltzmann constant [W/m ² K ⁴] | | |
| <i>τ</i> | Transmittance [%] | | |
| <i>μ</i> | Thomson coefficient [uV/K] | | |

ABSTRACT

PV systems in practice experience excessive thermal energy dissipation that is inseparable from the photo-electric conversion process. The temperature of PV cells under continuous illumination can approach 40°C above ambient, causing a drop in the electrical performance of about 30%. The significance of elevated temperature on PV cells inspired various thermal management techniques to improve the operating temperature of the cells and hence their conversion efficiency. Hybrid PV/Thermal (PV/T) collectors that can supply both electrical and thermal energy are attractive twofold solution, being able to cool the PV cells and thus improving the electrical power output as well as collecting the thermal energy by-product for practical utilization. The challenges present on the performance of PV systems due to elevated operating temperature is considered the research problem within this work.

In this research, an integrated hybrid heat pipe-based PV/Thermoelectric (PV/TEG) collector is proposed and investigated theoretically and experimentally. The hybrid collector considers modular integration of a PV absorber rated at 170W with surface area of 1.3 m² serving as power generator as well as thermal absorber. Five heat pipes serving as the heat transport mediums were attached to the rear of the module to extract excessive heat accumulating on the PV cells. The extracted heat is transferred via boiling-condensation cycle within the heat pipe to a bank of TEG modules consisting of five 40 mm x 40 mm modules, each attached to the condenser section of each heat pipe. In principle, the incorporation of heat pipe-TEG thermal waste recovery assembly allow further power generation adopting the Seebeck phenomena of Thermoelectric modules.

A theoretical numerical analysis of the collector proposed is conducted through derivation of differential equations for the energy exchange within the system components based on energy balance concepts while applying explicit finite difference numerical approach for solutions. The models developed are integrated into MATLAB/SIMULINK environment to assess the cooling capability of the integrated collector as well as the addition power generation through thermal waste heat recovery. The practical performance of the collector proposed is determined experimentally allowing for validation of the simulation model, hence, a testing rig is constructed based on the system requirements and operating principles.

Reduction in the PV cell temperature of about 8°C, which account for about 16% reduction in the PV cell temperature response compared to a conventional PV module under identical conditions is attained. In terms of the power output available from the PV cells, enhanced power performance of additional 5.8W is observed, contributing to an increase of 4% when compared with a PV module. The overall energy conversion efficiency of the integrated collector was observed to be steady at about 11% compared to that of the conventional PV module (9.5%) even at high ambient temperature and low wind speeds. Parametric analysis to assess the performance enhancements associated to the number of heat pipes attached to the PV module is conducted. Increasing the number of heat pipes attached to 15 pipes permits improved thermal management of the PV cells realised by further 7.5% reduction in the PV module temperature in addition to electrical output power improvement of 5%.

Chapter 1

Introduction

Throughout the history of humanity, major advances in civilisation have been accompanied by increased consumption of energy. Today, energy consumption appears to be directly related to the level of living of the populace and the degree of industrialization of countries. The shift in energy consumption between the industrial and technological eras had nearly tripled, Fig. 1.1. Societies have depended on different types of energy in the ancient past, and societies have been forced to change from one energy type to another, and so the cycle shall continue along with further advancements in civilisation. Recognising the great potentials of energy utilization, superpower states have established an exclusive market governed by energy price tags. It allowed some countries with large supplies of low-cost energy to use such resources as political and economic weapons to achieve ends that could not be realized by diplomatic means.

In the first half of the twentieth century, energy sources were exploited with the primary consideration given to economy – low cost. Today, innovative ideas have merged to develop technologies that can produce great quantities of energy at low cost with minimal impact on the environment. In this regard, proper balance of energy, economy, and ecology resembles a major challenge. The increased world population, and improved standards of living in developing countries have led to an increased global energy consumption, which averages about 2% per year (Ngo and Natowitz, 2009). If this rate of energy consumption is to be sustained, an energy consumption growth by 7 times is estimated between 2000 and 2100, Fig. 1.2. As far as fossil resources are concerned, this is clearly unsustainable.

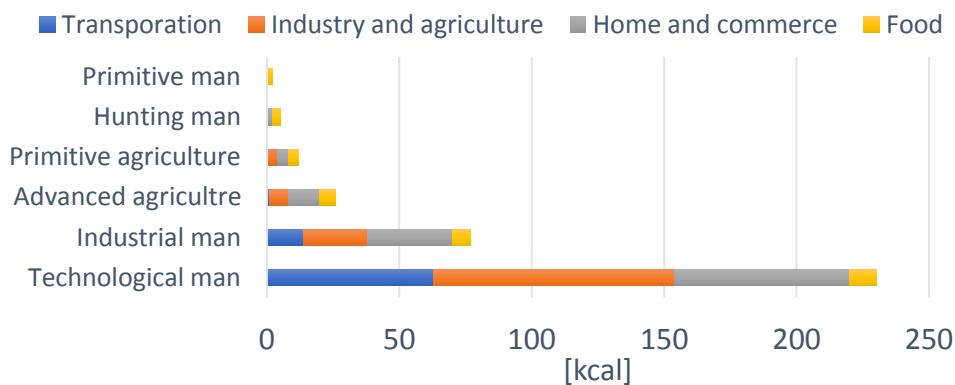


Fig. 1.1 Estimated energy consumption per person per day over the ages (Cook, 1971)

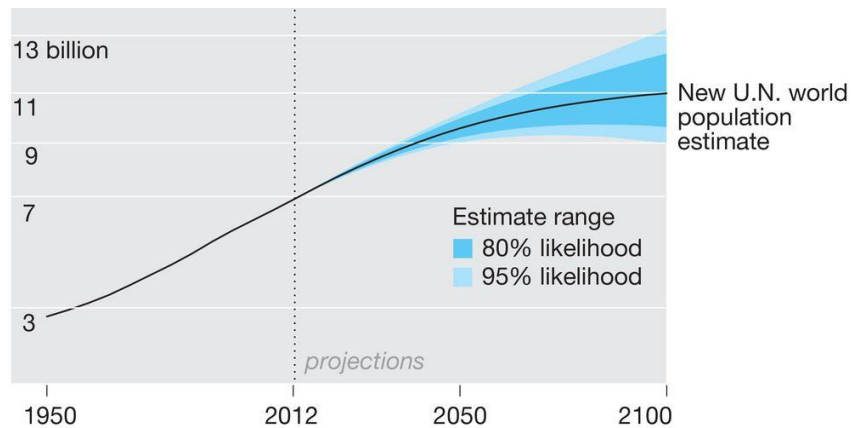


Fig. 1. 2 United Nations prediction of world's population (George, 2011)

1.1 The Ultimate Energy Source

Energy consumed in various forms on our planet originates in the power of the atom (Suhkatme et al., 2008). Nuclear fusion reactions energize the Sun, and the resulting sunlight has profound effects on our planet. The majority of energy sources that we use, except for geothermal and nuclear energies, are derived initially from solar energy, Fig. 1.3. The fossil fuel that we use today – coal, and natural gas – are derived from organisms that grew over several hundreds of million years, storing the solar energy which reached the earth’s surface. Renewable energies – hydro, biomass, and wind – are also directly or indirectly derived from the energy of our sun. The energy intercepted on earth warms the planet’s surface, powering transfers of heat and pressure in weather patterns and ocean currents (Miller, Spoolman, and Miller, 2014). The resulting air currents drive wind turbines.

Solar radiation aids evaporation of water that falls as rain and builds up behind dams, where its motion is used to generate electricity via hydropower. The energy available within solar radiation can also be harvested using Photovoltaic and Solar Thermal technologies which are continuously growing in both utilisation and efficiency. Solar energy, though technically not renewable, is normally classified as such because it is effectively inexhaustible on any practical timescale (Ngo and Natowitz, 2009). It is in the process of transforming energy from one form to another that we are able to harness part of it for our own benefit.

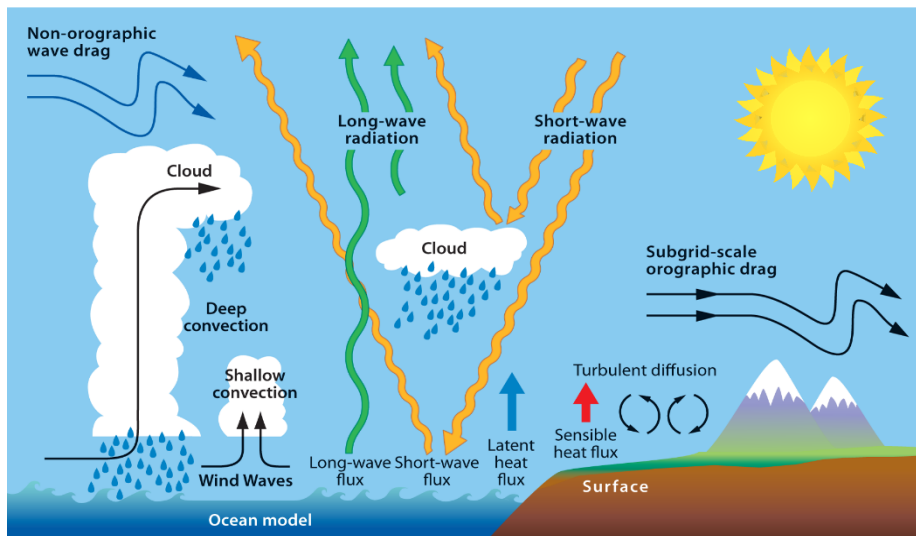


Fig. 1. 3 The ultimate energy source (European Centre for Medium-Range Weather Forecasts)

The total power available from the sun is about (3.9×10^{26} Watts) of electromagnetic waves radiated uniformly in all directions away from the source (Walker, 2013). In perspective, the average radiation reaching the

earth's surface annually is around 197 W/m^2 (Wallace and Hobbs, 2006). Although this figure is considered a very small proportion, it accounts for about 10,000 times (1.76×10^{17} Watts) as much energy as that consumed annually by humankind (Watt Committee on Energy, 1999). Major technological advances including steam engine, discovery of oil's use as fuel, and the discovery of nuclear power are often the catalysts for change in the global energy mix (Fanchi, 2011). The modern transition to a new energy mix is being driven by the desire to replace non-renewable fossil fuels, the concern that fossil fuel combustion is having an adverse effect on the environment, and the desire to achieve future energy security.

In this research, Solar Photovoltaic and Thermal conversion technologies are the focus of the investigation. Solar Photovoltaic is further highlighted being the subject for enhanced performance and optimized design. Nevertheless, the principle of thermal conversion is inseparable even when electrical generation using Photovoltaic technologies is considered.

1.2 Solar Energy Utilisation

Solar radiation can be converted to other forms of energy by several conversion processes as shown in Fig. 1.4. Thermal conversion relies on the absorption of radiation within the solar spectrum to heat a cooler surface. Thermal absorbing collectors have been widely applied exploiting the energy

available from the sun. Photovoltaic conversion however, produce electrical power by the generation of an electrical current as a result of the interaction of light photons with certain types of conducting materials (Fanchi, 2011). Depending on the technology within solar cells, the conversion efficiency of the cells is varied. In addition, solar energy is a key element to synthesize biologically chemical compounds as realized in photosynthesis process in plants.

The solar resource is enormous compared to our energy needs. It varies in quantity and quality in places as well in time, in ways that are not entirely predictable. Hence, making the choice to which is more favourable strictly dependant on the resources available within a location, as well as energy demand.

Solar radiation is simply transformed into heat through absorption by gaseous, liquid or solid materials. Heat can then be used for various applications including, water/space heating, evaporative processes, and drying crops (Thirugnanasambandam, Iniyar, and Goic, 2010). Heat can also be transformed into mechanical work or electricity, and it can run or facilitate chemical or physical transformations and thus industrial processes or the manufacture of various energy vectors or fuels (Goswami, Kreith, and Kreider, 2000).

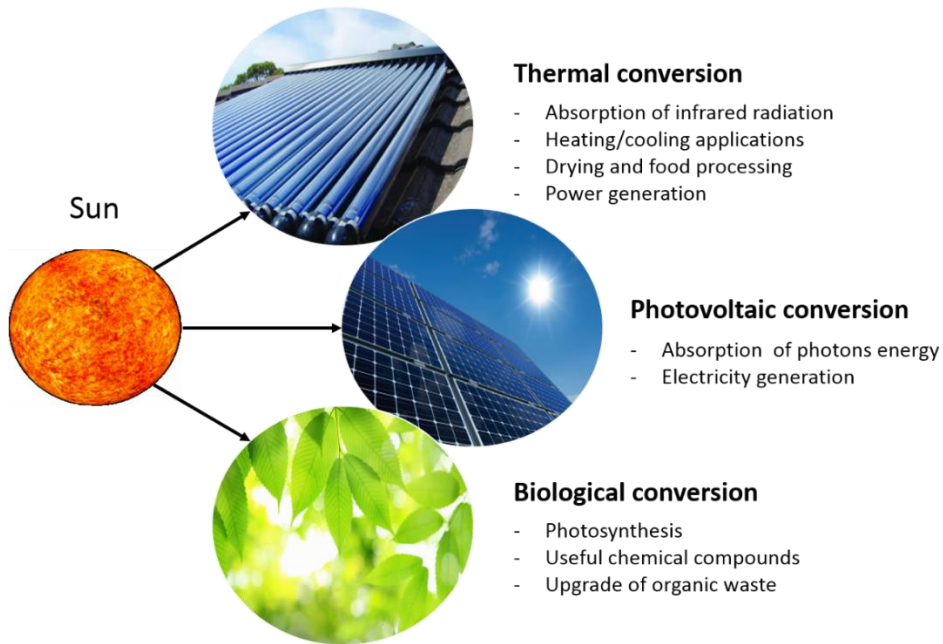


Fig. 1.4 Solar energy utilization

Solar radiation can also be viewed as a flux of electromagnetic waves or photons (Iqbal, 1984). Photons from the sun are highly energetic, and can promote photo-electrical conversion such as in photosynthesis, and generate conduction of electrons in semiconductors. Hence, enabling direct photovoltaic conversion of sunlight into electricity (Luque, 2010). The two fundamental methods to capture energy from the sun – heat and photoreaction – can also be combined in several ways to deliver combined energy vectors. In attempt to improve energy efficiency per surface area of receiving panels, manufacturers now offer hybrid systems, which produce electricity and heat simultaneously, thereby achieving a combined cogeneration efficiency that can approach 80% (Yan, 2015).

1.3 Aim & Objectives

1.3.1 Aim

The research aims on improving the energy conversion efficiency of Photovoltaic energy systems through investigating strategies to provide effective cooling and permit utilization of waste heat for useful applications. The investigation adopts a hybrid design that incorporates Photovoltaic (PV) technology in combination with Thermoelectric Generators (TEGs) and Heat Pipes for PV thermal management as well as efficient utilization of solar energy within the solar spectrum.

1.3.2 Objectives

The research objectives describing the tasks accomplished at each stage of the research are summarised as follows:

- ❖ Reviewing main challenges encountered within PV technologies and addressing the significance of temperature influence on the performance of PV modules in practice.

- ❖ Studying various cooling techniques and hybrid photovoltaic designs towards an optimum solution to the temperature rise experienced in PV collectors operating in practical conditions.

- ❖ Developing a mechanism to improve the operating conditions of PV cells while harnessing thermal waste energy available from PV panels through employing thermoelectric generators and heat pipes for improved conversion efficiency.
- ❖ Studying the heat transfer processes associated within the system to aid the derivation of a mathematical model based on the energy balance concepts.
- ❖ To predict, and optimise the performance of the system under investigation through computer simulations using the mathematical model implemented.
- ❖ Performing experimental tests to predict the practical performance of the system under various operating conditions and optimise the system performance through incorporating different techniques, technologies, and materials.

1.4 Novelty and Contributions

1.4.1 Novelty

The novelty of the system presented in this research lies behind the system design in which potential benefits can be attained. The novelty in the proposed system are summaries as follow:

- ❖ Few researchers have investigated the integration of TEG modules with PV technology, however, mostly have adopted a small scale impractical approach; either by attaching a single TEG module to a PV cell, or populating the rear of a PV module to cover the whole surface area with TEG devices. As TEG modules available commercially are expensive, the investigated system proposed employment of heat pipes as a solution for minimal use of TEG modules possible in an attempt to reduce the number of TEG modules attached and hence promote the feasibility of the system for improved power supply. The integration of TEG modules directly to the rear a PV module can achieve better heat extraction and hence improved thermal management for the cell; promoting minimal thermal losses. However, the power generation cost is further increased due to the increased number of TEG modules utilised to cover the entire rear of the module, making such integration less attractive; solving one part of the problem while introducing other challenges.
- ❖ Heat pipes are considered as absorbers for the thermal energy available from the PV module; facilitating thermal energy transport to the hot plate of the TEG module for supplemental power supply. Additionally,

utilisation of heat pipes within the proposed hybrid collector promotes a flexible design where the location of the TEGs are not limited to the surface requiring thermal management.

- ❖ The integrated hybrid heat pipe-based PV/Thermoelectric (PV/TEG) collector proposed considers a modular integration with a PV module rather than a small cell scale integration.
- ❖ A mathematical simulation model of a modular scale hybrid PV/TEG collector applying conservation of energy principle was developed, validated and programmed using MATLAB software. Both transient and steady state numerical simulations for varying operating conditions are also considered.
- ❖ The developed model can be applied for performance prediction under various climatic conditions in any particular region in the world. The model could also be helpful in selecting the optimum elements and design parameters of the integrated hybrid collector for further enhancements. Furthermore, this work has shown that experimental investigations are no longer restricted to specific solar insolation regions and the simulation model makes it possible to simulate solar insolation conditions anywhere in the world.
- ❖ The system avoids complex and expensive operating cycles, it also eliminates the use of additional pumps. Moreover, the system does not use pressure or high temperatures, so can be constructed largely of plastic materials that have a lower and inexpensive cost than metals.
- ❖ Low technology operation and easy maintenance reduces barriers to entry and applicability, especially where local skill levels could be a constraint.

1.4.2 Contributions

This research work would have a great benefit at various levels to tackle performance deterioration of PV cells due to elevated temperature especially in countries with abundant supply of solar energy and high ambient temperature as countries in Africa and the Middle East region. The outcomes of this research will have significant impact on the scientific community, researchers and industries. This research has the potential to open the market for this novel system. The system prototype can assist manufacture and supply companies in expanding their business as the system can be replicated in a variety of settings worldwide.

The application of the integrated collector has the potential to contribute in tackling increased energy demands through promoting thermal waste recovery for addition power especially for concentrated solar applications. Therefore, such system can have a direct benefit to the communities in rural areas. Significant environmental impacts in reducing greenhouse gas emissions; and improving the quality of life in many poor developing countries can also be attained.

In terms of new knowledge, an innovative technique for thermal waste heat recovery from PV modules is introduced where efficient utilisation of solar energy available from the sun is permitted. Since the research is

concerned with thermal management of PV cells, the development of an innovative cooling scheme for PV technology and potential results from this investigation will be of great interest to many research institutes and academic communities over the world.

1.5 Thesis Outline

This research has been conducted in several stages and covered many tasks and activities as presented in this thesis. The thesis comprises nine chapters divided as follows:

Chapter one presents a brief introduction on the increasing global energy consumption associated to growing population and level of industrialization, in addition to the challenges of proper balance of energy, economy, and ecology for emerging energy technologies. The chapter emphasizes on utilization of solar energy as a potential solution for electrical and thermal energy supply, which can also be combined in several ways to deliver combined energy vectors. The chapter then lays down the aim of this research and the objectives considered to tackle the significance of elevated temperature on the performance of PV cells. The novelty, impacts and benefits to science, and industry is also deliberated in this chapter. The chapter then concludes with the thesis outline.

Chapter two highlights the utilisation of solar energy for power generation through Photovoltaic technology. The factors affecting the practical performance of PV cells are also discussed, where elevated temperature is addressed as the most critical factor hindering the generation capability of the cells. The significance of temperature on the electrical performance of PV cells is then deliberated through electrical characteristic curves. The chapter then discusses means of thermal management for PV cells in operation including passive and active techniques, in addition to the additional benefits of thermal waste heat recovery. Background research on the technologies incorporated within the proposed hybrid collector including PV technology, heat pipes, and thermoelectric devices is presented along with theory and operating principle.

Chapter three presents an extensive review of the literature on various techniques applied for thermal management for PV systems. The chapters consider advancements in PV cells performance adopting hybrid PV integration. Techniques for thermal management of PV cells deliberated in this chapter include, air, liquid, Phase change material, heat pipe, and thermoelectric -based collectors. A comprehensive discussion of each hybrid PV collector category including design, operation principle, advantages and limitations, as well as possible improvement arrangements are also

presented. The conclusions drawn from the literature review which sets the motivations for the system proposed are also illustrated.

Chapter four presents the proposed hybrid integration of heat pipe-based Photovoltaic/Thermoelectric generation system. The collector design, operating principle, and considerations building on the limitations of the reviewed technologies in chapter three is also described. Execution of the research through both theoretical analysis and empirical investigation is deliberated in the methodology section of this chapter. The computer modelling process including, theory, derivation of energy balance equations, and numerical solution approach for implementation into MATLAB/SIMULINK environment is also described. The performance parameters considered for quantitative analysis of the system proposed including electrical power output and conversion efficiencies are given in this chapter. The chapter concludes with a brief description of experimental work conducted, which is further presented in detail in chapter 7.

Chapter five presents the derivation of two-dimensional differential equations of the system components within the hybrid collector proposed; applying conservation of energy and concepts of thermal resistance network. The main three modes of thermal energy transfer including, conduction, convection, and radiation, are also discussed within this chapter highlighting their contribution on thermal state of the system. The numerical

solution approach applying finite difference approximation to the derived equations is also presented in this chapter. Finally, the solution routine for the system equations implemented in MATLAB/SIMULINK is presented.

Chapter six presents the theoretical simulation results of the hybrid collector under investigation including both transient and steady state electrical and temperature responses. Results illustrated in this chapter considered three collectors to facilitate comparisons and realize the significance of the heat pipe-based PV/TEG collector with and without insulation present at the rear of the module compared against a conventional PV module under identical operating parameters. The results are intended to assess the heat pipe capability to transport thermal energy accumulating on the PV cells, as well as the ability of the TEG to convert low grade thermal energy absorbed from the PV module under varying irradiance, wind speed, and temperature conditions. The chapter concludes with the overall energy conversion efficiency of the integrated collector.

Chapter seven presents the experimental work conducted to assess the practical performance of the hybrid collector. The main experiments designed and conducted in this research include; initially testing of an artificial solar simulator utilised as a light source, in which light intensity and uniformity tests were performed, in addition to evaluation of the practical performance of the collector under controlled lab environment. This chapter

illustrates the fabrication process of the hybrid collector utilising the technologies described in chapter 2. The list of measuring instrument including pyranometer, thermocouples, data loggers, and solar module analyser to monitor the practical performance are also presented. The testing procedure and considerations adopted within the experimental investigation are also highlighted. The list of parameters measured and monitored including the electrical characteristics and thermal responses for both PV and TEG modules are also listed in at the end of this chapter.

Chapter eight presents the results obtained from experimental tests for the three collectors considered in this investigation. The practical results illustrate the electrical and thermal characteristics of the PV module and TEG employed. The results obtained are then utilised to validated the computer model developed in the computer model validation section. Optimisation of the collector considered is also presented in this chapter to evaluate improvements associated to increasing the number of heat pipes and TEG modules incorporated in the designed collector

Chapter nine concludes the research with a summary of the tasks accomplished to achieve the aim of this research. Additionally, the key findings of are presented along with most remarkable results attained by the hybrid collector studied. The chapter then lays down limitations within the research and recommendations for future work are also discussed.

Chapter 2

Thermal Management of Solar Photovoltaics

Solar energy is one of the most widely exploited energy sources that can be utilized in various applications such as, thermal management using thermal collectors or electricity generation through special optical solar cells, also known as *Photovoltaic* (PV) cells. PV cells are semiconductor devices that have the ability to convert the energy available in both dispersed and concentrated solar radiation into direct current (DC) electricity (Emery, 1999), (Markvart, 2000), (Radziemska, 2003), (van Helden, van Zolingen, and Zondag, 2004), (Luque, 2010), (Kurtz, 2012). Conversion of solar energy into electricity through PV cells is achievable at different efficiency ratings varying between 10-40% and determined primarily by the type of semiconductor material from which the cells are made (Emery, 1999), (Kurtz, 2012). PV technologies have been adopted in many regions world-wide as solar energy is ubiquitous and abundant on the

earth's surface. PV systems offer wide range of applications from direct power supply for appliances to large power stations feeding electricity into the grid and serving large communities. Although PV systems have been commercially available and widely operated for many years, certain barriers stand towards the widespread application of this technology.

Issues such as limited conversion efficiency, elevated temperatures, and dust accumulation are considered critical due to their significant impact on the performance of PV cells, especially in sun-drenched hot climate regions. Wide range of cooling techniques for thermal regulation of PV systems has been investigated. Among the proposed systems, air and liquid based cooling of PV systems are considered mature technologies and have been investigated widely in practice. The utilization of heat pipe, phase change materials (PCM), and thermoelectric devices to aid cooling of PV cells remain at the research and development stage. Although various techniques have been investigated, practical solutions have not been identified for wide implementation. The challenges present on the performance of PV systems due to elevated operating temperature is addressed in this chapter.

2.1 Temperature Influence on Photovoltaic Cells

PV cells absorb up to 80% of the incident solar radiation, however, the proportion of converted incident energy into electricity depends on the conversion efficiency of the PV cell technology (van Helden, van Zolingen, and Zondag, 2004). The remainder energy is dissipated as heat and the PV module can reach temperatures as high as 40 °C above ambient. This is due to the fact that PV cells convert a certain wavelength of the incoming irradiation that contributes to the direct conversion of light into electricity, while the rest is dissipated as heat (Luque, 2010), Fig. 2.1. The photoelectric conversion efficiency of commercially available single junction solar cells ranges between 10-25% under optimum operating conditions. The efficiency is mainly determined by the semiconductor material from which the cell is made (Radziemska, 2003), (Kurtz, 2012). However, PV systems do not operate under standard conditions, thus variation of operating temperatures limit the efficiency of PV systems. Such limited efficiency is associated with the band-gap energy of the semiconductor material (Markvart, 2000), (Luque, 2010). Crystalline silicon PV cells can utilize the entire visible spectrum and some part of the infrared spectrum. Nonetheless, the energy of the infrared spectrum, as

well as the longer wavelength radiation are not sufficient to excite electrons in the semiconductor material to cause current flow (Luque, 2010). Similarly, higher energy radiation spectrum which is capable of producing current flow; is unusable. Consequently, radiation with high and low energies is ineffective for electricity generation, and instead is dissipated at the cell as thermal energy, accounting for losses above 50% of the absorbed light.

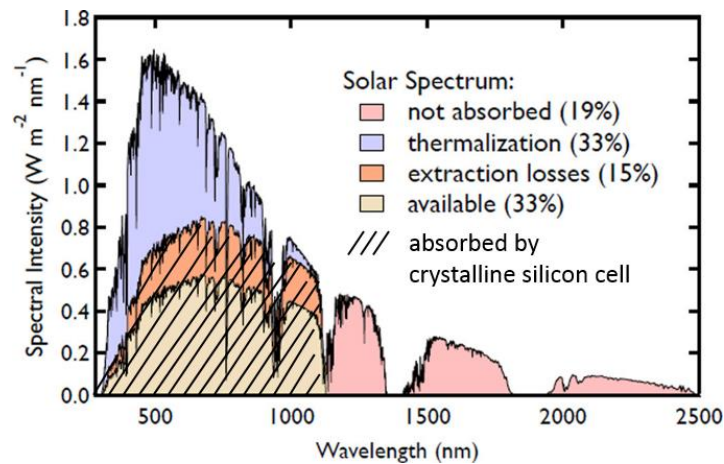


Fig. 2. 1 Fraction of terrestrial sunlight absorbed by crystalline silicon device (Kulish and Object, 2016)

Various elements affect the performance of PV modules in outdoor applications. Factors such as low irradiance, soiling, and high operating temperature contribute toward dramatic degradations in the conversion efficiency and the technical life-time of the solar cells (Du, Hu, and Kolhe, 2012), (Chatterjee and TamizhMani, 2011). However, PV cells under continuous

sunlight illumination tend to be affected mostly by high operating temperature, especially at concentrated radiation which tends to further elevate the temperature of the PV junction. The PV cell performance decreases with increasing temperatures, fundamentally owing to increased intrinsic carrier concentrations which tend to increase the dark saturation current of the p-n junction (Luque, 2010), (Michael, 2009). Reduction in band-gap due to high doping also serves to increase the intrinsic carrier concentration (Luque, 2010).

The increase in dark saturation current causes the open-circuit voltage to decrease linearly, which for silicon at 300K correspond to about 2.3 mV/°C (Luque, 2010). Huang et al. (2011) performed experimental investigation to observe the variation of open-circuit voltage over temperature range of (40-80°C) for practical of solar irradiance levels of (200-1000 W/m²), Fig. 2.2. Temperature rise of the PV cell has an adverse effect on the short-circuit current however; with a slight increase due to decline in the band-gap energy, Fig. 2.3. Andreev et al. (1997) estimated an increase in the short circuit current of 0.1%/°C due to reduction in the band-gap of the solar cell with temperatures varying between (20-100°C). Despite such increase in current flow, the degradation of the open-circuit voltage contributes to a noticeable decrease in

the available maximum electrical power which can be better observed through the characteristic curves of a PV module at different operating temperature in Fig. 2.4. For crystalline silicon PV cells, a drop in the electrical power output of about 0.2–0.5% was reported for every 1°C rise in the PV module temperature primarily due to the temperature dependence of the open-circuit voltage of the cell (Radziemska, 2003), (King and Eckert, 1996), (Moshfegh and Sandberg, 1998). Such property of PV cells is known as the *Temperature Coefficient* of the PV cell. According to Del Cueto (2002), the reduction in efficiency due to temperature dependence is in the range of an absolute 1–2% over a temperature span of 30°C. Table 2.1 presents the temperature coefficients of various PV technologies along with their typical efficiencies (Yang et al., 2010), (Petter Jelle, Breivik, and Drolsum Røkenes, 2012).

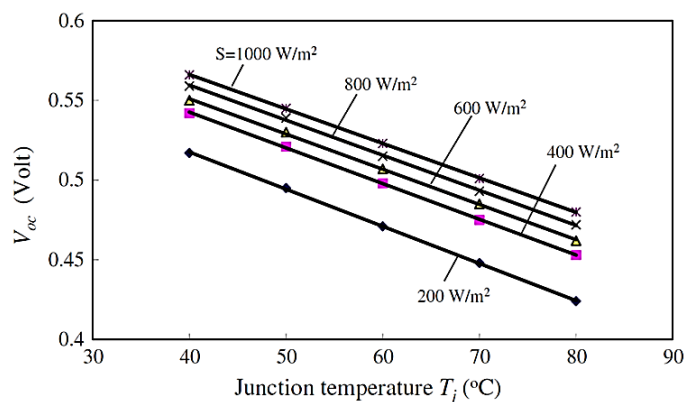


Fig. 2. 2 Open-circuit voltage variation against temperature - 40-80°C (Huang et al., 2011)

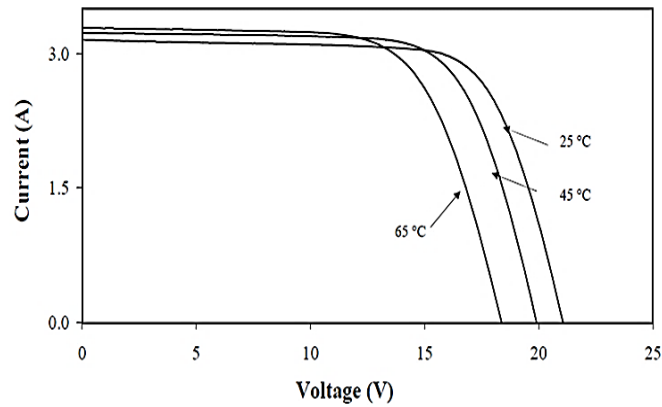


Fig. 2. 3 Slight increase in short circuit current observed with increasing temperature (Michael, 2009)

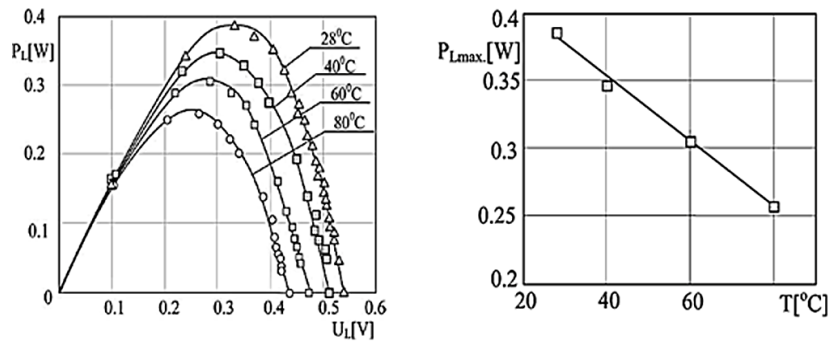


Fig. 2. 4 Linear drop in maximum power output of PV module with temperature increase (Radziemska, 2003)

Table 2. 1 Temperature coefficients of various commercially available PV technologies

| T_{ref} (°C) | η_{Tref} | β_{ref} (°C ⁻¹) | PV Technology | Ref. |
|----------------|---------------|-----------------------------------|---------------|----------------------|
| 25 | 16-24% | 0.0041 | Mono-cSi | (Zhang et al., 2012) |
| 25 | 14-18% | 0.004 | Poly-cSi | (Zhang et al., 2012) |
| 25 | 4-10% | 0.011 | a-Si | (Zhang et al., 2012) |
| 25 | 7-12% | 0.0048 | CIS | (Kurtz, 2012) |
| 25 | 10-11% | 0.00035 | CdTe | (Kurtz, 2012) |

In addition, for a given power output of a PV module where several cells are electrically connected in series, the output voltage increases while the current decreases due to series connection, hence reducing *Ohmic Losses* (Xu et al., 2012). Nonetheless, the cell producing the least output in series string of cells limits the current; this is known as *Current Matching* issue (ROYNE, DEY, and MILLS, 2005). Because the cell efficiency decreases with increasing temperature, the cell having the highest temperature will limit the efficiency of the entire string. Consequently, maintaining a homogeneous low temperature distribution across the string of cells is essential for an optimum performance of PV systems.

2.2 Thermal Management of PV Cells

Due to the temperature influence on the performance of PV cells, the energy that is unutilised for electrical energy conversion must be extracted to prevent excessive cell heating and deteriorated performance. Therefore, solar cell cooling must be an integral part of PV systems, especially in concentrated PV collectors in order to minimize the effect of elevated temperature on the PV module power output. Furthermore, with the current state of incentives and

the decreasing prices of solar modules, PV system prices are decreasing almost annually and industries are primarily concerned with ensuring maximum system output and prolonged lifetime (Du, Hu, and Kolhe, 2012). Hence, the cost, referred to as (£/kWh) of the total kWh generated from a system on an annual basis can be lowered as the PV collector would experience less losses. With primary interest of improving systems' overall performance, extensive efforts have been devoted to considering mechanisms for waste heat recovery to compensate for the low array electrical efficiency.

Various methods can be employed to achieve cooling of PV systems. However, the optimum cooling solution is critically dependent on several factors such as the PV technology employed, types of concentrators' geometries, and weather conditions at which the system operates. Challenges are mainly present in hot and humid climate regions where cells may experience both short and long-term degradation due to excessive temperature. Methods of cooling PV panels fall mainly into two categories, namely passive and active cooling.

Passive cooling techniques refer to means applied to extract and/or minimize heat absorption from/of the PV panel without additional power

consumption. The mechanism implies transporting heat from where it is generated and dissipating it to the environment (Royne, 2005). Wide varieties of passive cooling options are available, simplest forms involve application of solids of high thermal conductivity metals, such as aluminium and copper, or an array of fins or other extruded surfaces to enhance heat dissipation to the ambient (Theodore, 2011). More complex systems involve the use of Phase Change Materials (PCMs), in addition to the use of Heat Pipes that are able to transfer heat efficiently through a boiling-condensation process (Royne, 2005). However, in such thermal management systems heat dissipation is limited by the contact point between the heat-sink and the ambient, where the convective heat transfer coefficient and to a much less degree the radiative heat transfer are limiting factors (Royne, Dey, and Mills, 2005). An example illustrating passive cooling of PV panels can be of an array installed on a roof of a house with heat-sinks attached at the rear surface, in a way that allows air to naturally flow behind the panels, and extracts away heat through air convection, or the use of white-coloured roof that prevents the surfaces around the panels from heating up causing additional heat gain. Conversely, with passive cooling the main heat transfer mechanism for a PV system on a windless day is through

radiation and free convection, and both mechanisms are of the similar low order of magnitude, therefore, the need for a cooling system that can actively dissipate heat is essential especially in hot climate regions.

On the other hand, active thermal management techniques comprise of heat extraction utilizing devices such as blowers/fans to force air or pump water to the panels under operation allowing for excessive thermal energy to be extracted (Royne, Dey, and Mills, 2005). Active cooling means are powered using energy to affect some kind of heat transfer usually by convection and conduction. Although an active system consumes power, they are commonly applied in situations where the added benefit to the panels is greater than the energy demanded to power the system. These systems may also be used in situations where some additional benefit can be achieved, such as waste heat recovery for domestic space and water heating applications.

For both passive and active cooling systems, the commonly used cooling mediums are air and water. However, the thermal properties of air make it less efficient as a coolant medium (Xu et al., 2012). Therefore, air cooling is not well suited to the extraction of thermal energy from the PV collectors operating in hot regions. This implies that more parasitic power to operate fans will be

needed to achieve the same cooling performance of water, in addition to the limitations affecting thermal-waste recovery when using air as heat extracting medium. Nonetheless, in some situations where water is limited, air may still be the perfect option. Water cooling on the other hand, permits operation at much higher temperature levels and allows waste heat recovery to be employed more efficiently. Hence, air cooling is less favourable option in many cases. Many active cooling systems work in tandem with passive cooling elements to function more effectively. Therefore, the choice of the cooling approach and medium is highly dependent on the PV system design requirements and the conditions at which the system operates.

2.3 Waste Heat Recovery

Waste heat refers to energy that is generated in industrial processes without being put to practical use. Energy recovery comprises of practical means of minimizing the input of energy to an overall system by the exchange of energy from one sub-system of the overall system with another (Al-Hawaj, 2011). Mostly appearing as thermal energy exchange in either sensible or latent heat forms. Heat recovery from waste presents an ever-increasing opportunity for

economical operation of thermal systems. The selection of the mode of heat recovery depends on the characteristics of the application, the processes applied within a system, and the economic need for a given application (Boyen, 1980). Sources of waste heat include hot combustion gases discharged to the atmosphere, industrial thermal waste, and heat transfer from hot surfaces. It has been estimated an industrial waste heat as much as 20-50% of the industrial energy consumption (US Department of Energy, 2009).

Solar photovoltaic systems in operation experience great deal of thermal energy that is inseparable from the photo-electric conversion process. The challenges solar heat present on the performance of PV modules inspired ideas of various technique for thermal management, particularly realised in solar hybrid systems. Thermal energy recovery within PV systems is twofold, serving as cooling mean to the PV module and thus improving its electrical performance as well as collecting the thermal energy by-product, permitting its use in various applications. Hybrid collectors can serve as electrical generators and aid either water or space heating. Alternatively, the thermal energy can be harnessed in a thermo-electric conversion processes when electrical energy is of higher demand.

As practical operating conditions in regions of elevated levels of solar radiation are considered harsh for commercially available technologies, a practical solution for efficient operation is demanded. A thorough review of the literature has been conducted assessing different techniques applied to achieve thermal management for PV systems in an attempt to further enhance their power generation capabilities. Techniques vary from the methods heat is extracted by to the product of the thermal heat recovery. The following chapter highlights the main techniques applied within hybrid solar PV collectors, assessing their cooling capabilities and conversion efficiencies, reliability, and aspects of collector's design. The work presented in the following chapter is part of article "*Advancements in hybrid photovoltaic systems for enhanced solar cells performance*" published in Renewable & Sustainable Energy Reviews Journal.

2.4 Technologies Considered

The decision on the technologies incorporated is based on the potential a technology can offer to both existing and future emerging technologies within the PV industry. The need for a solution that can be applied to existing installations, is as important as application to state-of-the-art PV technologies.

As the primary target of PV technology is power supply, it is more desirable to use the thermal energy by-product to generate supplemental electricity. For that purpose, thermoelectric generators are very attractive being able to convert the difference in temperature to electricity. Few researchers have investigated the integration of TEG modules with PV technology, however, mostly have adopted a small scale impractical approach, either by attaching a TEG module to a single PV cell, or populating the rear of a PV module to cover the whole surface with TEG devices, solving one part of the problem while introducing other challenges.

The integration of heat pipes and thermoelectric generators have been widely investigated by automotive industry leaders. The integration of these technologies in such industry reflects the potential gain as seen in the development and commercialization of hybrid and electric cars. The technologies adopted reflect their reliability; operating in such environments in addition to flexibility they provide over the design. The use of heat pipes and TEGs allow for heat transfer and power production without introducing extra moving parts. In addition, the use of heat pipes promotes more flexible designs where the location of the TEGs are not limited to the surface requiring thermal

management. In that regard, the incorporation of heat pipes and thermoelectric generation technologies for thermal management of PV cells is investigated.

2.4.1 Photovoltaic (PV) Cells

Solar PV cells are the primary element of PV systems, and mainly are semiconductor devices that can convert solar radiation into DC electricity when exposed to sunlight. Such optical cell consists of a P-N junction formed on a thin light sensitive material primarily silicon (Si) (Bag, 2009a). The P-N junction of the cell is formed by doping silicon wafer with impurities (Chaosook, 2002), hence creating two layers with different electrical properties. The physical process through which solar cells convert solar radiation into electricity is known as the *Photovoltaic Effect* (Chaosook, 2002), (Bag, 2009b), (Luque, 2010). Photons available in sunlight makes electricity generation possible using PV cells. The basic process of electricity generation when a PV cell is exposed to sunlight is shown in Fig. 3.1. As sufficient photon energy is absorbed by a PV cell, electrons migrate from the negative layer to the positive layer of the cell, resulting in potential difference across the P-N junction, and therefore, current flow to the load through an external circuit (Luque, 2010).

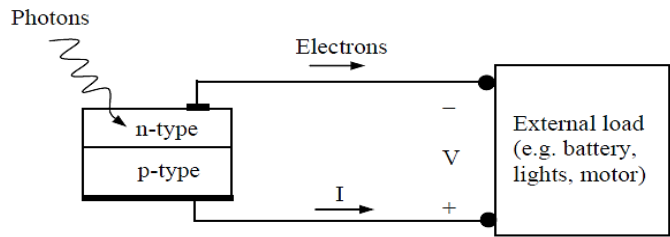


Fig. 3. 1 PV Electricity Generation Process

2.4.1.1 Efficiency

Commercially available PV cells are about 14-22% efficient in converting solar energy into electricity depending on the cell technology. Since PV technology is becoming more advanced, higher conversion efficiencies have been achieved. As by June 2016, *SunPower* holds the record for the world's most efficient rooftop solar module, achieving conversion efficiency of 24.1% (Wesoff, 2016). Table 3.1 presents some of the most efficient PV module available.

Table 3. 1 Most efficient solar PV panels available commercially (The Eco Experts, 2015)

| Manufacturer | Model | Type | Efficiency |
|--------------|-------------------|-----------------|------------|
| SunPower | X21-345 | Monocrystalline | 21.5% |
| Sanyo | HIT Double 195 | Monocrystalline | 20.5% |
| AUO | SunForte PM318B00 | Monocrystalline | 19.5% |
| Phono Solar | PS330P-24/T | Polycrystalline | 17.0% |

2.4.1.2 I-V Characteristic Curves:

The I-V characteristics of a PV cell defines the power output under variable load and atmospheric conditions. Fig. 3.2 shows the characteristics of a cell under various testing conditions (Duran et al., 2009). The characteristic play key role in PV system designs in which they define the parameters of a cell such as, short circuit current (I_{sc}), open circuit voltage (V_{oc}), maximum power point (P_{max}), and fill factor (FF) (Enrique et al., 2005).

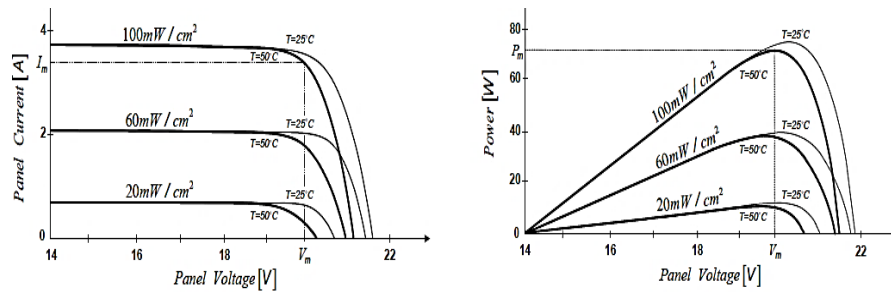


Fig. 3. 2 I-V and P-V characteristic curves of PV cell under various operating conditions

The P-V characteristics show that there is a point on the P-V curves at which the PV cell produces maximum output power as a result of irradiance interception. Typical experimental procedures applied to obtain IV curves consist of connecting the cell to variable load and measuring the voltage and current output. Alternatively, DC-DC converters with variable duty cycle is used, in which power loss of the systems operating in active zone is minimized (Enrique et al., 2005).

2.4.2 Thermoelectric Generators (TEGs)

Thermoelectric converters are solid-state semiconductor devices that can convert thermal energy directly into electricity or vice versa. Thermoelectric devices are categorized into two types of converters depending on the energy conversion process; Thermoelectric Generators (TEGs), and Thermoelectric Coolers (TECs). Thermoelectric generators have immense potential for waste heat recovery from power plants, automobile vehicles, and solar energy applications as discussed earlier (McEnaney et al., 2011), (Kraemer et al., 2012), (El-Genk and Saber, 2002). BMW and Ford are two of the automobiles companies who implemented waste heat recovery systems in their vehicles by integrating TEGs in the exhaust system of the vehicles. The results of the TEG integration design by BMW using single layer TEG showed fuel economy increase of 1-7% achieved through waste heat recovery of exhaust for temperature difference across TEG plates in the range of 220-820 °C (Liebl et al., 2009). In addition, such devices provide reliable power in remote areas such as is space and mountain top telecommunication sites using a phenomenon called the *Seebeck Effect*. One of the most common fields in which TEG devices are applied in is the oil and gas industry, where these devices are used to power

remote telemetry units, gas analyzers and metering equipment as well as for routine operating functions and emergency shutdown (kreazone, 2012). The minimal maintenance requirement of TEGs is a distinct advantage as site visits can be reduced to coincide with the annual preventive maintenance cycle of the telecom equipment powering in remote areas. Therefore, TEG device have proven to be the most reliable power source available for the rugged demands of the industry and various scale applications. Fig. 3.3 shows application of TEG devices in different scales.



Fig. 3. 3 Waste heat recovery in vehicle (left) and TEG devices powering communications and cathodic protection of gas pipeline, India (right)

On the other hand, thermoelectric coolers have been widely used in electronic devices and medical instruments as they can provide refrigeration and temperature control for such devices allowing them to operate at a certain temperature level utilizing the *Peltier Effect*. The use of thermoelectric

generators (TEGs) for the thermal management design proposed for PV systems is considered in this research.

2.4.2.1 Theory of Thermoelectric Conversion:

The direct conversion of temperature difference into electricity can be explained by the *Seebeck Effect*, which states that a voltage is induced when a temperature gradient is applied to the junctions of two differing materials (MacDonald, 2006). Fig. 3.4 illustrates this concept in a thermocouple, the materials are n-type and p-type semiconductor materials, the junctions are the substrate for the thermoelectric module, T_H represents the absorber temperature, T_L represents the heat sink temperature, and the voltage difference is measured across a load or open circuit. The induced voltage is proportional to ΔT by the difference in the Seebeck coefficients of the two materials. The Seebeck coefficients are considered to be material properties and are assumed to be constant at all temperatures.

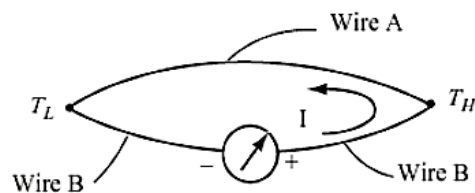


Fig. 3. 4 Schematic of basic thermocouple (Lee, 2010).

Similarly, the Peltier Effect describes the inverse of this behavior – when an electrical current is passed through the junction of two differing materials, heat is either lost or absorbed at the junction according to the direction of the current (MacDonald, 2006). The Peltier coefficient demonstrates the proportionality between the heat flowing from a material due to a current and the current itself; this is illustrated in Fig. 3.5. Both the *Seebeck* and *Peltier Effects* are functions of material state, but these effects are only seen when two differing materials are connected. Additionally, these effects are distinct from Joule heating, which is present in any semiconductor with a current flowing through it (MacDonald, 2006). Further details on the physics of thermoelectric converters are available in (MacDonald, 2006), (Lee, 2010).

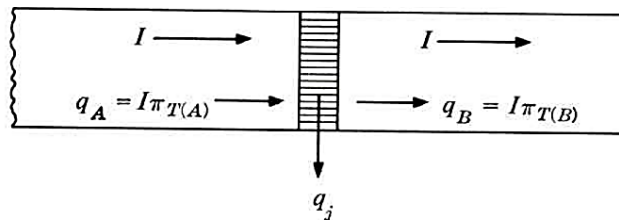


Fig. 3. 5 Current flow through dissimilar materials (Lee, 2010)

2.4.2.2 Thermoelectric Modules

In a typical thermoelectric module, alternating n-type and p-type thermoelectric elements are connected by substrates, electrically in series and thermally in parallel, Fig. 3.6. Heat is absorbed at the top substrate and flows through the thermoelectric elements; it is then rejected at the cold substrate. Loads can be attached to the module's external electrical connection (Angrist, 1982).

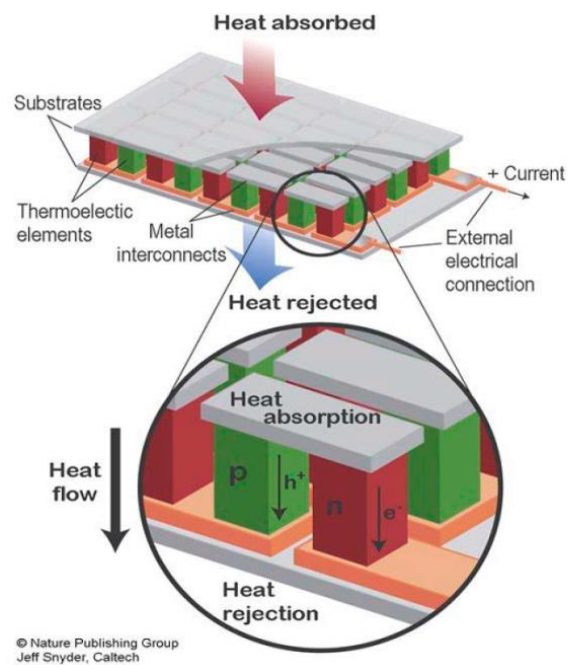


Fig. 3. 6 Thermocouple in thermoelectric module (California Inst. of Tech., 2013)

2.4.3 Heat Pipes

Heat pipes are passive heat transfer devices of high thermal conductance utilizing an efficient boiling-condensing process to transfer thermal energy by two-phase circulation of fluid. The heat transfer capability of heat pipes ranges from one hundred to several thousand times that of an equivalent piece of copper due to its two-phase heat transfer mechanism (Dunn, Reay, 1994). Hence, making heat pipes optimum solution in many cooling related applications as seen in electronic industry. Heat pipes are also often referred to as superconductors of heat as they possess enhanced heat transfer capacity and rate with almost no heat loss (Reay, Kew, and McGlen, 2006). The basic idea of heat pipes is based on an evaporation and condensation processes, whereas a working fluid goes through evaporation (hot side), while condensation of the working fluid releasing the thermal energy takes place at the condenser section.

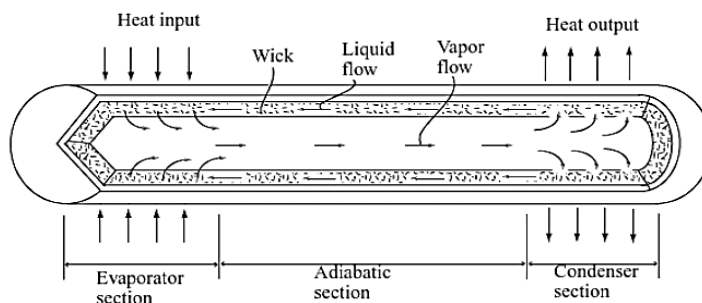


Fig. 3. 7 Cutaway view of heat pipe (Lee, 2010)

2.4.3.1 Heat Pipes Structure and Operation

Heat pipes comprise of a sealed tubular container with a wick structure lined on the inner surface and small amount of fluid such as water at the saturated state, Fig. 3.7. The pipe consists of three main regions, the evaporator section, condenser section, and adiabatic section in between. At the evaporator section, heat is absorbed causing the working fluid to vaporize and flow towards the condenser section through the core of the heat pipe. The vapor is then condensed at the condenser section and heat is rejected to the environment while the liquid phase of working fluid returns to the evaporator section through the wick of the heat pipe. The adiabatic section in between, is where the vapor and liquid phases of the fluid flow in opposite directions to complete the cycle. Therefore, the operation of a heat pipe is mainly based on the thermodynamic properties of the working fluid.

2.4.3.2 Heat Transport Limitations of Heat Pipes

The most important heat pipe design consideration is the amount of power the heat pipe is capable of transferring. The maximum heat transport capacity for a heat pipe is governed by five different limits which are function of the heat

pipe operating temperature i.e., the sonic limit, the entrainment limit, the boiling limit, the viscous limit, and the capillary limit, Fig. 3.8 (Lee, 2010), (Reay, Kew, and McGlen, 2006). If heat pipes are driven beyond its capacity, the effective thermal conductivity of the heat pipe will be significantly reduced.

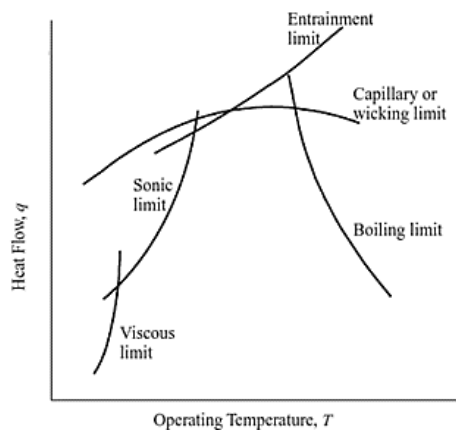


Fig. 3. 8 Schematic of limits on heat pipe performance (Lee, 2010)

The five heat transport limitations can be simplified as follow:

- I. Sonic limit - the rate that vapors travels from evaporator to condenser.
- II. Entrainment limit - Friction between working fluid and vapor that travel in opposite directions.
- III. Capillary limit - the rate at which the working fluid travels from condenser to evaporator through the wick.
- IV. Boiling limit - the rate at which the working fluid vaporizes from the added heat.
- V. Viscous limit - at low temperatures the vapor pressure difference between the condenser and the evaporator may not be enough to overcome viscous forces.

2.4.3.3 Wick Structure of Heat Pipes

The wick structure in a heat pipe facilitates liquid return from the evaporator from the condenser. The main purposes of wicks are to generate the capillary pressure, and to distribute the liquid around the evaporator section of heat pipe. The commonly used wick structure is a wrapped screen wick; however, other designs are available to meet certain requirements and applications. Each wick structure has its advantages and disadvantages and every wick structure has its own capillary limit. Fig. 3.9 shows common wick structures used in commercially produced heat pipes.

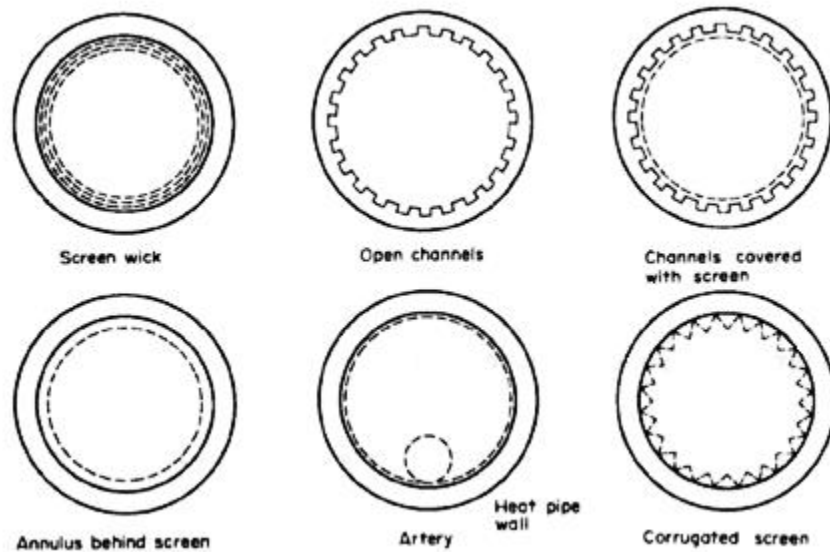


Fig. 3. 9 Wick section structures of heat pipes (Lee, 2010)

2.4.3.4 Working Fluid

Different working fluid options are available for heat pipes to suit different temperature requirements. In heat pipe design, a high value of surface tension is desirable in order to enable the heat pipe to operate against gravity and to generate a high capillary driving force. In addition to high surface tension, it is necessary for the working fluid to wet the wick and the container material, i.e. contact angle should be zero or very small. The vapor pressure over the operating temperature range must be sufficiently great to avoid high vapor velocities, which tend to setup large temperature gradients and cause flow instabilities. Table 3.2 lists few of the common working fluids used in heat pipes.

The prime requirements of the working fluid in heat pipes design are:

- a. Compatibility with wick and wall materials
- b. Good thermal stability
- c. Wettability of wick and wall materials
- d. High latent heat
- e. High thermal conductivity
- f. Low liquid and vapor viscosities
- g. High surface tension

Table 3. 2 Working fluid options for heat pipes and useful temperature range (Byon, 2016)

| Range | Name | Temp(°C) | Pressure(bar) |
|------------------|-------------|-----------|---------------|
| Cryogenic | Helium | -271:-268 | 0.06:2.29 |
| | Nitrogen | -203:-150 | 0.48:28.8 |
| Low | Ammonia | -60:120 | 0.27:90.44 |
| | Water | -20:200 | 0.02:16.19 |
| | Ethanol | -30:130 | 0.01:4.30 |
| | Acetone | -40:140 | 0.01:10.49 |
| Medium | Naphthalene | 100:400 | 0.02:17.5 |
| | Mercury | 150:750 | 0.01:63 |
| High | Sodium | 500:1300 | 0.01:15.91 |
| | Caesium | 375:825 | 0.02:3.41 |
| | Lithium | 1030:1730 | 0.07:8.90 |

Chapter 3

Advancements in Hybrid Photovoltaic Collectors

The thermal energy accumulating on PV cells due to continuous illumination of solar energy can be utilized in hybrid system designs instead of simply dissipating it to the environment. Hybrid Photovoltaic-Thermal (PVT) systems offer a practical solution to increase the electrical power production from PV panels in addition to the recovery of the heat extracted from the panels (Kern and Russell, 1978), (Zondag, Vries, and Van Steenhoven, 1999), (Zhang et al., 2012). Waste heat recovery permits the utilization of waste heat to supply space or water heating in a way allowing improved overall system efficiencies to as high as 70% to be achievable (Zhang et al., 2012). However, with most systems there are often instances where the heat can never be put to practical use, and so the overall efficiency of the system is usually lower. Furthermore, since the primary target of PV technology is electrical supply, it may be more desirable to use the thermal energy by-product to generate supplemental electricity.

A comprehensive discussion on Hybrid PVT modules is presented in the next section with diverse designs proposed in the literature in an effort to achieve optimum operating conditions and improved system efficiencies. In order to increase the electrical efficiency of PV cells and make good use of the incident solar radiation, it is most desired to remove the accumulated heat from the concealed PV surface and recover this heat appropriately. Hybrid PVT collectors are able to do so by simultaneously converting solar radiation available from the sun into electricity while permitting thermal energy recovery.

3.1 Hybrid PV–Thermal Collectors

The concept of PVT collectors was initially addressed by Kern and Russell (1978). For a PVT module, the solar irradiation of wavelength between 0.6-0.7 μm is absorbed by the PV cells and converted into electricity, while the remaining irradiation is dissipated as heat. Consequently, PVT modules could collect and convert higher fraction of the solar energy absorbed than neither individual PV panel nor thermal collector does for an equal absorber area (Zondag, Vries, and Van Steenhoven, 1999),(Zhao et al., 2011), and therefore, offers a potential for creating low cost and highly efficient solution for heat and power generation. PVT systems are classified into

distinct categories depending on the structure or functionality of the designs. In terms of heat extraction technique employed, PVT modules can be classified as *Air*, *Liquid*, *Heat Pipe*, *Phase Change Materials (PCMs)*, and *Thermoelectric* -based types, Fig. 3.1 The integration of thermoelectric generators with PV systems allows utilizing the heat by-product from the PV module to generate supplemental electricity, hence improving the power generation of the system. While, other hybrid PV configurations offer both electricity generation and thermal energy capture simultaneously. In terms of the system structure, the modules could be classified as flat-plate, concentrated, and building integrated (BIPV) types. A comprehensive review of various methods employed for thermal regulation of PV cells along with assorted hybrid PVT designs are deliberated in this chapter.

3.1.1 Air-based PVT Collectors

Air-based PVT collectors are fabricated by incorporating air channels often present at the rear of a PV laminate allowing naturally or forced ventilated air to flow and extract accumulated heat through convective heat transfer. The use of forced air enhances heat extraction resulting in further improved performance of the PV cells when compared with naturally ventilated ones (ROYNE, DEY, and MILLS, 2005).



Fig. 3. 10 Classification of PVT modules based on heat extraction mechanism

Nevertheless, parasitic power losses are introduced due to the use of air blowers, hence affecting the net electrical output. Several design concepts have been illustrated and investigated with respect to air flow patterns in addition to the presence of front glazing to achieve optimum performance of PV modules, Fig. 3.2. Owing to minimal use of material and low operating costs among other PV cooling technologies, ventilated PVT and PV façade systems have found broad range of applications in which warm air is required for space heating, agriculture/herb drying, as well as electricity generation (Zhang et al., 2012), (Janjai and Tung, 2005). However, due to low density and small heat capacity of air, improvements in the practical

performance of air-based PVT collectors are limited, making air thermal management techniques less favourable option in certain situations. Nonetheless, such designs are attractive in situations where water is limited. In the following section a review on the recent advancements as well the limitations of ventilated PVT and PV façade systems are presented.

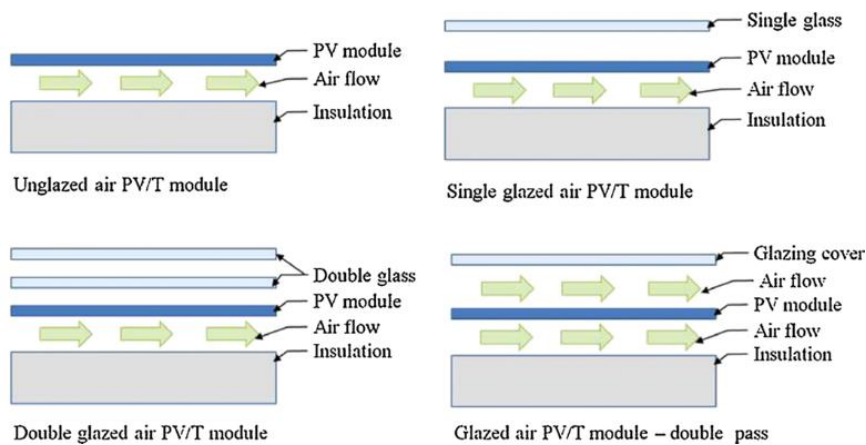


Fig. 3. 11 Different designs of air-based PVT collectors (Zhang et al., 2012)

Dubey et al. (2009) studied analytically and experimentally different configurations of PV modules under typical New Delhi climatic condition, Fig. 3.3. Four different configurations were investigated, namely, (1) glass-to-glass PV module with duct, (2) glass-to-glass PV module without duct, (3) glass-to-tedlar PV module with duct, and (4) glass-to-tedlar PV module without duct. Higher electrical efficiency and outlet temperature were achieved with the glass-to-glass PV module type with duct compared to the glass-to-tedlar type PV module with duct owing to radiation being

transmitted through the back glass. Meanwhile, in the case of glass-to-tedlar the radiation is absorbed by the tedlar layer and conducted away resulting in higher cell temperature, Fig. 3.4. The theoretical models were experimentally validated and good agreement was observed. Improvement of 6.6% in the annual average efficiency was reported with the glass-to-glass type PV module with duct.

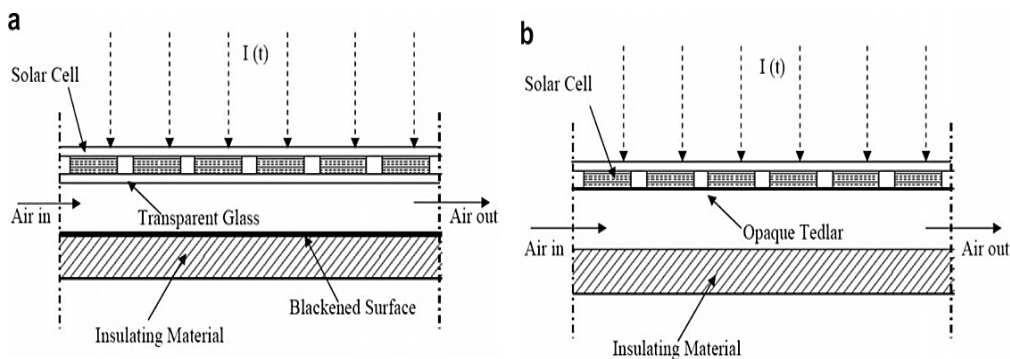


Fig. 3.12 (a) Glass-to-glass module with duct, (b) Glass-to-tedlar module with duct Dubey et al. (2009)

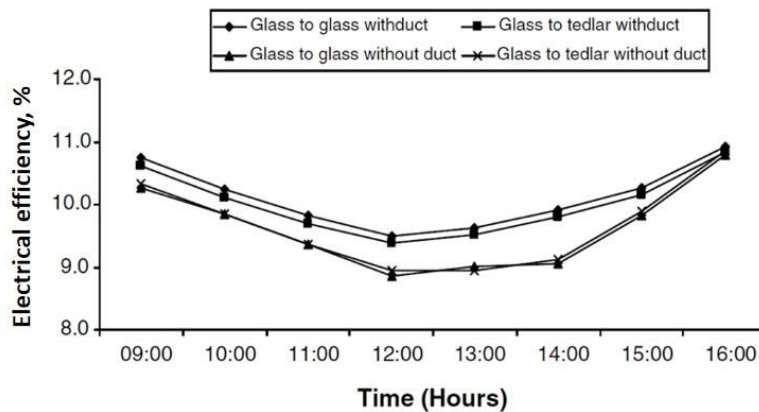


Fig. 3.13 Electrical efficiency of PV cells for collectors investigated in Dubey et al. (2009)

Numerical models of two low cost modification techniques to enhance heat transfer in air-based PVT collectors through natural ventilation were

considered by Tonui and Tripanagnostopoulos (2008). The modifications consisted of a thin metal sheet suspended at the middle of the air channel (TMS), and a finned metal sheet at the back wall of the air duct (FIN), Fig. 3.5. The models were validated against the experimental data for both glazed and unglazed PVT collectors using a commercial poly-crystalline silicon (pc-Si) PV module rated at 46Wp, with an aperture area of 0.4 m² having a rectangular air duct channel of 0.15 m depth. Good agreement between predicted values and measured data was observed. The effect of channel depth on the PV temperature was studied and results showed an optimum channel depth at which the PV module temperature was least, Fig. 3.6. Results showed that at a channel depth of 0.15 m, the unglazed TMS and FIN systems achieved reduced PV module temperature of about 3°C compared to the reference system, which contributes to about 1–2% improvement the electrical efficiency. It was concluded that such modifications are suitable for building integration and can be applied in solar chimneys for natural ventilation of buildings.

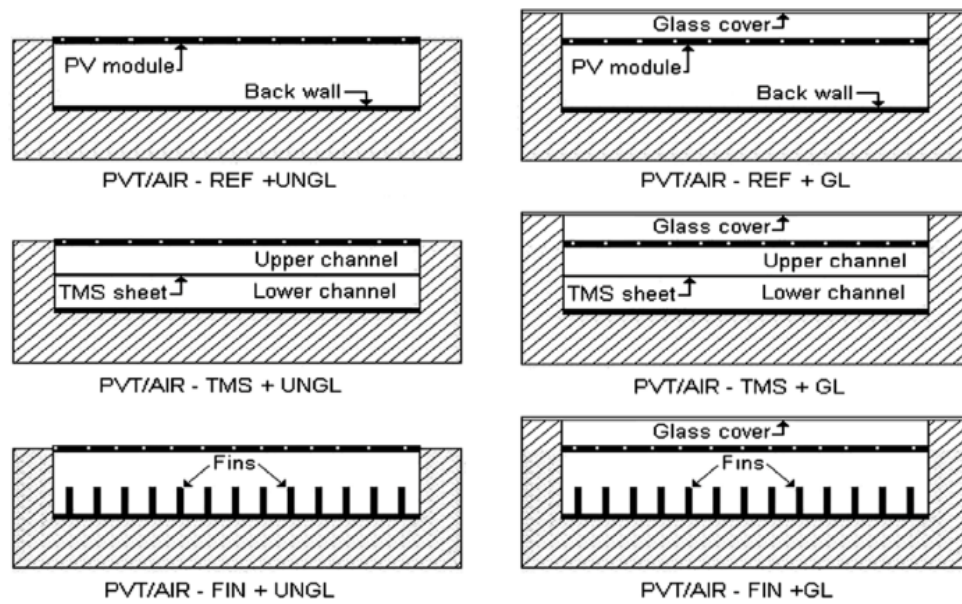


Fig. 3. 14 Air-based PVT collectors with thin metal sheet and finned metal sheet Tonui and Tripanagnostopoulos (2008)

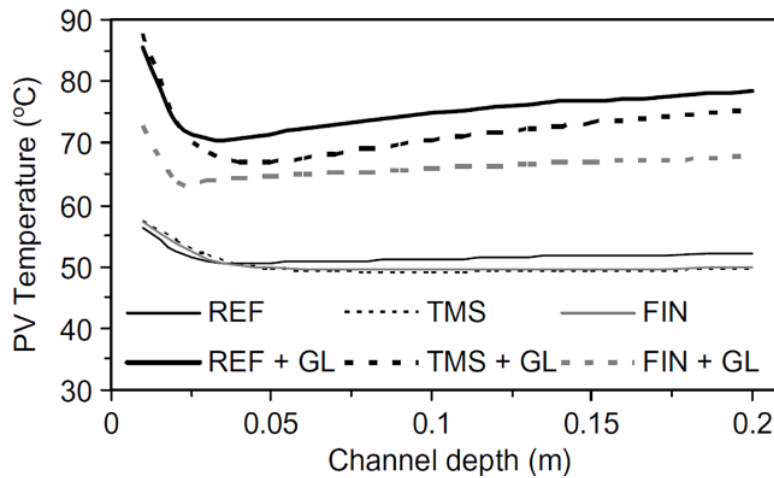


Fig. 3. 15 PV surface temperature as function of air duct depth Tonui and Tripanagnostopoulos (2008)

The performance of a PVT air solar heater was studied analytically and experimentally considering various design parameters under controlled indoor conditions by Solanki, Dubey, and Tiwari, (2009). The prototype

consisted of three modules of mono-crystalline silicon (mc-Si) solar cells, each rated at 75Wp and have dimensions of 0.45x1.2m² mounted on a wooden duct allowing inlet and outlet air to pass below the PV modules to extract thermal energy from the back surface of the modules. The effect of the mass flow rate on the electrical, thermal, and overall efficiency at solar radiation intensity of 600W/m² and inlet air temperature of 38°C is shown in Fig. 3.7. It was concluded that enhanced performance of PV cells can be achieved through air cooling in which temperature drop of about 10°C at the PV cell level was achieved, Fig. 3.8. The reported electrical, thermal, and overall efficiency were 8.4%, 42%, and 50%, respectively.

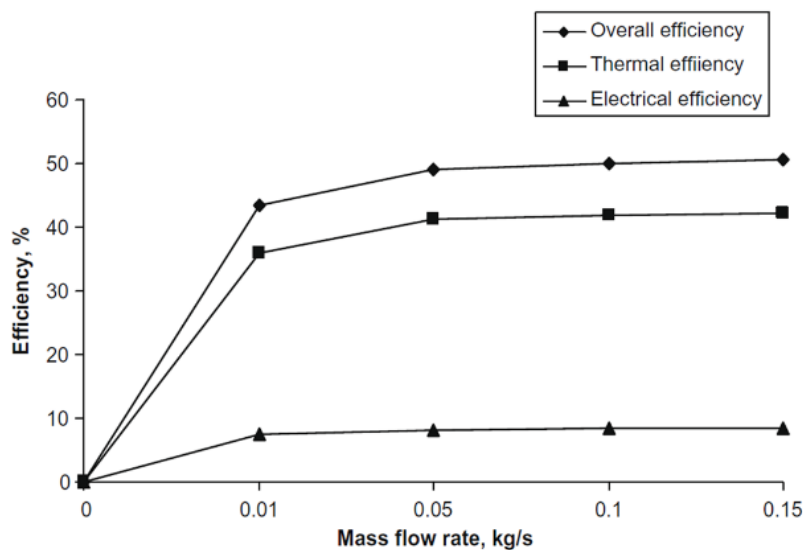


Fig. 3. 16 Electrical efficiency variation with mass flow rate (Solanki, Dubey, and Tiwari, 2009)

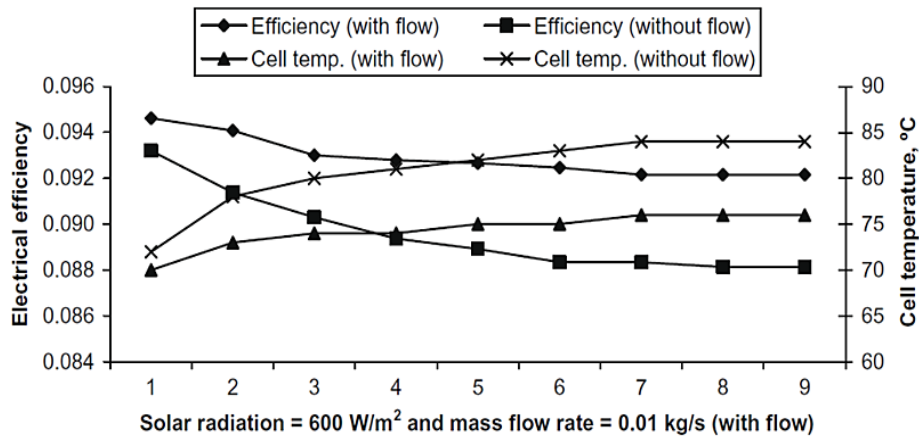


Fig. 3. 17 Variation of electrical efficiency and cell temperature (Solanki, Dubey, and Tiwari, 2009)

Bambrook and Sproul (2012) investigated experimentally the enhancements of both electrical and thermal energy of a PVT collector using air as a heat extraction medium. The cooling system comprised of an open loop single pass duct using extraction fan capable of producing high air mass flow rates (0.02-0.1 kg/s/m²) at low input power (4-85W), Fig. 3.9. Enhanced electrical power in excess of the fan requirements was reported for air mass flow rates ranging between 0.02 and 0.08 kg/s/m², with thermal efficiencies in the range of 28–55% and electrical PV efficiencies between 10.6% and 12.2% at mid-day, Fig. 3.10. The system performance was also compared with the energy requirement of the fan for a range of air mass flow rates. It was concluded that, the low grade thermal energy output makes such system suitable for residential thermal management applications.

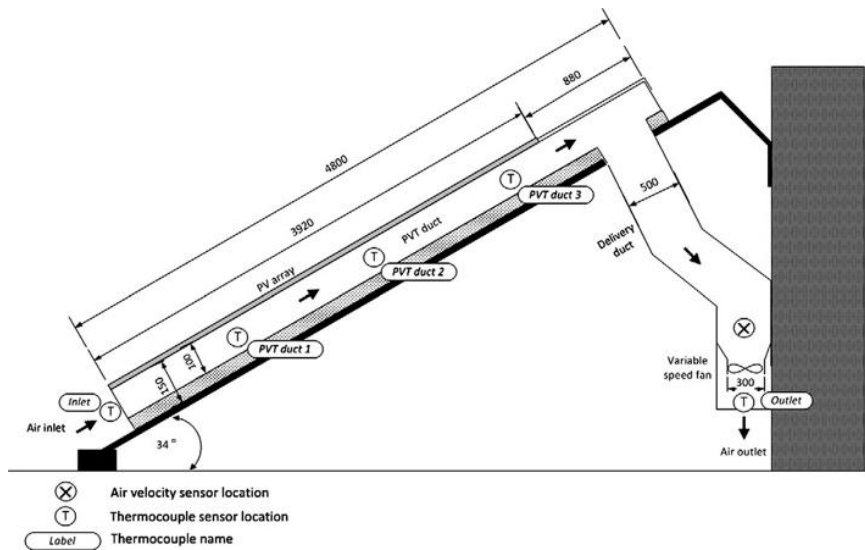


Fig. 3. 18 Air-based PVT with open loop single pass duct Bambrook and Sproul (2012)

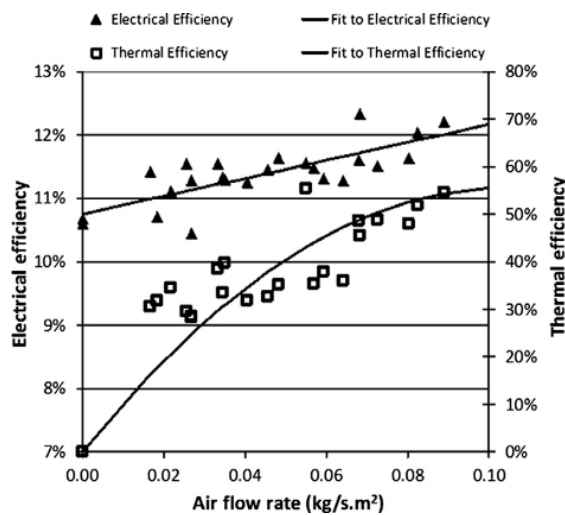


Fig. 13 Electrical and thermal efficiency variation of PVT with open loop single duct Bambrook and Sproul (2012)

Amori and Al-Najjar (2012) investigated theoretically the performance of a hybrid PVT air collector for two different case studies under Iraqi climatic conditions. Improved thermo-electrical mathematical model of the PVT air collector considering the effect of radiative heat transfer in the air duct, and

the convective heat transfer coefficient from both the PV module rear and inner surface of insulation to the working fluid were accounted for. The effective sky temperature correlation for relative humidity was also adopted in the model. Modified boundary conditions for better convergence and accuracy of the electrical model were also considered. The model presented was validated against previously published experimental results and theoretical simulations of similar designs by Joshi et al. (2009) and (Garg and Adhikari, 1997). A better alternative amongst the existing models was observed in Amori and Al-Najjar's design. The electrical and thermal efficiencies for the two cases considered were 12.3% and 19.4% for the winter day, while that for the summer day were 9% and 22.8% respectively. Although the output power in the summer was observed to be higher than that of winter season (1.7 times at solar noon), the efficiency recorded in winter was higher due to the negative temperature coefficient of efficiency and higher fill factor.

Recently Amori and Abd-ALRaheem (2014) carried out a quantitative comparative study on different conceptual hybrid PVT collectors for Iraq climate conditions. Four air-based PVT collectors were adopted in experimental work, namely; (I) PV modules without cooling, (II) Hybrid PVT collector with single duct double pass, (III) Hybrid PVT collector with double duct single pass, (IV) Hybrid PVT collector with single duct single pass. A DC

fan of power of (6W) at the ducts' outlet was installed to pull air. A mathematical expression of the PVT collector model IV was also developed based on energy balance to analyse the thermal and hydraulic performances of the model. Model IV attained better electrical performance compared to model II and III, while the overall efficiency of model III was higher compared to model II and model IV due better heat extraction. Measurements also showed that optical losses were introduced due to presence of glass cover in models II and III as the electrical efficiency deviated before and after solar noon when compared to model I, which agrees with the findings in Shahsavari and Ameri (2010).

Yun et al. (2007) investigated a ventilated PV façade system considering building characteristics and façade configuration for both preheating during winter and natural ventilation in summer, in addition to cooling of PV modules. The system incorporated transparent windows, opaque PV panels with air gap and concrete composite wall, and air dampers, Fig. 3.10. The researchers introduced the effectiveness of a PV façade (PVEF) parameter to evaluate the building performance in terms of heat transmission, ventilation, and daylight, in addition to the electrical efficiency of the PV modules. Results for the hottest recorded day exhibited an approximate improvement of 15% of PV module efficiency through the ventilated system when compared with that without ventilation, Fig. 3.11.

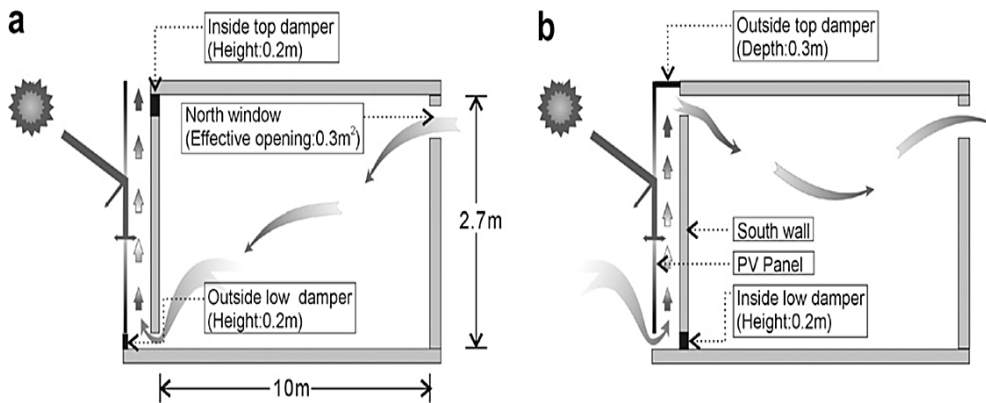


Fig. 3. 19 Ventilated PV façade system (a) summer, (b) winter Yun et al. (2007)

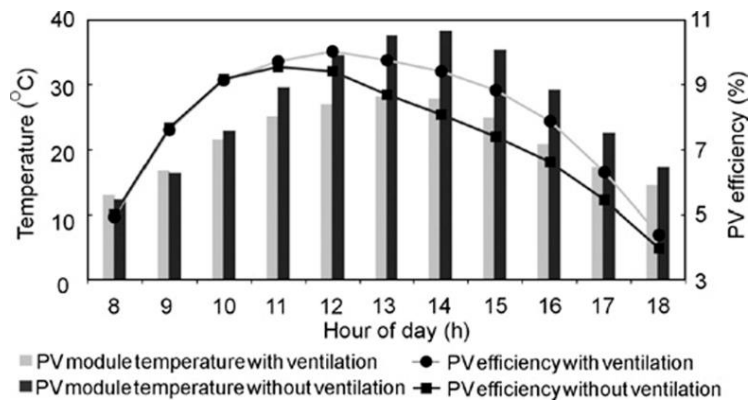


Fig. 3. 20 PV efficiency and module temperature of ventilated PV façade Yun et al. (2007)

Sukamongkol et al. (2010) studied the dynamic performance of condenser heat recovery with air PVT collector for desiccant regeneration to reduce energy consumption of air conditioning for a room in tropical climates. The system comprised of a living space, desiccant dehumidification and regeneration unit, air conditioning system, PVT collector, and air mixing unit. Warm dry air of 53°C and 23% relative humidity were reported in this investigation. In addition, energy saving in air conditioning of about 18% was

reported through such integration. However, electrical efficiency of only 6% of the daily total solar radiation was recorded.

Temperature prediction of a multi-junction solar cell based on passive cooling was performed through theoretical thermal modelling by Min et al. (2009). A linear relationship between the heat sink area and the concentration ratio was observed in order to maintain acceptable cell temperature. More recently, active air cooling of concentrator multi-junction solar cells by convection and surface radiation was studied theoretically by Al-Amri and Mallick (2013). In their study, a triple-junction GaInP/GaAs/Ge solar cell with a Cu-Ag-Hg front contact was considered where air was forced within ducts underneath aluminium base plate. Noticeable effect of surface radiation on the temperature of the PV cell was observed which agreed with the findings of a study conducted by Moshfegh and Sandberg (1998). Analysis also revealed that increasing the emissivity of the duct walls promoted the effect of the surface radiation. Simulation results under concentration ratio of 100x predicted a drop in solar cell temperature from 240°C to 150°C as the emissivity was increased from 0 to 0.98. The effect of thermal conductivities of solar cell holders and accessories in addition to air inlet velocity, channel width, and thicknesses were also examined and found to have profound influence on the maximum cell temperature and critical concentration ratio.

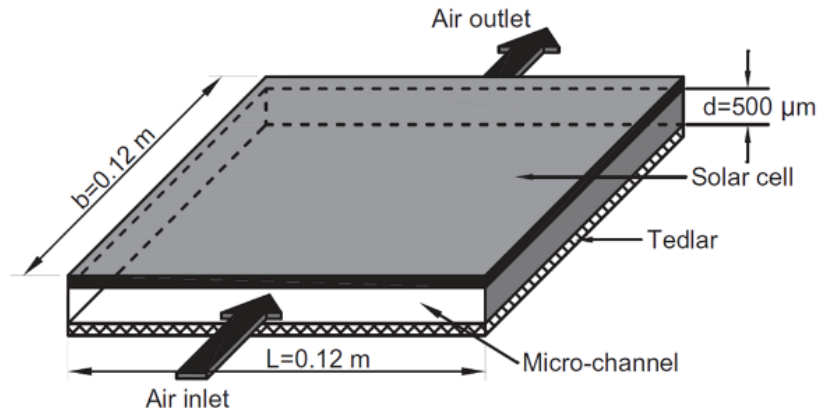


Fig. 3. 21 Micro-channel solar cell thermal (MCSCT) tile (Agrawal and Tiwari, 2011)

Utilizing micro-channels, Agrawal and Tiwari (2011) presented the concept of series and parallel air flow arrangement of micro-channel solar cell thermal tiles. The system comprised of air channels of depth 500mm made between a 0.0144m^2 cell and tedlar allowing for the thermal resistance of tedlar to be eliminated, Fig. 3.12. Nine rows of four series-connected micro-channel solar cell thermal (MCSCT) tiles were connected in parallel to form a micro-channel PVT (MCPVT) module. Performance of the MCPVT in terms of overall energy, exergy and exergy efficiency was compared with that of single channel PVT module studied by Dubey et al. (2009) with same (micro depth) flow rate. Results revealed that the MCPVT module achieved higher overall exergy efficiency, Fig. 3.13. Agrawal and Tiwari extended their study to validate their aforementioned MCPVT module, in addition to other MCPVT module configurations being investigated (Agrawal and Tiwari, 2011).

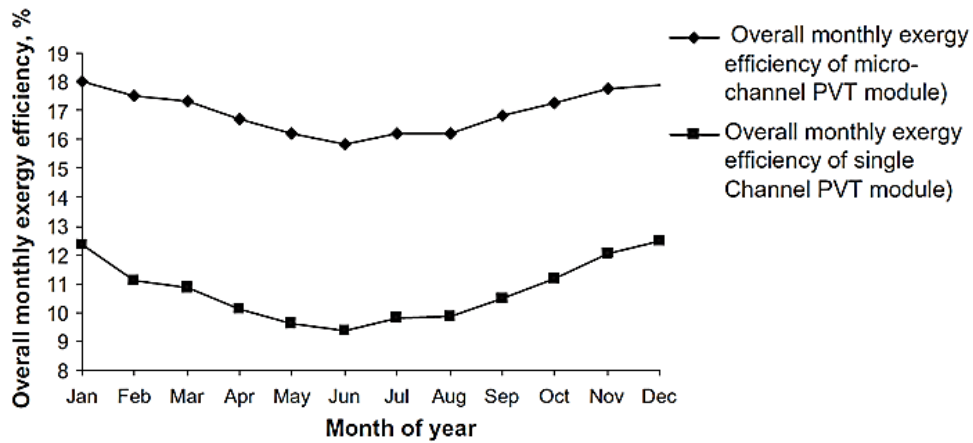


Fig. 3. 22 Exergy efficiency utilising micro-channel solar cell thermal tile with air cooling Agrawal and Tiwari (2011)

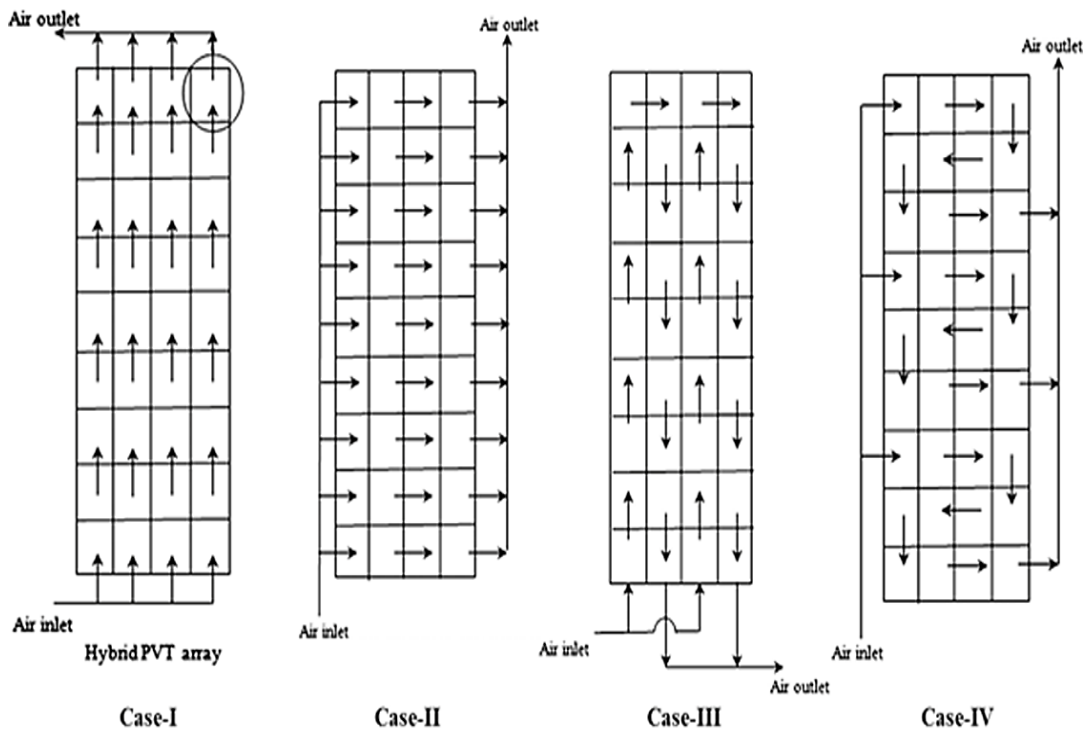


Fig. 3. 23 Series and parallel arrangement of ventilated micro-channel solar cell tiles (Agrawal and Tiwari, 2011) (Rajoria, Agrawal, and Tiwari, 2012)

Theoretical analysis and optimization were carried out by Rajoria et al. (2012) adopting the designs proposed in (Agrawal and Tiwari, 2011), Fig. 3.14. Due to low value of bottom and side losses, case-II achieved the highest value of overall thermal energy among other arrays. Nevertheless, higher grade of energy was achieved through the configuration in case-III with average electrical efficiency of 11.3% resulting in further 12.9% improvement in overall exergy efficiency than that of case-II. Owing to increased number of PVT module connected in series, case-III achieved the highest outlet air temperature.

In a recent study by Rajoria et al. (2013) utilizing the same concept, the flow arrangement was modified such that air was passed under two parallel-connected columns of 18 modules each having 36 series-connected PVT tiles. Results were compared with array in case-III in (Rajoria et al. 2012), and the innovative design was observed to be more efficient. Further improvements in electrical efficiency, outlet air temperature, and annual overall exergy efficiency of 6.5%, 18.1%, and 10.4% respectively were observed compared to that of case-III under the same climatic conditions. The study was extended to investigate the CO₂ mitigation and environmental cost utilizing exergoeconomic analysis to reflect the financial gain/savings that can be obtained for four different cities in India. On a similar study, carbon credit analysis for different air-based PVT arrays was conducted,

enabling price comparison between systems in respect to CO_2 emissions for the Indian city (Agrawal and Tiwari, 2013).

Three heat exchanger designs, namely, V-groove, honeycomb and stainless-steel wool incorporated at the rear of PV module were investigated experimentally (Othman, 2013), Fig. 3.15. Under irradiance of $830\text{W}/\text{m}^2$ and mass flow rate of $0.11\text{ kg}/\text{s}$ PVT module with honeycomb heat exchanger achieved better performance with reported thermal and electrical efficiencies of 87% and 7.13% respectively. This was attributed due to larger surface area in direct contact with the PV module in addition to the uniform air flow resulting in enhanced heat transfer from the PV module to flowing air.

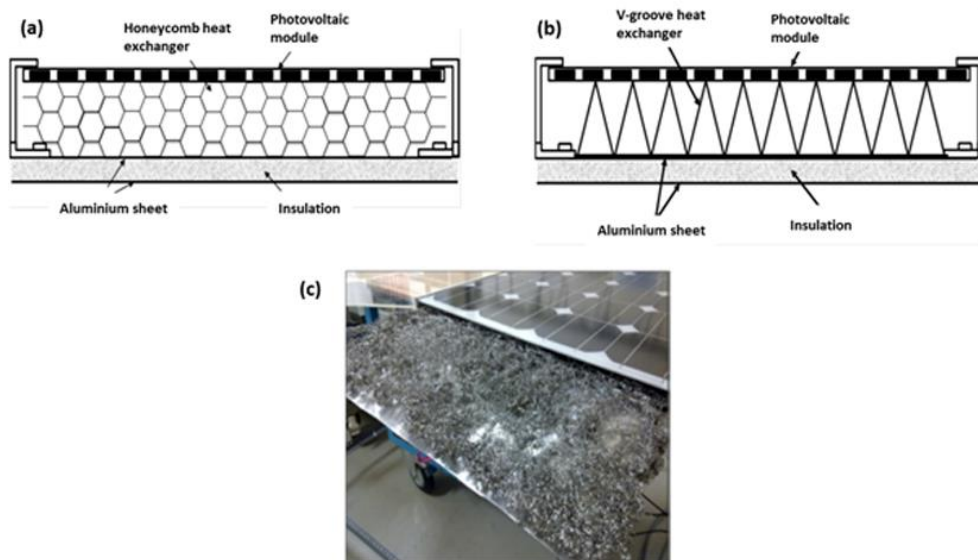


Fig. 3. 24 PV modules with different heat exchanger designs (a) Honeycomb, (b) V-groove, (c) stainless steel wool (Othman, 2013)

Air PVT and ventilated PV façade systems have found broad range of applications offering a simple mechanism to cool PV cells and low grade thermal energy for space heating in residential applications. Nevertheless, the low density and small heat capacity of air limits the improvements in the performance of air PVT collectors, hence making air less favourable option. At high operating temperature conditions, air cooling fails to accommodate for the temperature rise at the surface of PV cells causing critical drop in their conversion efficiency.

3.1.2 Liquid-based PVT collectors

Liquid cooling offers a better alternative to air cooling utilizing coolant as heat extraction medium to maintain desired operating temperature of PV cells and a more efficient utilization of thermal energy captured (Daghigh, Ruslan, and Sopian, 2011) (Chow, 2010) (Tyagi, Kaushik, and Tyagi, 2012). Liquid-based PVT collectors are superior to air-based collector's due to higher specific heat capacity of coolants employed, leading to further improved overall performance (Daghigh, Ruslan, and Sopian, 2011), (ROYNE, DEY, and MILLS, 2005). In addition, liquid-based PVT collectors offer less temperature fluctuations compared to air-based PVT making them more favourable (Daghigh, Ruslan, and Sopian, 2011). The most common liquid-based PVT collector design comprises of metallic sheet-and-tube absorber in

which heat extraction is attained via pumped fluid circulation through series/parallel connected pipes adhered to the rear of PV collector (Zhang et al., 2012), (Du, Darkwa, and Kokogiannakis, 2013) (Zondag et al., 2002) (de Vries, 1998). As a result, improved conversion efficiency is achieved and useful thermal energy is made available for utilization in domestic and industrial applications. Fluid circulation in such type of collectors is accomplished utilizing either gravity-assisted circulation or circulation pumps. Liquid-based PVT systems are commonly distinguished according to the working fluid employed (Bouzoukas, 2008). Water is the most common fluid employed; however, refrigerants that are able to undergo phase change at a relatively low temperature have been adopted in many systems recently (Zhao et al., 2011). In this section, a review on liquid-based PVT collector system utilizing water and other liquid refrigerants as heat extraction fluids is presented.

3.1.2.1 Water-based PVT collectors

Several water-based PVT conceptual designs having different flow patterns have been introduced and investigated both theoretically and experimentally to assess improvements associated with PV cells operating temperature, Fig. 3.16. However, the most common collector design studied consists of a PV module attached to an absorbing collector with serpentine

of a series or parallel tubes at the rear surface of PV modules (sheet-and-tube), Fig. 3.17. The PVT water collector operates such that water is forced to flow across tubes extracting the excessive heat from the PV cells, hence reducing the operating temperature of PV cells and transferring heat to be utilized for water and/or space heating. Researchers have identified several environmental and design parameters affecting the performance of such type of collectors including; mass flow rate, water inlet temperature, number of covers, absorber to fluid thermal conductance, PV cells packing factor, collector length, duct depth, and absorber plate design parameters (Amori and Taqi Al-Najjar, 2012) (Charalambous et al., 2007).

An early theoretical study on combined PVT water system was conducted by Garg and Agarwal (1995). The system comprised of a roof-mounted flat plate thermal collector with PV laminate pasted on top of an absorber plate, a storage tank, water pump for water circulation through pipes, and a control system to control on/off switching of the pump. Simulation was performed for different operating and design parameters including, PV cell areas, mass flow rates and water masses. Zondag et al. (2002) performed numerical analysis on water-based PVT collectors having different water flow patterns that were discussed by de Vries (1998). Results in terms of electrical efficiency revealed that sheet-and-tube achieved conversion efficiency of 9.7%, higher than that of PVT collectors with water channel,

free flow, or two-absorber. However, the thermal efficiency predicted of the sheet-and-tube collector was about 13–21% less than that of other designs. Huang et al. (2001) compared the performance of an integrated PVT solar system with conventional solar water heater experimentally. Polycrystalline PV cells were laminated on a thermal collector comprising of a corrugated polycarbonate panel and thermal insulation layer attached at rear to form a PVT module. Thermal efficiency of 38% was reported (about 76% of conventional solar water heater) electrical efficiency of 9%, and primary-energy saving efficiency of 60%, higher than either sole water heater or PV systems.

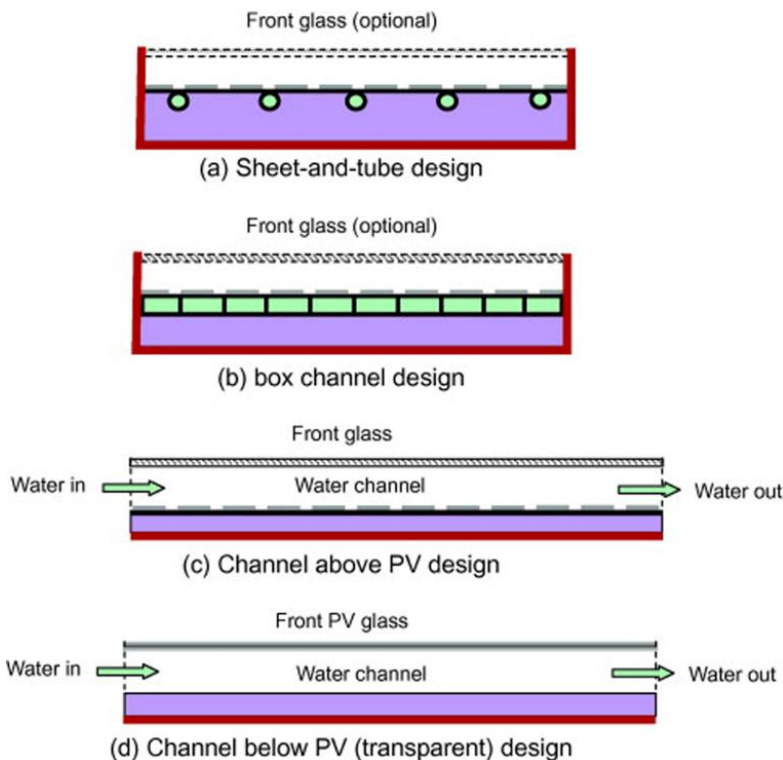


Fig. 3. 25 Various configurations of water-based PVT collectors (Chow, 2010)

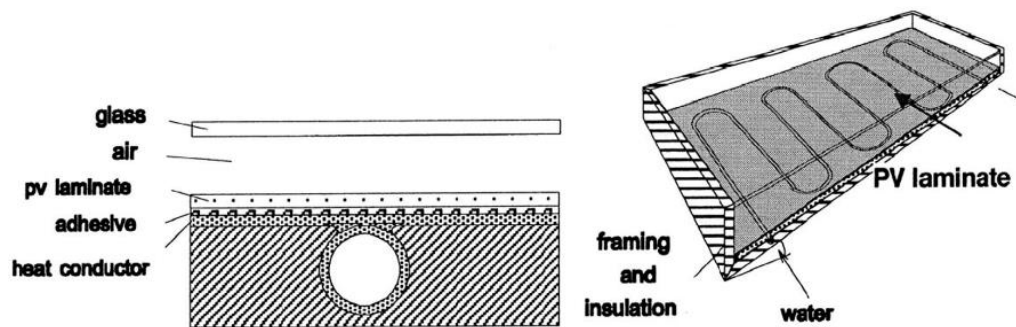


Fig. 3. 26 Sheet-and-tube PVT collector (Zondag et al., 2002)

A PVT collector utilizing aluminium-alloy flat-box for domestic water heating was constructed and experimentally investigated (Chow, He, and Ji, 2006) (He et al., 2006). PV cells were adhered on the surface of the aluminium alloy absorber which comprised of multiple extruded aluminium alloy box-structure modules having their ends connected to two aluminium traverse headers in which water circulation was achieved through the thermosyphon effect, Fig. 3.18. A thermal simulation model of the hybrid system was developed and results agreed well with the measured data (Chow, He, and Ji, 2006). The validated model was used to examine the steady state performance of the collector under different operating conditions of China. Under $800\text{W}/\text{m}^2$ of solar irradiation, 20°C ambient air temperature, $2.5\text{m}/\text{s}$ wind speed, and water mass flow rate of $76\text{ kg}/(\text{h m}^2)$ the ranges of the averaged daily thermal and electrical efficiencies were $37.6\text{-}48.6\%$ and $10.3\text{-}12.3\%$, respectively (Chow, He, and Ji, 2006). Such variation in efficiencies was observed to be dependent on the corresponding

water temperature and the level of solar radiation. Moreover, incorporation of anti-freeze closed-loop design was suggested to overcome water-freezing problems inside the flow channels arising during severe cold days in winter. He et al. (2006) observed a slightly lower value of the overall thermal-absorption of hybrid PVT system compared to conventional solar hot water collector attributed to lower optical absorption of the PV module as compared to the mat-black thermal absorber surface. However, energy-saving efficiency of 52% was achieved, which was above the conventional solar hot water collector and slightly higher than the performance of the unglazed PVT system using plastic channel absorber under forced circulation tested by Huang et al. (2001). In a later study by Chow et al. (2009), computer simulation model of a vertical wall-mounted water-based PVT was developed. The annual average thermal and cell conversion efficiencies of PVT collector with flat-box type thermal absorber and polycrystalline silicon cell were 37.5% and 9.39%, respectively.

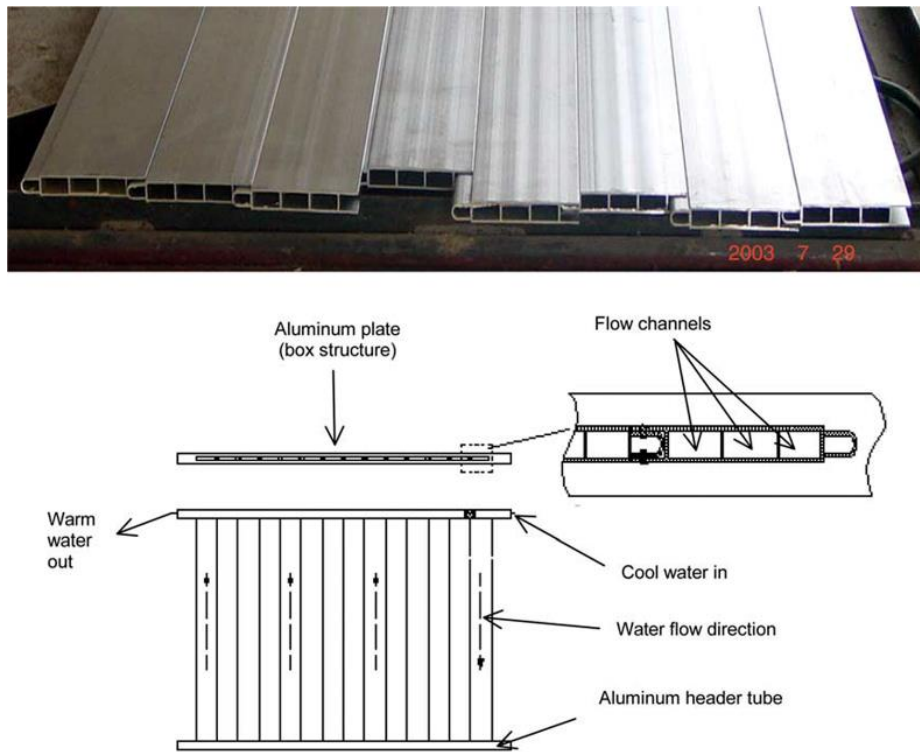


Fig. 3. 27 Flat-box aluminium-alloy heat exchanger (Chow, He, and Ji, 2006) (He et al., 2006)

Ji et al. (2006) presented a numerical model of wall-mounted water-based PVT collectors for electricity and hot water supply, in addition to improving the thermal insulation of the building envelope. The work adopted the PVT collector design presented earlier in (Chow, He, and Ji, 2006) (He et al., 2006). Air gap was incorporated between the front glazing and the PV surface to aid ventilation, which was addressed by Brinkworth et al. (1997) to assist reduction in operating temperature of PV modules. The BIPVT system comprised of six PVT collectors each of aperture area 1.173 m², a 420-litre water storage tank, a water circulation pump and connecting

pipes, Fig. 3.19. The influence of packing factors, water flow rate, and water delivery pipe size, on the electrical and thermal efficiencies was analysed to enable optimal set of design parameters to be identified. Results revealed that as the pipe diameter increased from 0.01 to 0.02 m, the required pumping power reduced dramatically. Nevertheless, further increase in the pipe diameter results in increased thermal loss at the exterior pipe surface. The effect of water mass flow rate was observed to improve the thermal efficiency and PV cooling as the heat removal factor was enhanced. However, the advantage of increased flow rate diminishes when the critical flow rate is exceeded, thereby decreasing thermal efficiency.

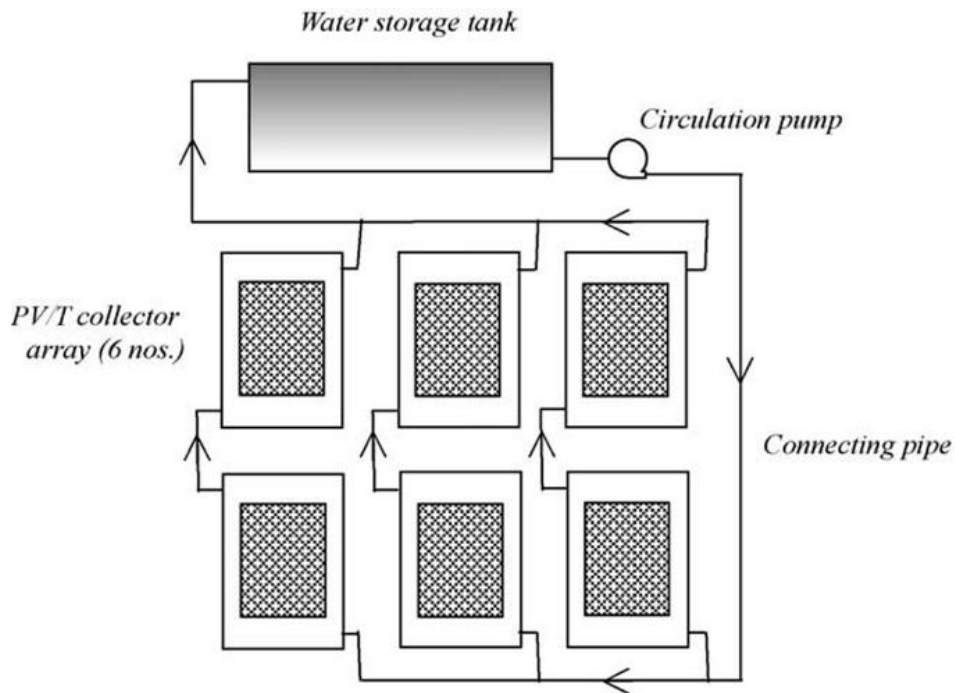


Fig. 3. 28 Wall-mounted water-based PVT collectors Ji et al. (2006)

The performance of water-based PVT collectors having different configurations of absorber collectors was studied theoretically by Ibrahim (2009), Fig. 3.20. The PVT collector comprised of polycrystalline PV cells with hollow tubes attached underneath. Under water flow rate of 0.01 kg/s with spiral flow design proved to be the best design with the highest thermal and cell efficiencies of 50.12% and 11.98% respectively and output temperature of 31 °C. Different output temperatures were observed and attributed to the design configuration of the absorber, in which the closer spacing between tubes enabled more heat to be absorbed. In a further study, Ibrahim et al. (2009) investigated the water type PVT collector with spiral flow design experimentally and compared it with single pass rectangular tunnel absorber collector for air flow. Electrical and thermal efficiency of 64% and 11% respectively were achieved under same water flow rate in the previous theoretical study. Compared to the single pass rectangular collector absorber with water flow, spiral flow design offers better heat extraction and overall efficiency having low surface temperature.

Based on a theoretical model, Dubey and Tiwari (2009) analysed the thermal energy, exergy and electrical energy yields of water-based PVT collectors by varying the number of collectors in use, series/parallel connection patterns, and operating conditions. The study concluded that the decision of PV cells covering factor would depend on the system

requirements, in which partially covered by PV cells would be beneficial when hot water production is a priority. On the other hand, fully covered collectors enhanced electrical energy yield leading to higher exergy efficiency. Dubey and Tiwari extended their work to identify the economic and environmental benefits of their system through evaluation of the optimum hot water withdrawal rate (Tiwari et al., 2009).

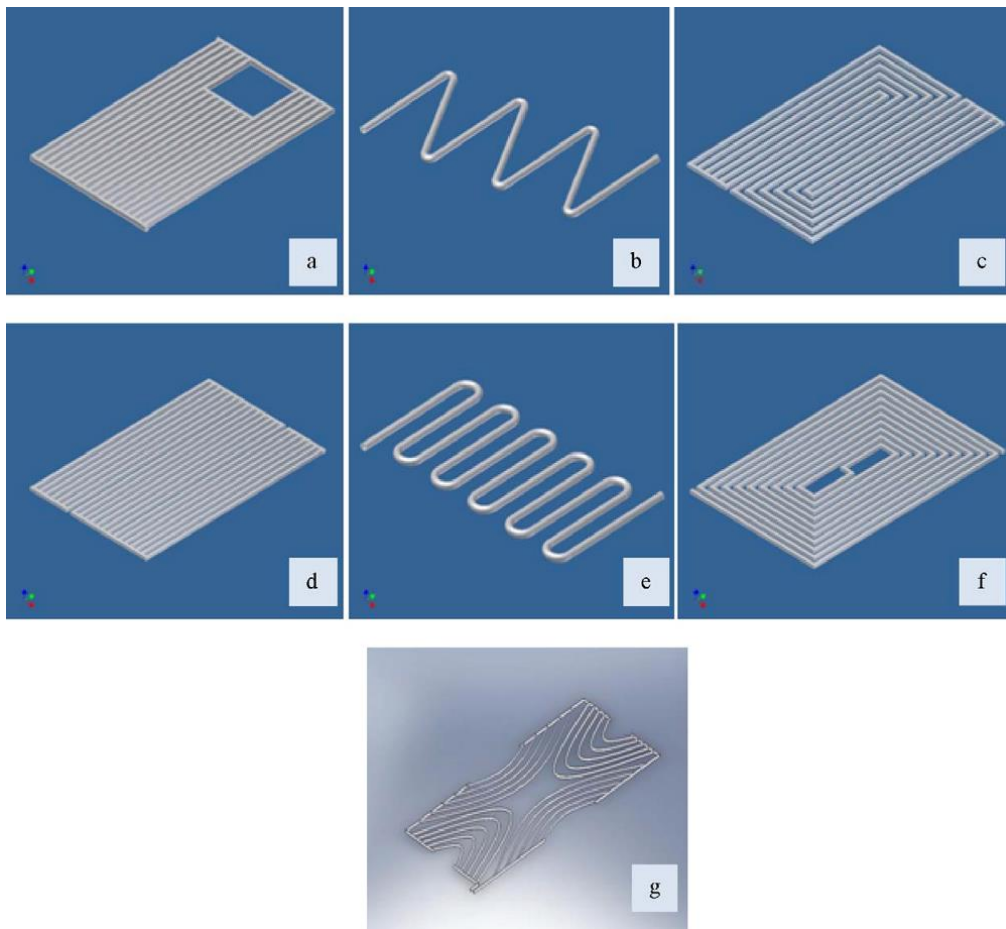


Fig. 3. 29 (a) Direct flow design, (b) serpentine flow design, (c) parallel-serpentine flow design, (d) modified serpentine-parallel flow design, (e) oscillatory flow design, (f) spiral flow design, (g) web flow design (Ibrahim, 2009)

Brogren and Karlsson (2002) used active water cooling method to cool a hybrid PVT system with stationary parabolic reflectors for low concentration ratio. The system consisted of a row of monocrystalline silicon cells laminated on a copper fin thermal absorber with a water tube welded on the back. Results of the experiment under 3 concentration ratios measured a short-circuit current of 5.6 A compared to identical module without concentration having a short-circuit current of 3 A, hence showing a true optical concentration of only 1.8. Brogren and Karlsson justified the losses were attributed to geometrical imperfections of the concentrating element and optical losses in the reflector and the cover glazing. Meanwhile, significant amount of thermal energy 3-4 times the electric energy was produced at a water temperature of 50 °C.

Zhu et al. (2011) conducted experimental work investigating dielectric liquid immersion cooling for concentrator PV system using 250x dish concentrator. Mono-crystalline silicon PV cells with back contacts were mounted on copper-clad electrically insulating substrates to form modules, each having 88 cells connected in series. Under 250 suns with direct normal irradiance of 900 W/m², cooling water inlet temperature of approximately 31 °C and ambient temperature around 17 °C peak module temperature of 49 °C was observed. Moreover, temperature distribution difference along the surface of less than 4 °C was attained. Due to eliminated contact thermal

resistance of back cooling, liquid immersion facilitated improved cell performance to be achieved. In a more recent work, improvement in electrical efficiency of about 8.5–15.2% was reported through 1.5 mm thickness liquid layer over the cell surface by Han et al. (2013)

Prudhvi (2012) proposed improving the efficiency of the PV by active cooling to reduce the temperature losses considerably and decrease reflection losses. A thin layer of water to flow on the surface of the solar panel was investigated. The system considers closed circuit flow, whereas *Ground Water Tunnelling* mechanism was applied to cool water absorbing the heat from the surface of the PV cells. Practical calculation based on the developed model presented a net 7.7% improvement in efficiency.

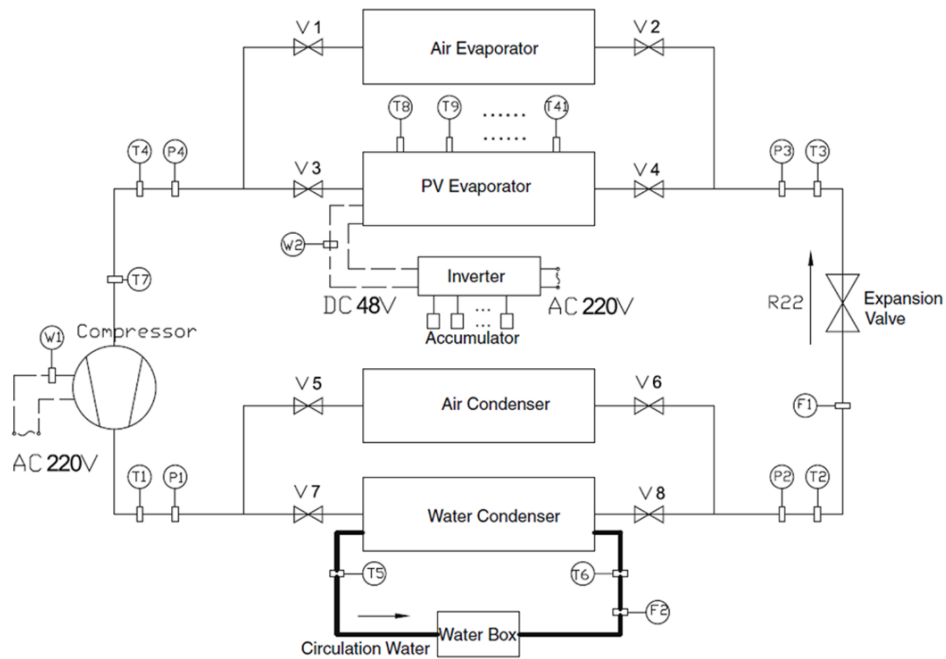
3.1.2.2 Refrigerant-based PVT collectors

Refrigerant fluids are generally used in systems combining PVT collectors and solar-assisted heat pumps (SAHP), in which the PVT collector serves as an evaporator where the refrigerant absorbs thermal energy available at the PV cells (Ji et al., 2008) (Ji, Pei, et al., 2008). Low evaporation temperature (0–20 °C) of refrigerant allows efficient cooling of PV cells to be achieved leading to significant improvement in the performance (Ji et al., 2008) (Ji, Pei, et al., 2008) (Zhao et al., 2011).

The performance of PVT solar-assisted heat pump co-generation system was investigated theoretically and experimentally by Ji et al. (2009). The system comprised of nine (3x3) mono-crystalline PVT collectors serving as direct-expansion evaporators for the heat pump in which R22 refrigerant inside copper coil vaporizes at low temperature transferring absorbed heat to the condenser section, Fig. 3.21. Dynamic distributed model was developed to predict various parameters including the pressure distribution of the PV evaporator and along the copper coil attached, temperatures of PV cells and base panel thermal collector, thermal and electrical efficiencies of the system, in addition to vapour quality and enthalpy. Validation of the simulation results exhibited good agreement with measured data except for the pressure drop of the PV evaporator which was found much higher than the simulation prediction, attributed to underestimation of the saturated temperature gradient and higher temperature gradient along the copper coil observed during the experiment. Under solar irradiation of 840 W/m^2 and ambient temperature of $14 \text{ }^\circ\text{C}$, the electrical and thermal efficiencies were 12% and 50% respectively implying enhanced cooling effect of the PV.

A novel PV/evaporator (PV/e) roof module for electricity generation and acting as an evaporator of a heat pump system was designed by Zhao et al. (2011), Fig. 3.22. The performance was evaluated theoretically with R134a refrigerant based on various parameters including, top cover material, PV

cells technology, and evaporation and condensation temperature of the heat pump. An optimized system configuration comprising of mono-crystalline PV cells, borosilicate top cover, evaporation and condensation temperatures of 10 °C and 60 °C respectively was suggested. The PV/e heat pump system was simulated under typical Nottingham (UK) weather conditions, and thermal and electrical efficiencies of 60.93% and 9.21% respectively were reported.



T1-T41, Thermocouples; V1-V8, Cut-off valves; P1-P4, Pressure sensors;
F1-F2, Flow meters; W1-W2, Wattmeters

Fig. 3. 30 Schematic diagram of PV solar-assisted heat pump (Ji et al. 2009)

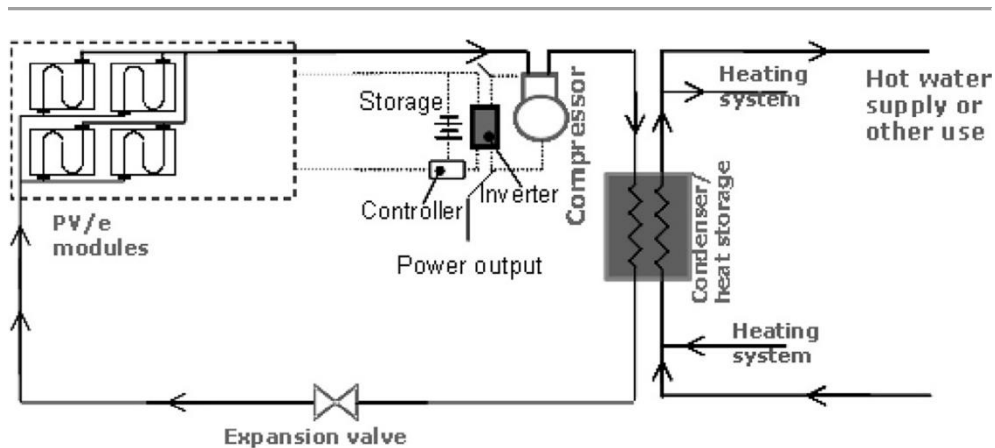


Fig. 3. 31 PV/evaporator heat pump system (Zhao et al. 2011)

Improved performance of PVT collector is attained through utilising refrigerant cooling. Nevertheless, the practical feasibility of such systems encounters several challenges including, unbalanced refrigerant distribution, possible leakage of refrigerant, and maintaining pressurization and depressurization at various parts of the system (Zhang et al., 2012) (Zhang et al., 2013). In attempt to override such challenges, Zhang et al. (2013) presented a novel PV/loop-heat-pipe (PV/LHP) heat pump solar system, Fig. 3.23. The design utilized loop heat pipe structure with three-ways tube combining the PVT module and the heat pump operations to overcome 'dry-out' problem encountered in conventional heat pipe cooling. Theoretical evaluation and experimental tests were conducted to define the performance of the system in terms of thermal and electrical efficiencies, and the system's overall performance coefficient. Predicted simulation results showed fair agreement with data measured. Parametric analysis on

the impact of several operational parameters including; solar radiation level, ambient temperature, air velocity, evaporation temperature of heat pump, top glazing cover, and heat pipe absorbing number was performed using the validated model. Results under laboratory condition reported electrical, thermal, and overall efficacies of about 10%, 40%, and 50%, respectively. Overall coefficient performance of about 8.7 was measured contributing to improvement of two to four times than that for conventional solar/air heat pump water heating systems.

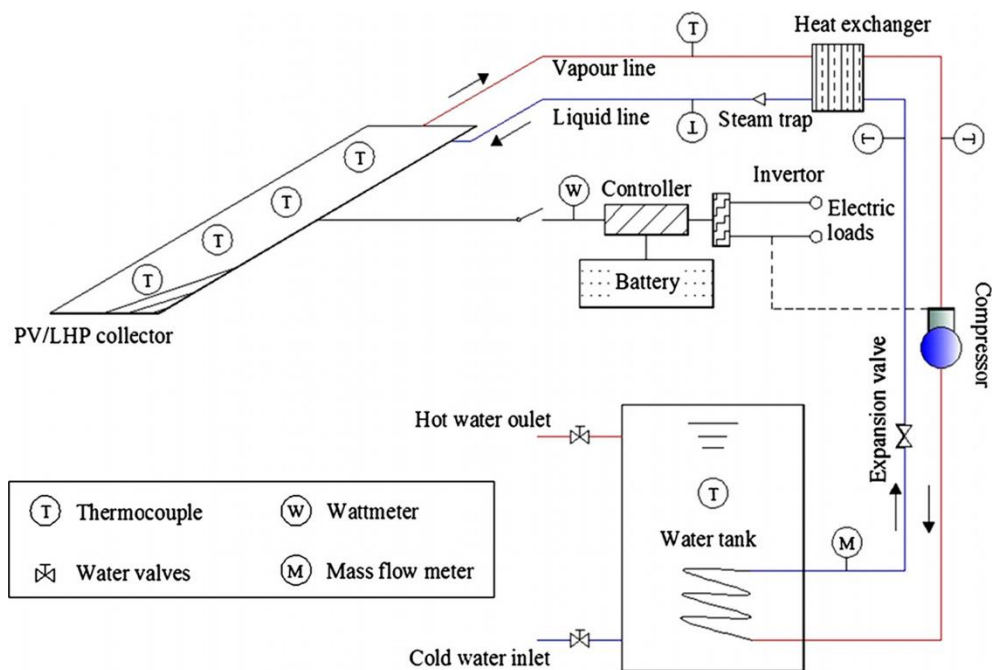


Fig. 3. 32 PV/loop-heat-pipe (PV/LHP) heat pump solar system (Zhang et al., 2013)

In a similar concept, Xu et al. (2011) adopted refrigerant cooling to absorb heat from PV cells under low concentration using parabolic

concentrator reflecting the incident sunlight onto the surface of PVT collector. Under climatic conditions of Nanjing (China) and low concentration, the PVT integrated heat pump (LCPVT-HP) achieved an electrical efficiency of 17.5%, which was observed to be 1.36 times higher than that of LCPV system without cooling. The effective cooling of the refrigerant can be seen clearly in Fig. 3.24, where comparison between base panel temperature of the LCPVT with and without the presence of cooling is presented.

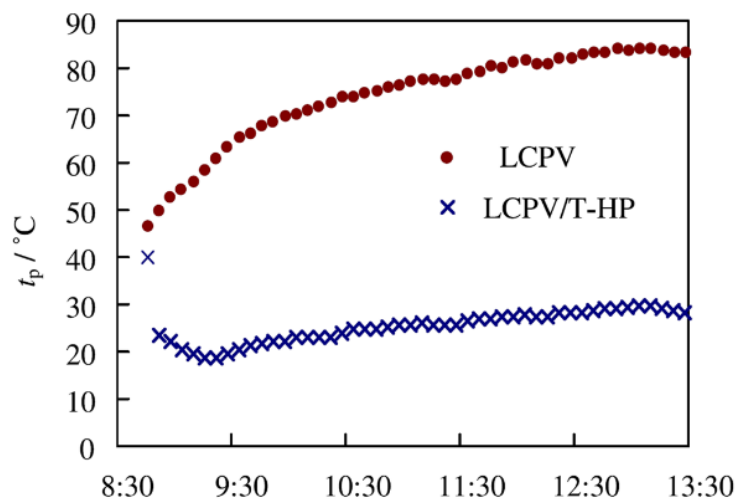


Fig. 3. 33 PV cell operating temperature of low concentrating PVT integrated heat pump (LCPVT-HP) (Xu et al. 2011)

Liquid cooling offers a better alternative to air cooling utilizing coolant as heat extraction medium to maintain desired operating temperature of PV cells and a more efficient utilization of thermal energy captured. In addition, liquid-based PVT collectors offer less temperature fluctuations compared to

air-based PVT making them more favourable in aiding a homogenous temperature distribution on the surface of PV modules. The low evaporative temperature (0–20°C) of refrigerants allows efficient cooling of PV cells to be achieved leading to improved performance compared to water cooling. Nevertheless, the practical feasibility of such systems encounters several challenges as discussed earlier.

3.1.3 Heat pipe-based PVT collectors

Heat pipes are considered efficient heat transfer devices that combine the principles of both thermal conductivity and phase transition. A typical heat pipe consists of three sections namely; evaporator, adiabatic, and condenser sections, Fig. 3.25. Heat pipes provide an ideal solution for heat removal and transmission, with one end serving as a thermal energy collector and the other end as a thermal energy dissipater (Du, Darkwa, and Kokogiannakis, 2013). Heat pipes have been considered for thermal management applications of PV technology due to the advantages such technology provide over other cooling means such as aiding uniform temperature distribution of PV cells, elimination of freezing that thermosyphon tube can suffer from in higher latitudes, in addition to resistance to corrosion. However, the design of efficient heat pipe involves

careful selection of a suitable combination of the heat pipe container material, working fluid, and wick structure (Dunn, Reay, and Dunn, 1994).

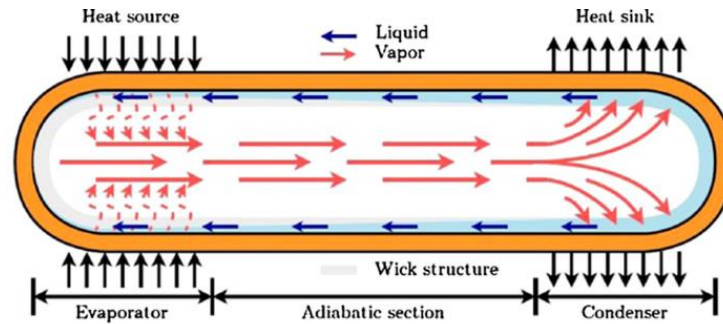


Fig. 3. 34 Schematic diagram of heat pipe (Zhang et al., 2012)

Russell (1982) developed a cooling approach for concentrated PV (CPV) systems utilising heat pipes, to enable operation at elevated temperature and utilization of extracted heat for beneficial use. The systems comprised of a row of PV cells mounted on the outer surface of a heat pipe, where heat pipes are arranged next to each other to form a panel, and Fresnel lenses were used to provide high solar energy intensity, Fig. 3.26. The heat pipe used had internal tubes for circulating a fluid coolant through the heat pipe vapour field to promote heat extraction. Details of the performance parameters were not revealed in this study. Heat pipe approach for CPV system under concentration ratio of about 24 suns was presented by Feldman et al. (1987). The pipe was made from extruded aluminium surface and the evaporative working fluid was benzene. Under ambient temperature of 40 °C and concentrated solar radiation of 19.2 kW/m², a

minimum wind speed of 1 m/s was required to keep the evaporator temperature below 140 °C which limits the cooling capability of such system.

Akbarzadeh and Wadowski (1996) utilized a passive cooling approach using two heat exchangers piped together and filled with refrigerant to cool down the rear of the solar cells for a system designed for concentration ratio of 20 suns, Fig. 3.27. The cooling mechanism proposed has a lower heat exchanger which is an evaporator and flooded with liquid refrigerant, and an upper saturated vapour heat exchanger acting as a condenser. PV cells in this system were attached to the evaporator and the upper condenser was exposed to natural convective air cooling, in addition to fins attached to the condenser to extend the external heat transfer area. Results showed that the solar cell's surface temperature did not exceed 46 °C. Improved performance of 50% was observed, generating 20.6 W compared to 10.6 W for the case without cooling arrangement.

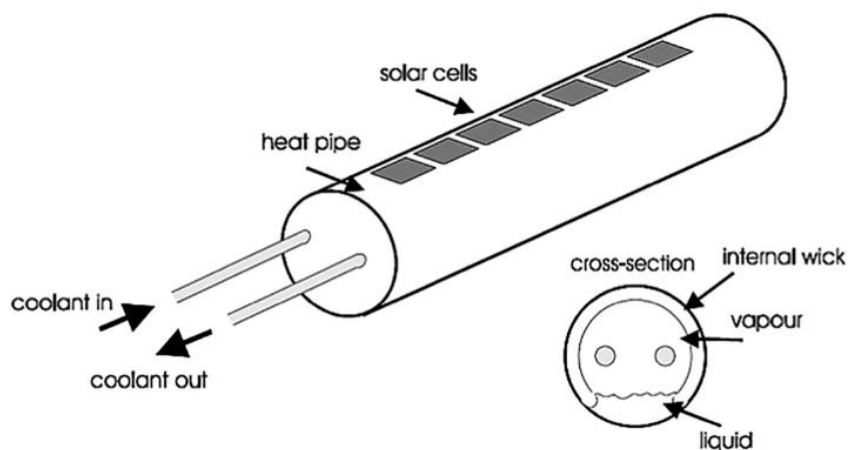


Fig. 3. 35 Heat pipe cooling of PV cells (Russell, 1982)

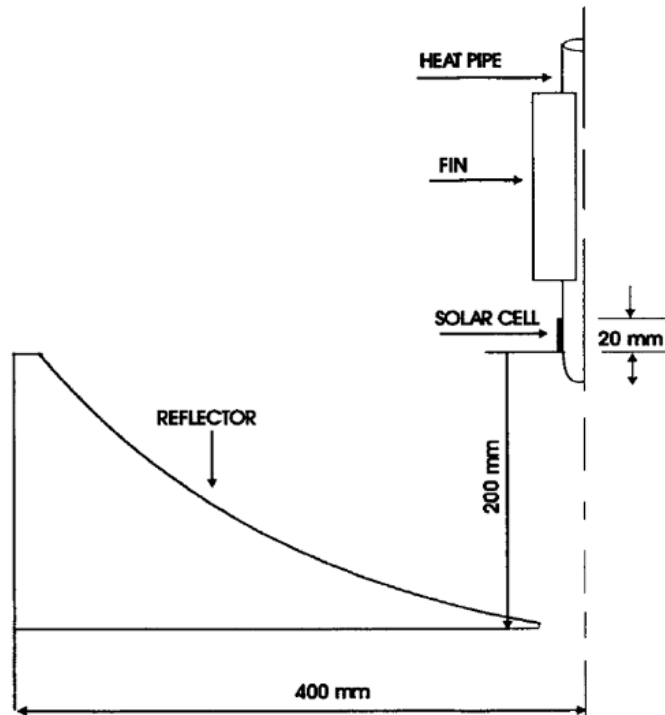


Fig. 3. 36 Cooling of low concentrator PV cell with heat pipe extruded fin Akbarzadeh and Wadowski (1996)

Farahat (2004) conducted experimental tests to evaluate the cooling capability of two approaches for concentrator PV cells using water and heat pipe cooling. The study investigated the influence of actual cell temperature on the performance of PV cells by observing the electrical characteristics of PV cells when both cooling techniques were employed. Results showed the influence of temperature on the open circuit voltage which tended to decrease, while the short circuit current increased with the increase in temperature. A comparison of the annual yield of different configurations revealed that decreased temperature of PV cells and a more reliable thermal performance were achieved when heat pipe cooling was applied.

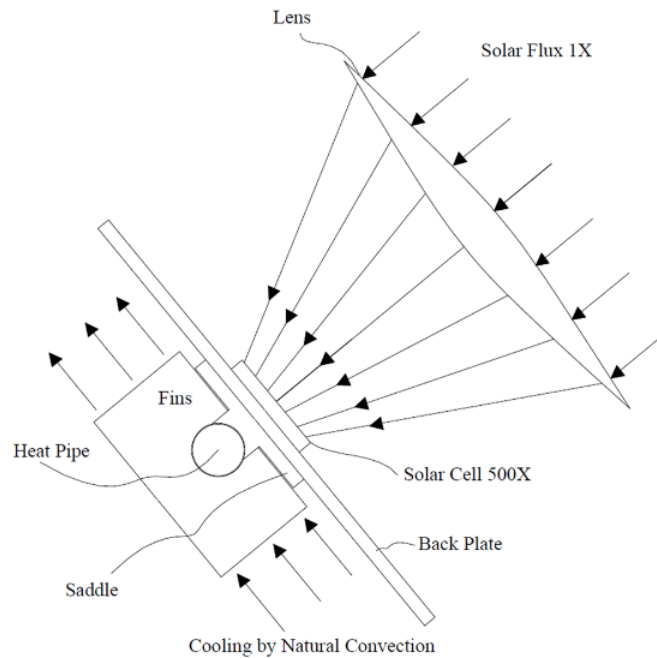


Fig. 3. 37 Cooling PV concentrator through copper/water heat pipe with aluminium fins (Anderson et al. 2008)

Anderson et al. (2008) investigated a design to cool PV concentrator under concentration ratio of 500 suns utilizing a copper/water heat pipe with three wraps of mesh along with aluminium fins to enhance cell cooling with the aid of natural convection. Comparison between different working fluids compatible with copper heat pipes revealed that copper/water heat pipes were able to carry more than six times the power of other working fluids. The heat pipe was fabricated and attached to an aluminium saddle in which the CPV cell sits on, Fig. 2.28. Optimum fin size and spacing for rejecting heat by natural convection were determined through series of CFD analysis. Heat rejection to the environment through natural convection achieved cell-to-ambient difference of 43 °C when input heat flux of 40

W/cm² was applied, whereas temperature difference of 110 °C was measured when aluminium plate was used for PV cells cooling. Adopting the same concept design, Hughes et al. (2011) performed CFD analysis to model the heat transfer from a conventional flat plate PV module. A prototype of the system was fabricated and tested under weather conditions of Dubai, UAE. With the aid of finned heat pipe arrangement and natural convection, the operating temperature of solar cells was regulated at 30 °C under ambient temperature of 42 °C and wind speed of 4.2 m/s.

Tang, Quan, and Zhao (2010) utilized micro heat pipe arrays to investigate the performance of conventional flat plate PV module using both air and water as heat extraction mediums from the condenser section of the micro heat pipe array, Fig. 3.29. Experimental results of both systems were compared to an ordinary PV panel without cooling. Using water to cool the heat pipes contributed in achieving a maximum difference in electrical efficiency of 3% and average increase of 0.5%, while air cooling attained 2.6% and 0.4% respectively when compared to ordinary panel without cooling. In terms of output power, the water and air-cooled systems achieved average increase of 9% and 6.3% respectively.

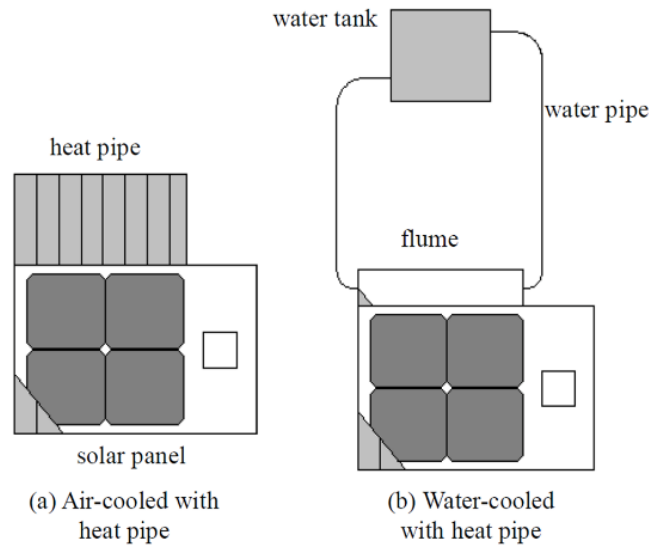


Fig. 3. 38 Micro heat pipe array cooling for conventional flat-plate PV module using (a) air, (b) water

The performance of a water thermosyphon PVT and a heat pipe PVT collector which was part of a solar assisted heat pump (SAHPHP) was compared experimentally in Hefei, China in a study conducted by Pei et al. (2011). Heat pipes were used to overcome the freezing issues associated with water thermosyphon PVT collectors in high latitudes and improve the conversion efficiency of PV cells. Heat pipes filled with R600a were utilized and a heat exchanger was incorporated in a water tank (acting as a condenser section of heat pipe), where the working fluid condensed and released its latent heat into the water. The thermal efficiency of the heat pipe PVT collector recorded (23.8%) was 27.9% less than that of the water thermosyphon (33%) attributed to large thermal inertial of the heat pipe PVT system. However, improvement of 6.7% in the electrical efficiency with an

average electrical efficiency of 9.5% was achieved through utilizing heat pipe cooling due to small temperature difference between the PV cells compared to that of the water thermosyphon which attained electrical efficiency of 8.9%. The study revealed that utilization of heat pipes in SAHP-HP system has potential in reducing the power consumption of heat pumps as the heat pipe replaced part of the work of the heat pump.

More recently, Gang et al. (2012) conducted dynamic modelling of a PVT collector utilizing heat pipe for heat extraction for PV modules. The collector comprised of 9 water-copper heat pipes joined together at the back of aluminium plate incorporated at the rear of a PV module. Low-iron tempered glass was used as a top cover glass of the installation preventing thermal losses and the entry of dust particles. The model was validated with experimental measurements performed under the weather conditions of Hefei, China, and good agreement was observed. Reported average electrical and thermal energy efficiencies were 10.2% and 45.7% respectively with average overall exergy efficiency of the 7.1%. (Gang et al. 2012) extended the research to provide a comprehensive parametric analysis based on the validated dynamic model to investigate the effect of water flow rates, PV cell covering factor, tube space of heat pipes, and different solar absorptive coatings of the absorber plate. It was noted that both thermal and electrical efficiencies can be improved by decreasing the

inlet water temperature and increasing the mass flow rate. However, the packing factor has an influence on the electrical efficiency greater than that of the thermal efficiency. Cost analysis was also presented in terms of the overall performance improvements that could be achieved by increasing the PV cell covering factor and reducing the tube space of heat pipes. Results of the analysis revealed that heat pipe spacing of 0.09 m was the most suitable and cost-efficient option, further reduction in tube spacing resulted in an increased number of heat pipes required for producing a collector at an additional cost with only small improvement in the overall performance. In a similar design, Wu et al. (2011) investigated the influence of heat pipe cooling on maintaining a uniform cooling for PV cells by absorbing the excessive heat accumulating on solar cells isothermally. Results showed that the use of heat pipe cooling can assist uniform temperature of solar cells on the absorber plate with variation of solar cell temperature less than 2.5 °C. The overall thermal, electrical, and exergy efficiencies of the heat pipe PVT hybrid system reported were 63.65%, 8.45%, and 10.26% respectively.

Redpath et al. (2012) investigated the performance of a linear axis compound parabolic concentrating solar PVT (CPC-PVT) with heat pipe integrated for heat removal. The system was compared to a simple flat plate PVT (FP-PVT) with headers and risers. Reported heat loss coefficient of the heat pipe-integrated PVT exhibited lower value than flat plate. Under

concentration ratio of 1.8x the CPC-PVT system attained additional 2.5% in the electrical conversion efficiency, while only 0.9% added efficiency was observed from the FP-PVT comparing both to a reference PV panel. A novel hybrid-structure flat plate heat pipe for a concentrator photovoltaic was fabricated and investigated by Huang et al. (2012) The temperature regulation mechanism comprised of a flat copper pipe with a sintered wick structure, and a coronary-stent-like rhombic copper mesh supports. Such modifications could effectively reduce the thermal resistance of the heat pipe allowing for further heat to be extracted. Experimental results with 40 W concentration on the cell achieved improvement of 3.1% in the electrical conversion efficiency compared to an aluminium substrate in a single solar cell.

3.1.4 PCM-based PVT collectors

Phase changes Materials (PCMs) are substances that can absorb and release large amount of energy as latent heat through a reversible isothermal process at a particular phase transition temperature (Huang, Eames, and Norton, 2004), (Al-Mosawi, 2011), (Biwole et al. 2013), (Lo Brano et al., 2013). Latent heat storage using PCMs is superior to sensible heat storage due to their higher energy storage density within a smaller temperature range (Bouzoukas, 2008). These materials are classified as

organics consisting of paraffin wax and fatty acids, inorganics consisting of salt hydrates, and eutectic mixtures of organic and inorganic PCMs (Malvi, Dixon-Hardy, and Crook, 2011), (Jun Huang, 2011), (Hassan, 2010). A thorough review of the three classified PCMs and their desirable characteristics, advantages, disadvantages, and behaviours during phase transition are available in literatures (Sharma et al., 2009), (Agyenim et al., 2010), (Dincer, Rosen, and Dincer, 2002).

PCMs have been used widely as heat sinks for electronic devices (Abhat, 1983), (Wirtz, Zheng, and Chandra, 1999) and in passive thermal storage and management of buildings by adding encapsulated PCM particles during material production processing known as microencapsulated PCMs (MEPCM) or by laminating PCM layers onto construction panels (Cerón, Neila, and Khayet, 2011), (Hasse et al., 2011), (Koo et al., 2011), (Chan, 2011), (Lai, Chen, and Lin, 2010), (Ansuini et al., 2011). Incorporating PCMs in wallboards, roofs, and ventilation heat exchangers can significantly reduce peak cooling/heating loads leading to reduced energy consumption, in addition to improving human comfort by reducing temperature swings (Peippo et al. 1991), (Hawes et al. 1993), (Pasupathy and Velraj, 2008), (Arkar and Medved, 2007), (Paris, Villain, and Houle, 1999), (Shapiro et al., 1987). As for electronic devices, incorporating PCMs into traditional heat sinks for electronic chips within mobile phones and computers have been proven

effective for thermal regulators (Lu, 2000), (Kandasamy et al. 2007), (Tan and Fok, 2007).

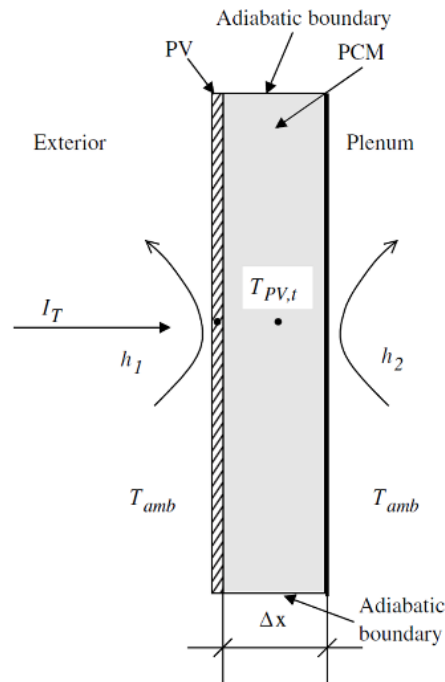


Fig. 3. 39 Schematic drawing of a PV/PCM system (Huang et al. 2004) .

As far as PV systems are concerned, conventional passive cooling techniques are unable to provide the required cooling during peak solar radiation periods leading to a deteriorated performance of PVs. Furthermore, inhomogeneous temperature profiles which affect the generation capacity of PV systems stand as a limitation in other passive cooling methods (Di Vincenzo and Infield, 2013), (Domenech-Garret, 2011). Recently, few studies were conducted to investigate the incorporation of PCMs in PV systems to tackle temperature significance on PV cells operation.

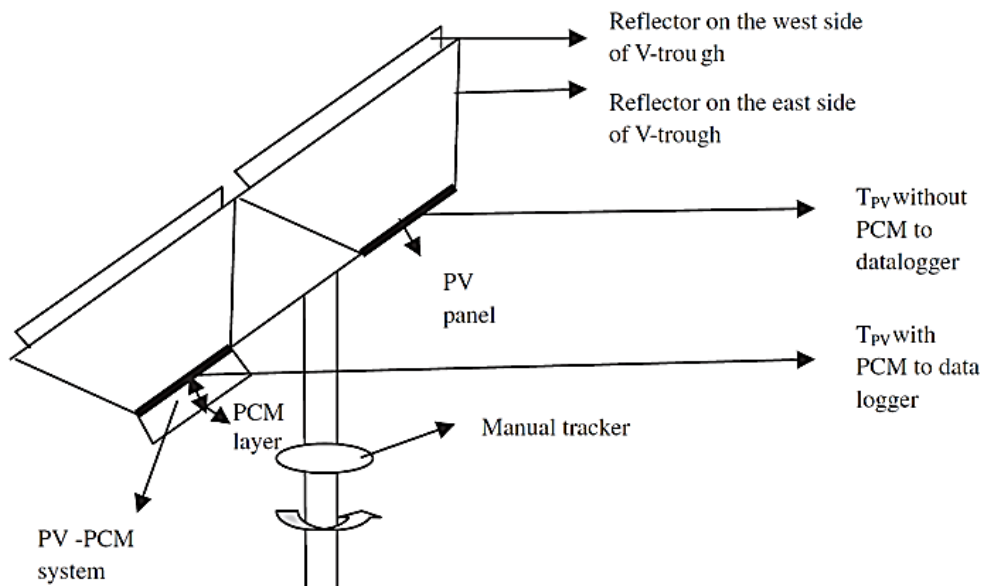


Fig. 3. 40 V-trough stand-alone PV/PCM system (Maiti et al., 2011)

Various PCM-based PV concept designs have been reported in literatures. The most common system studied considers incorporation of PCMs in Building Integrated Photovoltaic (BIPV), Fig. 3.30, (Huang et al. 2004), (Huang, Eames, and Norton, 2006), (Hasan et al., 2010), (Ho et al., 2013). Stand-alone PV collectors with PCM thermal storage have also been reported in few literatures, Fig. 3.31, (Maiti et al., 2011), (Kourvisianos, 2013). These designs have the same basic components in common from which the system is constructed. However, diversity in the heat transfer mechanisms from the PV module was noted. The unutilized part of solar radiation striking the surface of PCM-based PV systems is conducted as heat to the PCM through the PCM container material causing increased temperature of PCM. At a certain phase transition temperature, the PCM

starts melting and due to continuous temperature rise the melt extends into the PCM. During latent heat transfer process the PCM effectively acts as a heat sink maintaining a regulated temperature of the PV modules close enough to its melting/freezing point. Once the melting process is complete, any further heat stored will manifest as a temperature rise. Such process is reversible wherein solidification cycle takes place as the temperature drops below the melting point.

Non-linear motion of solid–liquid interface, presence of buoyancy driven flows in the melt, and volume expansion of the PCM during melting/solidification introduce complexities in the analytical investigation of PCM-based applications (Huang et al. 2004). Therefore, numerical and experimental investigations represent majority of the work reported in this field. Huang et al. (2004) developed a two-dimensional model to investigate the use of solid-liquid PCM to regulate the temperature of BIPV near its characterizing temperature of 25 °C. The model was validated with experimental measurements and good agreement was achieved. Parametric analysis based on the validated model was conducted to predict the thermal control of a range of PV/PCM configurations and operating conditions in order to optimize the PV/PCM design. Insolation level had a profound influence on the thermal regulation of the PCM in which the time required for PCM to completely melt was reduced as solar intensity increased, Fig.

3.32. Improvements in the thermal management of the PCM were achieved through incorporating metal fins extending in the PCM as observed in Fig.

3.33.

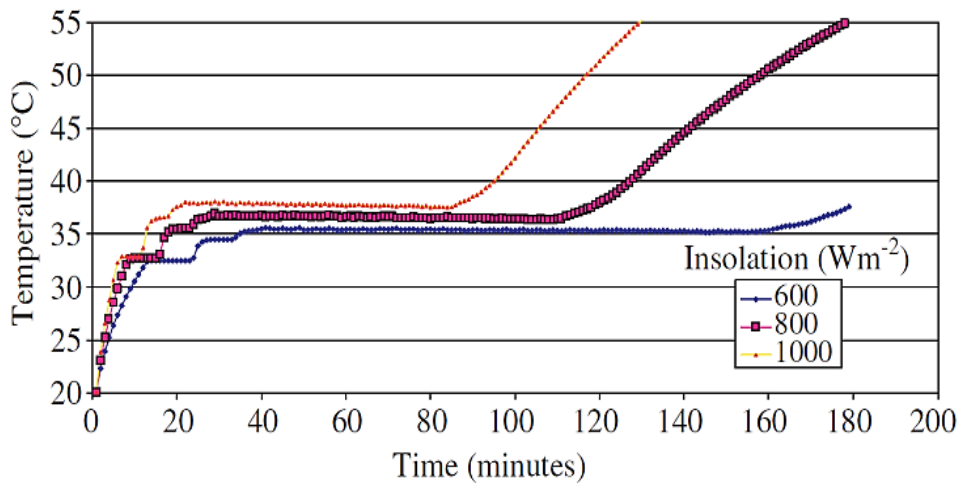


Fig. 3. 41 Surface temperatures at different levels of insolation and ambient temperature of 20°C

Thermal performance of different internal fin arrangements to enhance the thermal conductivity of bulk PCM was investigated experimentally using RT25 and GR40 paraffin waxes by Huang, Eames, and Norton (2006). Of the different fin arrangements investigated straight fins of width 36 mm led to the lowest surface temperature. Soft-iron wire matrix however, sustained stable temperature during phase transition under 750 W/m² and ambient temperature of 23±1 °C as shown in Fig. 3.34. Reported thermal control of solid-liquid RT25 PCM was superior to granular GR40 PCM as a thermal regulation of below 32 °C for a period of 150 min was achieved. Increasing the width of the fin resulted in a longer duration at which the temperature

was regulated, while decreasing the spacing between fins further reduced the temperature at the surface of the PV modules at the expense of the temperature control duration. The study concluded that the temperature was mainly influenced by the number, dimension, form of fins, and type of PCM material used.

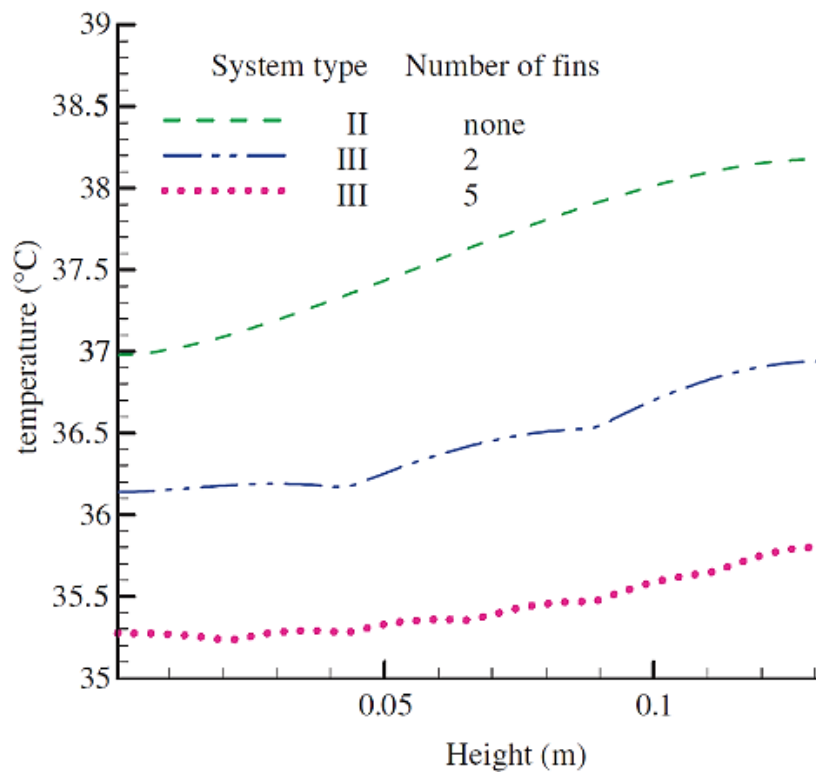


Fig. 3. 42 Surface Temperatures of PV/PCM systems with and without internal fins at a particular operating condition

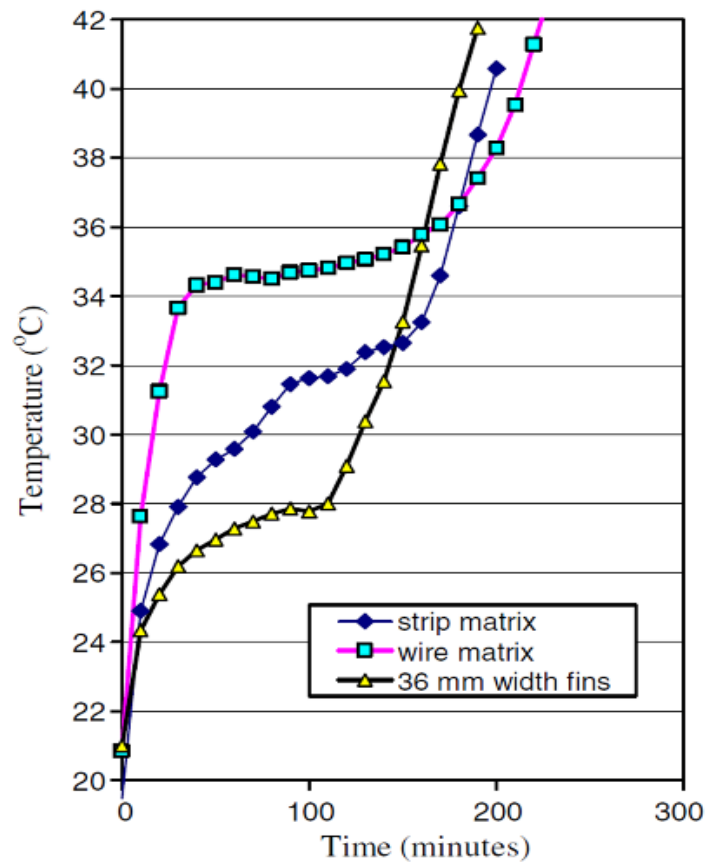


Fig. 3. 43 Average measured surface temperature of finned PV/PCM systems (Huang, Eames, and Norton 2006)

With regards to the declined thermal regulation period noted through the use of internal fin arrangements, a modified PV/PCM system integrated with two PCMs with different phase transient temperatures was investigated (Jun Huang, 2011). Various cases using different combinations of PCMs with different melting temperatures in triangular shaped cells were considered, Fig. 3.35. Compared with the previously studied straight fins PV/PCM, Huang reported that the system with triangular cells was able to dissipate the stress resulting from volume expansion and extended the

thermal regulation period. Results of the research revealed that the thermal regulation performance of the PV/PCM depended on the thermal mass of PCM, position of PCMs inside the PV/PCM system, and thermal characteristics of both PCM and PV/PCM system structure. Furthermore, for the combination of PCMs the lower phase transition PCM dominated the whole system performance. Under insolation level of 1000 W/m^2 and ambient temperature of 20°C the system with PCMs RT27-RT21 had the lowest temperature rise due to its lower melting temperature, while RT27-RT27 was able to regulate the temperature for a longer period, Fig. 3.36.

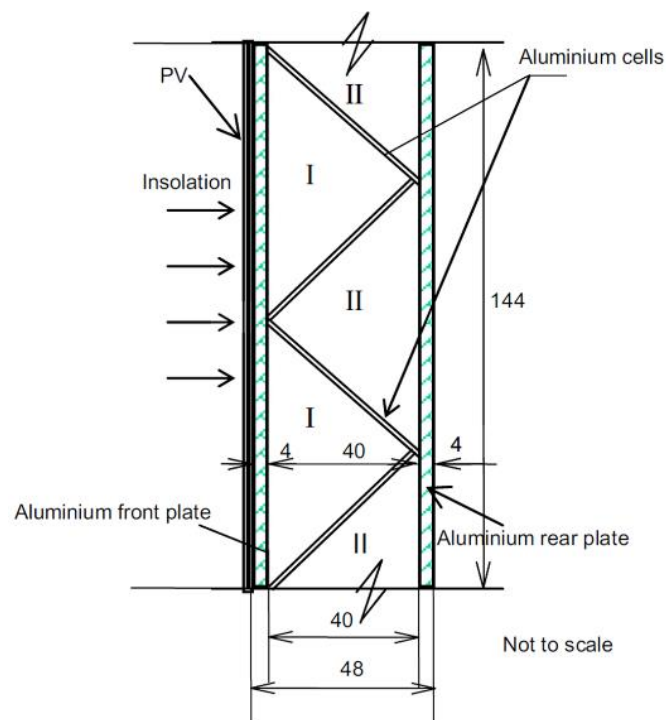


Fig. 3. 44 Schematic diagram of PV/PCM system with triangular cell (Jun Huang, 2011).

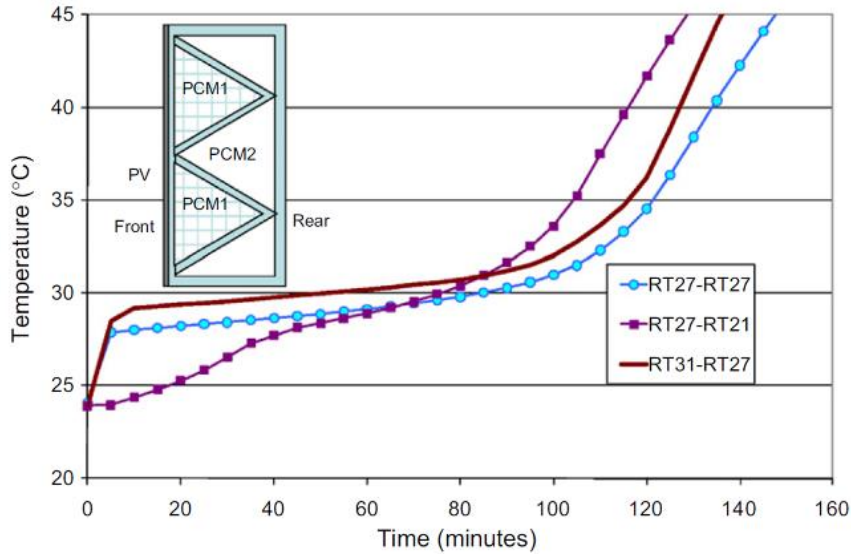


Fig. 3.45 Predicted surface temperature evolution using different combinations of PCMs within PV/PCM system (Jun Huang, 2011).

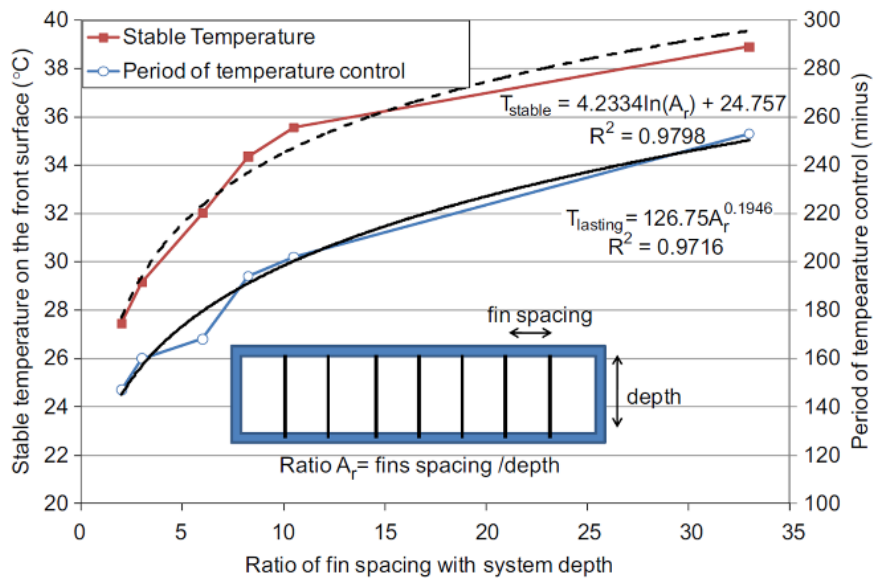


Fig. 3.46 Temperature regulation with the ratio of fins spacing on PV/PCM system design (Huang et al. 2011).

The effect of crystalline segregation and convection in melted PCM was also investigated by Huang et al. (2011). The physical structure of bulk PCM

in PV/PCM system with phase transition was examined. Increased porosity in the centre of the bulk PCM due to the effect of volume contraction when the PCM solidified was observed, resulting in an increased heat transfer resistance. Although horizontal metal fins enhanced the heat transfer process, obstruction of the movement of bubbles formed under the fins during PCM melting was observed leading to increased heat transfer resistance. Thermal stratification was as well examined through temperature measurements within the PCM, and results showed that with certain fin interval (12–24 mm) the thermal stratification could be reduced and convection had improved effect on heat transfer rate leading to more uniform temperature distribution in the PV/PCM system and improved thermal regulation period. A correlation between the ratio of fins spacing to system depth that can be used to characterize the period of temperature control and temperature regulation capacity is shown in Fig. 3.37.

Hasan et al. (2010) conducted experimental tests and observed the effect of the thermal conductivity of the container material wherein the PCM resides and the effect of thermal mass of PCM on the PV thermal regulation at different insolation levels. Aluminium and Perspex were used as containers attached to the rear of PV module to absorb excessive heat, and various PCMs with different conductivities were examined. Results revealed that salt hydrate CaCl_2 PCM in aluminium container achieved the best

thermal regulation performance at insolation level of 1000 W/m^2 and ambient temperature of $20 \pm 1 \text{ }^\circ\text{C}$ as shown in Fig. 3.38. It was evident that the thermal regulation performance of PCMs depended on both the thermal mass of the PCM and the thermal conductivities of both PCM and the overall PV/PCM assembly.

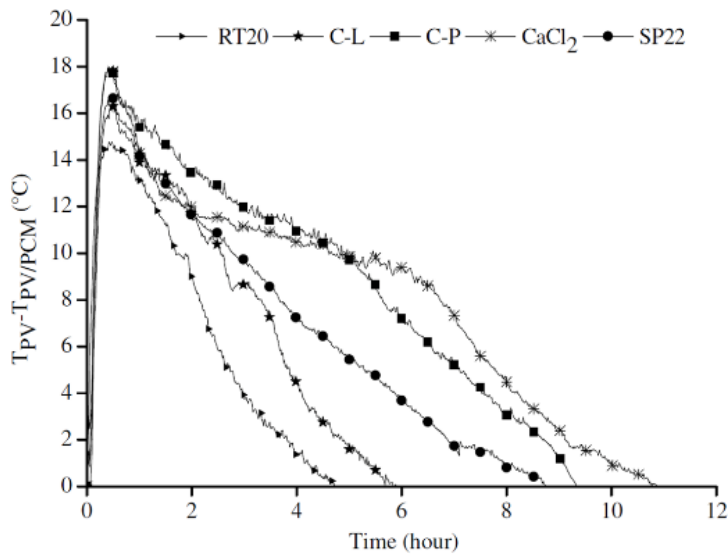


Fig. 3. 47 Temperatur edifference from reference PV using four different PCMs (Hasan et al. 2010)

Thermal regulation of an enhanced solar insolation stand-alone PV/PCM system using V-trough was conducted by Maiti et al. (2011), Fig. 3.31. Temperature regulation of $65 \text{ }^\circ\text{C}$ under 1.7 average enhancement of solar insolation was attained. The investigated system achieved 55% improvement in the overall power generation through incorporating a bed of metal-embedded paraffin wax as PCM at the rear of the PV module, even

under low wind velocities and moderately high insolation and ambient temperature conditions, Fig. 3.39.

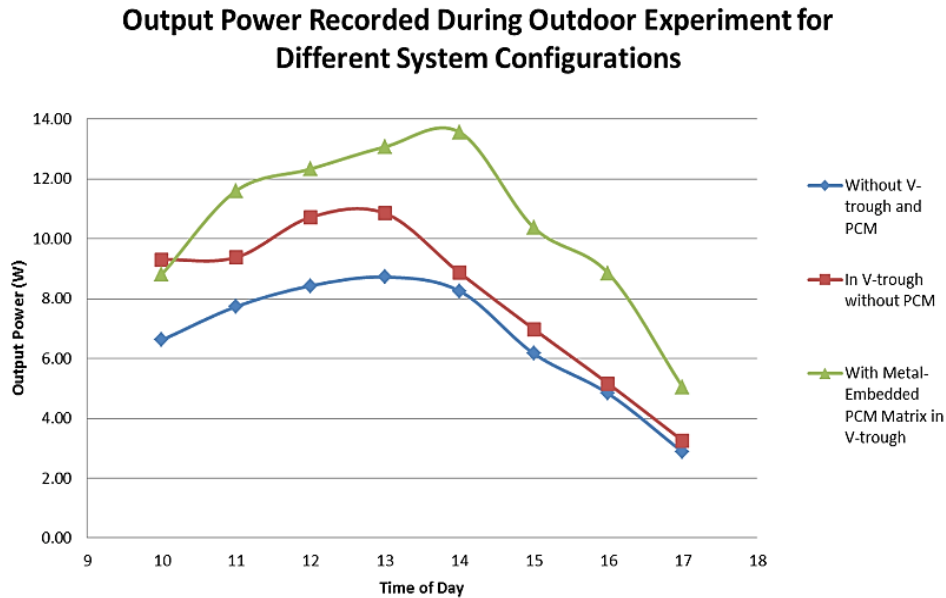


Fig. 3. 48 Output power data of different system configuration taken from (Maiti et al. 2011).

Ho et al. (2012) conducted a numerical investigation on MEPCM incorporated in a building structure to realize the thermal and electrical performances of BIPV module under various operating parameters. The significance of PCM melting point choice to match the operating conditions was addressed and proved to be influential on the PCM phase transition cycle completion. In a more recent study, the effectiveness of using a layer of water-saturated MEPCM as a passive thermal management medium for BIPV was explored by Ho et al. (2013). Improvement in average electrical efficiency of 2% over the corresponding efficiency for a reference PV module

was achieved through integrating a layer MEPCM with a melting point of 30°C and thickness of 30 mm. PCM with water circulation integrated at the rear of the PV module was as well examined by (Bouzoukas 2008). Among other approaches to cool PV systems PCMs presented fair performance improvements leading to enhanced electrical efficiency and low heat loss coefficient as compared to that of air-, water-, and heat pipe-based systems investigated.

3.1.5 Thermoelectric (PV-TE) Systems

Thermoelectric (TE) modules are solid-state semiconductor devices that are able to convert thermal energy directly into electrical energy or vice versa. A TE module comprise of thermoelectric elements made of two dissimilar semiconductors, p- and n-type junctions connected electrically in series and thermally in parallel (Hamid Elsheikh et al., 2014). TE modules possess salient features of being compact, lightweight, noiseless in operation, highly reliable, maintenance free and no moving or complex parts (Omer, 1998), (Hamid Elsheikh et al., 2014), (Omer and Infield, 2000), (Riffat, Omer, and Ma, 2001), (Kane and Verm, 2013). Such devices are categorized into two types of converters depending on the energy conversion process; *Thermoelectric Generators* (TEGs), generating electricity from a temperature gradient, and *Thermoelectric Coolers* (TECs), converting a direct current into

a temperature gradient (Omer and Infield, 2000), (Ahiska, Dislitas, and Omer, 2012), Fig. 3.40.

Thermoelectric generators have potential in waste heat recovery from power plants, automobile vehicles, and solar energy applications where direct heat-to-electricity conversion can occur using a phenomenon called the *Seebeck effect* (Harman, 1958), (McEnaney et al., 2011), (Kraemer et al., 2012), (El-Genk and Saber, 2002). For the past 10 years several studies have been conducted to investigate the feasibility of incorporating TEGs with PV technology in a combined cell-scale, flat plate, or even concentrator type systems to harvest energy through thermal waste utilization (Vorobiev et al., 2006), (Leonov et al., 2010), (Zhang and Chau, 2011), (Chávez-Urbiola et al., 2012), (Deng et al., 2013), (Li et al., 2014). On the other hand, thermoelectric coolers have been widely used in electronic devices and medical instruments as they are capable of providing refrigeration and temperature control for such devices allowing them to operate at a certain temperature level utilizing the *Peltier effect* (Kane and Verm, 2013), (Najafi and Woodbury, 2013), (Choi, Ko, and Chung, 2010), (Xi, Luo, and Fraise, 2007). In this section, a review on the most recent advancements of incorporating of TE modules with PVs to aid lower temperature regulation using TE coolers (TECs) or energy harvesting through direct thermal-to-electricity conversion through TE generators (TEGs) are presented.

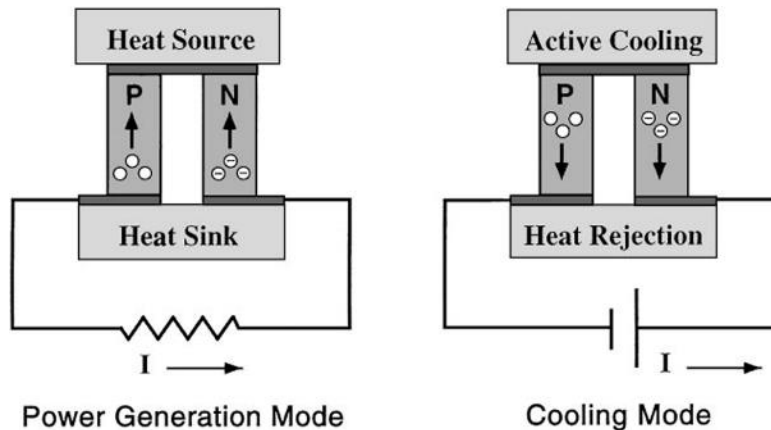


Fig. 3. 49 Operation modes of thermoelectric TE module (Nolas et al., 1999).

TE coolers operate in such way that supplying a low DC voltage to a TEC module enables heat to transfer from one side to the other. Incorporation of TE coolers with PV modules have been studied extensively for refrigeration and temperature management systems, however; these systems are out of the scope of this work. A comprehensive review on PV-driven TEC systems is available in (Xi, Luo, and Fraise, 2007). Meanwhile, limited research has been done in the application of TE coolers to regulate the temperature of PV cells. The most common design of TE cooler for PV (PV-TEC) systems comprise of TEC module installed at the rear PV cell with aluminium sheet in between so as to spread the heat dissipated at the back surface of the PV cell, Fig. 3.41 (Kane and Verm, 2013), (Najafi and Woodbury, 2013), (Choi, Ko, and Chung, 2010). In such system, a fraction of the generated power by the PV cell is fed to the TEC module to provide the necessary cooling effect for the PV cell. The cooling effect of a TEC module

considered a TEC module attached to the back side of a single PV cell, Fig. 3.41. The model was used to estimate the temperatures within the system, the required power to supply the thermoelectric cooling module, and the additional power produced by PV cell due to the cooling effect. Evaluation of power saving due to temperature reduction in the PV cell minus the utilized power by the TEC module was estimated through genetic algorithm based optimization in which an optimum value of the supplied electrical current for the TEC module was estimated. This leads to the maximum net generated power at a specific operating condition. Results revealed that additional power due to cooling was generated, nevertheless, for the optimal current the cooling effect was insignificant and the temperature reduction did not exceed 8 °C. Moreover, it was noted that the performance of the system strongly depended on the figure of merit of the TE module.

Kane et al. (2013) utilized TE coolers to aid cooling of PV modules in a building integrated system. A dynamic model of the BIPV/TE system with consideration to PV panel temperature was developed to assess the performances improvement of the TE coolers on PV. The BIPV/TE system comprised of TE module attached at the back of PV module with heat sink attached to the other side of the module to increase heat transfer process. Results revealed that BIPV/TE combined system can be operated at 53 °C PV module temperature without loss of PV power thus module can be cooled

down by 10 °C which will enhance life of PV module, and therefore its performance.

Thermoelectric coolers for improved performance of building integrated photovoltaic (BIPV) modules were investigated experimentally by Choi et al. (2010). As control of thermoelectric elements can be regulated independently in an outdoor environment using a micro-controller, the operating temperature of PV cells can be maintained near the characterizing temperature of 25 °C. A control algorithm was built to control the DC current fed into the TE module to achieve the required cooling effect. Comparison between BIPV modules using a ventilator and thermoelectric elements was presented. The TEC was operated when the temperature of the BIPV module exceeds a set temperature, hence operating the BIPV module within the control value only during days with high radiation to achieve additional net power generation. Experimental results showed that average module temperature of 24.48°C was observed for the BIPV system using a thermoelectric element, while that with ventilator attained average module temperature of 33.31°C. The output power of the BIPV system was observed to be higher than that with the conventional method and the efficiency of BIPV system was increased.

On the other hand, the incorporation of TE generators with PV cells has been studied extensively to harvest the solar energy available for the sun. In

an investigation on the possibility of using TEGs in solar hybrid system carried out by Vorobiev et al. (2006), two distinctive designs were theoretically studied, Fig. 3.42. To increase the electricity production in PVT the author suggested directing the heat flux originating between the PV module and heat extractor through thermoelectric generator. In the first model the PV cells operated at low temperature, and the thermal solar radiation was concentrated onto the hot side of the elevated temperature stage (HTS). Therefore, high temperature can be converted to electrical energy through the use of TEGs as the HTS. On the other hand, the second design considered was a system without solar spectrum division, in which PV cells operate at high temperature. The investigation considered two types of PV cell technologies; GaAs single junction cell for model (A), and multi-junction GaAs-based cell for model (B) with corresponding room temperature efficiencies of 24% and 30% respectively under concentration ratio of 50 Suns. Predicted results showed that model (A) was able to enhance overall system efficiency by 5–10% while model (B) with PV cells operating at high temperature did not exhibit much influence on improving the overall conversion efficiency. The investigation however, relayed on theoretical calculation for the investigated models without experimental justifications besides, predictions were given for TEG modules with assumed high figure of merit that are not available in current stage of TEG technology.

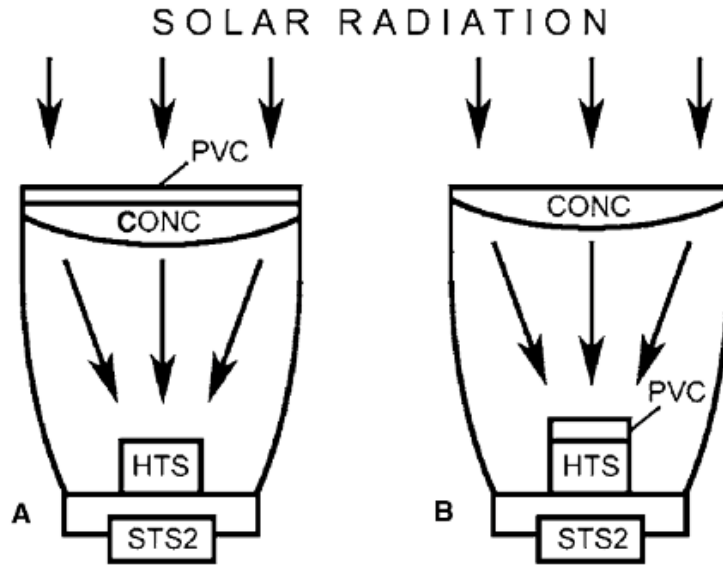


Fig. 3. 51 Incorporation of TE generators with PV cell (a) non-concentrated (b) concentrated (Vorobiev et al. 2006)

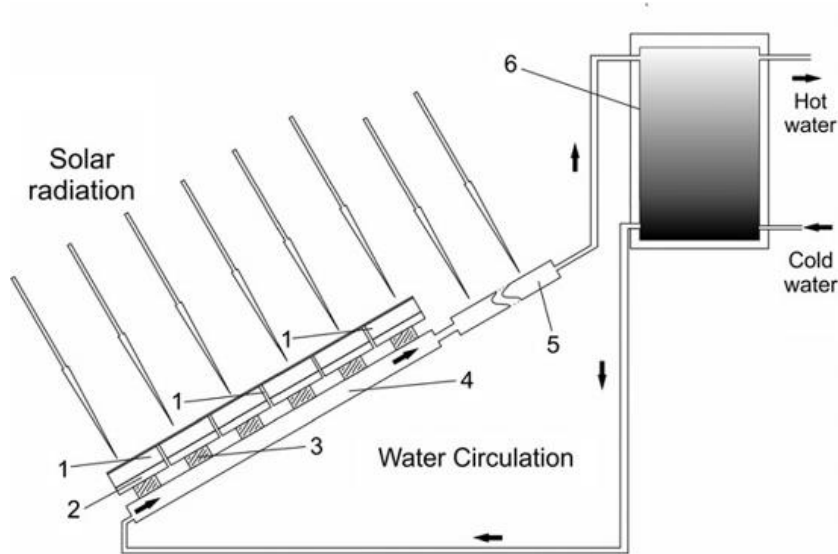


Fig. 3. 52 A scheme of hybrid PV/T system with TEGs: (1) solarcell, (2) cell's back electrode, (3) TEG, (4) heat extractor, (5) plane collector, (6) thermal tank (Chávez-Urbiola et al., 2012).

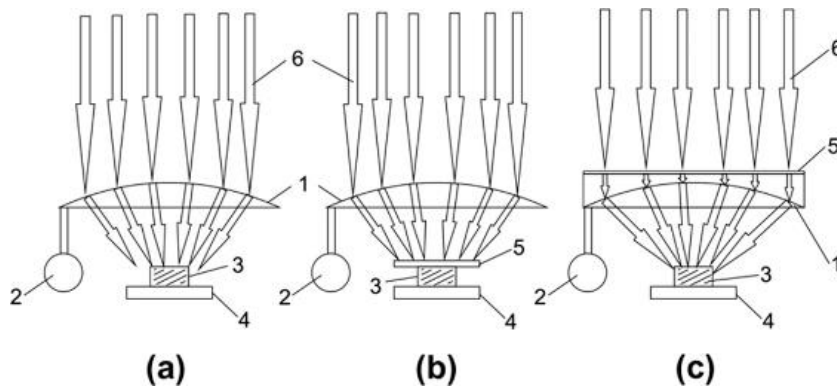


Fig. 3.53 Scheme of hybrid system with TEG and concentrated solar radiation: (1) concentrating lens, (2) tracking system, (3) TEG, (4) heat extractor, (5) PV panel, (6) solar radiation

Adopting similar design as in (Vorobiev et al. 2006), an experimental investigation was performed to assess the integration of TEGs in a solar hybrid system in (Chávez-Urbiola et al., 2012). The model utilized the heat generated under one sun in each PV cell and passed it through individual TEG that have good thermal contact with this cell from one side, and with heat extractor from the other side. The general scheme of the system is shown in Fig. 3.43, where direct non-concentrated sunlight falls onto the PV panel where each cell possesses a back electrode with high thermal conductivity. The electrodes have direct thermal contact with the hot plate of corresponding TEG. It was noted from the efficiency estimations that with traditional TEGs, one cannot expect significant improvement in electrical efficiency. Due to heat flux losses on the way to TEG, the expected increase of electrical efficiency provided with this TEG model ($ZT=0.7$) was around 1%. Taking the value of ZT equal to 2.4 larger increase due to TEG of 3.2%

will be obtained; with $ZT=4$, the efficiency will be 4.1%. Thus, the use of existing traditional TEGs in the system studied cannot be really effective, but the advanced TEG might be useful. The authors extended their research to investigate the potentials of achieving better conversion efficiency through concentrated radiation based on three different geometries shown in Fig. 3.44. From the results obtained it was observed that the conversion efficiency of TEG in concentrated sunlight comparable to that of commercial PV panels can be achieved as presented in Table 3.1. Although the cost of TEGs currently is slightly higher than that of PV modules of equal surface area, critical reduction can be attained taking into account area reduction of TEG at concentrated irradiation. The second system utilizing concentrated illumination is represented by Fig. 3.44 (b) in which both PV module and TEG work in concentrated irradiation and at elevated temperature, the efficiency of PV decreases with an increase of temperature whereas the TEG's efficiency increases. Therefore, an optimal temperature corresponding to the maximum value of electrical efficiency of the whole device and depending upon the parameters of its components can be identified, Fig. 3.45. In relation to the hybrid system shown in Fig. 3.44 (c) a transparent a-Si based PV modules with efficiency of 10% and low temperature coefficient compared to c-Si PV modules were used, such modules have the advantage of withstanding high temperature due to the high concentration ratios. The

thermal part of the solar spectrum that passes through the cell was determined by the value of band gap, in which for a-Si was 1.6 eV (45% taking into account reflection losses). As per Table 3.1 the system design (c) in Fig. 3.44 can be quite efficient with PV cells made of semiconductor with higher band gap such as CdSe, and using TEG with advanced materials.

Table 3. 3 Efficiency of TEG-based concentrator systems for maximum irradiance (Chávez-Urbiola et al., 2012).

| System | Concentrator-TEG | | PVM-Concentrator-TEG | |
|------------------|------------------|------|----------------------|------|
| PV | – | – | a-Si | a-Si |
| ΔT (K) | 150 | 250 | 150 | 250 |
| x-ratio | 55 | 95 | 122 | 211 |
| $\eta_{0.7}$ (%) | 4 | 6 | – | – |
| $\eta_{2.4}$ (%) | 12.4 | 15.3 | 15.6 | 17 |

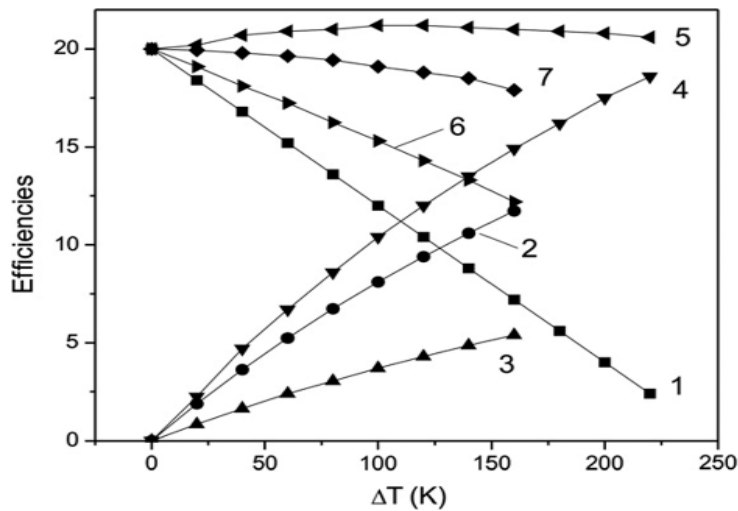


Fig. 3. 54 Calculated temperature dependence efficiency as function of the temperature difference: (1) PVcells, TEG with different $ZT=2.4$ curve (2) 0.7curve (3), and 4 curve (4), total efficiency with different TEGs ($ZT=4$ curve (5), 0.7curve (6), and 2.4 curve (7) . (Chávez-Urbiola et al., 2012)

Sark (2011) conducted theoretical investigation on the feasibility and performance enhancements utilizing thermoelectric converters for electricity generation in a PV integrated system. A hybrid module was formed by attaching a series of low temperature thermoelectric converters (i.e. $ZT \geq 1$ at 300 K) to the rear surface of a PV module to utilize thermal waste available from the module. To maintain temperature difference of about 50-60 °C across the TE convertor plates, the converters were mounted on a heat sink to keep the cold plate cooled convectively. The developed model takes into account the influences of irradiance, temperature, and figure of merit on the performance of the PV-TE hybrid module. Results revealed that for the current near-maximum value of $Z=0.008K^{-1}$ additional efficiency of 1.53% was estimated by incorporating thermoelectric converters, while for the current maximum value of $Z=0.004K^{-1}$, PV-TE efficiency of 14.03% was estimated, which resembles the generated power when the PV module was operating at a constant temperature of 25 °C (STC), Fig. 3.46. The annual performance of the developed system for two cities, namely; Malaga, Spain, and Utrecht, the Netherlands was also evaluated using set of hourly average irradiances and daily ambient temperature and an increase by 14.7% and 11%, for Malaga and Utrecht, respectively was found through the integration of TE converters. Nevertheless, the model ignored the influence of radiation loss through top cover and assumed that

the temperature at the hot side of the TE converter equaled the ambient temperature, which may not be realized in practice.

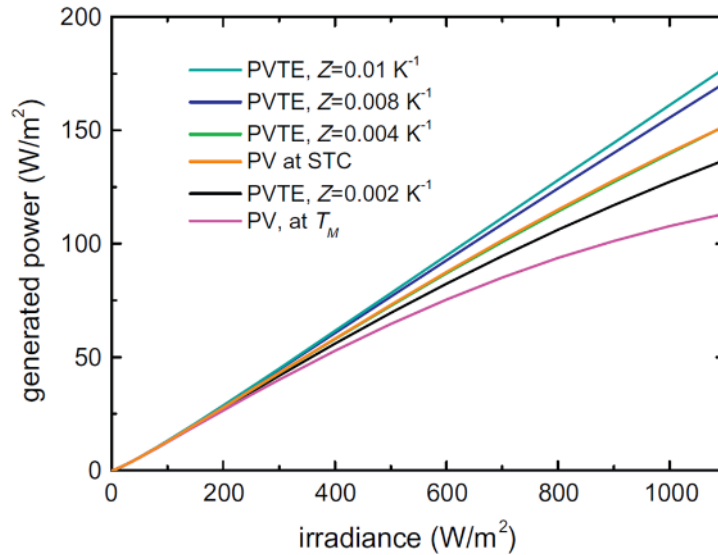


Fig. 3. 55 Generated PV-TE power as a function of irradiance for four values of the figure of merit Z , and generated PV power as a function of irradiance at STC and module temperature (Sark, 2011)

More recently, experimental and theoretical investigation on solar hybrid generation system consisting of 170 mm 40 mm silicon thin film solar cell, thermoelectric generators, and heat collector was conducted by (Deng et al., 2013b). The hybrid system developed was in principle similar to the PV-TE hybrid module discussed earlier by (Sark, 2011), however, an optimized heat collector design with three layers namely; absorbing, conducting, and insulation layers was introduced to obtain larger temperature difference across the TEG, Fig. 3.47. The absorbing layer was used to enhance the absorption of sun light, and for that purpose three distinct types of heat

absorbing layer were tested, namely; Graphite, optical-thermal thin film, and black polymer tape. A bowl-shaped copper foil was fabricated and fixed to the side and back of the solar cell to accelerate heat conduction to the TEG, while a layer of foam was applied to prevent heat loss. To enhance heat dissipation and maintain larger temperature difference across the TEG plates, both aluminium fin heat sinks attached at the cold side of converter and water cooling was investigated. To assess the performance of the TEG in the hybrid system the open circuit voltages and short circuit currents for the design with black polymer tape as an absorbing layer and aluminium fins to cool the TEG were recorded in Table 3.2. Results showed that the integrated design had an enhanced overall performance. The numerical simulation performed on TEG estimated increased heat flux on the hot side of the converter by more than tenfold using the optimized thermal collector design.

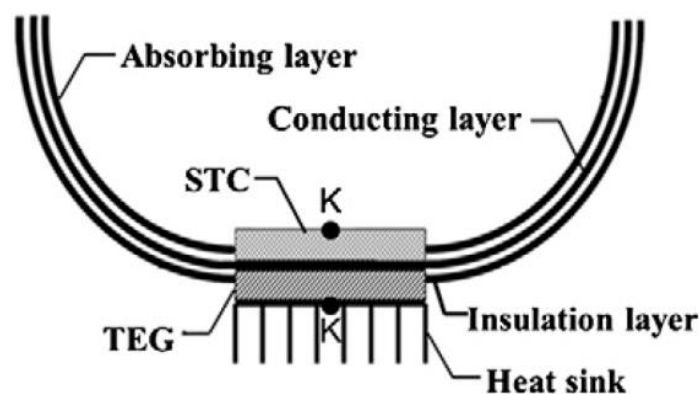


Fig. 3. 56 Schematic of PE-TE hybrid module (Deng et al., 2013b)

Table 3. 4 Performances of TEG, solar cell and hybrid PV-TE module (Deng et al., 2013b)

| | FF | Voc (V) | | Isc (A) | | Pmax (W) | |
|----------------------|------|---------|--------|---------|--------|----------|--------|
| | | Max | Stable | Max | Stable | Max | Stable |
| TEG | 0.24 | 3.25 | 0.86 | 0.26 | 0.07 | 0.204 | 0.146 |
| Solar Cell | 0.43 | | 2 | | 0.22 | | 0.189 |
| Hybrid module | - | | - | | - | 0.393 | 0.204 |

3.2 Discussion

Various methods can be employed to achieve cooling action for PV systems. However, the optimum cooling solution is critically dependent on several factors such as, system arrangement, PV technology employed, types of concentrators' geometries, and weather condition at which the system is installed. Hybrid PV System offer a practical solution to increase the electrical power production from PV panels and reduce the heating loads, in addition to the recovery of heat extracted from the panels. Heat extraction from PV modules utilizing various mechanisms was presented. Various designs employing air, liquid, heat pipe, PCM, and thermoelectric modules to aid cooling of PV cells were discussed along with the parameters influencing the system performance.

Air cooling of PV system provides a simple technique to thermally regulate the temperature of PV cells owing to minimal use of material and low operating cost among other PV cooling technologies. Forced air enhances heat extraction resulting in further improved performance of air PVT systems when compared with naturally ventilated ones at the expense of some parasitic power losses introduced due to the use of air blowers. Nevertheless, the low density and small heat capacity of air, limits the improvements in the performance of air PVT collectors making air less favourable option. On the other hand, liquid cooling offers a better alternative to air cooling utilising coolant allowing a more efficient utilization of thermal energy captured. In addition, liquid-based PVT collectors offer less temperature fluctuations compared to air-based PVT making them more favourable in aiding a homogenous temperature distribution on the surface of PV modules. Water is the most common fluid employed in liquid-based cooling of PV systems; however, refrigerants that are able to undergo phase change at a relatively low temperature have been practically investigated and offered better performance. The use of heat pipe cooling of PV cells aids a uniform temperature distribution of PV cells in addition to elimination of freezing that thermosyphon tube used in water-based cooling. PCMs however, offer both high heat transfer rates and heat absorption due to latent heating, which make them attractive for PV cells cooling application.

The incorporation of thermoelectric devices with PV systems seems very attractive when operating at generation mode, however, the supplemental energy generated by the thermoelectric device requires large temperature difference across the hot and cold plates of the device, making improvement in performance limited with the current technologies available.

3.3 Conclusions

The conclusions from the reviewed literature are summarised as follows:

- Solar PV systems benefit from the abundant supply of solar energy; hence PV technology has immense potential to tackle ever increasing energy demands. Nevertheless, heating of PV cells is considered one of the main challenges towards widespread applications.
- Elevated temperature can cause serious degradation to the PV performance, hence cooling of the PV cells must be an integral part of PV systems for efficient operation.
- Cooling of PV cells can be achieved through various techniques; passively, actively, or both working in tandem, with various degrees of cooling capabilities and system complexity.

- Air cooling techniques are considered mature and have been applied in diverse designs, however, improvements in the PV performance are limited due to low density and small heat capacity of air.
- Liquid cooling offers a better alternative to air cooling to accommodate larger margins of temperature rise in addition to efficient capture of thermal energy. However, water in many situations is limited.
- Phase change materials have been applied widely to electronic components for thermal management, and ideas have emerged to assess integration with PV technology, however, the utilisation of the thermal energy is complicated, due to the bulkiness of such integration, introducing further complexities and challenges.
- Heat pipes are attractive heat transport mediums functioning as highly concentrating heat exchangers based on the ratio of the evaporator to condenser sections, and thus, heat pipes promote efficient waste heat recovery. Heat pipes are mainly integrated for electronics cooling and realized in many water heating applications.
- Thermoelectric modules have been widely implemented for waste heat recovery applications as power generators, however, they are limited by the operating temperature. Nevertheless, they are solid devices with no moving parts or chemical reactions therefore less

maintenance required due to wear and corrosion. In addition, TEGs are also considered one of the few options for direct thermo-electrical conversion.

The list of advantages and disadvantages of each of the cooling technologies for PV cells discussed earlier are given in Table 3.3. A summary of some of the various systems that have been reviewed is provided in Table 3.4.

Table 3. 5 Advantages and disadvantages of different thermal management techniques (Makki, Omer, and Sabir, 2015)

| | Natural air circulation | Forced air circulation | Liquid cooling | Heat pipes | Thermoelectric Cooling | PCM |
|----------------------|---|--|---|---|---|---|
| Advantages | <ul style="list-style-type: none"> - Passive heat exchange - Low initial cost - No maintenance - Easily integration - Longer life - No Noise - No electricity consumption | <ul style="list-style-type: none"> - Higher heat transfer rates compared to natural circulation of air - Independent of wind direction and speed - Higher mass flow rates than natural air circulation achieving high heat transfer rates - Higher temperature reduction compared to natural air | <ul style="list-style-type: none"> - Higher heat transfer rate compared to natural and forced circulation of air - Higher mass flow rates compared to natural and forced circulation of air - Higher thermal conductivity and heat capacity of water compared to air - Higher temperature reduction | <ul style="list-style-type: none"> - Passive heat exchanger - Efficient heat transfer - Simple - Easy to integrate | <ul style="list-style-type: none"> - No moving parts - Noise Free - Small size - Easy to integrate - Low maintenance costs - Solid state heat transfer | <ul style="list-style-type: none"> - Higher heat transfer rates compared to both forced air circulation and forced water circulation - Higher heat absorption due to latent heating - Isothermal natural of heat removal - No electricity consumption - Passive heat exchange - No maintenance cost |
| Disadvantages | <ul style="list-style-type: none"> - Low heat transfer rates - Accumulation of dust in inlet grating further reducing heat transfer - Dependent on wind direction and speed - Low thermal conductivity and heat capacity of air | <ul style="list-style-type: none"> - High initial cost for fans, ducts to handle large mass flow rates - High electrical consumption - Maintenance cost - Noisy system - Difficult to integrate compared to natural air circulation system | <ul style="list-style-type: none"> - Higher initial cost due to pumps - Higher maintenance cost compared to forced air circulation - Higher electricity consumption compared to forced air circulation - Leakage and pressurization issues | <ul style="list-style-type: none"> - Expensive - Dust accumulation on the inlet grating - Dependent of wind speed and direction - Dry out - Hot spots - Leakage | <ul style="list-style-type: none"> - Heat transfer depends on ambient conditions - No heat storage capacity - Require electricity - Requires efficient heat removal from warmer side for effective cooling - Costly for PV cooling | <ul style="list-style-type: none"> - High PCM cost - Some PCMs are toxic - Some PCMs have fire safety issues - Some PCMs are strongly corrosive - PCMs may have disposal problem after their life cycle is complete |

Table 3. 6 Summary of some of the various systems reviewed

| | Work | Configuration | PV Type | Electrical Efficiency | Thermal Efficiency | PV cell temperature |
|-------------------|--|---|------------|----------------------------|--------------------|---------------------|
| Air-Based | Dubey et al. | Glass-to-glass PV (forced air) | N/A | 10.41% | N/A | 55-75 °C |
| | Tonui and Tripanagnostopoulos | Unglazed PVT with metal sheet at the middle of the air channel (Natural Convection) | Pc-Si PV | 1-2% Impr. | 13% | 3 °C(drop) |
| | | Glazed PVT with metal sheet at the middle of the air channel (Natural Convection) | Pc-Si PV | 4% Impr. | 12% | 4 °C(drop) |
| | | Unglazed PVT with finned metal sheet at air duct (Natural Convection) | Pc-Si PV | 1-2% Impr. | 18% | 3 °C(drop) |
| | | Glazed PVT with finned metal sheet at air duct (Natural Convection) | Pc-Si PV | 10% Impr. | 40% | 10 °C(drop) |
| | Solanki et al. | PVT air solar heater | Mc-Si PV | 8.40% | 42% | 10 °C drop |
| | Bambrook and Sproul | PVT with open loop single pass duct and extraction fan | Mc-Si PV | 10.6-12.2% | 28–55% | 22-28 °C |
| | Amori, and Al-Najjar | PVT with single pass air duct | Mc-Si PV | 12.3%(Winter), 9% (Summer) | 19.4%(W), 22.8%(S) | N/A |
| | Min et al. | Concentrator PV with metal plates heat sink (400x) | MJ PV | N/A | N/A | 37 °C |
| | Al-Amri and Mallick | Triple-junction solar cell with forced air cooling (100x) | MJ PV | N/A | N/A | 150 °C |
| Rajoria et al. | Micro-channel PVT tiles (Case III) | Mc-Si PV | 11.30% | N/A | N/A | |
| Rajoria et al. | Micro-channel PVT tiles | Mc-Si PV | 6.5% Impr. | 18.1% Impr. | | |
| Othman et al. | Air-based PVT module with honeycomb heat exchanger | Mc-Si PV | 7.13% | 87% | 4 °C drop | |
| Water-Based | Chow et al. | PVT collector with aluminium-alloy flat-box | Pc-Si PV | 10.3–12.3% | 37.6–48.6% | N/A |
| | Chow et al. | Vertical wall-mounted water-based PVT | Pc-Si PV | 9.39% | 37.50% | N/A |
| | Ibrahim et al. | PVT collector with spiral flow | Pc-Si PV | 11% | 64% | N/A |
| | Zhu et al. | Dielectric liquid immersion cooling for CPV | Mc-Si PV | N/A | N/A | 49 °C |
| Refrigerant-Based | Ji et al. | PVT solar-assisted heat pump co-generation with R22 | Mc-Si PV | 12% | 50% | N/A |
| | Zhao et al. | PV/evaporator roof module of heat pump system with R134a | Mc-Si PV | 9.21% | 60.93% | N/A |
| | Zhang et al. | PV/loop-heat-pipe (PV/LHP) heat pump solar system | N/A | 10% | 40% | N/A |
| | Xu et al. | Low concentrating PVT with heat pump (LCPVT-HP) using R134a | N/A | 17.5±0.4% | N/A | 51 °C |

Chapter 3 Advancements in Hybrid Photovoltaic Systems

| | | | | | | |
|-----------------|---|---|------------|-------------|--------|------------------------|
| Heat Pipe-Based | Akbarzadeh and Wadowski | Heat pipe cooling for CPV 20x | N/A | N/A | N/A | 46 °C |
| | Anderson et al. | Heat pipe with aluminium fins cooling for CPV | N/A | N/A | N/A | 43 °C above ambient |
| | Hughes et al. | Finned heat pipe and natural convection for flat plate PV | N/A | N/A | N/A | 30 °C |
| | Pei et al. | Heat pipe PVT collector with R600a (part of a solar assisted heat pump) | N/A | 9.50% | 23.80% | N/A |
| | Pei et al. | Heat pipe cooling for flat plate | N/A | 10.20% | 45.70% | N/A |
| | Wu et al. | Heat pipe cooling for flat plate | N/A | 8.45% | 63.65% | N/A |
| | Redpath et al. | Compound parabolic concentrating solar PVT (CPC-PVT) with heat pipe | N/A | 2.5% Added | N/A | N/A |
| Huang et al. | flat plate heat pipe for CPV | N/A | 3.1% Impr. | N/A | N/A | |
| PCM-Based | Huang et al. | Flat plate PV with PCM | N/A | N/A | N/A | 37.5 °C |
| | Huang et al. | Flat plate PV with finned PCM | N/A | N/A | N/A | 27 °C |
| | Huang | BIPV with container having two PCM separated in triangles | N/A | N/A | N/A | 28 °C |
| | Hassan et al. | Flat plate PV with PCM | N/A | N/A | N/A | 18 °C(drop) |
| | Maiti et al. | V-trough metla-wax matrix Flat plate PV with PCM (1.7x) | N/A | N/A | N/A | 65 °C |
| | Ho et al. | MEPCM incorporated in a building structure for BIPV | N/A | N/A | N/A | 30.5 °C (W), 47 °C (S) |
| Ho et al. | BIPV integrated with a layer of water-saturated MEPCM | N/A | 2% Impr. | N/A | N/A | |
| TE-Based | Najafi and Woodbury | PV cell with TE cooler | N/A | N/A | N/A | 8 °C drop |
| | Arati Kane et al. | BIPV with TE cooler | N/A | N/A | N/A | 53 °C PV(10 °C drop) |
| | Choi et al. | BIPV with TE cooler | N/A | N/A | N/A | 24.48 °C |
| | Cha´vez-Urbiola et al. | PV cell with TE generator | c-Si PV | 1% Added | N/A | N/A |
| | Van Sark et al. | Combined PV-TEG | N/A | 8–23% Impr. | N/A | N/A |

Chapter 4

Proposed System Design and Research Methodology

The conclusions reached from the review of the literature highlight the challenges solar heat introduce in solar photovoltaic systems. The limitations are challenged in this research; building on various techniques implemented to improve the operating temperature of PV module in hot climates. The integration of Heat Pipe-based PV/TEG collector is therefore presented and discussed along with the operating principle adopted. Execution of the research through both theoretical analysis and empirical investigation is deliberated in order to facilitate implementation of the tasks of each stage within this research to accomplish the aim of this investigation.

4.1 Proposed System Design and Operation Principle

4.1.1 Proposed System Design

The system proposed suggests the integration of a Photovoltaic (PV) module and thermoelectric generation modules (TEG) as a cooling strategy, in an attempt to improve the operating temperature of the PV cells, Fig. 4.1 (a). The absorber of the PV-TEG collector consists of a PV module serving as power generator as well as thermal absorber. Heat pipes were attached to the rear to extract excessive heat accumulating on solar cells, therefore providing cooling to maintain the cells at a desirable operating temperature. The extracted heat is transferred via boiling-condensation process to a bank of TEG modules attached to the condenser section of each heat pipe, and waste-heat is recovered via direct conversion of the temperature difference across the TEG plates to electrical energy. The layers from which the collector consists of are depicted in Fig. 4.1 (b). A layer of PV cells is laminated onto the surface of an aluminum plate base panel. In between the PV layer and the aluminum base panel a layer of black tedlar-polyester-tellar (TPT) exists in addition to a transparent TPT and ethylene-vinyle-acetate (EVA) layers laid at the top of the

PV cells. Such TPT layers play role in the electrical insulation of the PV cells in addition to enhancing the absorption of solar radiation (Wu et al., 2011). Anterior to the PV cells, a transparent cover of glass is used preventing entry of dust particles and rain. The evaporator sections of the heat pipes are attached to the rear of the PV module using aluminum base panels serving as fins, enlarging the heat transfer area at the evaporator section of the heat pipe. The sheets are fabricated with a groove for the heat pipe to sit in with thermal grease applied to fill air gaps and improve thermal heat conduction. Moreover, thermal insulation layer (mineral wool) is placed underneath the aluminum plate to minimize thermal losses. All these layers are integrated into one module and are enclosed in a weather tight system.

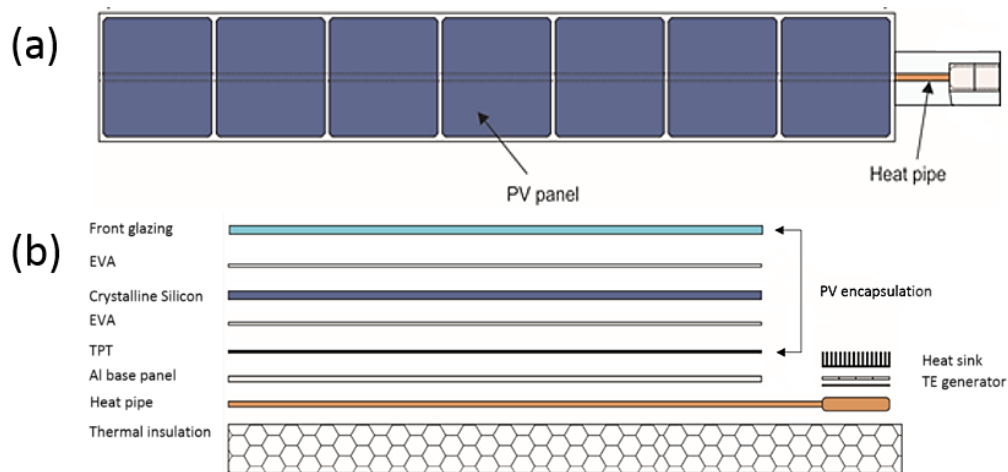


Fig. 4. 1 (a) PV module with heat pipes attached at rear (b) Side section view for heat pipe-based PV/TEG collector with technologies incorporated.

To maintain sufficient temperature difference across the TEG plates, a fan-heat sink assembly is attached at the cold plate of the TEG, Fig.(s) 4.2-3. The system schematic showing how the heat pipes are spaced and attached to the rear of the PV module is given in Fig. 4.3 (a), while Fig. 4.3 (b) illustrates the layout of the waste heat recovery system attached to the condenser section of heat pipe. The incorporation of the TEG module with the condenser section of the heat pipe is shown in Fig. 4.2, while the fan-heat sink assembly components are depicted in Fig. 4.4.

An aluminum heat exchanging block is utilized to contain the condenser section of the heat pipe, and thus, thermal energy is transferred to the TEG hot plate attached to the aluminum block via conduction. The use of heat pipes in such design permits converting low heat flux absorbed from the PV module into high heat flux by changing the ratio of the evaporator to condenser areas at an almost constant temperature (He et al., 2012). The fan-heat sink assembly is attached to the cold plate of the TEG module to maintain sufficient temperature difference across the TEG plates. The power generation capability of the thermoelectric generator is majorly influence by the temperature difference available, hence the addition of the blowing fan for improved heat extraction.

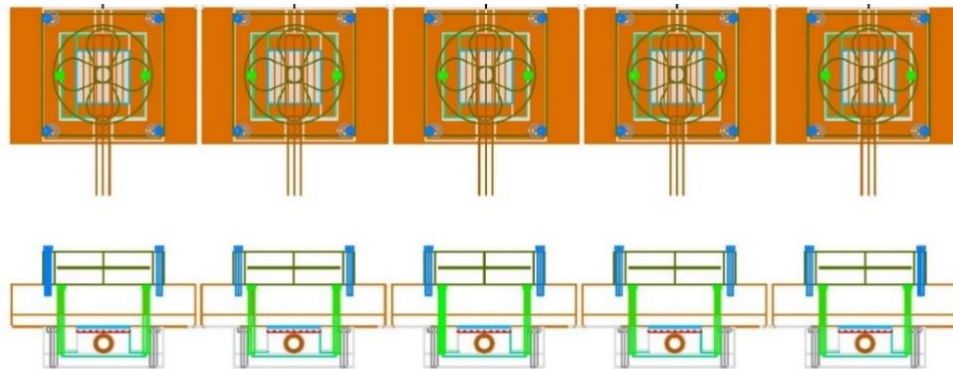


Fig. 4. 2 Heat recovery system utilizing heat pipes and thermoelectric generators of PV cooling

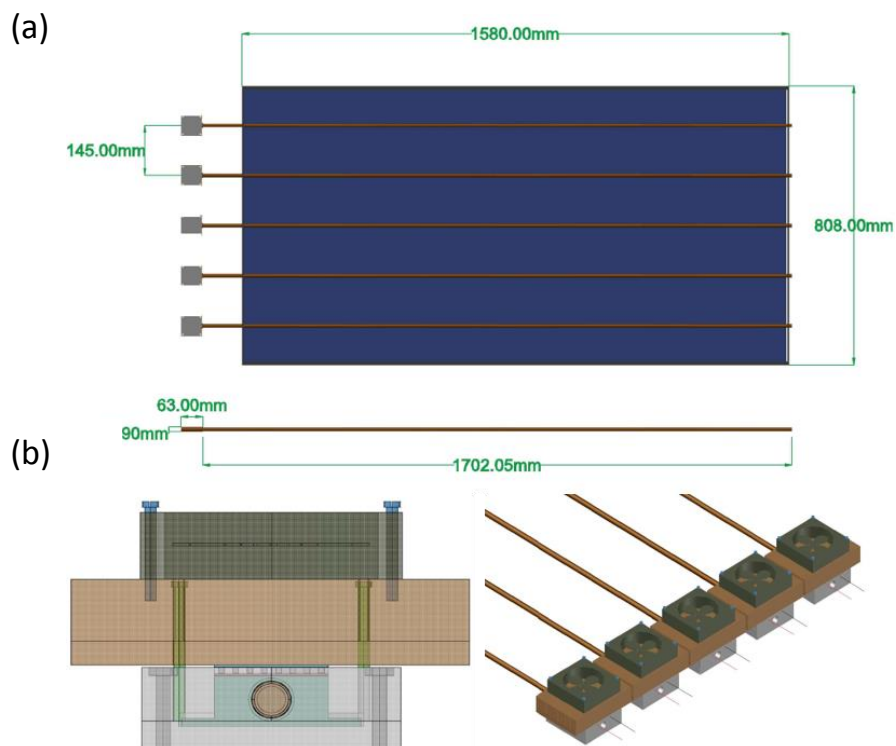


Fig. 4. 3 (a) Top view of collector proposed showing 5 heat pipes attached at rear. (b) TEG-fan heat sink assembly for waste heat recovery front view and layout

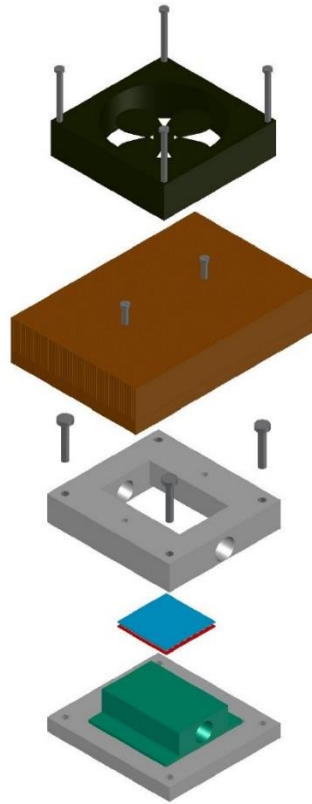


Fig. 4. 4 TEG-fan heat sink assembly

4.1.2 Operation Principle

As solar radiation passes through the transparent cover and strikes the PV layer, most of the radiation is absorbed by the PV cells and the black TPT layer. Part of the absorbed radiation is converted directly into DC electricity according to the Photoelectric effect of silicon PV cells, while the other part is dissipated as thermal energy and is conducted to the aluminum base panel, Fig. 4.5.

A relatively high transmittance from a wavelength of about 600-1100 nm can be absorbed from the spectrum, however, only part of this radiation contributes toward electricity conversion and the other portion is dissipated as heat, Fig. 4.6 (Tseng et al., 2011), (Oksengendler et al. 2009). On the other hand, the aluminum base substrate selective absorber has a markedly low reflectance in the wavelength range from 600-1100 nm (Wang et al., 2011). This indicates that the transmitted radiation through the PV cell can be well absorbed by the aluminum substrate with thermal absorption and reflectance of 95% and 5% respectively. Therefore, converting the residual radiation transmitted through the PV cells into thermal energy.

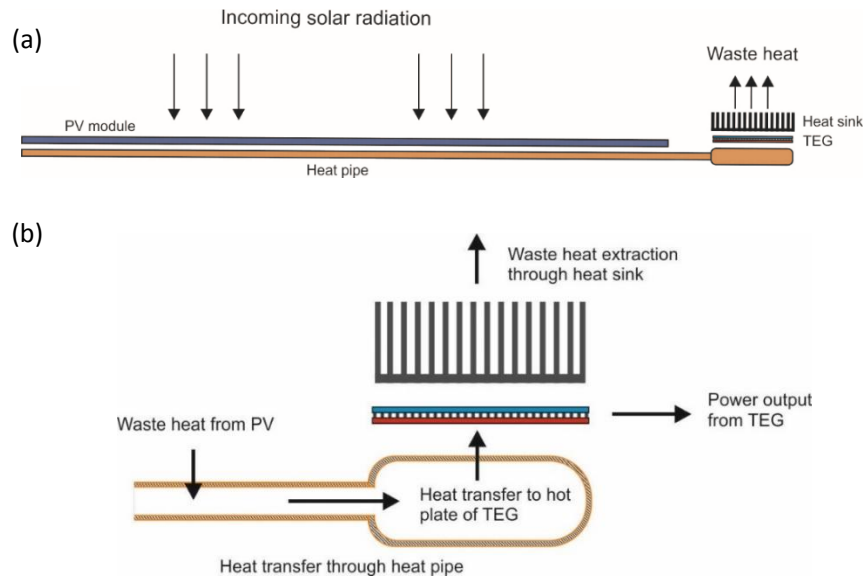


Fig. 4. 5 Operating principle; energy balance: (a) Heat pipe-base PV collector (b) TEG-fan heat sink assembly.

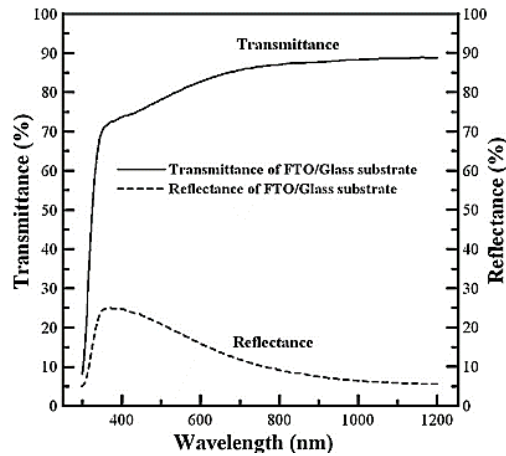


Fig. 4. 6 Optical transmittance and reflectance versus wavelength for the FTO/glass substrate (Tseng et al., 2011)

Heat available at the rear surface of the PV layer is conducted along the aluminum plate to the evaporator section of the heat pipe, and then the wall of the wick heat pipe evaporator section. The absorbed heat causes the working fluid inside the heat pipe to vaporize by the intense heat transferred from the wall evaporator section by convection. The generated vapor moves toward the wick heat pipe condenser section where it releases the evaporation latent heat and conducts thermal energy to the TEG module, Fig. 4.3 (b). Such arrangement allows the heat to be conducted to the TEG module through an efficiency boiling-condensation process of heat pipe and further electricity generation takes place through the Seebeck effect. Consequently, this hybrid design allows absorption of wide wavelength range of incident solar radiation, and hence leads to higher energy conversion efficiency.

Few researchers have investigated the integration of TEG modules with PV technology, however, mostly have adopted a small scale impractical approach; either by attaching a single TEG module to a PV cell, or populating the rear of a PV module to cover the whole surface area with TEG devices. As TEG modules available commercially are expensive, the investigated system proposed employment of heat pipes as a solution for minimal use of TEG modules possible in an attempt to promote the feasibility of the system for improved power supply. The integration of TEG modules directly to the rear a PV module can achieve better heat extraction and hence improved thermal management for the cell; promoting minimal thermal losses. However, the power generation cost is further increased due to the increased number of TEG modules utilized to cover the entire rear of the module, making such integration less attractive; solving one part of the problem while introducing other challenges.

Heat pipes are considered as absorbers for the thermal energy available from the PV module; facilitating thermal energy transport to the hot plate of the TEG module for supplemental power supply. Additionally, utilization of heat pipes within the proposed hybrid collector promotes a flexible design where the location of the TEGs are not limited to the surface requiring thermal management.

4.2 Research Methodology

The research was carried out through building insights of Photovoltaic technology and challenges encountered in such field at preliminary stages of the research; hence a qualitative research was carried out focusing on solar heat challenges on PV technologies and techniques to tackle the adverse temperature influence on the performance. On the other hand, quantitative methods were applied to quantify the performance and practicality of the system proposed. The quantitative methods considered in the research involve two sequential stages; the computer modelling stage, and the experimental testing stage. Computer modelling considered building a mathematical model for the purpose of simulation using MATLAB/SIMULINK packages to allow prediction of the system performance. Consequently, system prototype construction took place for the empirical study after the model is finalized and various results were obtained. In the following sub-sections, each stage is further clarified including the variety of results considered in this research. The summary of the process and tasks implemented in this investigation are presented in Fig. 4.7.

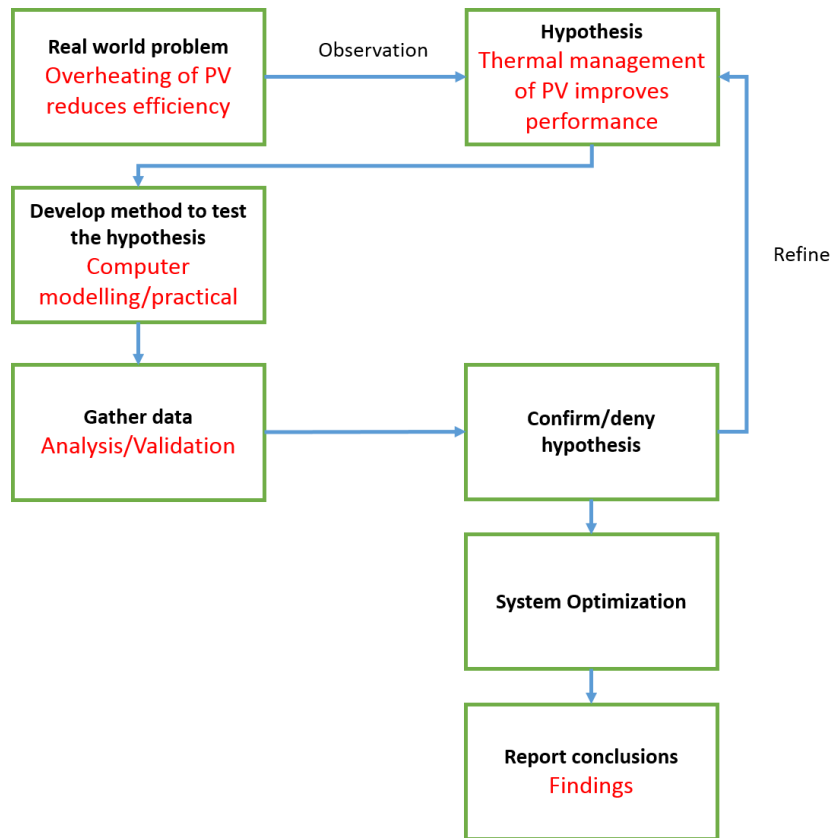


Fig. 4. 7 Research methodology adopted in this investigation

4.2.1 Computer Modelling

This stage involved studying each sub-system, component, and device involved in the proposed design, including mainly; PV modules, Thermoelectric Generators, and Heat Pipes. The theoretical study is conducted as per the diagram in Fig. 4.8. Problem formulation is considered the background and review of literature accomplished at an earlier stage; which led to the final

decision on the proposed system design. Moving on, construction of the system was partially completed by building the system structure graphically and studying the energy balance equations of each sub-system. Hence, the next step taking place involved the completion of the model construction using MATLAB/SIMULINK before model validation against empirical results. During the validation stage, assumptions made at the construction stage will be examined to better understand their influence on the system performance. In addition, the sub-systems (i.e. PV panel, thermoelectric generator, and heat pipe) were simulated individually to ensure their performance is in accordance to presumed results and to allow modelling of each sub-system at satisfactory level of details. The evaluation of the model to quantify the cooling system performance on the PV panels for various input conditions is presented and discussed for both theoretical predictions and experimental test in chapters 6 and 8 respectively.



Fig. 4. 8 Computer modelling development process

The theoretical study has been conducted as follow:

- ❖ A theoretical background research of technologies and components incorporated in the integrated hybrid collector including mainly, Solar Photovoltaics, Heat Pipes, and Thermoelectric Generation technologies, presented in Chapter 2.
- ❖ Reviewing theory of heat transfer and different modes of thermal exchange; namely, Conduction, Convection, and Radiation, and how such mechanisms are applied to solar thermal and PV systems.
- ❖ Derivation of differential equations for the energy exchange within the system components based on the energy balance concept, and applying finite difference numerical approaches for solutions.
- ❖ Integration of mathematical models of technologies incorporated in a suitable simulation environment allowing assessment of the model implemented.
- ❖ Validation and calibration of the theoretical model against empirical results leading to a refined and improved simulation model.
- ❖ Simulation of proposed hybrid solar collector under realistic operating conditions

4.2.1.1 Heat Transfer

Heat is defined as a form of energy that can be transferred from one system to another as a result of temperature difference. The theoretical analysis of the system under investigation is formulated through heat balance, which is concerned with the amount of heat transfer as a system undergoes a process from one equilibrium state to another. Heat transfer always occurs from the higher-temperature medium to the lower-temperature one, and heat transfer stops when the two mediums reach the same temperature, *Steady State*. Thermal energy can be transferred between mediums in three different modes; namely, *Conduction*, *Convection*, and *Radiation*, under the presence of temperature difference between mediums.

Energy balance at a plane surface is accomplished by keeping track of interactions at the surface through applying the conservation of energy principles, Fig. 4.9. A surface can be viewed as a fictitious system whose energy content remains constant during a process, hence the energy balance of a surface can be expressed by Eq. 4.1 extending its validity for both steady and transient conditions. The energy balance for the outer surface of the wall in Fig. 4.10. can be expressed by Eq. 4.2.

$$\dot{Q}_1 = \dot{Q}_2 + \dot{Q}_3 \quad (4.1)$$

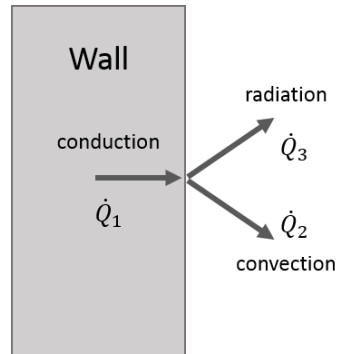


Fig. 4. 9 Energy interaction on a surface

$$\dot{E}_{in} = \dot{E}_{out} \quad (4.2)$$

Although the three modes of heat transfer are encountered in the thermal analysis of this investigation, not all three can exist simultaneously in a system. For example, heat transfer is only by conduction in opaque solids as for the PV absorber, but by conduction and radiation in semi-transparent solids as encountered at the front cover of the collector. Therefore, a solid may involve conduction and radiation but not convection. However, it is vital to mention that a solid may also involve heat transfer by convection and/or radiation on its surfaces exposed to a fluid or other surfaces, defined by boundary conditions, while the inner region of the solid experiences heat transfer via conduction. This case in particular is observed in the following sections of this chapter, as the incoming solar radiation striking the collector and other operating conditions

alter the system state at the front surface of the module, while thermal energy induced due to radiation and convection is transferred through the system layers via conduction.

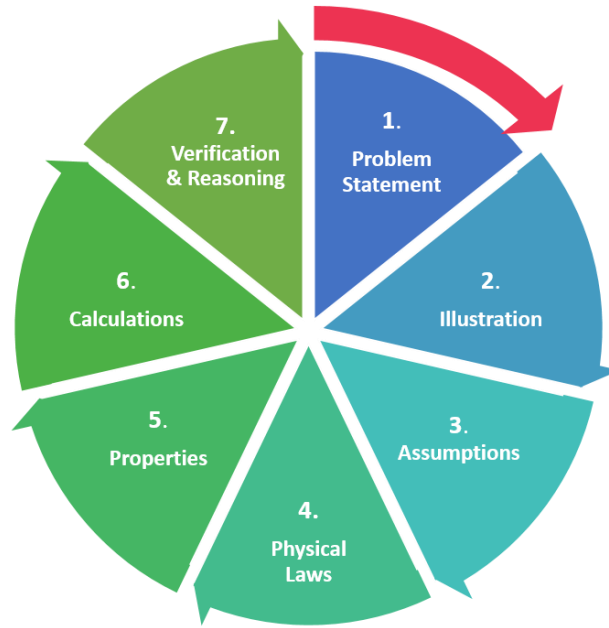


Fig. 4. 10 Computer modelling approach implemented

4.2.1.2 Problem Solving Technique

Solving energy balances in real world applications is complex, especially for transient response, hence a pragmatic approach is adopted. Applying a step-by-step approach, the solution of complicated problems can be reduced to solution of series of simple problems. The steps applied for the theoretical performance analysis of the system under investigation are summarized in Fig. 4.10. The first

step involved defining the problem statement in addition to specifying the quantities to be evaluated. Realistic schematic sketch of the physical system further simplifies the problem by aiding visualisation of the entire energy interactions of the entire system at once. To add simplicity to the process, assumptions are made with justifications. Moving on, relevant physical laws and principles are applied utilising the assumptions made. Prior to the calculation process using computer aided software, the properties of components within the system are specified. Calibrations and validation are then applied to further improve the model for credible evaluation.

4.2.1.3 System Equations

The system equations are formulated over energy interactions at the surface of the collector through applying the conservation of energy laws and using the basic principles of heat transfer. Fig. 4.11 depicts the thermal energy balance within the system on a side view of the collector. For simplicity, the mathematical model is divided into two sections, namely; (1) Heat-pipe based PV collector, and (2) Thermoelectric Generator Fan-Heat Sink Assembly.

Energy Exchange

The energy exchange within the hybrid collector is better visualised through the schematic diagrams in Fig. 4.12. As the temperature of the PV module is the main quantity to characterize its performance improvements in this study, the thermal energy exchange of the module with the environment is specified. At the front surface of the collector, thermal energy transfer in the form of radiation and convection heat transfer is experienced. Convection and radiation heat transfer from the front and rear surfaces of the module have profound effect on the collector performance. However, conduction from the module to the structural framework support is considered negligible due to the small area of contact. In transient response, the rate of change of module temperature with time is considered to be significantly greater than zero. The resulting rate of temperature change with time for the collector is expressed as the sum of energy contributions the collector experience, Eq. 4.3, with the module heat capacity given by Eq. 4.4 where m denotes the layer within the collector. The thermal resistance network of the entire collector is given in Fig. 4.13.

$$C_{moduel} \frac{dT}{dt} = q_{rad(short)} + q_{rad(long)} + q_{conv} - P_{electrical} \quad (4.3)$$

$$C_{moduel} = A \cdot \rho_m \cdot \delta_m \cdot C_m \quad (4.4)$$

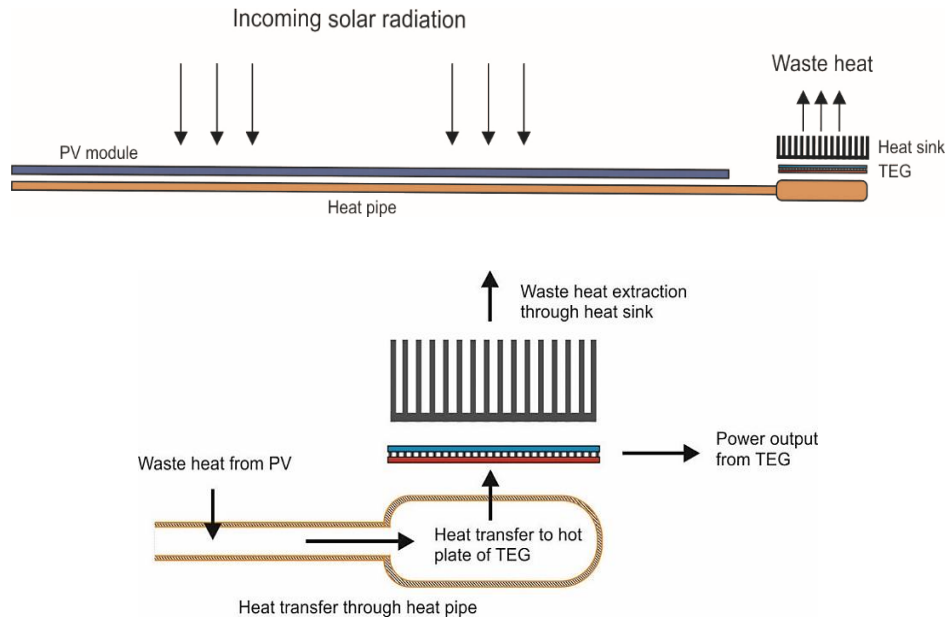


Fig. 4. 11 Schematic of energy flow within the integrated heat pipe PV/TEG collector

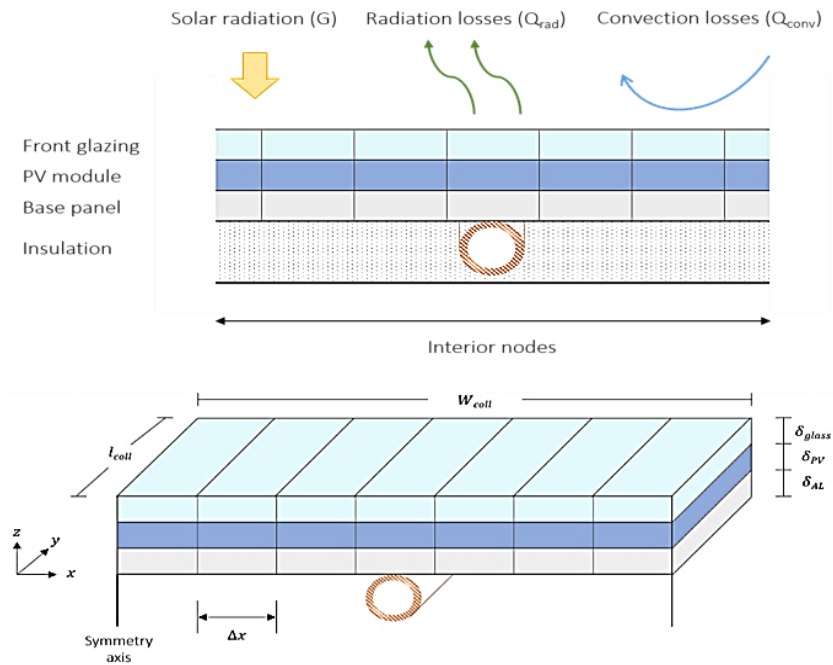


Fig. 4. 12 Schematic depicting energy interactions and layers from which the system is designed

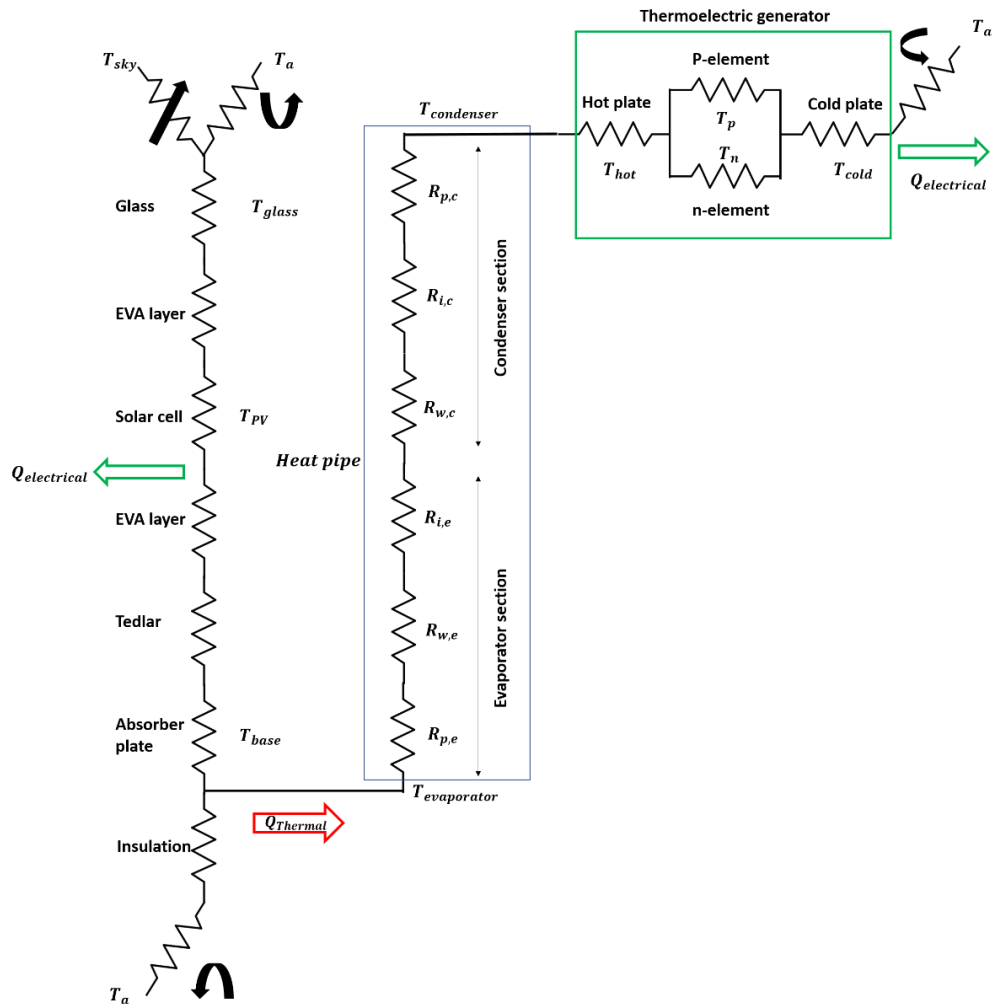


Fig. 4. 13 Thermal resistance network of integrated heat pipe-based PV/TEG collector

Where the thermal resistances for the heat pipe section are defined as follows:

$R_{p,e}$: Radial conduction resistance across the pipe wall at evaporator section

$R_{w,e}$: Resistance of the liquid-wick combination at the evaporator section

$R_{i,e}$: Thermal resistance at vapour-liquid interface at evaporator section

$R_{w,c}$: Resistance of the liquid-wick combination at condenser section

$R_{p,c}$: Radial conduction resistance across the pipe wall at condenser section

$R_{i,c}$: Thermal resistance at the vapor-liquid interface at condenser

4.2.1.4 Numerical Solution (Finite Difference Approximation)

The translation from differential equations $\left(\frac{\partial^2 T}{\partial x^2}, \frac{\partial T}{\partial x}, \frac{\partial T}{\partial t}\right)$ to numerical forms using finite difference approximations is presented in this section. The transformation using finite difference equation is obtained to a set of energy balance equations derived in Chapter 5. The result is a new set of equations that can be solved numerically using any kind of computer simulation environment. In this investigation, MATLAB packages offered a suitable yet simple implementation approach of the energy performance prediction model. Various sets of conditions and loops required for solving the energy balance models simultaneously at acceptable level of time and spatial steps was also implemented. The program routine of the energy prediction model is presented in the latter section. However, in this section numerical form representation of the set of energy balance models for each layer and subsystem are presented.

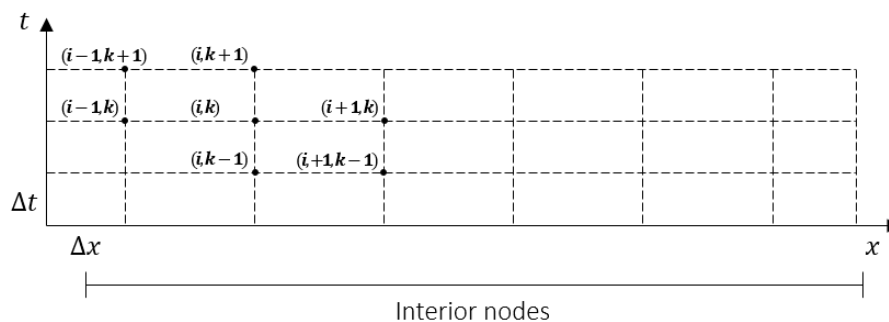


Fig. 4. 14 Nodal temperatures (discrete points in time as well as space)

Finite difference approximations:

The numerical form of the energy balance equations derived earlier is developed based on the nodal temperature scheme for transient heat transfer, Fig. 4.14. The finite difference representation of the second derivative at a general internal node (m) is given by Eq. 4.5. Note that the second derivative of temperature at a node (m) is expressed in terms of the temperature at node (m) and its two neighbouring nodes. The time derivative however, is expressed in forward difference (explicit) form by Eq. 4.6.

$$\frac{\partial^2 T}{\partial x^2} = \frac{T_{(i+1,j)} - 2T_{(i,j)} + T_{(i-1,j)}}{\Delta x^2} \quad (4.5)$$

$$\frac{\partial T}{\partial t} = \frac{T_{(i,j+1)} - T_{(i,j)}}{\Delta t} \quad (4.6)$$

The results intended from the computer simulation model which will set a base for evaluating the system performance include:

- ❖ Estimation of the hybrid system output, including:
 - Electrical performance
 - Thermal performance
 - Electrical and thermal efficiencies
 - Temperature variation and influence on performance
- ❖ Prediction of performance under various geographical and operating conditions
 - Various range of operating temperatures, wind speeds, and solar intensities, emphasizing on hot, sunny, and dry climatic regions
- ❖ Estimation of performance under various input parameters, design dimensions, and materials
- ❖ Comparison of the hybrid system performance with other available designs and conventional collectors and PV modules working side by side

4.2.2 Experimental Investigation

Performance analysis of the collector proposed is determined experimentally to permit the validation of the simulation model developed. A testing rig is constructed with the assistance of the lab technicians based on the system requirements and operating principles as a prototype for the system under investigation. The practical results obtained are vital to allow the comparison between the computer simulation model and the real system. In addition, the experiment will consider gathering data over various operating conditions and time periods. Likewise, the experimentation process involved collection of results of the same parameters and scenarios as in the computer simulation model presented earlier. The experiment conducted including the set-up, components, commissioning, and data logging are presented in detail in Chapter 7. Results from experimental testing are documented and discussed for the evaluation purpose of the system in Chapter 8. Finally, the system designed requirements for an efficient operation is concluded in Chapter 9 along with recommendations and further possible improvements.

Chapter 5

Energy Balance Equations

The research aims on optimizing the energy conversion efficiency of PV cells through a novel integration of heat pipe-based TEG assembly in a compact collector, this chapter presents the theoretical modelling of the system under investigation for computational implementation. Applying various forms of heat transfer while adopting numerical analysis techniques, the theoretical study was developed based on energy balance equations written for each component within the system. Investigation of the performance capability of the collector as well as optimization through parametric analysis is conducted. Within the theoretical study a set of objectives are accomplished and put together to deliver a simulation model that is utilised to predict the overall performance of the novel system described in the previous chapter. The chapter here includes, modelling, design and simulation of the hybrid collector with various configurations and operating conditions.

The energy exchange in the form of radiation at the surface of the panel is comprised of both long and short electromagnetic waves. The effective solar radiation intercepting the surface of the collector is a function of the intensity (G) of the direct and diffuse short-wave radiation inputs as well as the absorptivity (α) of the cell material, expressed by Eq. 5.1 (Jones and Underwood, 2002). The long wave radiation on the other hand, is described by the *Stefan-Boltzmann law* from a black body at surface temperature T , Eq. 5.2 (Armstrong and Hurley, 2010). Convection heat transfer however, occurs at both front and rear of the collector. The convective heat transfer is generally described by *Newton's law of Cooling*, yet different expression is applied at each surface. At the front, the convective energy is described by Eq. 5.3 (Jones and Underwood, 2002), while free convection given by (Holman, 2009) is considered at the rear, Eq. 5.4; due to having the PV module enclosed from wind effects. Thus, having buoyancy-driven free convection domination. Heat transfer via conduction as well is considered across not only the width of the module but also layers from which the collector is made, obtaining 2-dimensional thermal model, Eq. 5.5.

$$q_{rad(short)} = \alpha A G \quad (5.1)$$

$$q_{rad(long)} = \sigma \varepsilon T^4 \quad (5.2)$$

$$q_{conv} = A h_c (T_{amb} - T_{module}) \quad (5.3)$$

$$q_{conv(free)} = A \left(1.31 (T_{module} - T_{amb})^{\frac{1}{3}} \right) \cdot (T_{module} - T_{amb}) \quad (5.4)$$

$$\dot{Q} = -kA \frac{dT}{dx} \quad (5.5)$$

5.1 Heat pipe-based PV collector

For simplified modelling of the heat-pipe based PV collector, the following assumptions were made:

- Negligible ohm-electrical losses within the PV cells
- Edge losses within the collector were assumed to be negligible
- The pressure drops caused by vapor flow along the axial length of the heat pipe was assumed to be negligible
- Vapor space of heat pipe operate at steady saturation pressure
- Temperature gradient of the working fluid along the axial length of the heat pipe was neglected

5.1.1 Energy balance of the front glazing

Referring to Fig. 5.1, and taking into consideration heat transfer due to radiation and convection on the top glass cover of the collector, the 2-D energy balance within a single glazing cover in direct contact with the PV layer is expressed by Eq. 5.6.

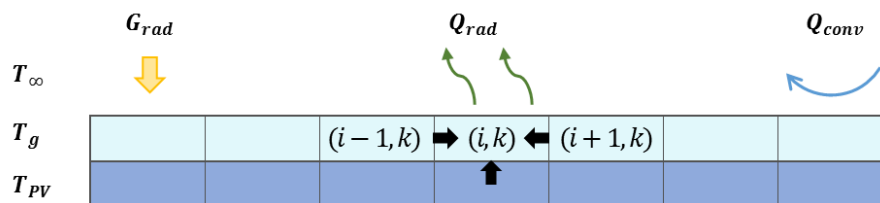


Fig. 5. 1 Energy interactions of front glazing at surface and layer underneath

$$\begin{aligned}
& \Delta x \Delta y (\rho C \delta)_{glass} \frac{\partial T_{glass}}{\partial t} \\
& = \Delta x \Delta y k_{glass} \delta_{glass} \frac{\partial^2 T_{glass}}{\partial x^2} \\
& + \Delta x \Delta y (h_{c_{forced}}) (T_{\infty} - T_{glass}) \\
& + \Delta x \Delta y h_{rad} (T_{surr} - T_{glass}) \\
& + \Delta x \Delta y \left(\frac{k_{glass}}{\delta_{glass}} \right) (T_{pv} - T_{glass}) \\
& + \Delta x \Delta y G_{rad} \alpha_{glass}
\end{aligned} \tag{5.6}$$

Where the parameters incorporated in the equation are defined as follow:

ρ_g : Density of low-iron glass, 2508 [kg/m³] (PPG Industries Inc., 2010)

δ_g : Thickness of front glazing, 4 [mm] (Gang et al., 2012)

C_g : Specific heat capacity of glass, 858 [J/(kg K)] (PPG Industries Inc., 2010)

G : Global solar radiation

α_g : Absorptivity of front glazing, 1% (PPG Industries Inc., 2010)

h_{wind} : Convective heat transfer coefficient [W/m² K]

$h_{r,g-a}$: Radiative heat transfer coefficient [W/m² K]

R_{pv-g} : Thermal resistance between front glazing and PV, [(K m)/W]

To include the influence of wind speed in the performance evaluation, Eq. 5.7 is considered for the forced convective heat transfer coefficient at the front surface (Duffie and Beckman, 2013). The evaluation of the radiative

losses coefficient at the surface is estimated using Eq. 5.8. Conduction to the layer underneath however, is estimated using the concept of thermal contact resistance, Eq. 5.9. The contact thermal resistance describes the influence the interface has in multilayer system on the heat transfer.

$$h_{wind} = 2.8 + 3 u_a \quad (5.7)$$

$$h_{rad} = \varepsilon_g \sigma (T_{glass}^2 + T_{surr}^2) (T_{glass} + T_{surr}) \quad (5.8)$$

$$R_{m-n} = \frac{\delta_m}{k_m} \quad (5.9)$$

Where,

u_a : Wind velocity [m/s]

ε_g : Emissivity of front glazing, 84% (Giovannetti et al., 2014)

σ : Stephan-Boltzmann's constant, 5.67×10^{-8} [W/(m² K⁴)]

T_{surr} : Sky Temperature, $T_{surr} = 0.0552 T_{amb}^{1.5}$ [°C] (Cengel, 2007)

k : Thermal conductivity [W/m K]

δ : Thickness of layer m [m]

m, n : Subscripts denoting layers above and underneath interface

5.1.2 Energy balance of PV layer

In similar a manner, however considering only thermal conduction from the layers adjacent to the PV encapsulation layer, the 2-D time dependent temperature variation for the PV layer given in Fig. 5.2 is estimated by solving the partial differential equation given in Eq. 5.10.

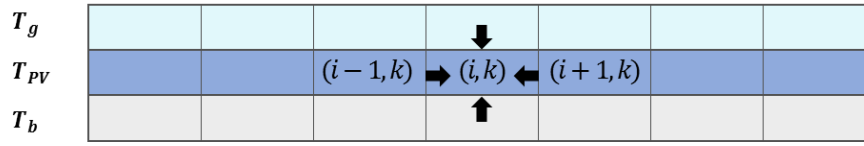


Fig. 5. 2 Energy interactions at PV encapsulation layer

$$\begin{aligned}
 & \gamma \Delta x \Delta y (\rho C \delta)_{PV} \frac{\partial T_{PV}}{\partial t} \\
 & = \Delta x \Delta y k_{PV} \delta_{PV} \frac{\partial^2 T_{PV}}{\partial x^2} \\
 & + \Delta x \Delta y (R_{pv-glass})^{-1} (T_{glass} - T_{PV}) \\
 & + \Delta x \Delta y (R_{base-pv})^{-1} (T_{base} - T_{PV}) \\
 & + \Delta x \Delta y G_{rad} (\tau\alpha)_{PV} - \Delta x \Delta y E
 \end{aligned} \tag{5.10}$$

Where the parameters incorporated in the Eq. 5.10 are defined as follow:

γ : PV cell coverage ratio, $A_{pv}/A_{collector}$

ρ_{pv} : Density of PV encapsulation [kg/m^3]

δ_{pv} : Thickness of PV cells layer [m]

C_{pv} : Specific heat capacity of PV cells [$\text{J}/(\text{kg K})$]

G : Global solar radiation [W/m^2]

$(\tau\alpha)_{pv}$: Effective transmittance-absorption product of PV layer

E : Electrical power output from PV module [W]

In practice the PV cell consists of several layers sandwiched together forming a PV encapsulation, Fig. 5.3. For the purpose of calculating the effective heat capacity of the module for estimating the change in

temperature, the module is considered as several layers of materials; flat sheet of silicon PV cells laminated within a Polyester/Tedlar tri-laminate (Jones and Underwood, 2002). Therefore, to calculate the product of the density, thickness, and specific heat ($\rho_{pv}, \delta_{pv}, C_{pv}$), each layer of the PV encapsulation (PV cell, EVA, Tedlar) must be taken into consideration as presented in Table 5.1.

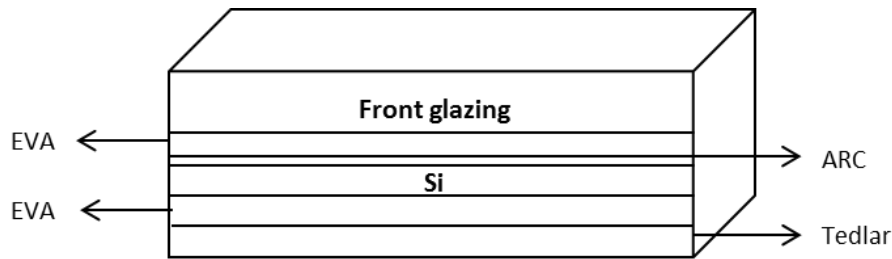


Fig. 5. 3 Illustration of PV cell encapsulation

Table 5. 1 Estimation of effective heat capacity of PV encapsulation (Armstrong and Hurley, 2010)

| Layer | Thermal conductivity k, (W/m K) | Thickness (m) | Density (kg/m ³) | Specific heat (J/kg K) | Product |
|---------------|---------------------------------|---------------|------------------------------|------------------------|----------------|
| PV cells (Si) | 148 | 0.0003 | 2330 | 677 | 473.22 |
| EVA | 0.35 | 0.0005 | 960 | 2090 | 1003.20 |
| Tedlar | 0.2 | 0.0001 | 1200 | 1250 | 150.00 |
| Total | | | | | 1626.42 |

The electrical power produced by the PV module is expressed by Eq. 5.11 (Gang et al., 2012). While the temperature dependant PV cell efficiency is calculated from the PV cell reference efficiency (η_r) at reference operating

temperature (T_{ref}) and temperature coefficient (β_{pv}) using Eq. 5.12 (Chow et al., 2007).

$$E = G(\tau\alpha)_{pv}\tau_{EVA}\eta_r[1 - \beta_{pv}(T_{pv} - T_{ref})] \quad (5.11)$$

$$\eta_{PV} = \eta_r (1 - \beta_{pv}(T_{pv} - T_r)) \quad (5.12)$$

The effective transmittance-absorption product of the PV layer $(\tau\alpha)_{pv}$ is calculated by the expression give in Eq. 5.13, where (α) is the weighted average of the absorption of PV cell (α_{pv}) and black TPT (α_{TPT}), given by, $\alpha = \gamma\alpha_{pv} + (1 - \gamma)\alpha_{TPT}$.

$$(\tau\alpha)_{pv} = \frac{\tau_g\alpha}{1 - (1 - \alpha)\rho_g} \quad (5.13)$$

τ_g : Transmittance of front glazing $\tau_g = \tau_\alpha\tau_\rho$, 91% (PPG Industries Inc., 2010)

τ_α : Transmittance of front glazing considering absorption

τ_ρ : Transmittance of front glazing considering reflection losses

ρ_d : Reflectance of front glazing for diffuse radiation, $\rho_g = 1 - \alpha_g - \tau_g$

α : Weighted average of the absorption of PV cell

The thermal resistance between the front glazing and PV encapsulation (Thermal resistance of adhesive layer EVA) is expressed by Eq. 5.14, while the interface resistance between the PV encapsulation and the underneath base panel is calculated based on Eq. 5.15.

$$R_{pv-glass} = \frac{\delta_{EVA}}{k_{EVA}} \quad (5.14)$$

$$R_{base-pv} = R_{pv} + R_{EVA} + R_{TPT} = \frac{\delta_{pv}}{k_{pv}} + \frac{\delta_{EVA}}{k_{EVA}} + \frac{\delta_{TPT}}{k_{TPT}} \quad (5.15)$$

Where;

δ_{EVA} : Thickness of EVA layer [m]

δ_{TPT} : Thickness of TPT layer [m]

k_{pv} : Thermal conductivity of PV layer [W/m K]

k_{EVA} : Thermal conductivity of EVA layer [W/m K]

k_{TPT} : Thermal conductivity of TPT layer [W/m K]

5.1.3 Energy balance of the aluminum base panel

The transient heat conduction along both thickness and width of the aluminum heat spreading sheet can be approximated to 2-dimensional dynamic heat transfer on an infinite flat plate. The base panel is divided into several nodes along the width of the aluminum sheet Fig. 5.4, and differential steps are used to estimate the heat transfer within each node. The temperature distribution across the heat spreader is assumed to be symmetrical relative to the position of the evaporator section of the pipe. Hence two energy balance equations are defined. The first equation derived describes the energy balance associated within the pipe node, Eq. 5.16.

While nodes surrounding the evaporator section of the heat pipe, are described by Eq. 5.17.

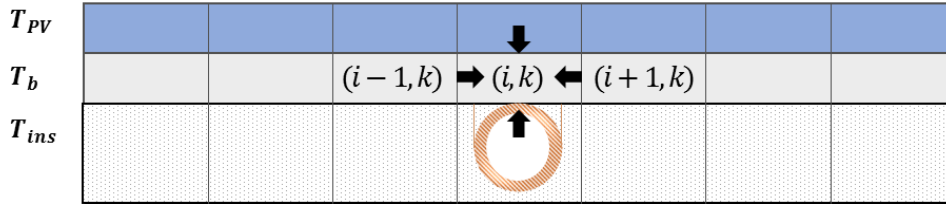


Fig. 5. 4 Conduction to/from base panel layer from/to PV and heat pipe at middle node

$$\begin{aligned}
 & \Delta x \Delta y (\rho C \delta)_{base} \frac{\partial T_{base}}{\partial t} \\
 &= \Delta x \Delta y k_{base} \delta_{base} \frac{\partial^2 T_{base}}{\partial x^2} \\
 &+ \Delta x \Delta y (R_{base-pv})^{-1} (T_{PV} - T_{base}) \\
 &+ A_{bond} (R_{base-pipe})^{-1} (T_{hp(eva)} - T_{base}) \\
 &+ \Delta x \Delta y \left(\frac{\delta_{ins}}{k_{ins}} + \frac{1}{hc_{free}} \right)^{-1} (T_{\infty} - T_{base})
 \end{aligned} \tag{5.16}$$

$$\begin{aligned}
 & \Delta x \Delta y (\rho C \delta)_{base} \frac{\partial T_{base}}{\partial t} \\
 &= \Delta x \Delta y k_{base} \delta_{base} \frac{\partial^2 T_{base}}{\partial x^2} \\
 &+ \Delta x \Delta y (R_{base-pv})^{-1} (T_{PV} - T_{base}) \\
 &+ \Delta x \Delta y \left(\frac{\delta_{ins}}{k_{ins}} + \frac{1}{hc_{free}} \right)^{-1} (T_{\infty} - T_{base})
 \end{aligned} \tag{5.17}$$

Where the parameters incorporated in the equation are defined as follow:

ρ_{base} : Density of Aluminium base panel, 2700 [kg/m³] (Gang et al., 2012)

δ_{base} : Thickness of base panel, 1.2 [mm] (Zhang et al., 2014)

C_{base} : Specific heat capacity of base panel, 930 [J/(kg K)] (Lee, 2010)

k_{base} : Thermal conductivity of base panel, 205 [W/m K] (Lee, 2010)

δ_{ins} : Thickness of insulation layer at rear 50 [mm]

k_{ins} : Thermal conductivity of insulation 0.018 [W/m K]

$T_{hp(eva)}$: Temperature of evaporator section of heat pipe [°C]

The thermal resistance between the base panel and evaporator section of pipe is given by Eq. 5.18 (Gang et al., 2012).

$$R_{base-pipe} = \frac{\ln\left(\frac{d_{o(eva)} + \delta_{base}}{d_{o(eva)}}\right)}{2 \pi l_{eva} k_{base}} \quad (5.18)$$

5.1.4 Energy balance of the heat pipe

The general method applied to model heat pipes is to analyze the two-phase flow within the pipe (Fadhil, 2014). The procedure is based on writing conservation of mass, momentum and energy equations which introduce complexity to the process. On the other hand, simplified modelling process can be applied based on the energy balances at each section of the heat pipe (Reay, Kew, and McGlen, 2006), (Lee, 2010), (Wu et al., 2011). In this regard, the assumptions mentioned earlier in this section were adopted, where;

- The pressure drops caused by vapor flow along the axial length of the heat pipe was neglected
- Temperature gradient of the working fluid along the axial length of the heat pipe was neglected

In general, the heat pipe design process includes estimating the geometry, the type and amount of fluid, and the material of the container in order to meet the requirements of heat transfer capacities at defined temperatures, in safely and durable way and at lower cost possible. For this research, the pipes utilized were of an evacuated tube solar thermal collector, thus the scope of the investigation does not cover the design aspect of the heat pipe, but instead to assess the incorporation of heat pipes for thermal heat recovery in a unique integration of a PV module and TEGs. Hence, the heat transfer and the associated temperature drop in the heat pipe are represented by thermal resistance network illustrated in Fig. 5.5 and described by Eq. 5.19.

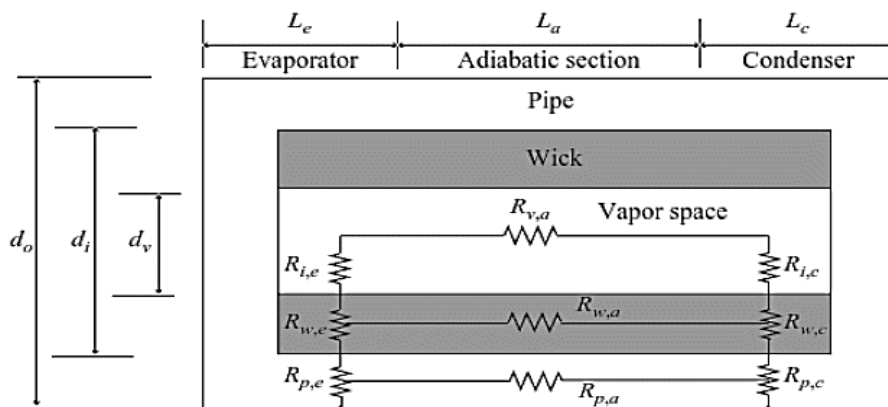


Fig. 5. 5 Heat pipe thermal resistance network (Lee, 2010)

$$R_{eva-con} = R_{p,e} + R_{w,e} + R_{i,e} + R_{w,c} + R_{i,c} + R_{p,c} \quad (5.19)$$

Where:

$R_{p,e}$: Radial conduction resistance across the pipe wall at evaporator section

$R_{w,e}$: Resistance of the liquid-wick combination at the evaporator section

$R_{i,e}$: Thermal resistance at vapour-liquid interface at evaporator section

$R_{w,c}$: Resistance of the liquid-wick combination at condenser section

$R_{p,c}$: Radial conduction resistance across the pipe wall at condenser section

$R_{i,c}$: Thermal resistance at the vapor-liquid interface at condenser

$$R_{p,e} = \frac{\ln\left(\frac{d_{o,eva}}{d_{i,eva}}\right)}{2 \pi k_p l_{eva}} \quad (5.20)$$

$$R_{w,e} = \frac{\ln\left(\frac{d_{o,wick}}{d_{i,wick}}\right)}{2 \pi l_{eva} k_{wick}} \quad (5.21)$$

$$R_{i,e} = \frac{2}{h_{eva} \pi d_{i,eva} l_{eva}} \quad (5.22)$$

$$R_{w,c} = \frac{\ln\left(\frac{d_{o,wick}}{d_{i,wick}}\right)}{2 \pi l_{con} k_{wick}} \quad (5.23)$$

$$R_{p,c} = \frac{\ln\left(\frac{d_{o,con}}{d_{i,con}}\right)}{2 \pi k_p l_{con}} \quad (5.24)$$

$$R_{i,c} = \frac{1}{h_{con} \pi d_{i,con} l_{con}} \quad (5.25)$$

Where;

d_i, d_o : Inner and outer diameter of heat pipe section

k_p, k_{wick} : Thermal conductivity of pipe container and wick materials

l_{eva}, l_{con} : Length of evaporator and condenser sections respectively

For screen mesh wick structure of the heat pipe, the effective thermal conductivity of the wick is evaluated from both liquid and wick thermal conductivities (k_l, k_{wick}), and wick porosity (ζ_{wick}) using Eq. 5.26 (Lee, 2010).

$$k_{wick(eff)} = \frac{k_l[(k_l + k_{wick}) - (1 - \zeta_{wick})(k_l - k_{wick})]}{(k_l + k_{wick}) + (1 - \zeta_{wick})(k_l - k_{wick})} \quad (5.26)$$

The porosity, defined as the ratio of pore volume to total volume is evaluated using Eq. 5.27 (Azad, 2008).

$$\zeta_{wick} = 1 - \frac{1.05 \pi n_{wi} d_{wi}}{4} \quad (5.27)$$

Where;

n_{wi} : Number of mesh per inch [in^{-1}]

d_{wi} : Wire diameter [m]

For a wick lined wall, the vaporization film coefficient (h_{eva}) is approximately equal to the thermal conductivity of the fluid divided by the wick thickness as Eq. 5.28 suggests (Azad, 2008). Heat transfer analysis of internal condensation however, is complicated by the fact that it is strongly influenced by the vapor velocity and the rate of liquid accumulation on the

walls of the tubes. The internal film condensation coefficient (h_{con}) for horizontal and inclined tube is described by Eq. 5.29 (Cengel, 2007).

$$h_{eva} = \frac{k_l}{\delta_{wick}} \quad (5.28)$$

$$h_{con} = 0.555 \left[\frac{g \rho_l (\rho_l - \rho_v) k_l^3}{\mu_l (T_{sat} - T_{con})} h_{fg}^* \right]^{\frac{1}{4}} \quad (5.29)$$

Where;

δ_{wick} : Thickness of wick [m]

g : Gravitational acceleration [m/s^2]

ρ_l, ρ_v : Densities of the liquid and vapor [kg/m^3]

μ_l : Viscosity of the liquid [$kg/m \cdot s$]

k_l, k_w : Thermal conductivity of the liquid, and wick respectively [$W/m \text{ } ^\circ C$]

T_{sat} : Saturation temperature of the condensing fluid [$^\circ C$]

h_{fg}^* : Modified latent heat of vaporization [J/kg], given by:

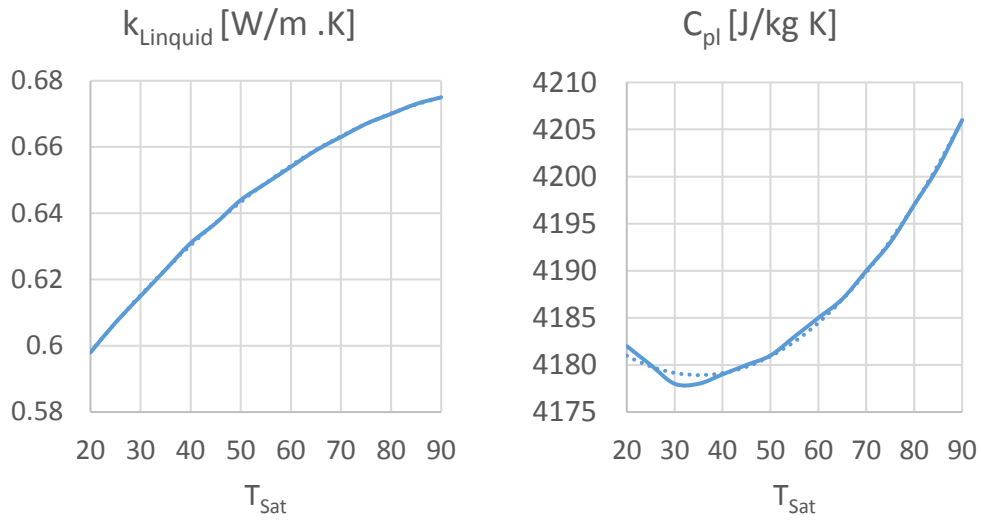
$$h_{fg}^* = h_{fg} + \frac{3}{8} C_{pl} (T_{sat} - T_{con}) \quad (5.30)$$

The heat pipe is modelled considering saturation temperature in the range of the operating temperature the collector is expected to operate within. Meaning, the working fluid will undergo a phase-change at a temperature only if its pressure equals the saturation pressure. Note, in the evaluation of the condensing film coefficient, all properties of the liquid are

evaluated at the film temperature ($T_f = 0.5 (T_{sat} - T_{con})$), while the latent heat of vaporization, and vapour density are evaluated at the saturation temperature. To incorporate the temperature dependant thermo-physical properties of saturated water, the temperature dependency trends presented in Fig. 5.6 are applied within the heat pipe model. The energy balance equation of the evaporator and condenser sections are then described by Eq. 5.31 and Eq. 5.32 respectively.

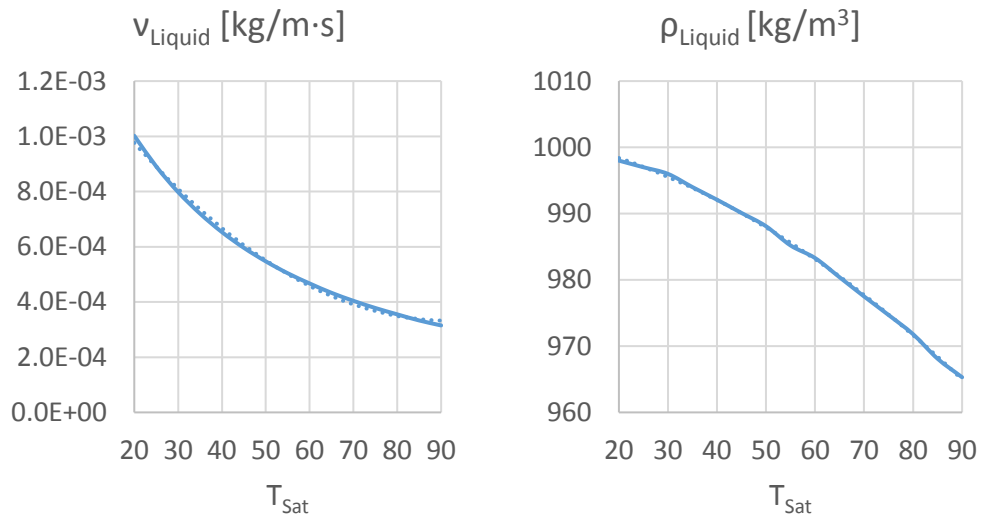
$$\begin{aligned}
 & \frac{1}{4} \pi (d_{o,eva}^2 - d_{i,eva}^2) (\rho C l)_{eva} \frac{\partial T_{eva}}{\partial t} \\
 & = \Delta x \Delta y (R_{base-pipe})^{-1} (T_{base} - T_{hp(eva)}) \\
 & + (R_{eva-con})^{-1} (T_{hp(con)} - T_{hp(eva)}) \quad (5.31)
 \end{aligned}$$

$$\begin{aligned}
 & \frac{1}{4} \pi (d_{o,con}^2 - d_{i,con}^2) (\rho C l)_{con} \frac{\partial T_{con}}{\partial t} \\
 & = \Delta x \Delta y (R_{TE-(con)})^{-1} (T_{TEG(hot)} - T_{hp(eva)}) \\
 & + (R_{eva-con})^{-1} (T_{hp(eva)} - T_{hp(con)}) \quad (5.32)
 \end{aligned}$$



$$k_L = -1.03E-05x^2 + 2.231E-03x + 5.576E-01$$

$$C_{pl} = 8.99E-03x^2 - 6.319E-01x + 4.190E+03$$



$$v_L = 1.25E-07x^2 - 2.298E-05x + 1.386E-03$$

$$\rho_L = -3.21E-03x^2 - 1.249E-01x + 1.002E+03$$

Fig. 5. 6 Thermo-physical properties of saturated water over range of operating temperatures (Cengel, 2007)

5.2 Thermoelectric Generator – Fan Heat Sink Assembly

The theoretical model applied in the computer simulation process to evaluate the heat recovery capabilities of the thermoelectric generator integration is illustrated in this section. The fan-heat sink assembly is intended to aid maintaining sufficient temperature difference across the TEG plates for direct thermo-electrical conversion. The section here is further divided to present the models for the thermoelectric generator (TEG), and the fan-heat sink assembly separately.

5.2.1 Energy balance of thermoelectric generator (TEG)

In this section, transient modelling of the thermoelectric generator through the coupling effects governing the conversion which includes, *Seebeck effect*, *Peltier effect*, *Thomson effect*, and *Joule heating* is illustrated. As the thermoelectric generators are subject to unsteady heat flux and operating conditions, transient modelling was considered, in which complexities can occur due to variation of electric currents with time (Nguyen and Pochiraju, 2013), (Cheng, Huang, and Cheng, 2010), (Lee, Kim, and Kim, 2010).

To introduce simplicity to the TEG model, the following assumptions are taken into consideration:

- Radiative and convective heat losses were assumed to be negligible

- Current flow is assumed one-dimensional
- 2-dimensional heat flow is considered
- All materials are homogeneous

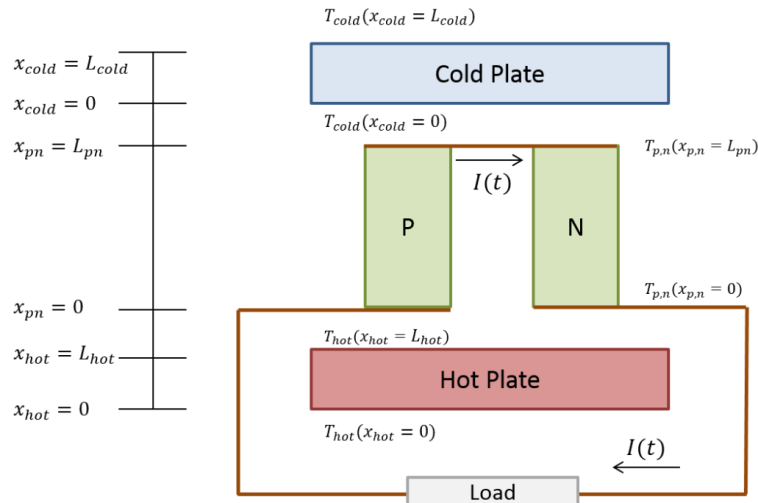


Fig. 5. 7 Thermoelectric generator schematic diagram

The schematic diagram of the thermoelectric generator shown in Fig. 5.7 consists of two dissimilar thermoelectric elements, p- and n- elements wired electrically in series and thermally in parallel. To simplify the modelling, the simulation dimension is divided into three frames; (i) Hot plate, (ii) p- and n- elements, and (iii) Cold plate. The energy balance at each junction is induced by the Seebeck and Peltier effects and direction of thermal conduction through the two elements. Operation either in generation or cooling mode is directly related to the direction of current flow through the load. The governing equations of the p- and n- elements are derived based on the energy balance equation of a differential element in space, given by Eq.(s)

5.33–5.34 (Nguyen and Pochiraju, 2013). The general energy balance across the hot and cold plates is considered a 2-dimensional transient heat transfer problem and is given by Eq.(s) 5.35 - 5.36. However, the equations need to be modified to account for interface boundaries between the plates and the thermo-elements as well as the heat source at the hot side and heat sink at the cold side. In addition, the hot plate is divided into three differential elements of a width equivalent to the condenser section diameter, Fig. 5.8.

$$A_p C_p \rho_p \frac{\partial T_p}{\partial t} = k_p A_p \frac{\partial^2 T_p}{\partial x_p^2} + \frac{\varepsilon_p}{A_p} I^2 - \mu_p I \frac{\partial T_p}{\partial x_p} \quad (5.33)$$

$$A_n C_n \rho_n \frac{\partial T_n}{\partial t} = k_n A_n \frac{\partial^2 T_n}{\partial x_n^2} + \frac{\varepsilon_n}{A_n} I^2 + \mu_n I \frac{\partial T_n}{\partial x_n} \quad (5.34)$$

$$A_{hot} \rho_{hot} C_{hot} \frac{\partial T_{hot}}{\partial t} = k_{hot} \frac{\partial^2 T_{hot}}{\partial x_{hot}^2} \quad (5.35)$$

$$A_{cold} \rho_{cold} C_{cold} \frac{\partial T_{cold}}{\partial t} = k_{cold} \frac{\partial^2 T_{cold}}{\partial x_{cold}^2} \quad (5.36)$$

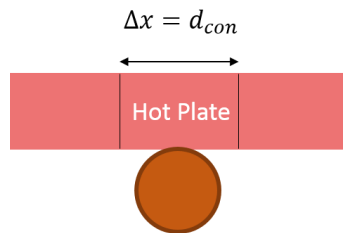


Fig. 5. 8 Condenser-TEG hot plate interface boundary with 3 differential elements

Initial and boundary conditions:

The initial temperature profiles of the three frames are set to ambient temperature. At boundary $x_{hot} = 0$, the temperature is conducted from the

condenser section of the heat pipe to the TEG hot plate, therefore, the energy balance at the interface is described by Eq. 5.37. The first term of the equation describes the thermal exchange to the side differential nodes, while the second and third terms describe the thermal energy transfer from both top and underneath layers respectively. Taking into account the cooling capacity of the fan-heat sink assembly, the boundary condition at the top cold side ($x_{cold} = L_{cold}$) was derived in similar manner. The temperature at the top of the cold plate considering the interface with both p-/n-elements as well as the fan-heat sink is given by Eq. 5.38.

$$\begin{aligned}
 A_{hot} (\rho C \delta)_{hot} \frac{\partial T_{hot}}{\partial t} &= \left(\Delta x k_{hot} \delta_{hot} l_{hot} \frac{\partial^2 T_{hot}}{\partial x^2} \right) \\
 &+ \left(A_{hot} \frac{k_{hot}}{\delta_{hot}} (T_{hp(con)} - T_{hot}) \right) \\
 &+ \left(A_p \frac{k_p}{\delta_p/2} (T_p - T_{hot}) + A_n \frac{k_n}{\delta_n/2} (T_n - T_{hot}) \right) \\
 &+ \alpha_{pn} T_{hot} I \tag{5.37}
 \end{aligned}$$

$$\begin{aligned}
A_{cold} (\rho C \delta)_{cold} \frac{\partial T_{cold}}{\partial t} &= \left(\Delta x k_{cold} \delta_{cold} l_{cold} \frac{\partial^2 T_{cold}}{\partial x^2} \right) \\
&+ \left(A_{cold} \frac{k_{cold}}{\delta_{cold}} (T_{fan-heatsink} - T_{cold}) \right) \\
&+ \left(A_p \frac{k_p}{\delta_p/2} (T_p - T_{cold}) + A_n \frac{k_n}{\delta_n/2} (T_n - T_{cold}) \right) \\
&- \alpha_{pn} T_{cold} I
\end{aligned} \tag{5.38}$$

$$\alpha_{pn} = \alpha_p - \alpha_n \tag{5.39}$$

In closed-circuit mode, the output voltage generated is essentially the difference between the open-circuit voltage and the voltage drop across the internal resistance computed using Eq.(s). 5.40 –41 (Lee, 2010). The open-circuit voltage however, is estimated using Eq. 5.42 (Nguyen and Pochiraju, 2013). While the current through the circuit is evaluated for a load resistance (R_L) connected across the TEG terminals using Eq. 5.43.

$$V = V_{emf} - IR \tag{5.40}$$

$$R_{internal} = \frac{\varepsilon_p L_p}{A_p} + \frac{\varepsilon_n L_n}{A_n} \tag{5.41}$$

$$V_{emf} = T_o \alpha_{pn}(T_o) - T_L \alpha_{pn}(T_L) \tag{5.42}$$

$$I = \frac{V_{emf}}{R_L + R} \tag{5.43}$$

The temperature-dependant thermo-electrical properties of the thermo-elements including; Seebeck coefficient (α) and electrical resistivity (ε_p) are evaluated using empirical equations supplied by the manufacturer (available in Appendix). To assess the direct relation the Thomson coefficient has on the Seebeck coefficient, Kelvin relationship was applied, Eq. 5.44 (Nguyen and Pochiraju, 2013). Substituting Eq. 5.44 into Eq. 5.39 results in the Seebeck coefficient of the device at junction temperature (T_{hot}, T_{cold}), Eq. 5.45.

$$\alpha_{p,n}(T) = \alpha_{p,n}^{ref} + \mu_{p,n} \ln\left(\frac{T}{T_{ref}}\right) \quad (5.44)$$

$$\alpha_{pn}(T) = (\alpha_p^{ref} - \alpha_n^{ref}) + (\mu_p - \mu_n) \ln\left(\frac{T}{T_{ref}}\right) \quad (5.45)$$

To translate results obtained from a TEG with several cells into that for a single cell, the number of p-n pairs counted in the actual thermoelectric generator and their parallel/serial network connections are determined. The voltage from the model is converted to the complete TEG response with the assumption that all p-n cells are operating under the same conditions. With N p-n cells electrically connected in series in the TEG (N=128), the relationship for electric quantities between the actual and the single TEG cell are given in Eq.(s) 5.46-48. Several material properties are required to successfully simulate the thermal, electrical and thermo-electrical behavior

of the TEG. Most material properties are obtained from the manufacturers' datasheet, however, some properties as the case for both p- and n- elements are adopted from the literature.

$$V_{emf}^{act} = NV_{emf}^{single} \quad (5.46)$$

$$I^{act} = I^{single} \quad (5.47)$$

$$R_{load}^{act} = NR_{load}^{single} \quad (5.48)$$

5.2.2 Fan-Heat sink assembly

Convection heat transfer between a solid surface and a fluid is proportional to the velocity of the fluid. The higher the velocity, the larger the flow rate and the higher the heat transfer rate. The fluid velocities associated with natural convection currents are naturally low, and thus natural convection cooling is limited with its cooling capabilities. Therefore, the rate of heat transfer is enhanced by incorporating a fan on top of the heat sink. The fan-heat sink assembly is capable of increasing the heat transfer coefficient by a factor of up to about 10 by increasing localized airflow while improving thermal efficiency (Aavid Thermalloy, 2016). A schematic diagram of the fan-heat sink assembly attached at the cold plate of the TEG is given in Fig. 5.9. The assembly was fabricated for incorporation in the experimental study.

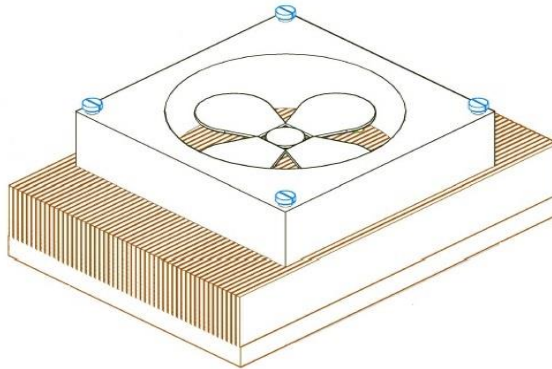


Fig. 5. 9 Fan-Heat sink assembly attached at the TEG cold plate

The cooling capability of the assembly is applied to the computer model by incorporating empirical equations based on tests performed on TEG module having the fan-heat sink attached and in operation while being subject to various heat flux. The cooling capability of the fan-heat sink assembly was obtained at the experimental investigation, in which tests were conducted to monitor the temperature change at the TEG cold plate, Fig. 5.10. The recorded results from the experiment aided obtaining a correlation between the temperature recorded at the surface of the collector and the temperature at the TEG cold plate. Integrating the empirical correlation, the temperature at the cold plate of the TEG can be estimated within the implemented computer model. Hence, the term ($T_{fan-heat sink}$) in Eq. 5.38 for the energy balance of the TEG cold plate is substituted with a value estimated based on the collector temperature in accordance to equation present in Fig. 5.10.

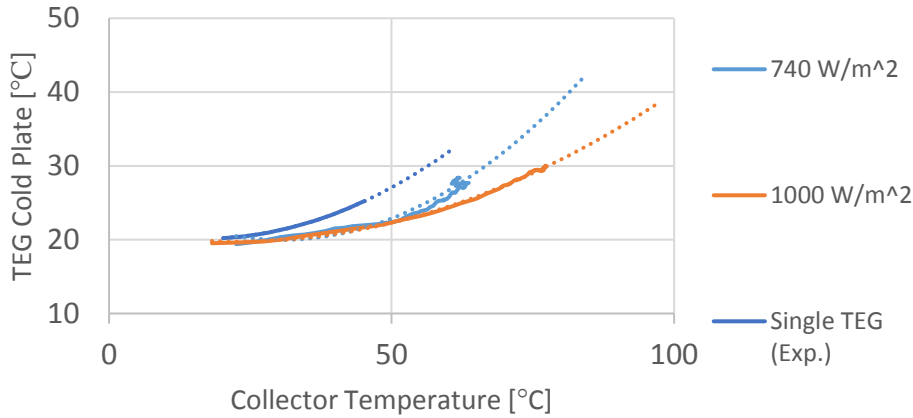


Fig. 5. 10 Correlation between collector and TEG cold plate temperatures

5.3 Discretising energy balance equations

Applying the finite difference approximations given above to the energy balance equations derived earlier will result in the following set of numerical equations for each individual component of the system.

❖ Front glazing layer

$$\begin{aligned}
 & \Delta x \Delta y \rho_g C_g \delta_g \frac{T_{g(i,j+1)} - T_{g(i,j)}}{\Delta t} \\
 & = \Delta x \Delta y k_g \delta_g \frac{T_{g(i+1,j)} - 2T_{g(i,j)} + T_{g(i-1,j)}}{\Delta x^2} \\
 & + \Delta x \Delta y (hc_{forced}) (T_{\infty} - T_{g(i,j)}) \\
 & + \Delta x \Delta y h_{rad(i,j)} (T_{surr(i,j)} - T_{g(i,j)}) \\
 & + \Delta x \Delta y \left(\frac{k_g}{\delta_g} \right) (T_{PV(i,j)} - T_{g(i,j)}) \\
 & + \Delta x \Delta y G_{rad} \alpha_g
 \end{aligned} \tag{5.49}$$

❖ **PV encapsulation layer**

$$\begin{aligned}
& \Delta x \Delta y \rho_{PV} C_{PV} \delta_{PV} \frac{T_{PV(i,j+1)} - T_{PV(i,j)}}{\Delta t} \\
& = \Delta x \Delta y k_{PV} \delta_{PV} \frac{T_{PV(i+1,j)} - 2T_{PV(i,j)} + T_{PV(i-1,j)}}{\Delta x^2} \\
& + \Delta x \Delta y \left(\frac{k_g}{\delta_g} \right) (T_{g(i,j)} - T_{PV(i,j)}) \\
& + \Delta x \Delta y \left(\frac{\delta_{si}}{k_{si}} + \frac{\delta_{EVA}}{k_{EVA}} + \frac{\delta_{TPT}}{k_{TPT}} \right)^{-1} (T_{b(i,j)} - T_{PV(i,j)}) \\
& + \Delta x \Delta y G_{rad} (\tau\alpha)_{PV} - \Delta x \Delta y E
\end{aligned} \tag{5.48}$$

❖ **Base panel layer**a) *Middle node:*

$$\begin{aligned}
& \Delta x \Delta y \rho_b C_b \delta_b \frac{T_{b(i,j+1)} - T_{b(i,j)}}{\Delta t} \\
& = \Delta x \Delta y k_b \delta_b \frac{T_{b(i+1,j)} - 2T_{b(i,j)} + T_{b(i-1,j)}}{\Delta x^2} \\
& + \Delta x \Delta y \left(\frac{\delta_{si}}{k_{si}} + \frac{\delta_{EVA}}{k_{EVA}} + \frac{\delta_{TPT}}{k_{TPT}} \right)^{-1} (T_{PV(i,j)} \\
& - T_{b(i,j)}) \\
& + \Delta x \Delta y \left(\frac{\delta_{ins}}{k_{ins}} + \frac{1}{hc_{free}} \right)^{-1} (T_\infty - T_{b(i,j)})
\end{aligned} \tag{5.49}$$

b) *Heat pipe node:*

$$\begin{aligned}
& \Delta x \Delta y \rho_b C_b \delta_b \frac{T_{b(i,j+1)} - T_{b(i,j)}}{\Delta t} \\
& = \Delta x \Delta y k_b \delta_b \frac{T_{b(i+1,j)} - 2T_{b(i,j)} + T_{b(i-1,j)}}{\Delta x^2} \\
& + \Delta x \Delta y \left(\frac{\delta_{si}}{k_{si}} + \frac{\delta_{EVA}}{k_{EVA}} + \frac{\delta_{TPT}}{k_{TPT}} \right)^{-1} (T_{PV(i,j)} \\
& - T_{b(i,j)}) + A_{bond} \left(\frac{k_b}{\delta_b} \right) (T_{hp(eva)}^{(j)} - T_{b(i,j)}) \\
& + \Delta x \Delta y \left(\frac{\delta_{ins}}{k_{ins}} + \frac{1}{hc_{free}} \right)^{-1} (T_\infty - T_{b(i,j)})
\end{aligned} \tag{5.50}$$

❖ **Evaporator section of heat pipe**

$$\begin{aligned}
& \frac{1}{4} \pi (d_{o,eva}^2 - d_{i,eva}^2) (\rho C l)_{eva} \frac{T_{eva(j+1)} - T_{eva(j)}}{\Delta t} \\
& = \Delta x \Delta y (R_{base-pipe})^{-1} (T_{base} - T_{hp(eva)}) \\
& + (R_{eva-con})^{-1} (T_{hp(con)} - T_{hp(eva)}) \quad (5.51)
\end{aligned}$$

❖ **Condenser section of heat pipe**

$$\begin{aligned}
& \frac{1}{4} \pi (d_{o,con}^2 - d_{i,con}^2) (\rho C l)_{con} \frac{T_{con(j+1)} - T_{con(j)}}{\Delta t} \\
& = \Delta x \Delta y (R_{TE(hot)-(con)})^{-1} (T_{TEG(hot)} - T_{hp(eva)}) \\
& + (R_{eva-con})^{-1} (T_{hp(eva)} - T_{hp(con)}) \quad (5.52)
\end{aligned}$$

Similarly, the finite difference approximations are incorporated to the energy balance equations governing the behaviours of the thermoelectric generator, leading to new set of equations that are solved numerically.

❖ **P-element**

$$\begin{aligned}
& A_p C_p \rho_p \frac{T_{p(i,j+1)} - T_{p(i,j)}}{\Delta t} \\
& = k_p A_p \frac{T_{p(i+1,j)} - 2 T_{p(i,j)} + T_{p(i-1,j)}}{\Delta x^2} + \frac{\varepsilon_p}{A_p} I^2 \\
& - \mu_p I \frac{T_{p(i+1,j)} - T_{p(i,j)}}{\Delta x} \quad (5.53)
\end{aligned}$$

❖ **N-element**

$$\begin{aligned}
& A_n C_n \rho_n \frac{T_{n(i,j+1)} - T_{n(i,j)}}{\Delta t} \\
&= k_n A_n \frac{T_{n(i+1,j)} - 2 T_{n(i,j)} + T_{n(i-1,j)}}{\Delta x^2} + \frac{\varepsilon_n}{A_n} I^2 \\
&+ \mu_n I \frac{T_{n(i+1,j)} - T_{n(i,j)}}{\Delta x}
\end{aligned} \tag{5.54}$$

❖ **TEG hot plate**

$$\begin{aligned}
& A_{hot} (\rho C \delta)_{hot} \frac{\partial T_{hot}}{\partial t} \\
&= \left(\Delta x k_{hot} \delta_{hot} l_{hot} \frac{T_{hot(i+1,j)} - 2 T_{hot(i,j)} + T_{hot(i-1,j)}}{\Delta x^2} \right) \\
&+ \left(A_{hot} \frac{k_{hot}}{\delta_{hot}} (T_{hp(con)} - T_{hot}) \right) \\
&+ \left(A_p \frac{k_p}{\delta_p/2} (T_p - T_{hot}) + A_n \frac{k_n}{\delta_n/2} (T_n - T_{hot}) \right) + \alpha_{pn} T_{hot} I
\end{aligned} \tag{5.55}$$

❖ **TEG cold plate**

$$\begin{aligned}
& A_{cold} (\rho C \delta)_{cold} \frac{\partial T_{cold}}{\partial t} \\
&= \left(\Delta x k_{cold} \delta_{cold} l_{cold} \frac{T_{cold(i+1,j)} - 2 T_{cold(i,j)} + T_{cold(i-1,j)}}{\Delta x^2} \right) \\
&+ \left(A_{cold} \frac{k_{cold}}{\delta_{cold}} (T_{fan-heatsink} - T_{cold}) \right) \\
&+ \left(A_p \frac{k_p}{\delta_p/2} (T_p - T_{cold}) + A_n \frac{k_n}{\delta_n/2} (T_n - T_{cold}) \right) - \alpha_{pn} T_{cold} I
\end{aligned} \tag{5.56}$$

5.4 Solution Routine (Flow Chart)

The theoretical model developed earlier is implemented in MATLAB in accordance to the simplified illustrative flow charts presented in Fig.(s) 5.11-12. The heat pipes based PV collector modelling process is initiated by defining the initial conditions, collector geometry and thermal and electrical properties of the PV module. The operating conditions are defined in the model to assess the performance for particular operating environments. adopting the nodal temperature scheme for transient heat transfer, the model is implemented to solve the equations explicitly in time. The energy balance equations of the PV thermal collector are solved to estimate the temperature values at each junction within the system. The condenser temperature is considered the interface between the heat pipe based PV collector and the heat waste recovery system which is highlighted in Fig. 5.12. Similarly, the TEG model was incorporated in the developed model and solved simultaneously with the energy balance equations of the PV collector. The flow charts below indicate the steps and loops executed for the integrated system performance prediction.

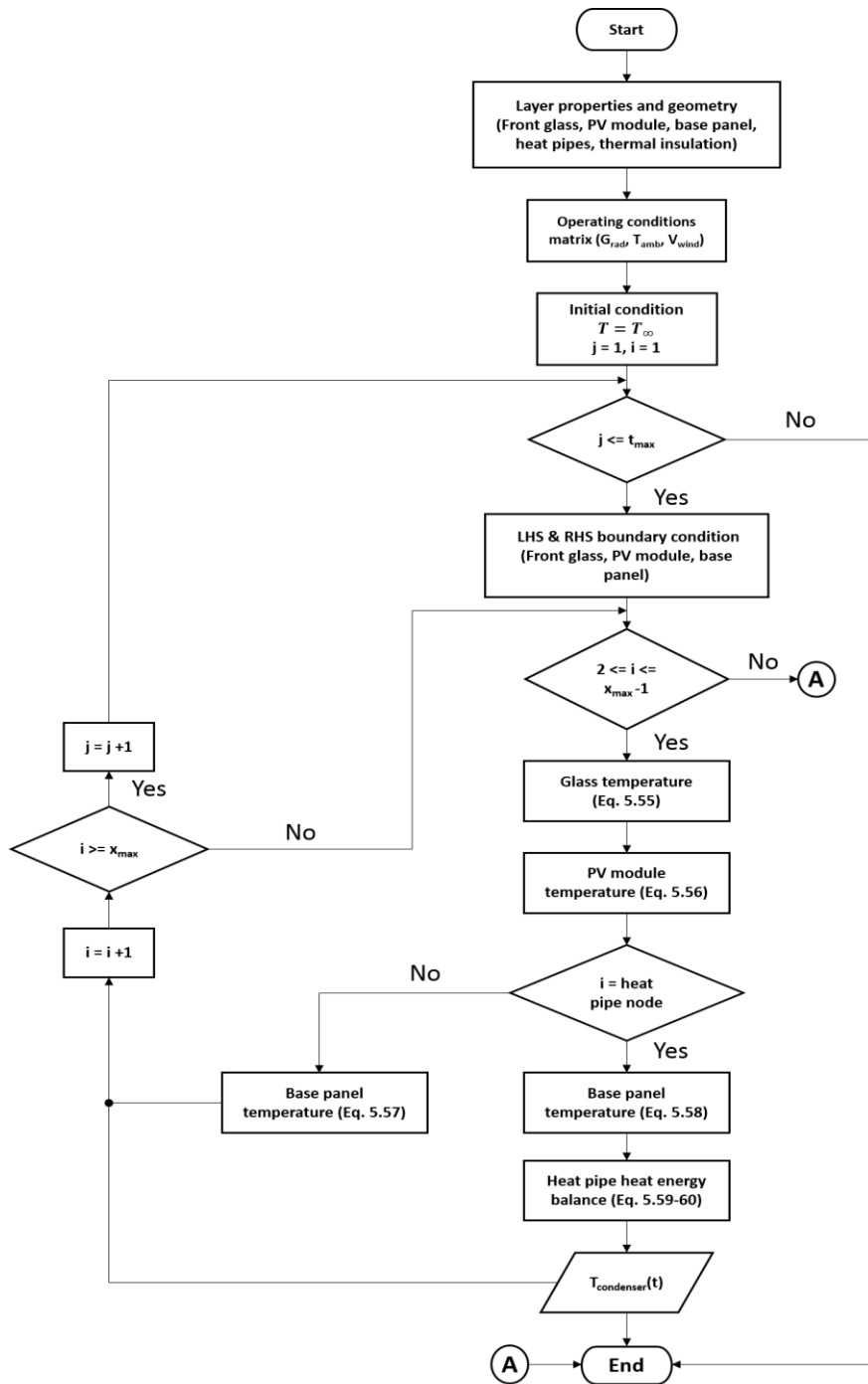


Fig. 5. 11 Heat pipe-based Photovoltaic collector thermal modelling flow chart

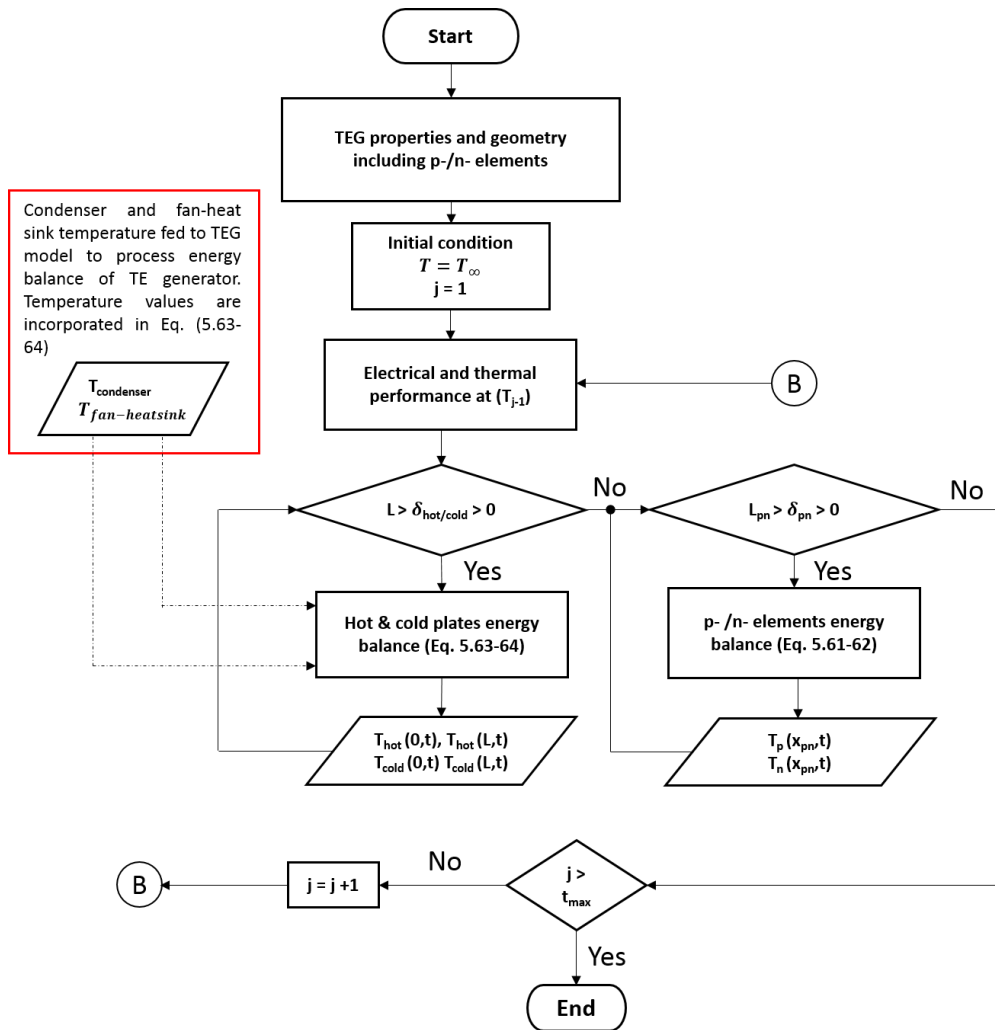


Fig. 5. 12 Thermoelectric generator computer model implementation flow chart

Chapter 6

Computer Model Results and Discussion

The integration of the heat pipe-based TEG assembly for thermal management of the PV module is evaluated through analysing the temperature and output power responses, in addition to the energy conversion efficiency of the collector. In order to evaluate and quantify the performance enhancements associated with the proposed integration, comparison against conventional PV module is conducted. In this section, three collectors are considered for the theoretical analysis purpose, including:

- a) Conventional PV module
- b) Integrated heat pipe-based PV-TEG collector
- c) Integrated heat pipe-based PV-TEG collector with insulation

The three collectors are simulated and compared against each other for identical operating conditions presented in Table 6.1.

Table 6. 1 Theoretical performance evaluation conditions applied

| Light intensity | Ambient temperature | Wind speed |
|---------------------|---------------------|------------|
| [W/m ²] | [°C] | [m/s] |
| 740 - 1060 | 20 – 50 | 0 – 5 |

6.1 Temperature response

The temperature response of the PV cells is considered the main parameter to characterize the effectiveness of the integrated cooling system. In this section, the temperature response of the conventional PV module is compared against the heat pipe-based PV-TEG collector. In order to develop insights of the system performance under varying operating conditions, both *Transient* and *Steady State* temperature responses of each collector are presented and discussed. The temperature elevation caused by increased light intensity, in addition to the combined influences of flow over the collector due to wind and the buoyancy-induced flow due to the external air are observed.

6.1.1 Steady State Response

Conventional PV module and Integrated PV-TEG Comparison

The correlation between the temperature of the PV cells against the radiation intensity and wind speed for the conventional PV collector, is given in Fig. 6.1. Note that during the experiment on the conventional PV panel

the condition applied at the test in terms of wind speed is of (0 m/s), as a result of the condition at the laboratory. However, since wind speed is a major factor in performance prediction of PV modules under realistic operating conditions, it is considered in this assessment for a broader range of speeds. The temperature of the PV cell is dramatically increased by the increased light intensity, due to absorption of sunlight by the PV module in regions which are not covered by solar cells as well as absorption of infrared radiation. Continuous light illumination on the surface of the PV module as well as high absorptivity of the PV cells material have a substantial influence on the PV cell temperature. At the absence of the wind influence, temperature change from 51°C to 86°C as the light intensity changes from 750-1060 W/m² was observed.

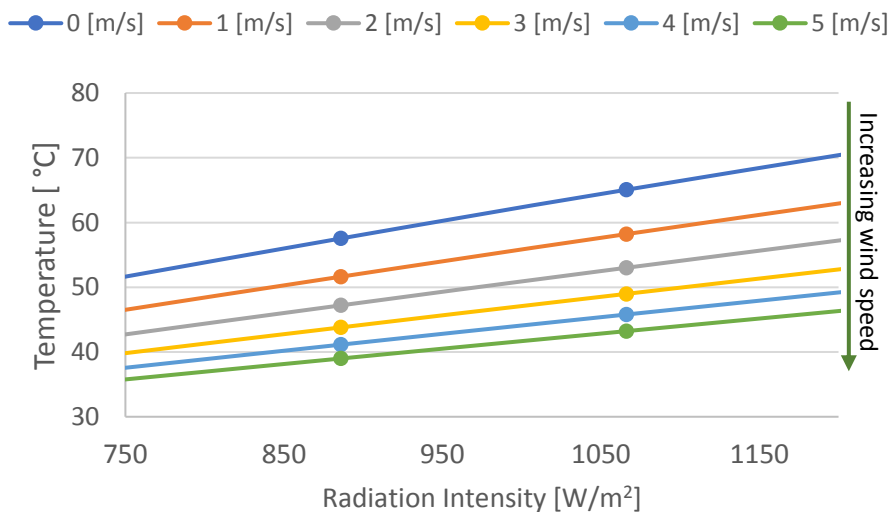
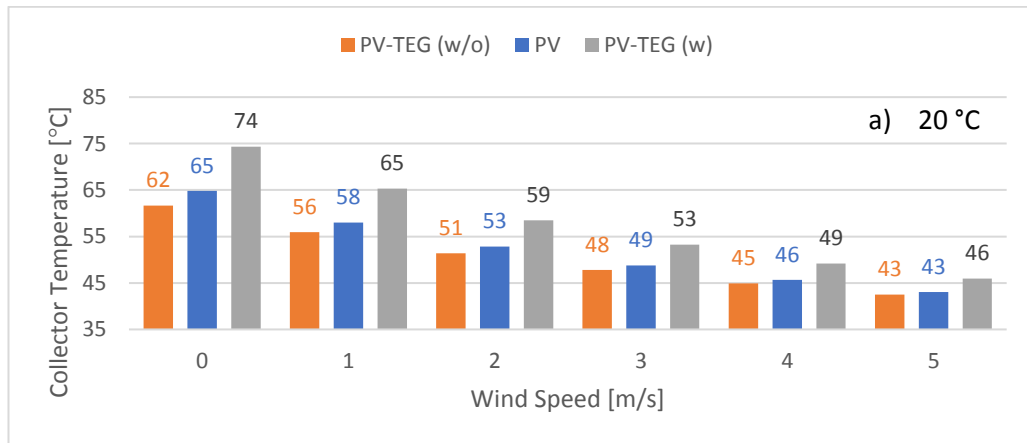


Fig. 6. 1 PV encapsulation temperature against radiation intensity for range of wind speeds

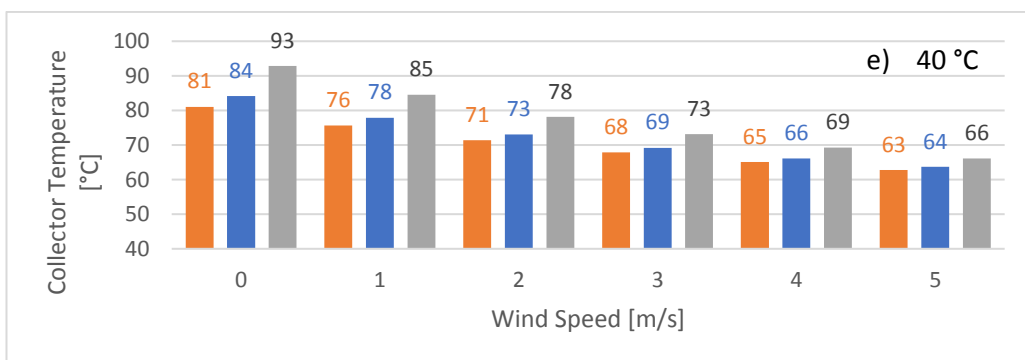
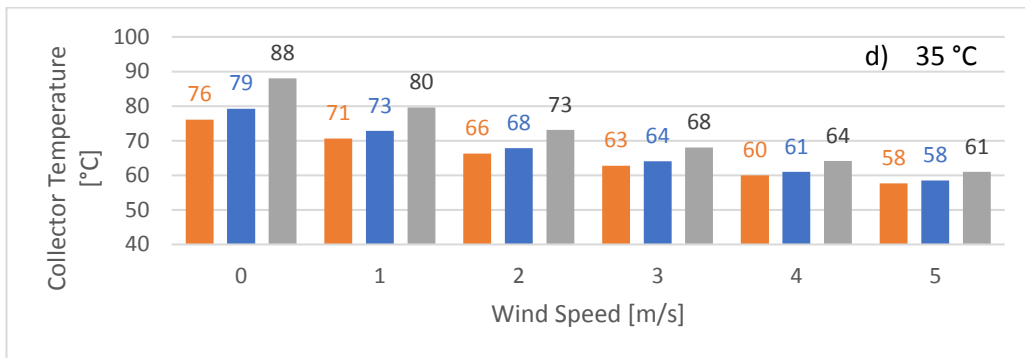
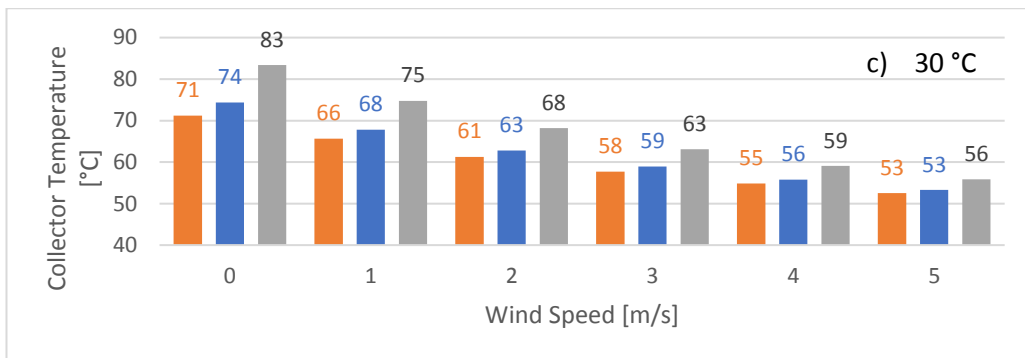
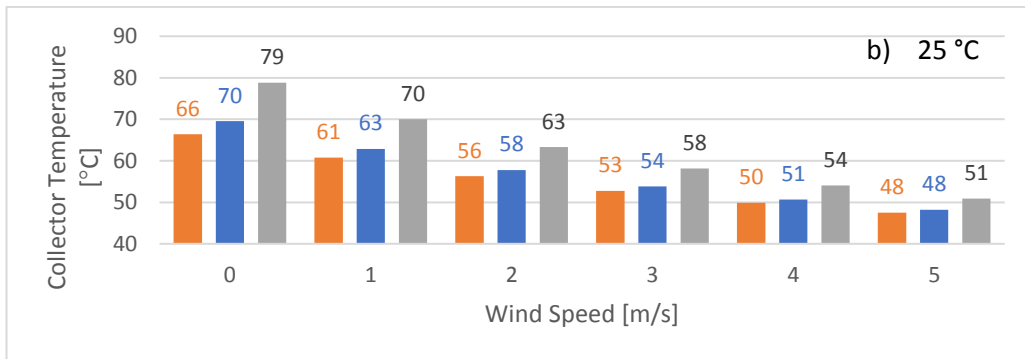
Similarly, it is clearly observed that change in the wind speed would alter the energy balance within the system. This is due to thermal energy exchange between the surface and the surrounding fluid (convection), described by Newton's law of Cooling. The influence of wind speed is incorporated through the convective heat transfer coefficient (h_{wind}), described previously Eq.5.7. Hence, convection from the collector is substantially increased by the presence of increasing wind speeds as presented in Fig. 6.1. In addition, free convection at the rear of the panel contributes to reduction in the predicted temperature of the collector to much less degree. In this situation, buoyancy-driven free convection dominates the convective heat transfer at the rear, in which surface-to-air temperature difference drives the convective thermal exchange. As a result, forced convection predominate in situations of windy surrounding, while free convection is experienced at the absence of wind and only the temperature difference between the surface and the surrounding quantifies the convective loss.

The steady state temperature responses of the collectors evaluated at maximum light intensity of ($G_{rad} = 1000 W/m^2$) is presented in Fig. 6.2. The light intensity is set constant while both wind speed and ambient temperature are varied each at a time. It is evident that the existence of insulation at the rear of the collector contributes to further rise the

temperature of the PV layer in the order of 2-10°C for the wind speed condition range of 0-5 m/s when compared against the conventional PV module. The temperature elevation or reduction due to the existence or absence of insulation at the rear of the integrated collector is better observed in Fig. 6.3. At the range of ambient temperatures conditions considered, the temperature difference between the PV-TEG collectors and the conventional module appears to be constant as presented in Fig. 6.3, and hence an average value is presented. Although elevated temperature has an adverse effect on the electrical performance of the PV cells, the thermal energy gained as a result is analysed to assess the performance enhancement possibilities in power output due to thermoelectric conversion.



Chapter 6 Computer Model Results and Discussion



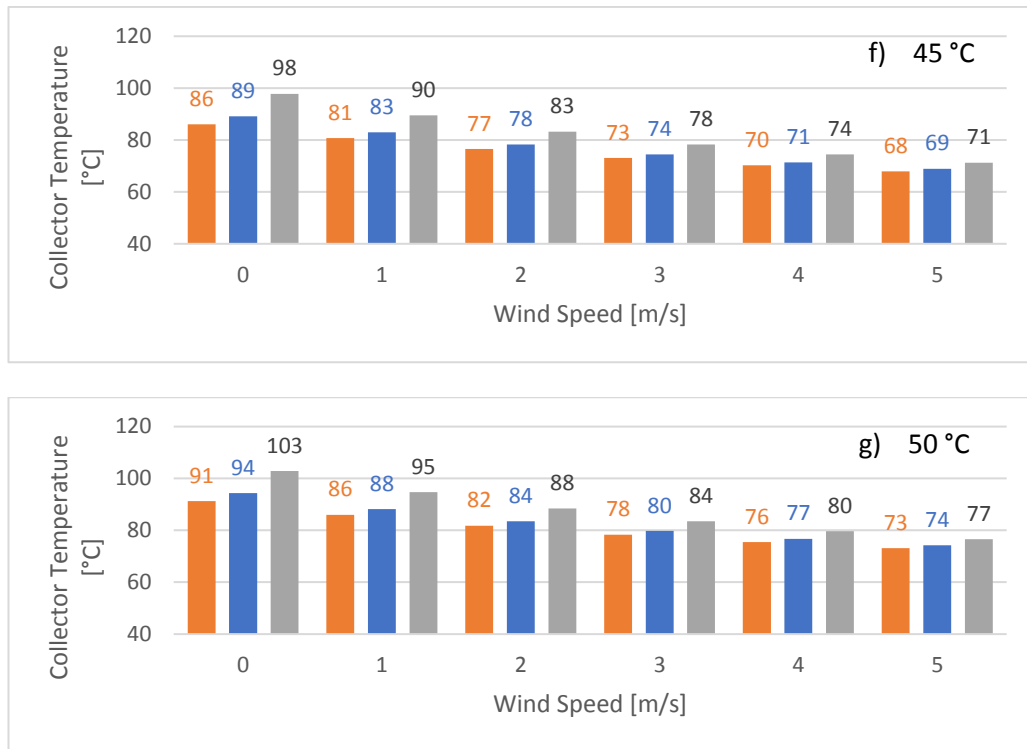


Fig. 6. 2 Steady state PV temperature response for ambient temperature range of 20-50 °C and Wind speed range of 0-5 m/s under light intensity of 1000 W/m²

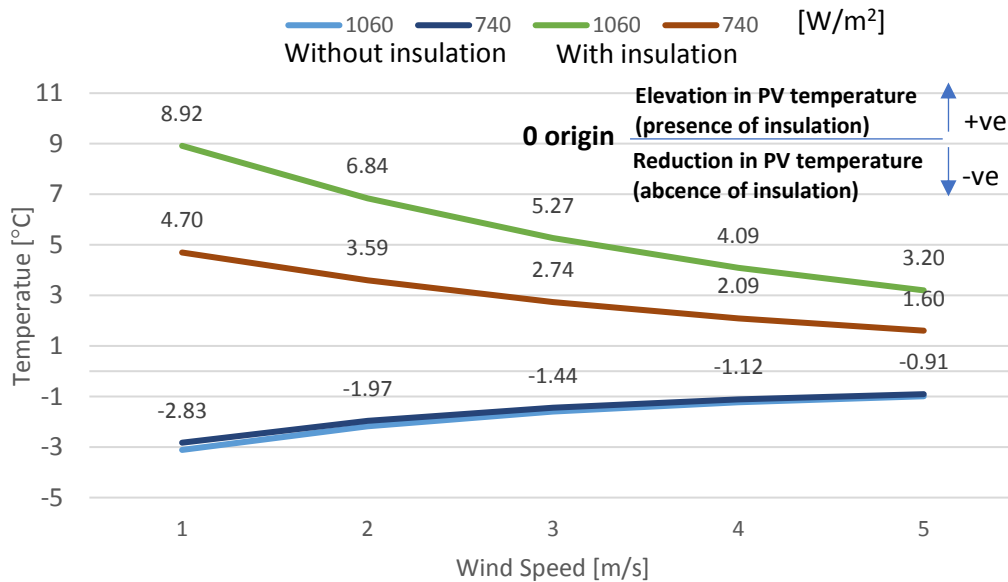


Fig. 6. 3 Influence of insulation on the temperature response of the integrated PV-TEG collector

For analysis purpose, the temperature responses of the three collectors against varying ambient operating temperature for fixed wind speed of (0 m/s) and light intensity of ($G_{rad} = 1000 W/m^2$) are presented in Fig. 6.4. It is apparent that the integrated heat pipe-based PV-TEG collector with no insulation exhibits the lowest temperature response for the range of the operating ambient temperature conditions considered amongst the collectors. The proposed collector design exhibits improved temperature response at low wind speeds, while at high wind speeds the three collectors display almost identical temperature response.

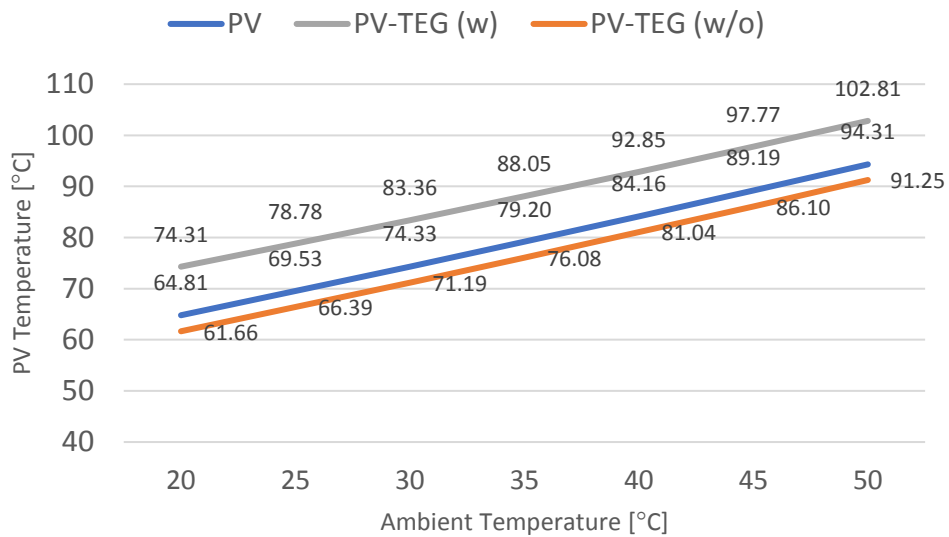


Fig. 6. 4 PV cells temperature for varying operating temperature and (0 m/s) wind speed

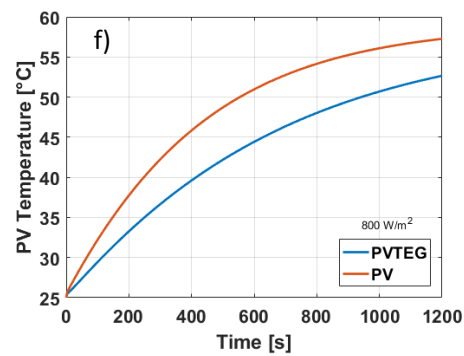
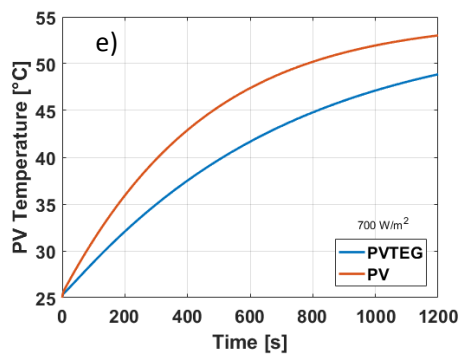
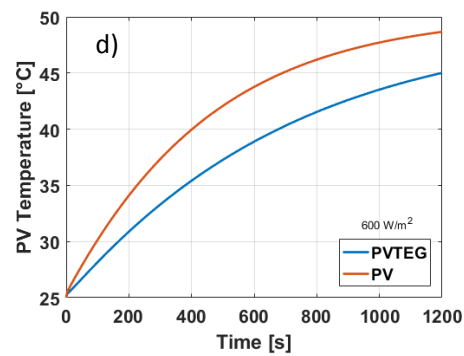
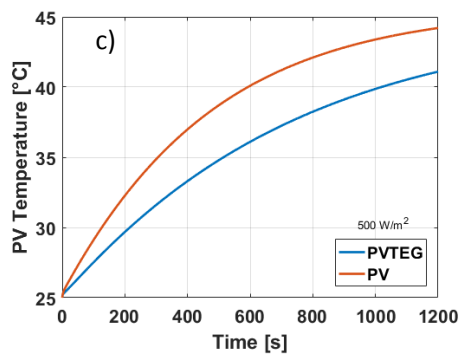
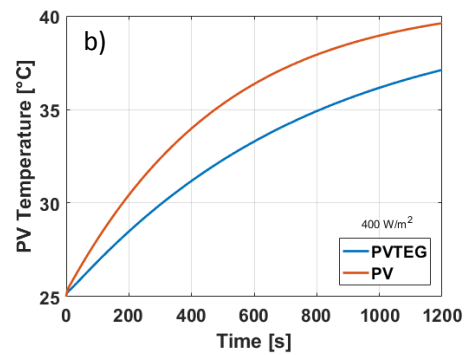
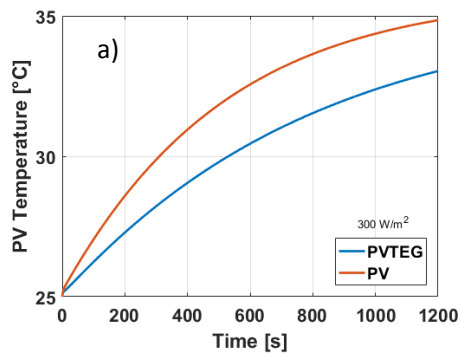
6.1.2 Transient Response

Conventional PV module and Integrated PV-TEG Comparison

The transient temperature response of the heat pipe based PV-TEG collector with no insulation relative to the conventional PV module for ambient operating temperature of ($T_{amb}=25\text{ }^{\circ}\text{C}$) and wind speed of ($v_{wind}=0\text{ m/s}$) is given in Fig.(s) 6.5. As the light intensity varies between 300-1000 W/m^2 , improved operating temperature was attained by the integrated PV-TEG collector for the PV cells. This improvement is directly linked to the power performance capabilities of the collector. Under light intensity of ($G_{rad}=1000\text{ W/m}^2$), maximum temperature difference between the collectors of 8°C was observed. The maximum temperature differences ($t=600\text{s}$) between the integrated collector without insulation and the conventional PV module for the light intensity range considered is given in Table 6.2. The integration of the heat pipes in collector assisted the temperature management of the system remarkably, showing immense potential especially under high light intensities with improvement of 16% in the operating temperature. For PV modules operating in practice, this is attractive as the associated high light intensity and temperature elevation as a result are controlled to a certain degree with the aid of the efficient heat transport capabilities of the heat pipes incorporated.

Table 6. 2 Temperature difference between PV-TEG and conventional PV collectors

| $G_{rad}[W/m^2]$ | 100 | 200 | 300 | 400 | 500 | 600 | 700 | 800 | 900 | 1000 |
|-------------------------------|-----|-----|-----|-----|-----|-----|-----|-----|-----|------|
| $Max\Delta T_{PV}[^{\circ}C]$ | 0.5 | 1.1 | 2.1 | 3.1 | 4.0 | 4.9 | 5.7 | 6.5 | 7.3 | 8.1 |
| T_{PV} imprv. | 2% | 4% | 7% | 9% | 11% | 13% | 14% | 15% | 16% | 16% |



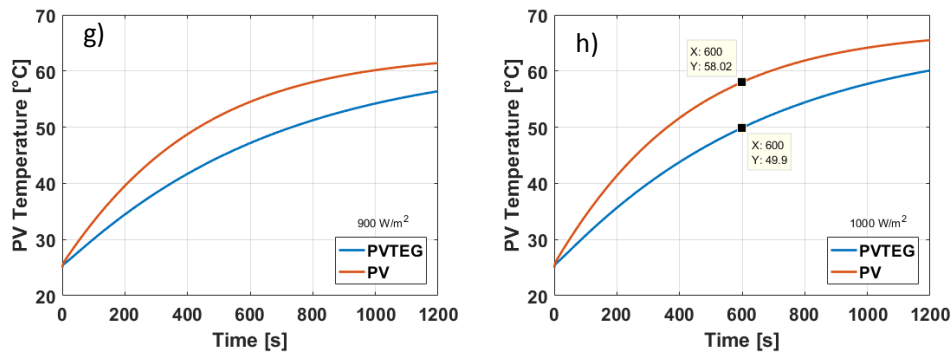


Fig. 6. 5 Transient PV Temperature response for range of light intensities at operating temperature $T_{amb} = 25$ °C and wind speed = 0 m/s; a) 300 W/m², b) 400 W/m², c) 500 W/m², d) 600 W/m², e) 700 W/m², f) 800 W/m², g) 900 W/m², h) 1000 W/m²

6.2 Low Temperature Thermal Waste Recovery

6.2.1 Thermal energy absorbed by Thermoelectric generators

The drop in the PV cells temperature of integrated collector due to heat extraction via the incorporated heat pipe-based TEG bank is also analysed in terms of the heat flux absorbed. The absorbed heat flux contributes to temperature drop of about 1-4°C across the wind speeds range considered as per Fig. 6.3. The absorbed heat flux is then utilised for thermal waste recovery contributing to further power generation; adopting the Seebeck phenomena of the TEG modules. The quantified heat flux absorber by a single TEG module and the TEG bank for the conditions considered for the maximum (8 m/s) and minimum (0 m/s) wind speed limits is given in Fig. 6.6. At the absence of the wind influence, the integration of the TEG bank proves

to be beneficial; resulting in the temperature drop of a higher degree when compared with that of elevated wind speeds. For the light intensity range of ($G_{rad} = 740$ and 1060 W/m^2), the heat flux absorbed under the ambient temperature range of ($T_{amb} = 20 - 50 \text{ }^\circ\text{C}$) and wind speed of (0 m/s) is presented in Fig. 6.7.

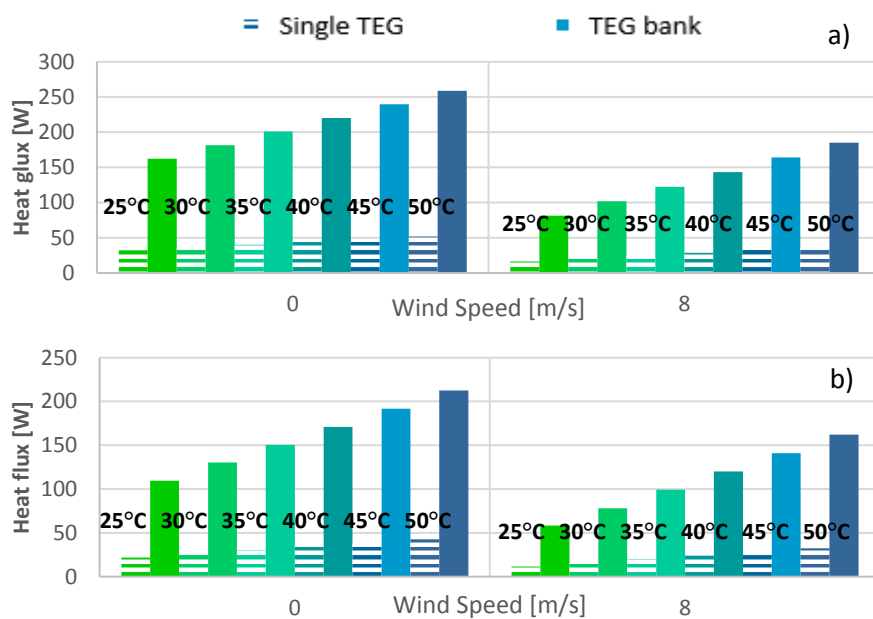


Fig. 6. 6 Thermal waste energy absorbed by TEG, a) 1060 W/m^2 , b) 740 W/m^2

The absorbed heat flux is observed to increase as both light intensity and operating temperature increase, while the wind speed expressed adverse effect on the amount of thermal waste energy absorbed. This confirms the observations made earlier for the PV cells temperature. Hence, at high light intensity the temperature of the PV cells is elevated resulting in enhanced thermal energy flux available.

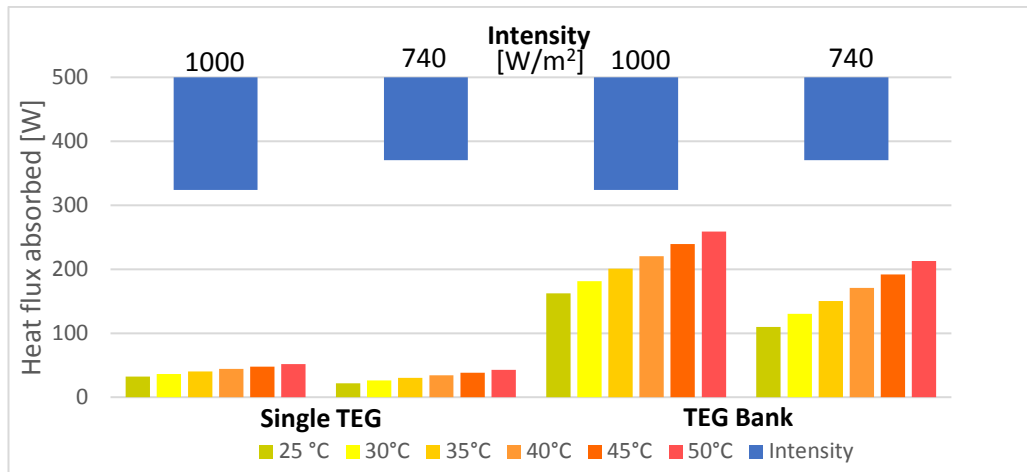


Fig. 6. 7 Thermal waste energy absorbed by thermoelectric generators for range of light intensities and operating temperatures at wind speed = 0 m/s

6.3 Electrical Performance

6.3.1 Steady State Response

Conventional PV module and Integrated PV-TEG Comparison

The relationship between the PV electrical power output against the radiation intensity for range of wind speeds for the conventional PV collector, is given in Fig. 6.8. The output power comparison between the three considered is given in Fig. 6.9 for radiation intensity level of 1000 W/m^2 and wind speed of 0 m/s. The power response against ambient temperature for both integrated PV-TEG collector with and without insulation considered the total power available from both PV module and integrated TEG module. For the range of ambient temperature considered the integrated PV-TEG collector without insulation displayed improved power output compared to

the other collectors with an almost constant power difference relative to the conventional PV module. Compared with the conventional module the integrated collector in the presence of the insulation slightly improved power performance is observed at elevated ambient temperature, due to the availability of higher grade thermal energy recovered by the integrated heat pipe-base recovery system.

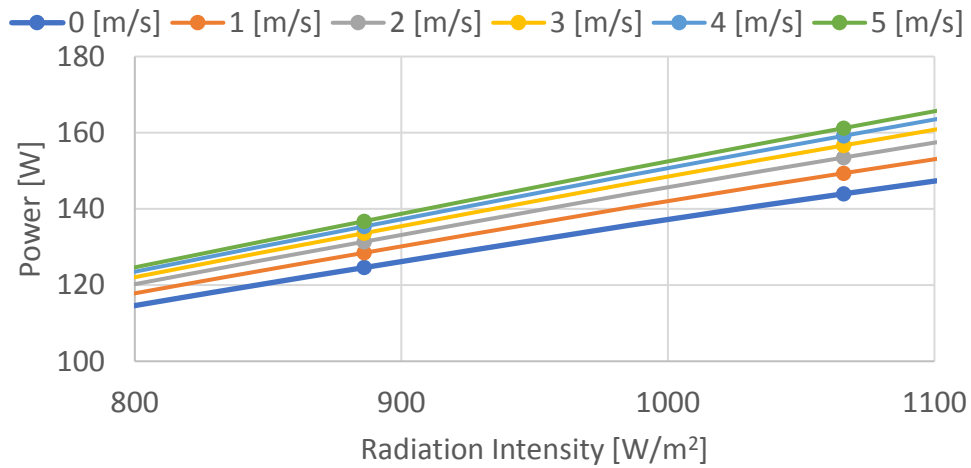


Fig. 6. 8 Conventional PV module power output for varying wind speed and light intensity.

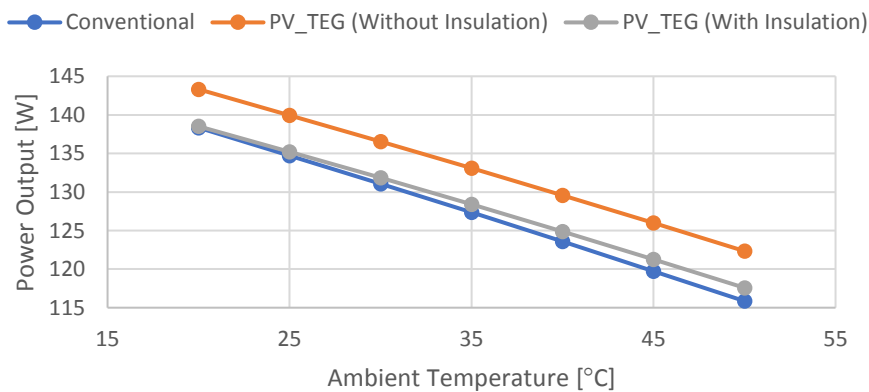


Fig. 6. 9 Output power comparison between the three considered for radiation intensity level of 1000 W/m² and wind speed of 0 m/s.

6.3.2 Transient Response

Conventional PV module and Integrated PV-TEG Comparison

The transient output power response of the heat pipe based PV-TEG collector with no insulation relative to the conventional PV module for ambient operating temperature of ($T_{amb}=25\text{ }^{\circ}\text{C}$) and wind speed of ($v_{wind}=0\text{ m/s}$) is given in Fig.(s) 6.10. As the light intensity varies between 300-1000 W/m^2 , enhanced power output from the PV cells was observed for the integrated collector. This improvement is directly linked to the reduction in the PV cells temperature discussed earlier. Under light intensity of ($G_{rad}=1000\text{ W/m}^2$), maximum power difference between the collectors of 5.8 Watts was observed. The maximum power difference ($t=600\text{s}$) between the integrated collector without insulation and the conventional PV module for the light intensity range considered is given in Table 6.3. The integration of the heat pipes in collector assisted the temperature management of the system remarkably, showing immense potential especially under high light intensities with improvement of 16% in the operating temperature, in which a corresponding enhancement of about 4% in the power output is achieved.

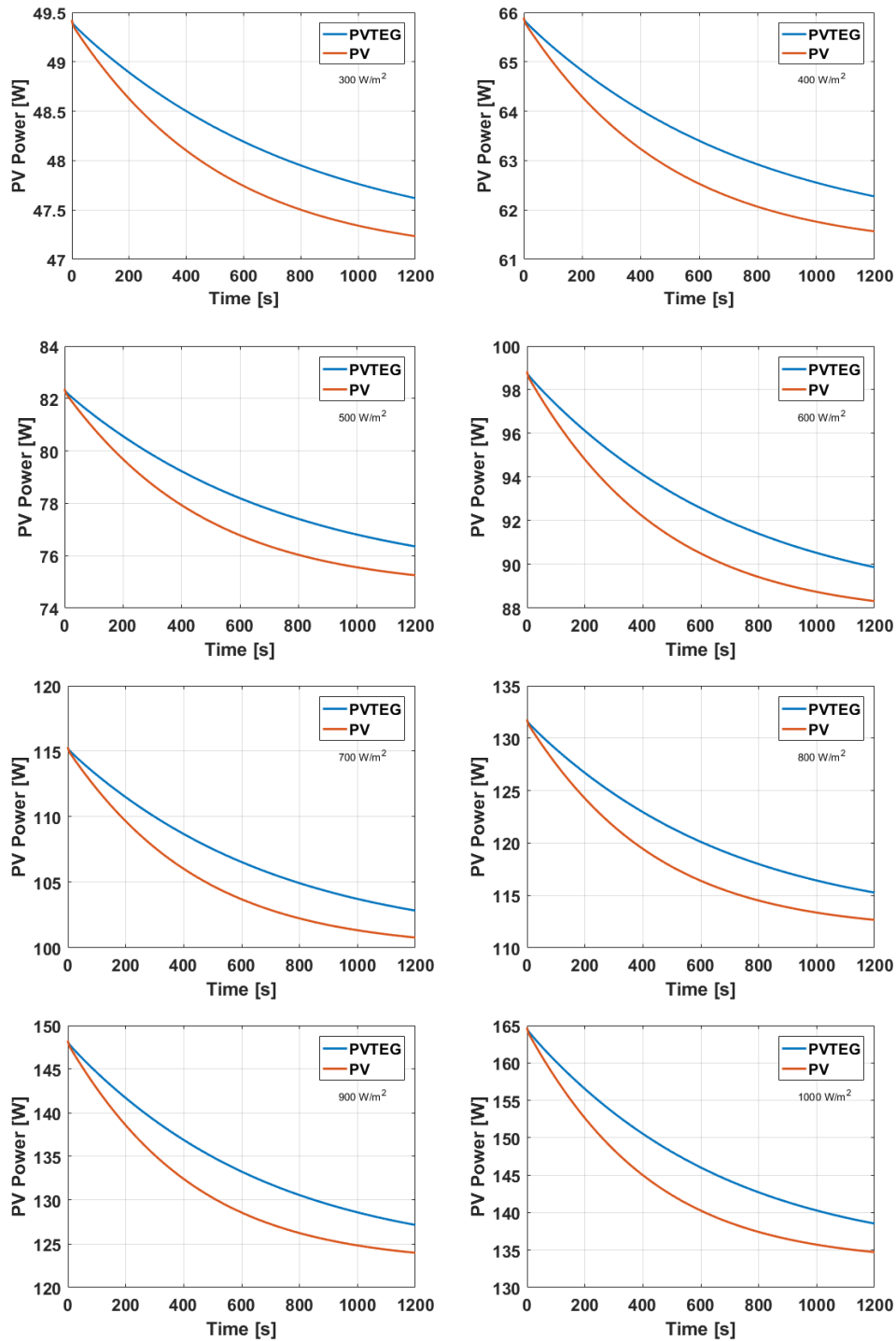


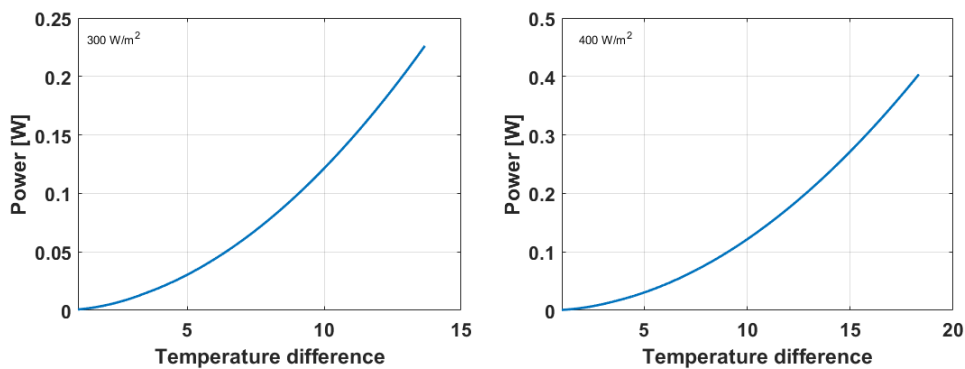
Fig. 6. 10 Transient PV Temperature response for range of light intensities at operating temperature $T_{amb} = 25\text{ }^{\circ}\text{C}$ and wind speed = 0 m/s; a) 300 W/m², b) 400 W/m², c) 500 W/m², d) 600 W/m², e) 700 W/m², f) 800 W/m², g) 900 W/m², h) 1000 W/m²

Table 6. 3 Power output difference between PV-TEG and conventional PV collectors

| $G_{rad}[W/m^2]$ | 100 | 200 | 300 | 400 | 500 | 600 | 700 | 800 | 900 | 1000 |
|---------------------|------|------|-----|-----|-----|-----|-----|-----|-----|------|
| Max ΔP_{PV} | 0.1 | 0.2 | 0.4 | 0.9 | 1.4 | 2.1 | 2.8 | 3.7 | 4.7 | 5.8 |
| P_{PV} improv. | 0.2% | 0.5% | 1% | 1% | 1% | 2% | 2% | 3% | 3% | 4% |

6.4 Thermoelectric Generator Electrical Performance

At steady state, the thermoelectric power performance against the temperature difference between the TEG plates is given in Fig. 6.11. As the radiation intensity is increased the thermal energy available for absorption is further enhanced; realized by the improved temperature difference across the TEG plates. At maximum radiation of $1000 W/m^2$, the temperature difference governing the TEG module power output is of 40 degrees allowing for heat to electricity conversion of an additional 2 Watts.



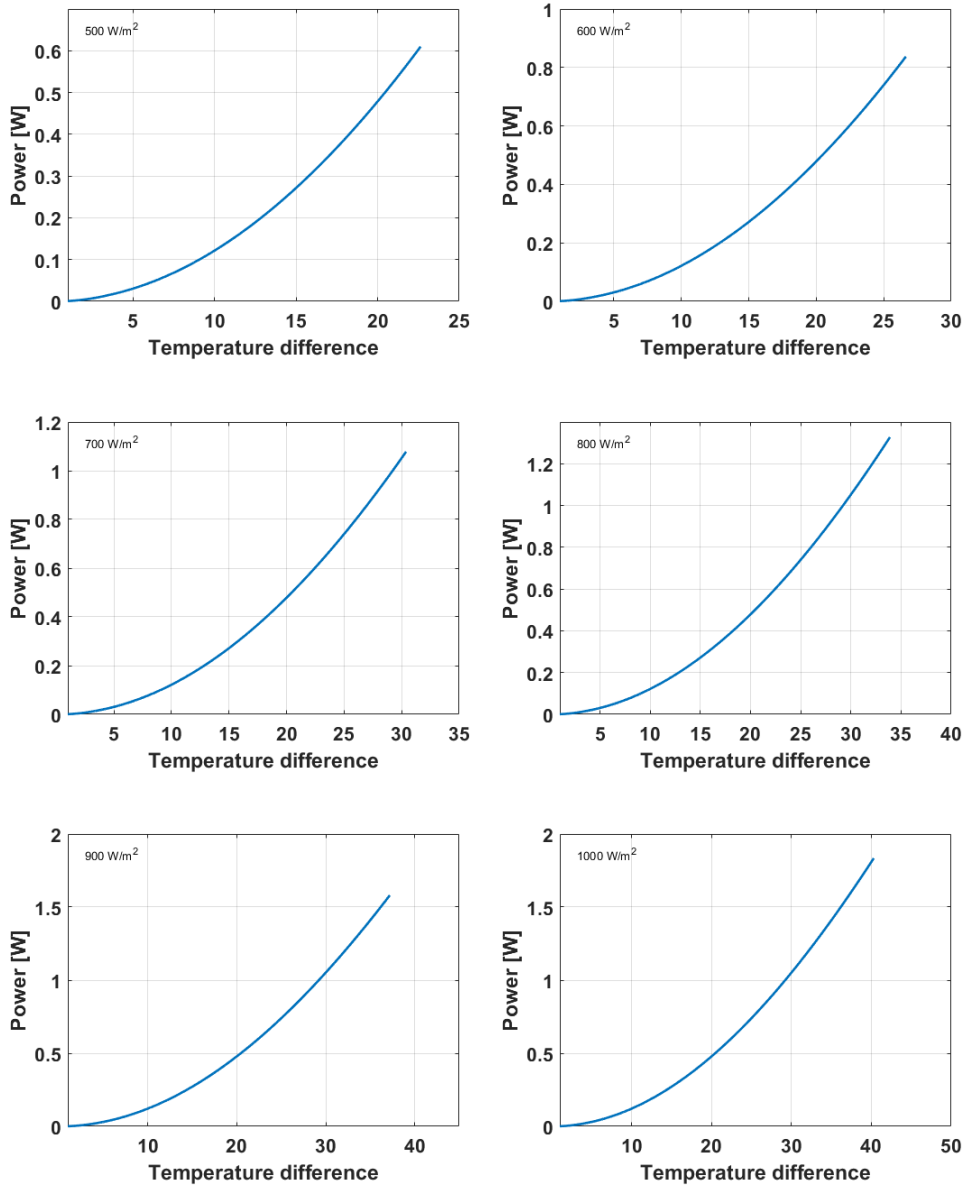


Fig. 6. 11 Thermoelectric generator power output against the temperature difference across TEG plates intensities at operating temperature $T_{amb} = 25\text{ }^{\circ}\text{C}$ and wind speed = 0 m/s; a) 300 W/m², b) 400 W/m², c) 500 W/m², d) 600 W/m², e) 700 W/m², f) 800 W/m², g) 900 W/m², h) 1000 W/m²

6.5 Conversion Efficiency

6.5.1 PV Cells Conversion Efficiency

The steady state PV conversion efficiency of the conventional PV module as function of the light intensity and wind speed experienced is given in Fig. 6.12. The transient conversion efficiency of the heat pipe based PV-TEG collector with no insulation relative to the conventional PV module for ambient operating temperature of ($T_{amb}=25\text{ }^{\circ}\text{C}$) and wind speed of ($v_{wind}=0\text{ m/s}$) is given in Fig.(s) 6.13.

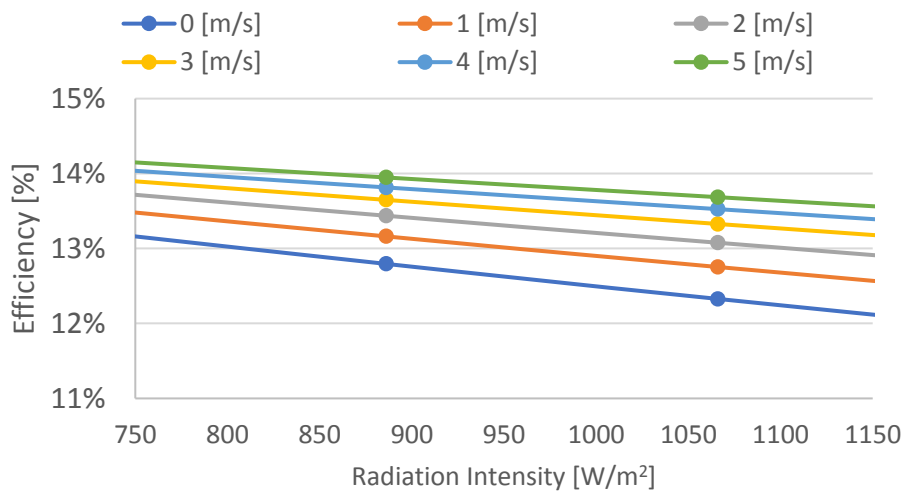


Fig. 6. 12 Steady State Electrical Conversion Efficiency Against Wind Speed

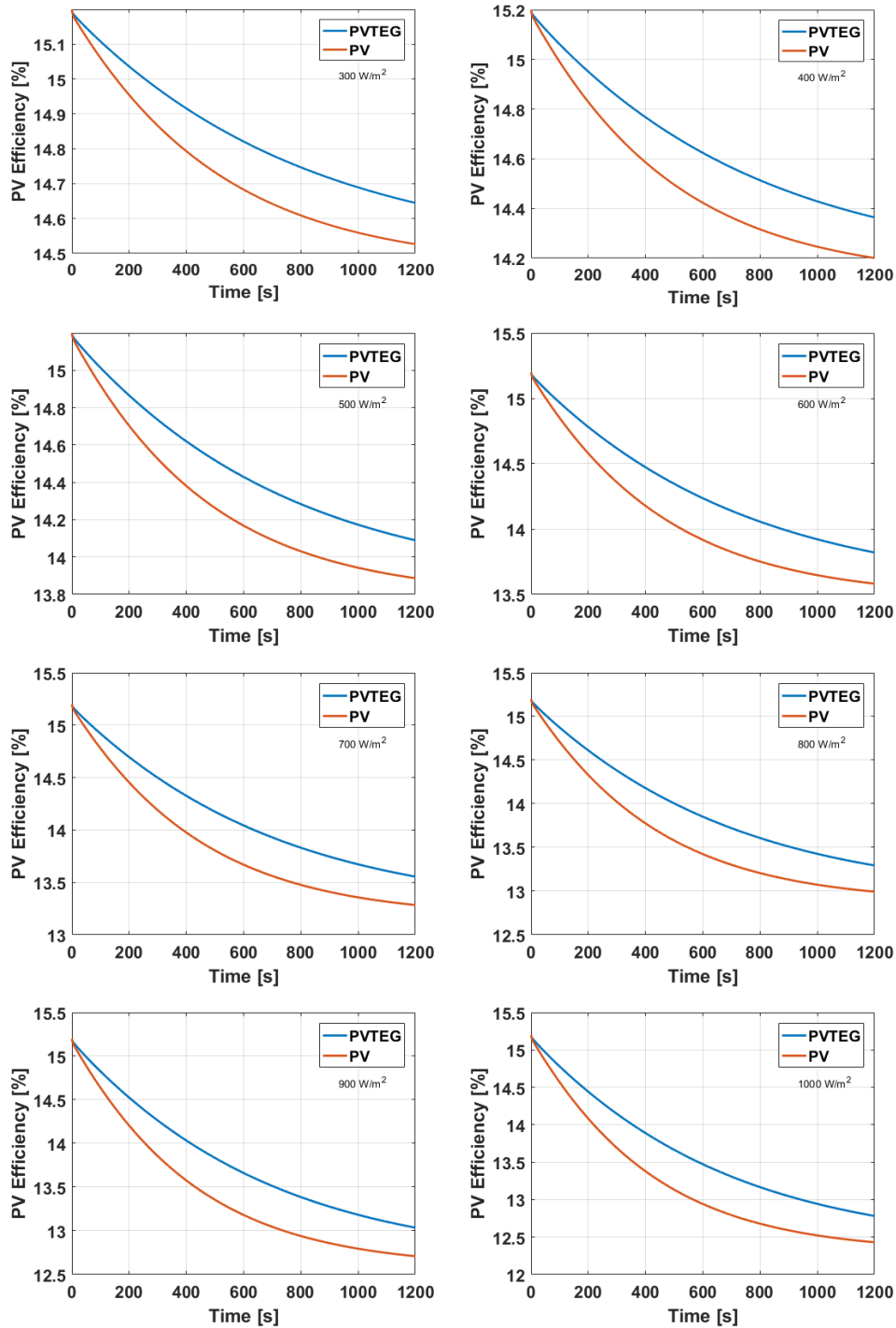


Fig. 6. 13 PV cells efficiency against the temperature difference across TEG plates intensities at operating temperature $T_{amb} = 25\text{ }^{\circ}\text{C}$ and wind speed = 0 m/s; a) 300 W/m², b) 400 W/m², c) 500 W/m², d) 600 W/m², e) 700 W/m², f) 800 W/m², g) 900 W/m², h) 1000 W/m²

6.5.2 Integrated PV-TEG Collector Efficiency

The PV panel and TEG module efficiencies as a function of various operating conditions of irradiance, wind speed, and ambient temperature is shown in Fig. (s) 6.14-16. Increased irradiance improves the PV panel efficiency as more solar energy is available at the collector per unit area for electricity generation, in addition to increased TEG conversion efficiency as higher radiation permits higher temperature difference across the TEG module plate. However, the PV panel efficiency is enhanced with increased wind speed due to the effect of convection on the surface of the collector, while the TEG module efficiency degrades as less temperature difference is available across the TEG plates for electrical conversion. On the other hand, ambient temperature has a reverse influence on the PV panel efficiency.

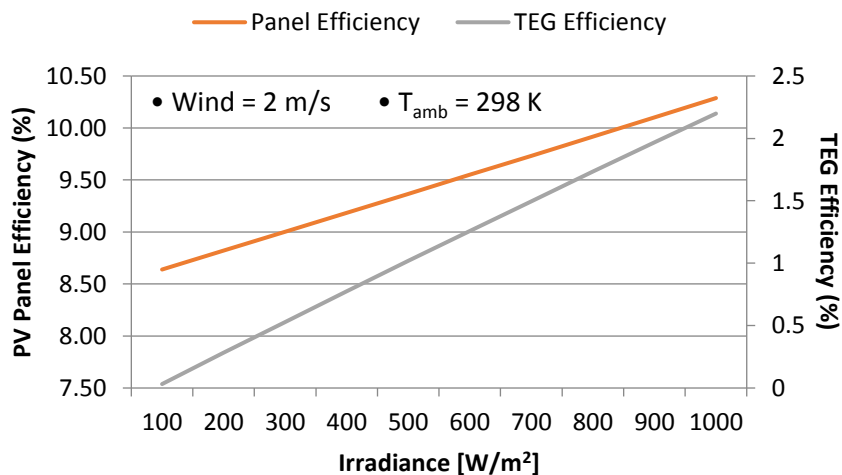


Fig. 6. 14 PV panel and TEG efficiencies as a function of irradiance

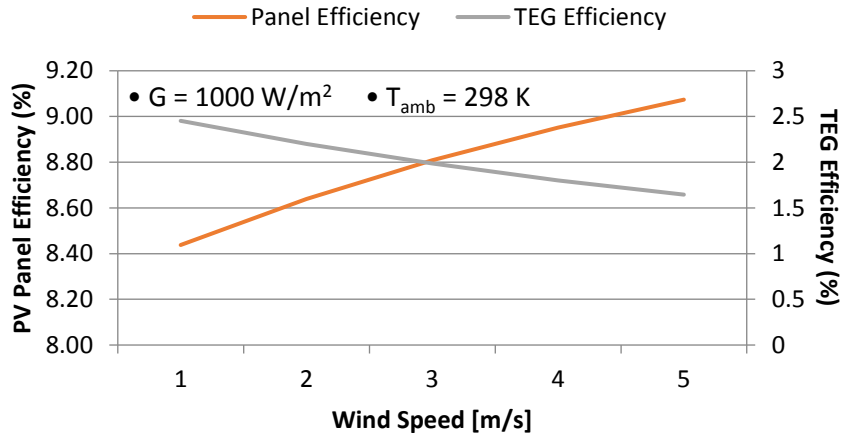


Fig. 6. 15 PV panel and TEG efficiencies against wind speed

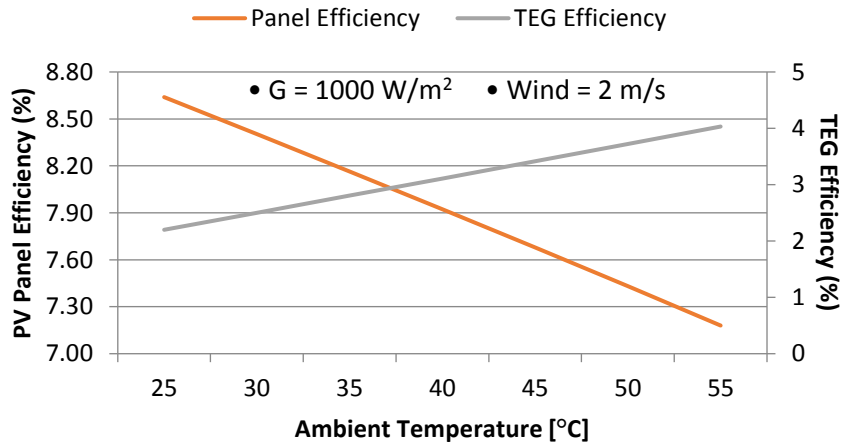


Fig. 6. 16 PV panel and TEG efficiencies as a function of ambient temperature

A comparison between the combined efficiency of the collector and the efficiency of a conventional PV panel of the same size as function of operating conditions of irradiance, wind speed, and ambient temperature is shown in Fig. (s) 6.17-19. It is observed that under all cases the hybrid collector permits further enhanced performance even at high ambient temperature and low wind speeds.

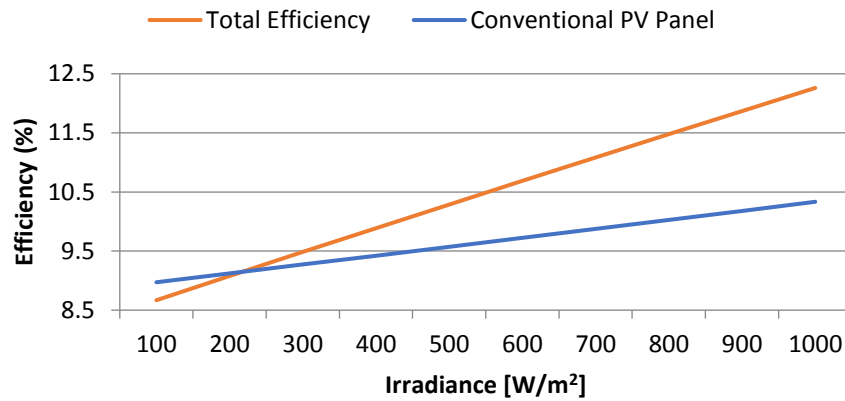


Fig. 6.17 Hybrid collector efficiency as a function of irradiance

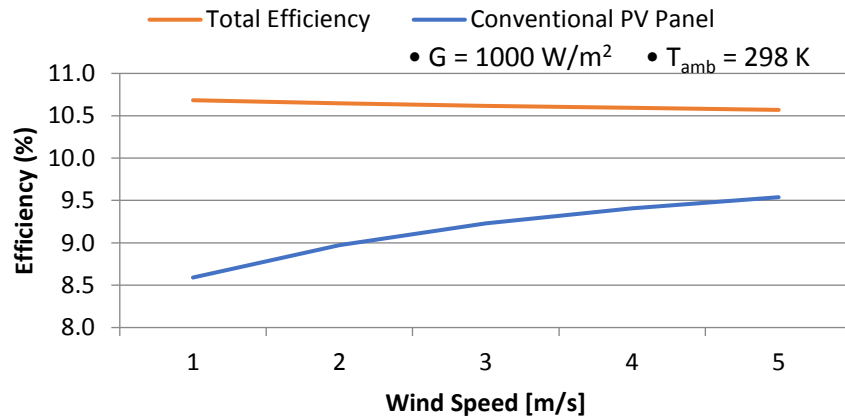


Fig. 6.18 Hybrid collector efficiencies as a function of wind speed

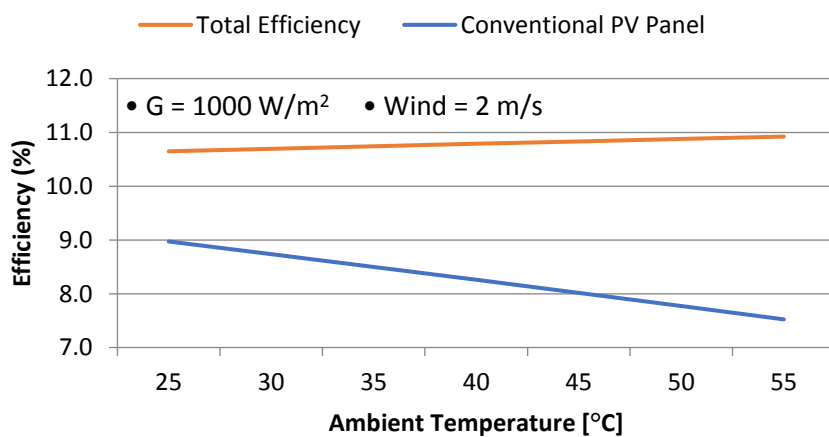


Fig. 6.19 Hybrid collector efficiencies as a function of ambient temperature

Chapter 7

Experimental Study

The practical performance of the collector proposed is determined experimentally allowing for validation of the simulation model, hence, a testing rig is constructed based on the system requirements and operating principles. The main experiments designed and conducted in this research involve testing of an artificial solar simulator utilised as a light source for the performance investigation of the integrated PV module. Therefore, the construction and set up to assess the solar simulator light intensity and uniformity is presented initially. On the other hand, fabrication of the integrated collector utilising the technologies presented in Chapter 2 is illustrated. The experimental set up for testing the integrated collector with the solar light source is then described. The experiment conducted including the set-up, components, and data logging are presented in detail in this chapter. Results from experimental tests however, are documented and discussed in Chapter 8.

7.1 Testing of Solar Simulator Intensity and Uniformity

The extensive research on the utilization of renewable energy sources, and of solar energy in particular have sparked the need for testing facilities in controlled environments. As far as PV technology is concerned, the development of artificial solar light simulators in conjunction with well-defined testing procedures have facilitated development and practical evaluation of state-of-the-art technologies as well as the production of certified nameplates of commercially available mature technologies. Characterization of PV modules performance in a stable environment is enabled while eliminating weather fluctuations that can be experienced in outdoor environments. Hence, providing a controlled environment, in which the influence of the design variables on the practical performance is better studied and realized. Solar simulators can be designed for both non-concentrating and concentrating solar applications by delivering high-flux thermal radiation onto the target (Shatat, Riffat, and Agyenim, 2013).

Nevertheless, artificial solar simulators are governed by some limitations, mainly associated to mismatch in the spectral response between artificial light source and natural sunlight, introducing measurement errors of the cells performance. As the irradiance of an artificial light source varies

depending on the lamp type and usage time, the type and construction of solar simulators for laboratory scale tests would vary according to the experiment requirement. For the purpose of experimental evaluation of the novel integrated collector constructed, the main requirements of the solar simulator are to provide a practical range of light intensities considering both low and high thermal radiation flux. Additionally, limited variations and even light distribution striking the surface of the solar PV module is highly desired. Satisfying these requirements enable understanding the practical performance of the collector based on the experienced conditions, as well as drawing justified conclusions on optimum system design.

7.1.1 Solar Simulator Construction

The construction and testing of an artificial solar simulator utilised for performance prediction of the collector proposed is presented in this section. Tungsten halogen lamps are utilised in the construction of the solar simulator, Fig. 7.1 (a). This type of lamps has been applied widely in solar beam experiments due to the stable smooth spectral output they provide compared to other light source options available, Fig. 7.1 (b). The wavelength range of tungsten halogen lamps falls between 360-2500 nm, providing a closer match to sunlight, especially in terms of thermal radiation, Fig. 7.2. The colour temperature provided of the lamps however is much less of natural sunlight, radiating at a black body temperature of about 3200K.

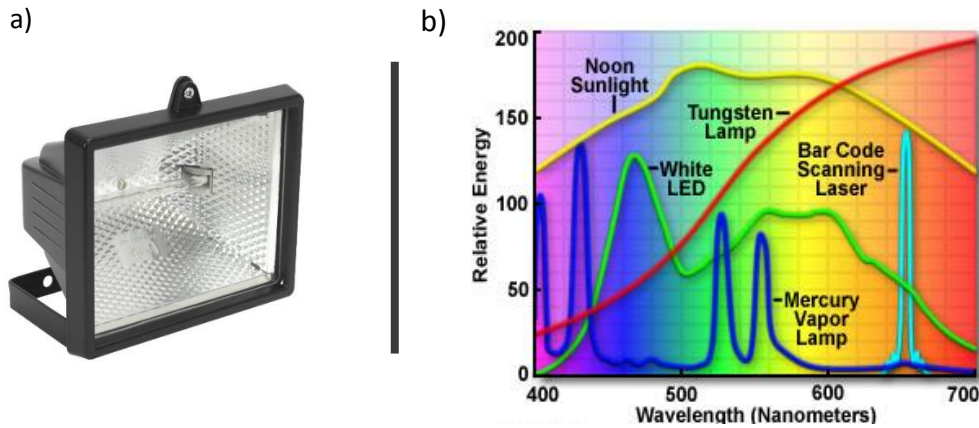


Fig. 7. 1 a) Tungsten halogen lamp. b) Spectra from common sources of visible light

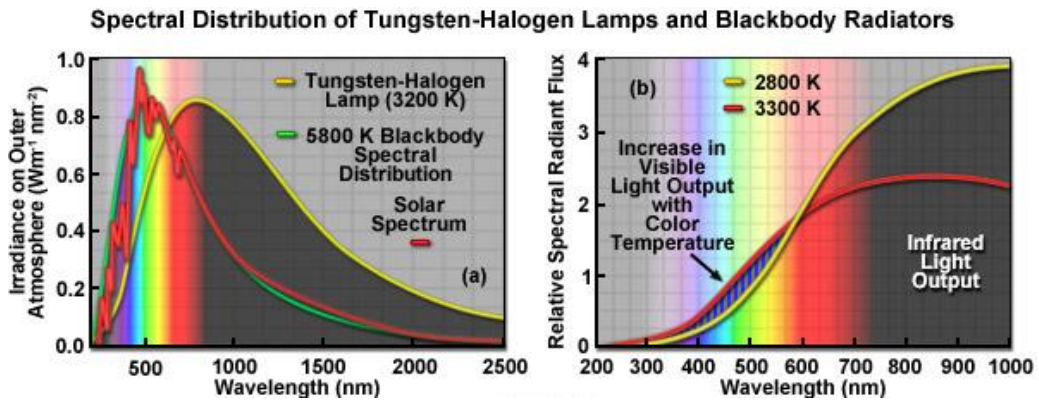


Fig. 7. 2 Spectrum distribution of Tungsten-Halogen lamps used for solar simulator

The simulator consists of 30 400 Watts floodlights fixed on an aluminium frame. The arrangement of the lamps and dimension of the solar simulator is shown in Fig. 7.3. The lamps are power by three-phase AC supply through a transformer connected to the grid. A Kipp & Zonen pyranometer with sensitivity of $17.99 \times 10^{-6} V/W/m^2$ was mounted on the tilted surface of the tested module to measure the striking radiation flux on the surface at evenly spaced points.

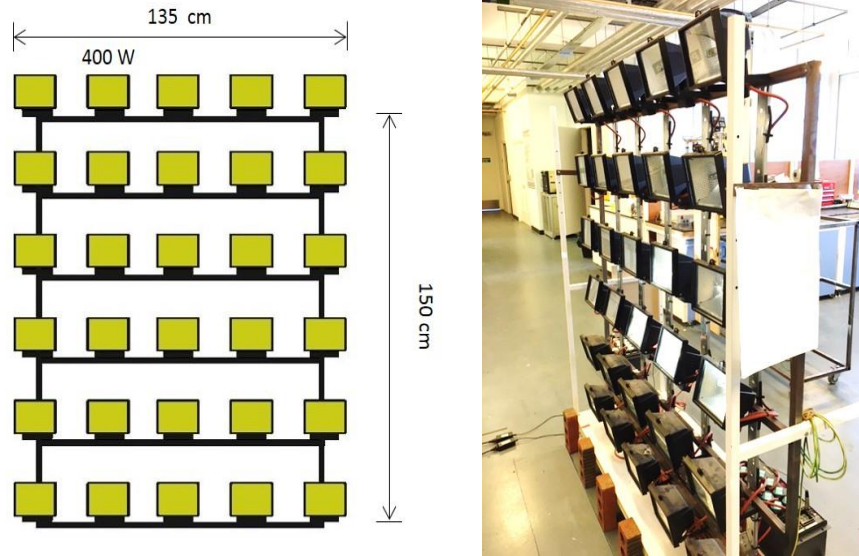


Fig. 7. 3 Solar simulator utilised for experimental performance characterization

7.1.2 Measurements of Light Intensity and Uniformity

The test performed on the solar light simulator and presented in this chapter includes radiation level intensity and evenness tests. Light intensity of various range is vital in this investigation to characterise the system performance under low and high light flux. Hence, leading to clear understanding of how the system performs in all levels of practical solar resources available in any location. Uniform light distribution however, is considered so as to eliminate effects of hot spots on the PV module surface as well as the performance evaluation the heat pipes attached. Hot spots can alter the system performance considerably, introducing further challenges and difficulties in assessing the capabilities of the PV cells as well as the integrated waste heat recovery system.

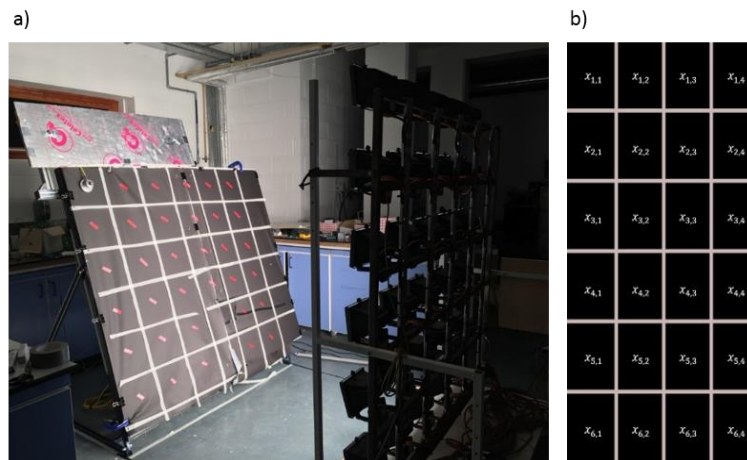


Fig. 7. 4 a) Artificial light intensity and uniformity test. b) Screen with grids indicating points of measurement for radiation intensity and uniformity assessment

The practical assessment of the solar simulator was performed by matching closely the international standard IEC 60904-1 for measurement of photovoltaic current-voltage characteristics under simulated sunlight. The standard procedure relevant to testing under simulated sunlight highlights the testing considerations in the following statements:

- ❖ Simulated solar irradiance usually varies spatially over the collector aperture as well as varying with time during test. It is therefore, necessary to employ a procedure for integrating the irradiance over the collector aperture.
- ❖ Time variations in irradiance are usually caused by fluctuations in the electricity supply and changes in lamp output with temperature and running time.
- ❖ The specifications of the lamp must be checked for warming up time, as some lamps take more than 30 min to reach stable working condition.

To measure the light source intensity, a black screen board of equidistant grids is used to indicate the location of measurement across the surface of the module, Fig. 7.4 (b). Prior to light intensity measurement, the solar simulator is allowed to stabilize for 30 minutes before recording measurements. The module at that point is shaded from the light source so as to not be affected by light until the solar simulator is considered stable. Consequently, a pyranometer is used to measure the irradiance, in which the device is placed on spots indicated on the black screen which was placed on the surface of the PV module. The distribution of irradiance over the PV panel aperture shall be measured using a grid of maximum spacing of 150 mm. The technique adopted is considered valid for testing in continuous solar simulator or natural light.

The pyranometer reads the light intensity as a potential difference (voltage) which is converted into irradiance according to Eq. 7.1. The mean solar intensity considered in the performance evaluation of the collector is taken as the average value of measured intensities across the collector aperture using Eq. 7.2. Where, E_{solar} is the irradiance [W/m^2], V_{emf} is the output voltage [μV], and S is the pyranometer sensitivity [$\frac{\mu V}{W/m^2}$]. At any time, the irradiance at any point on the grids shall not differ from the mean irradiance over the aperture by more than $\pm 15\%$. The light intensity of the simulator was varied by adjusting the distance between the simulator and collector.

The light intensity and uniformity of the light source were recorded at various departments away from the tested module, namely; 1.1, 1.4, 1.7, 2, 2.2 metres. Fig. 7.5, illustrate the displacement of the solar simulator with respect to the collector tested, both measured average light intensities with the respective displacement are presented. Further details on the results for both light intensity and uniformity tests are documented and presented in Chapter 7 prior to the validation of the computer simulation model. The unevenness is expressed in terms of the uniformity; defined as a measure of how the solar irradiance varies over a selected area and calculated from the maximum and minimum percentage differences from the mean irradiance as per Eq. 7.3.

$$E_{m,n_{solar}} = \frac{V_{emf}}{S} \quad (7.1)$$

$$Mean\ Solar\ Intensity = \frac{1}{n} \sum_{i=1}^n x_i \quad (7.2)$$

$$Unevenness\ (\%) = \pm 100 \left(\frac{E_{max} - E_{min}}{E_{max} + E_{min}} \right) \quad (7.3)$$

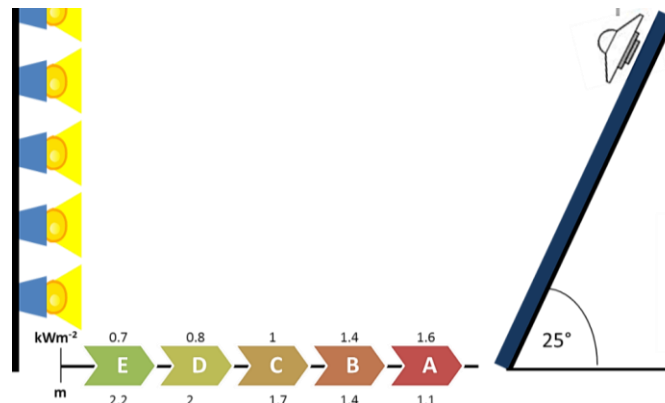


Fig. 7. 5 Schematic illustrating solar simulator displacement from PV module with respective recorded average light intensities.

7.2 Testing of Heat Pipe-based PV/Thermoelectric Collector

To verify the theoretical model of the integrated heat pipe-based PV/TEG collector proposed, a prototype collector is constructed as per the conceptual design presented in Chapter 4. First and foremost, the construction of the prototype for practical investigation is presented, including materials and equipment involved for this purpose. Furthermore, the practical testing procedures and considerations are laid down to enable precise measurement method and minimal errors associated to data collection. Characterization of the system is accomplished through the system variables evaluated against set of operating conditions. For that purpose, the list of dependant variables in addition to the testing conditions are provided. This section is intended to address the fabrication, testing procedures and practical considerations of the integrated collector to achieve the following set of goals:

- Characterise the practical performance of the integrated collector
- Facilitate validation of the theoretical computer model
- Assess discrepancies between theoretical models and practical tests
- Provide an insightful practical design of the system under investigation, towards further improvements and modifications

7.2.1 Fabrication of the Prototype Collector

The system under investigation consists of two main subsystems, namely the heat pipe-based PV collector, and the waste heat recovery system using thermoelectric generators. Integration of both subsystems is presented in the experimental apparatus section along with the instruments utilized for data recording and monitoring.

7.2.1.1 Materials and Instruments

The experimental set-up to investigate the performance of the proposed collector and the cooling capabilities associated with the integration of the waste heat recovery system require the following components and instruments. The components from which the system is constructed are summarized and listed in Table 7.1.

Photovoltaic Module:

The PV module considered in this experimental is characterized as per standard testing conditions with its performance parameters presented in Table 7.2. Such data presented in manufacturers' datasheet will be

considered as a reference to observe the factors affecting the practical performance of the panel and its efficiency.

Table 7. 1 List of components for experimental testing collector fabrication


| | |
|--|---|
|  | <ul style="list-style-type: none"> • PV Module The main component of power generation within the proposed system through photoelectric conversion. • Copper heat pipes Utilised to absorb excessive thermal energy accumulating on the PV module. • Thermoelectric generation modules Utilised for thermal waste recovery while assisting an improved operating temperature for the PV module. • Aluminium heat spreaders Grooved heat speeders for the pipe evaporator section attached at the rear of the module to enhance heat extraction. • Thermal grease Applied between the heat spreaders and the rear of the PV module, as well as the groove to eliminate air gaps and enhance heat transfer. • Thermal mineral wool insulation Applied at the rear of the collector to minimise convection and radiation thermal losses. • Aluminium heat sink Fabricated and attached at the cold plate of TEG module to assist temperature difference for thermal waste recovery. • Cooling fan Attached to the heat sink to create an air stream to enhance convective cooling at the cold plate of the TEG module |
|--|---|

Table 7. 2 PV Panel Specifications

| | |
|------------------------------------|-------------------------------------|
| Model | EQS170D-24 |
| Cells Type | Mono-crystalline Si cells 125×125mm |
| No. of series connected cells | 72(6×12) |
| Size | 1580 x 808 x 35 mm |
| Weight | 15 Kg |
| Maximum Power (P_{max}) | 170 W |
| Maximum Power Voltage (V_{mp}) | 35.3 V |
| Maximum Power Current (I_{mp}) | 4.82 A |
| Open Circuit Voltage (V_{oc}) | 44.3 V |
| Short Circuit Current (I_{sc}) | 5.29 A |
| Current temperature coefficient | $(0.065 \pm 0.015)\%mA/^\circ C$ |
| Voltage temperature coefficient | $-0.38\% mV/^\circ C$ |
| Power temperature coefficient | $-(0.5 \pm 0.05)\%/^\circ C$ |

Thermoelectric Generation Modules (TEGs)

Thermoelectric generation modules are power generating devices which use the Seebeck Effect in order to convert heat directly into electricity, Fig. 7.6. TEGs are utilised in this investigation for the waste heat recovery in which heat is absorbed at the top substrate and flows through the thermoelectric elements; it is then rejected at the cold substrate. The temperature difference across the TEG plates influences the electrical performance of such devices. The specifications of the modules employed in the designed collector are presented in Table 7.3.

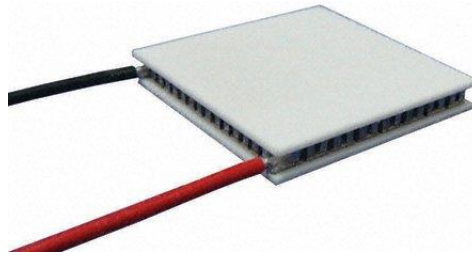


Fig. 7. 6 Thermoelectric generation module

Table 7. 3 Specification of thermoelectric generation modules employed

| | |
|---|-------------------------------------|
| Matched Load Output Power | 11.6W |
| Matched Load Resistance | 1.38Ω ± 15% |
| Open Circuit Voltage | 8.0V |
| Matched Load Output Current | 2.9A |
| Matched Load Output Voltage | 4.0V |
| Heat Flow Through Module | ~232W |
| Maximum. Compress. (non-destructive) | 1MPa |
| Max Operation Temperature | Hot side: 250°C Cold side: 175°C |
| Parameters for Hot Side Temp 250°C and Cold Side 30°C | |

Solar Simulator

The simulator presented and tested earlier is considered as the radiation source for the PV module. The simulator consists of several metal halide lamps used to provide light source for the PV panel. The metal halide lamps simulate sunlight and can be adjusted to various positions to project a range of light intensities on the PV module.

Pyranometer

The pyranometer is used to measure the illumination level by measuring the global radiation level, Fig. 7.7. Such device is designed to measure the short-wave irradiance on a plane surface which is a result from the sum of direct solar radiation and diffuse radiation incident from the hemisphere surrounding the device. The pyranometer is fixed on the panel to measure the sunlight or artificial light intensity in units of W/m^2 striking the PV panel surface.



Fig. 7. 7 Pyranometer for light intensity measurement

ISM 490 Solar Module Analyzer

The most common method of constructing the performance characteristics curves of the PV module is to measure both voltage and current for various load impedances as illustrated in Fig. 7.8. Initially, the output terminals of the panel are short circuited with a wire to measure the short circuit current. Next, the variable resistor is connected to the panel terminals starting with low resistance to higher. Varying the resistance from

a low value to a higher one causes the panel voltage to increase from zero towards the open circuit voltage (V_{oc}). The set of values obtained here are then used to construct the I-V and P-V characteristic curves of the panel for particular operating condition. However, the utilisation of a solar module analyser replaces the need to design the electrical circuit in order to sweep the electrical parameters across a range of load resistance to facilitate construction of the IV curves, Fig. 7.9 (a). The device utilises an electronic load instead for that purpose. Using the module analyser, obtaining the characteristics of the PV module is simplified to simply connecting the module leads as per Fig. 7.9 (b). The module serves as a datalogger as well in which data is logged automatically to a PC.

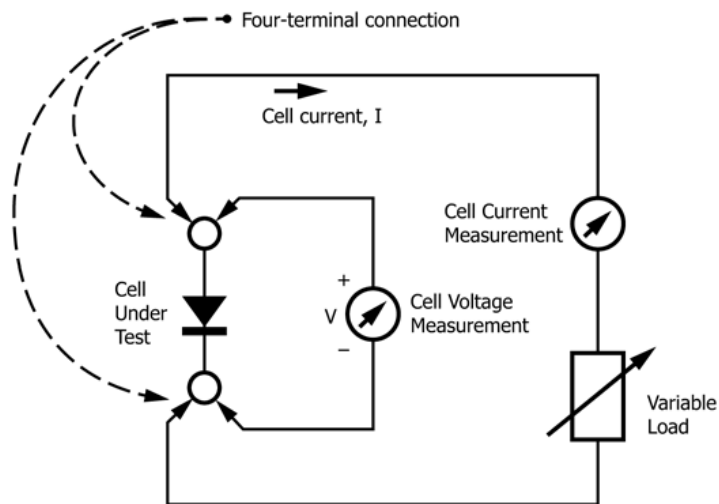


Fig. 7. 8 Wiring arrangement for current and voltage measurement of PV module

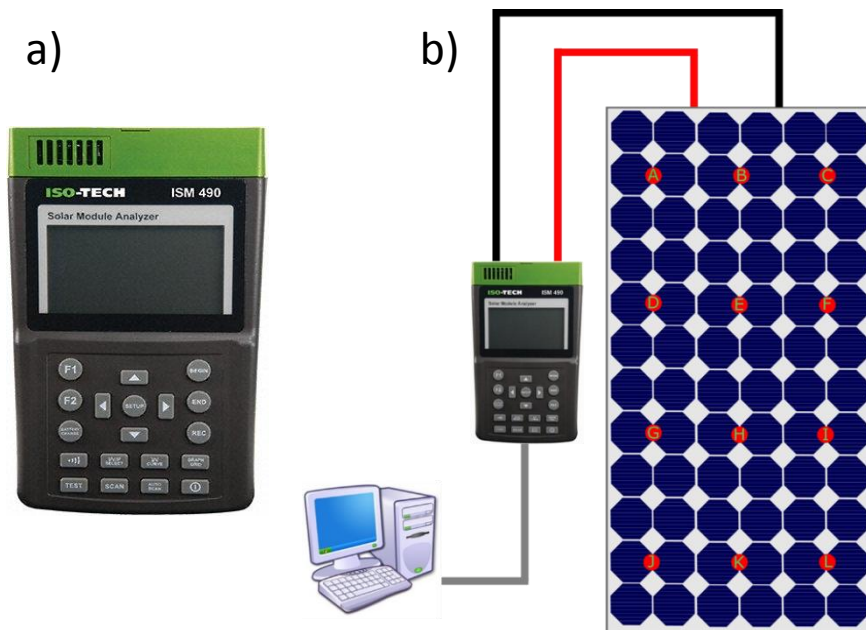


Fig. 7. 9 a) Solar module analyser ISO-TECH (ISM490) to characterize electrical performance of PV module. b) Wiring of PV module and solar module analyser

Thermocouples

Temperature measurements of the PV panel is obtained using thermocouples attached directly to both surface and rear of the PV panel at various locations. The other end of the thermocouples is connected to the data logger which is in turn connected to a PC to allow monitoring of data recorded. K-type thermocouples of Nickel-Chromium are employed in this investigation. The temperature range of K-type thermocouples is within the range of $-50^{\circ}\text{C} \rightarrow +250^{\circ}\text{C}$ with a time response of 0.7 and having measurement accuracy of $\pm 1.5^{\circ}\text{C}$ within temperature range $-40^{\circ}\text{C} < T < 375^{\circ}\text{C}$.

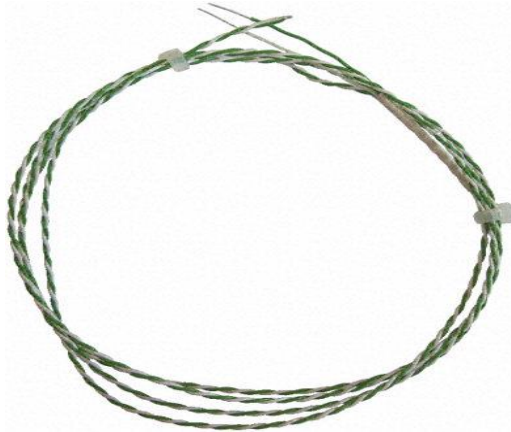


Fig. 7. 10 K-Type thermocouples for temperature measurements

Data logger

The temperature records are gathered using data loggers (DataTaker DT500/DT800), in which all transducers are configured and connected to specific channels. The data logger processes the data with a CPU through control software written on a PC and transferred to the logger.

Monitoring PC

The PC is used to configure the data logger with the relevant channels connected to the measurement devices by specifying the input data and the frequency at which data is collected. The PC also allows monitoring of the performance and gathering the data in more suitable format, allowing graphical representation using computer software.

7.2.1.2 Heat Pipe-based PV Collector Fabrication

The heat pipe-based PV collector is constructed of several main components and materials required to put the system together in a compact collector. Heat pipes were attached to the rear to extract excessive heat accumulating on solar cells, therefore providing cooling to maintain the cells at a desirable operating temperature. The evaporator sections of the heat pipes are attached to the rear of the PV module using aluminum base panels serving as fins, enlarging the heat transfer area at the evaporator section of the heat pipe. The sheets are fabricated with a groove for the heat pipe to sit in with thermal grease applied to fill air gaps and improve thermal heat conduction. Double-sided thermal conductive adhesive is used to secure the aluminum heat spreaders at the rear of the PV module as shown in Fig. 7.11.

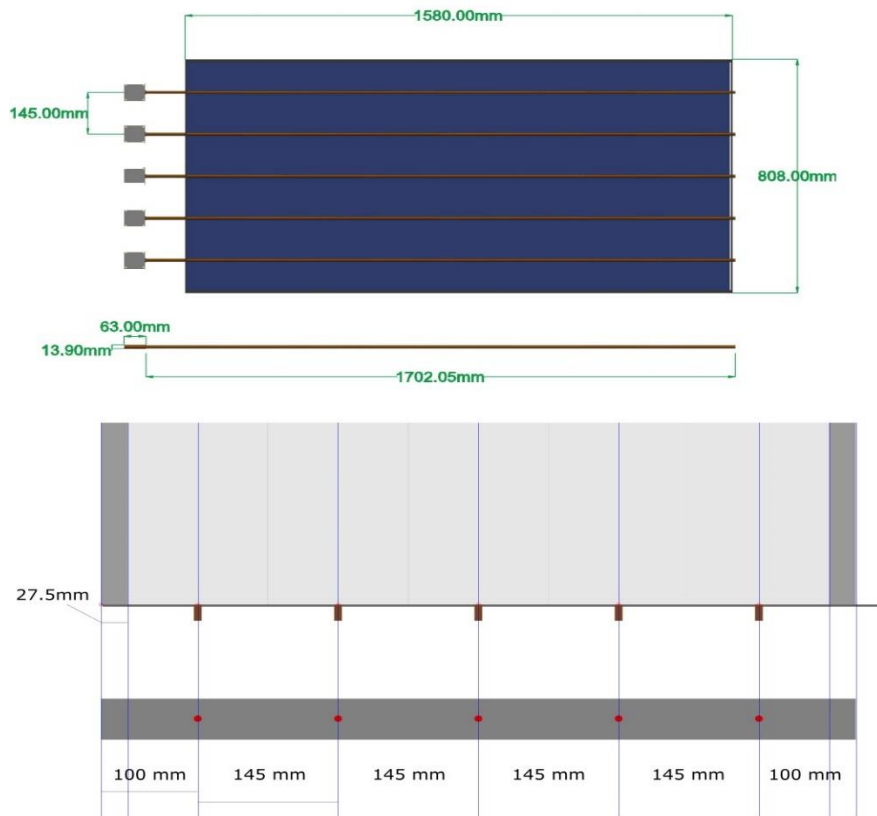
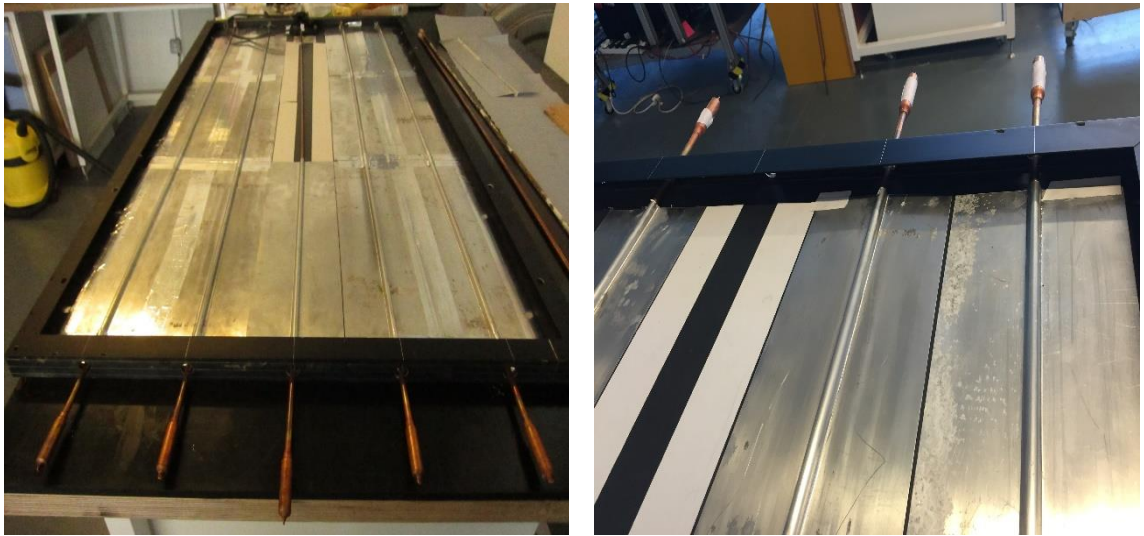


Fig. 7. 11 Fabrication of heat pipe-based PV collector

7.2.1.3 Waste Heat Recovery Assembly Fabrication

The heat recovery assembly is fabricated as per the schematic illustration in Fig. 7.12. A support system for the assembly is fabricated of acrylic material consisting of two parts in which the aluminium heating block and on top of it the thermoelectric generator is attached. Having low thermal conductivity, the support system serves as an insulation material, minimizing thermal losses. The heating block consists of an aluminum block having a width equivalent to that of the thermoelectric generator plates with a provision equivalent to the heat pipe condenser section diameter as illustrated in Fig. 7.13.

Thermal conducting paste is applied on both surfaces of the TEG to fill air gaps, and thus minimize associated losses, as well as in the provision for which the condenser section of the heat pipe is inserted in. At the cold plate of the TEG module, aluminium heat sink is attached for convective cooling to maintain temperature difference between the TEG plates. The addition of the cooling fan allows forced air hence improving the convective cooling of the heat sink and permitting higher temperature difference.

The actual waste heat recovery system resembling the assembly in Fig. 7.12 is shown in Fig. 7.14. For this experimental investigation, the 5 assemblies have been fabricated corresponding for the number of heat

pipes attached at the rear of the PV collector. Thermocouples for temperature difference detection are also attached at both sides of the TEG module plates. The assemblies are integrated with the heat pipe-based PV collector fabricated earlier by inserting the condenser section of each heat pipe to a single assembly, Fig. 7.15. The TEG modules of the 5 assemblies are connected electrically in series for their electrical performance assessment.

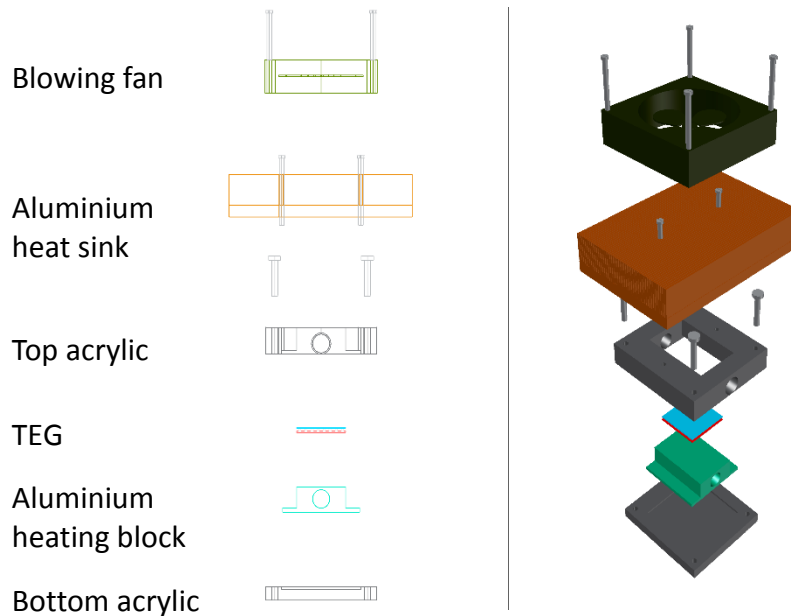


Fig. 7. 12 Schematic illustrating components of waste heat recovery system



Fig. 7. 13 Aluminium heating block integration to condenser section of heat pipe

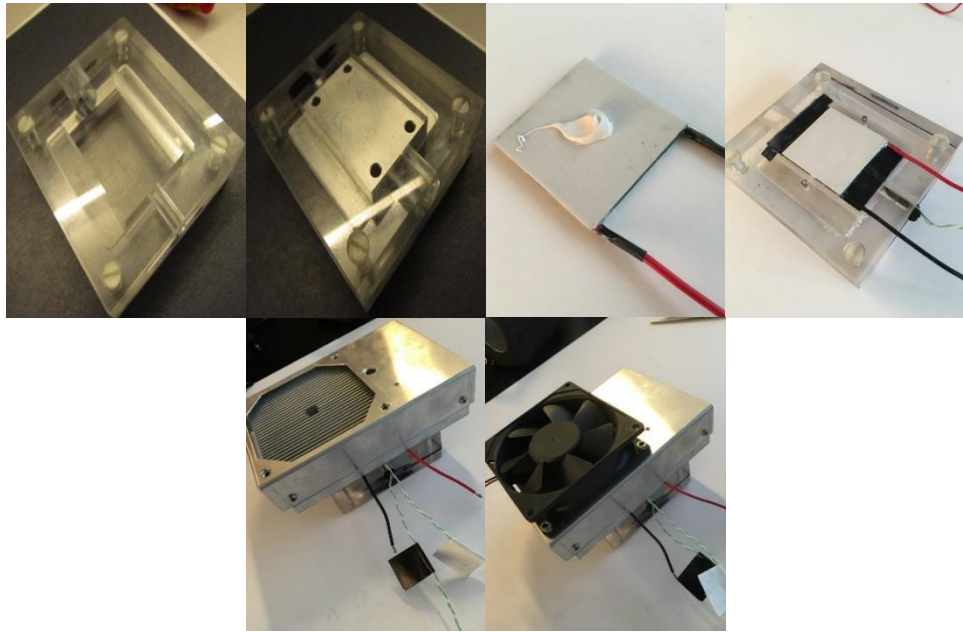
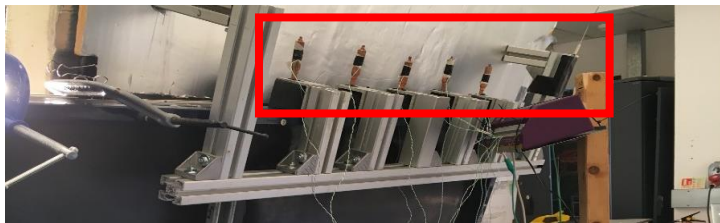


Fig. 7. 14 Actual TEG waste heat recovery assembly fabricated



Front view



Rear view



TEG-fan
heat sink
assembly
attached

Fig. 7. 15 Integration of TEG-fan-heat-sink waste heat recovery system with heat pipe-based PV collector

7.2.1.4 Performance Measurements

Photovoltaic Module Measurements

The practical characteristics of the PV panel is determined through the current versus voltage (I-V), and power versus voltage (P-V) curves. Through testing of PV modules, the properties of the panel which includes the *Short Circuit Current* (I_{sc}), *Open Circuit Voltage* (V_{oc}), *Maximum Power Voltage* (V_{mp}), *Maximum Power Current* (I_{mp}), and the *Maximum Power* (P_{max}) are obtained for set of operating conditions. Full set of voltage versus current readings to construct the characteristic curves of the PV panel are obtained through wiring the PV module and the solar module analyser as per Fig. 7.16. Using a four-wire Kelvin probe connected to the PV module output terminals, the electrical characteristics of the PV module are obtained. The list of electrical parameters recorded is given in Table 7.4, whereas a sampling rate of 1 minute and total test duration of 60 minutes is considered.

Table 7. 4 List of parameters measured

| Parameter | Unit | Parameter | Unit |
|---------------------------------|-------------|---------------------------------|-------------|
| Open circuit voltage, V_{oc} | [V] | Voltage at P_{max} , V_{mp} | [V] |
| Short circuit current, I_{sc} | [A] | Current at P_{max} , I_{mp} | [A] |
| Maximum power, P_{max} | [W] | Efficiency, η | [%] |

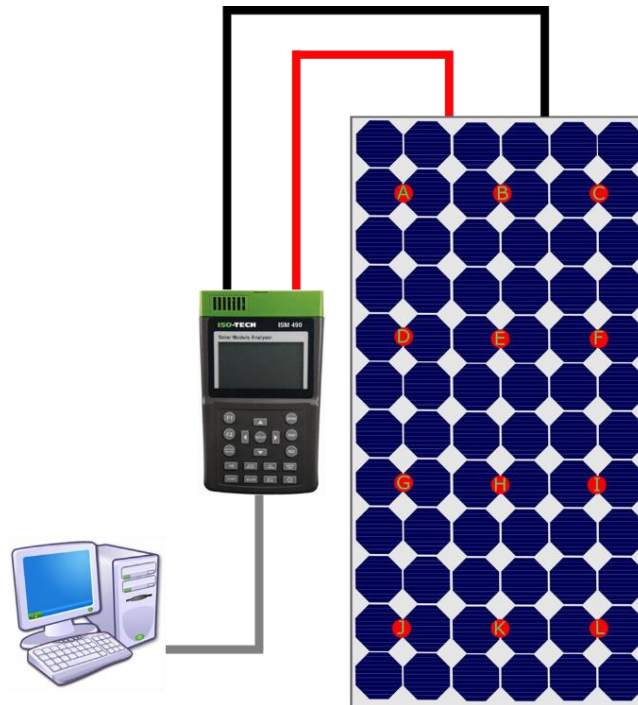


Fig. 7. 16 Wiring of PV module and solar module analyser (ISM 490) for electrical characterization of PV panel

Photovoltaic Module Temperatures Measurement

The tested collector is equipped with a set of K-type thermocouples with an accuracy of 0.1°C. The sensors were distributed evenly on the front surface of the tested collector as well as the rear of the panel. A datalogger is utilised to record the temperature response of the module at a sampling rate of 1 second. The locations of the thermocouples attached to the collector is presented in Fig. 7.17. The PV module effective temperature is evaluated based on averaged temperature values recorded at both surface and rear.

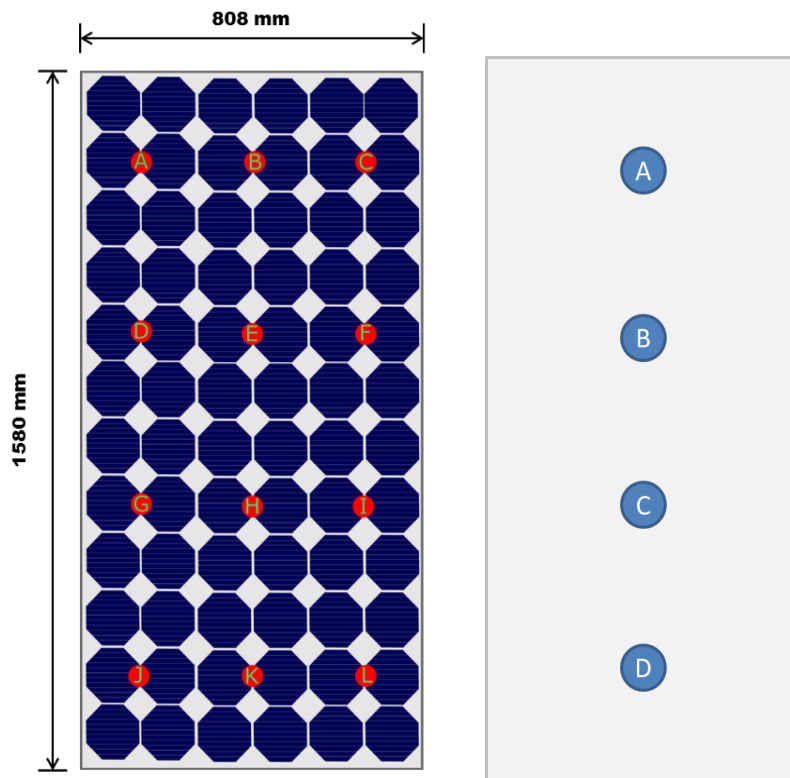


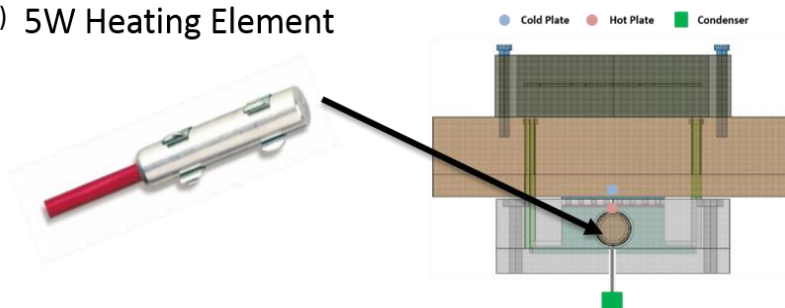
Fig. 7. 17 Locations of K-type thermocouples attached for temperature measurement

Average value of each row of temperature sensors is considered in the analysis. Subsequently, an average value between surface and rear is processed resulting in four temperature values averaged to present a single effective temperature, which is considered in the performance analysis of the system. This is in attempt to accommodate for the influence of any hot spots or the non-uniform distribution cause by the light source.

Thermoelectric Generator Measurements

The thermoelectric generation module employs direct conversion of thermal energy into electrical energy based on the Seebeck effect. Such phenomena harvests power depending on the temperature difference across the TEG plates when a closed loop is formed. TEGs are limited by the thermoelectric materials, thus the efficiency of the TEG system is limited to less than 5%. Despite of its relatively low conversion efficiency, utilisation for waste heat recovery make such devices very appealing in the sustainable energy field. To investigate the electrical performance of the TEG modules employed in this investigation, two tests are performed. The waste heat recovery assembly was tested using a heat source to heat the TEG hot side as in Fig 7.18 (a), in addition testing based on integration with the heat-pipe based PV was also performed as illustrated in Fig. 7.18 (b). To increase the thermal conductance between the TEG and the heat exchangers, pressure is applied by the fixing screw in addition to thermal grease applied between heat exchanging plate.

a) 5W Heating Element



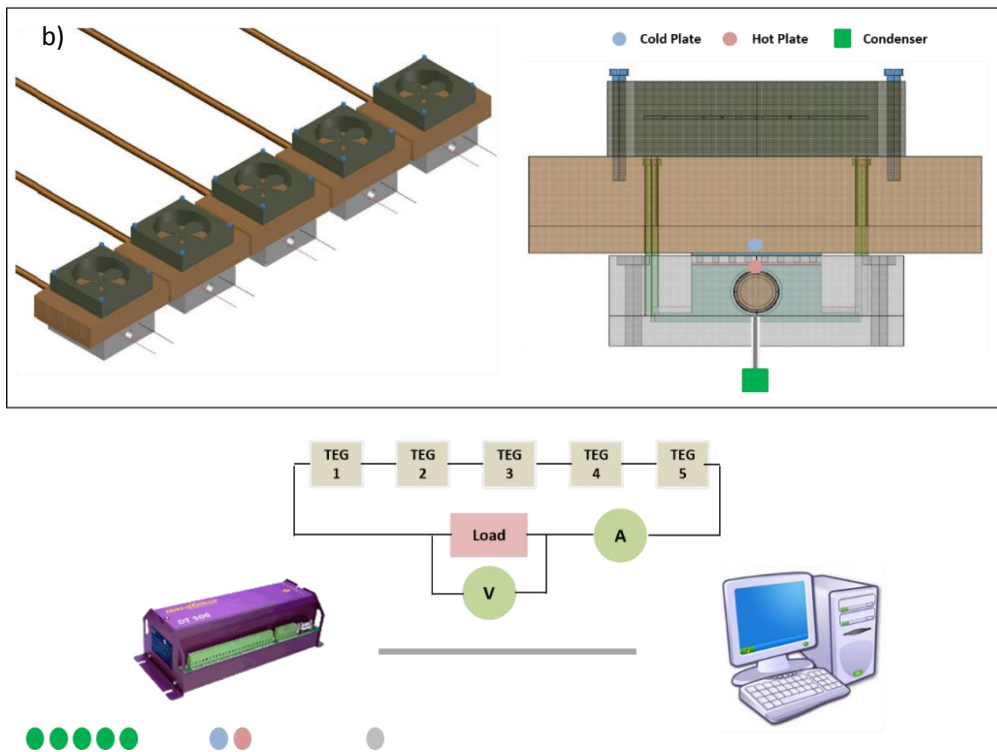


Fig. 7. 18 Experimental tests performed on waste heat recovery system.

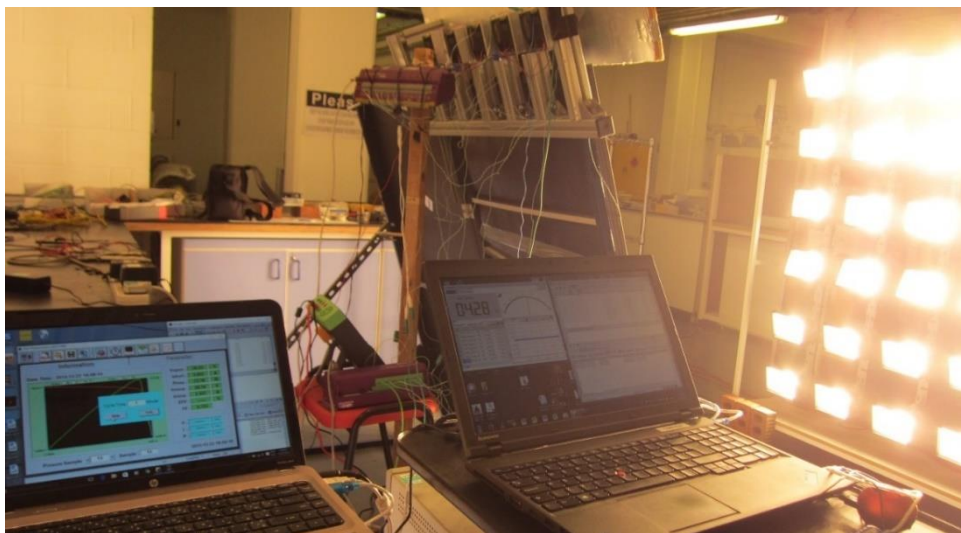


Fig. 7. 19 Photo showing test of integrated collector under artificial light simulator.



Fig. 7. 20 Photo showing tested collector and temperature sensors attached on surface as well as waste heat recovery assemblies at condenser section of heat pipe

Chapter 8

Experimental Results and Computer Model Validation

8.1 Experimental Results

8.1.1 Solar Simulator Testing Results

The tests performed on the solar light simulator is presented in this section including radiation level intensity and evenness tests. Light intensity of various range is vital in this investigation to characterise the system performance under low and high light flux. Hence, leading to clear understanding of how the system perform in all levels of practical solar resource available in any location. Uniform light distribution however, is considered to minimize effects of hot spots on the PV module surface as well as the efficient performance the heat pipes attached. The light intensity is varied by adjusting the distance between the light source and the collector. Fig. 8.1 displays the light intensity recorded for different displacements between the light source and the collector.

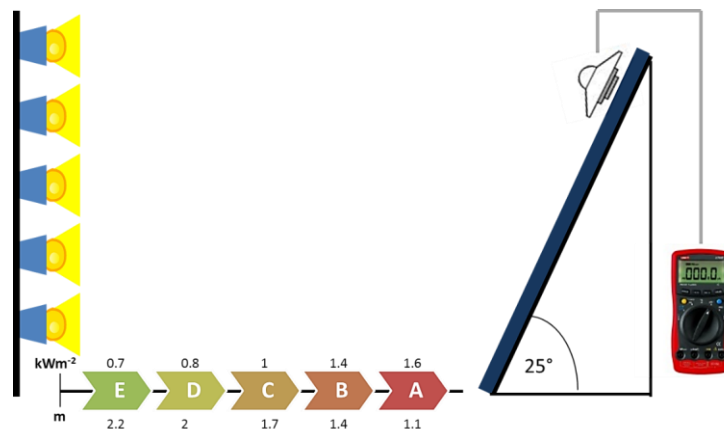


Fig. 8. 1 Schematic illustrating solar simulator displacement from PV module with respective recorded average light intensities

The variation of light source intensities projected on the surface of the collector is presented in Fig. 8.2 as per measurement taken on evenly spaced points discussed in Chapter 7. Variation at the upper most part of the collector is observed to have maximum deviation due to the length of the PV module utilised for the test; in which the solar simulator light projection area does not cover the whole collector under test. Nevertheless, Fig. 8.2 below confirms the requirement of light intensity with a variation of less than 15% for most of the points on the surface of the collector. The average deviation from the maximum light intensity value recorded is also displayed. The results of testing the solar simulator considering the light intensities and corresponding variation across the collector plate is summarised in Fig. 8.3.

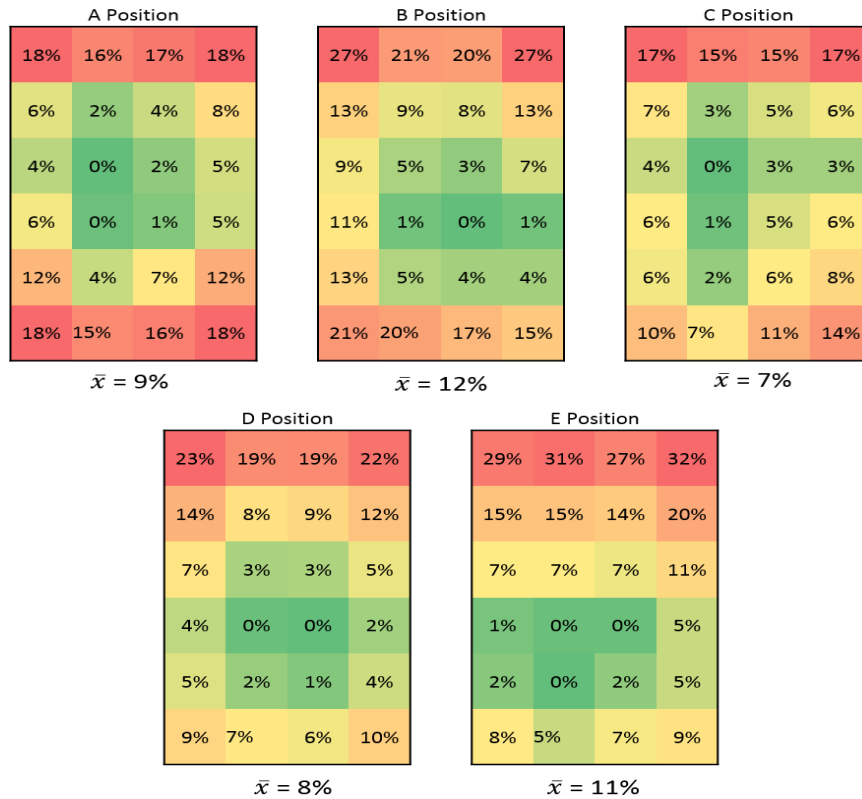


Fig. 8. 2 Variation percentage of light intensities at evenly spaced points

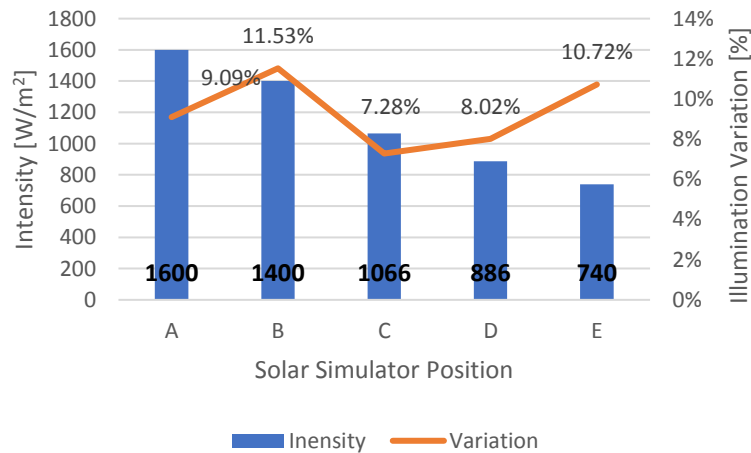


Fig. 8. 3 Solar simulator light intensities and uniformity percentage for different displacement of light simulator

8.1.2 Temperature Response

The temperature response of the integrated collector relative to the conventional PV module is presented in Fig. 8.4. The results are presented for varying light intensity, ambient temperature of 25°C, and wind speed of 0 m/s. The temperature response of the integrated collector at the absence of the insulation layer at the rear of the collector showed improved thermal management, exhibiting temperature values lower than that of the conventional PV module as well as the integrated PV-TEG module with insulation. Hence, incorporation of the heat pipes at the rear of the collector proves to be beneficial in assisting improved temperature of the PV cells.

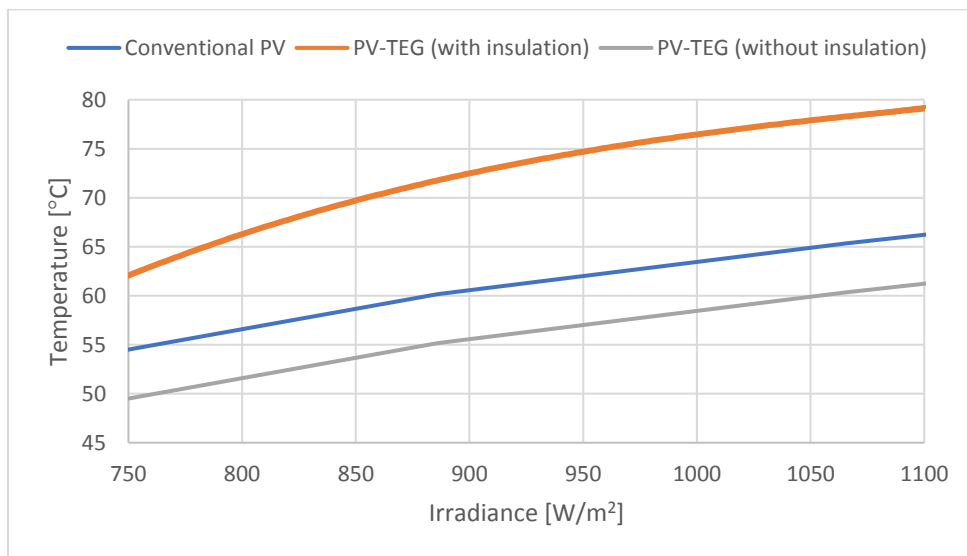


Fig. 8. 4 Temperature response of integrated PV-TEG with and without insulation relative to conventional PV module

The temperature distribution at the surface of the collector measured at evenly spaced points is given in Fig. 8.5. It is evident that the temperature distribution is far from uniform, however, to simplify the analysis the collector temperature is taken to be the average of all temperature values measured at the front glazing of the collector, to aid assessing the cooling capability of the integrated TEG-Fan-Heat sink assembly. Nevertheless, to assess the practical performance of the heat pipe, the appearance of hot spots within the collector can drastically affect the practical performance as it directly affects the boiling-condensation cycle.

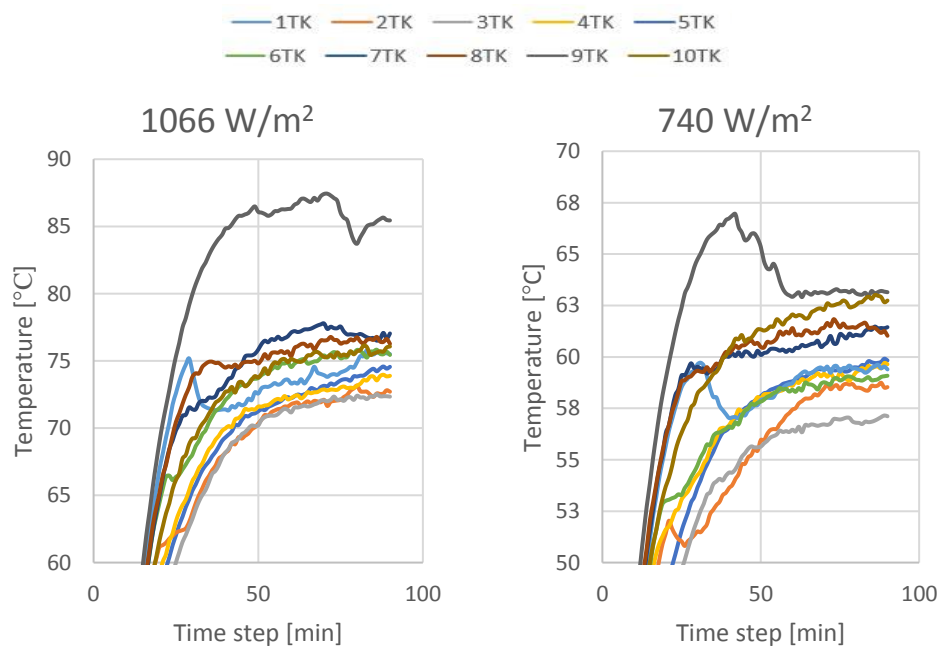


Fig. 8. 5 Temperature distribution at the surface of tested collector

At steady state the temperature values recorded for each light intensity scenario is better observed looking at Table 8.1. It is evident that at non-uniform temperature distribution exists across the collector, with an average deviation of (13.5%). The lowest temperature deviation across the collector was observed at light intensity of 740 W/m^2 , which when compared to the deviation of the condenser temperature at the identical light intensity, deviation of less than (5%) is observed. To assess how the non-uniformity affects the highest temperature recorded for each light intensity (thermocouple no. 9) is eliminated and the deviation of the temperature records is assessed, Table 8.1. The maximum temperature difference across the collector is reduced suggesting a more uniform distribution which if achieved, the heat pipe performance response is more likely to be matched for both simulation model and practical records. The reason why such non-uniformity can drastically affect the thermal transport capabilities of the heat pipe, is due to a non-complete boiling-condensation cycle. Additionally, in the computer model developed, the existence of the aluminium base panel heat spreaders at the rear of the collector assumes most of the thermal energy available from the incoming light intensity is transported to the heat pipe with only conduction losses through the base panel. Moreover, the thermal insulation suspended to maximise the

thermal energy captured serves as a perfect insulator. Thus, variation between the measured and simulated results is observed. Further discussion on such variation is addressed in the validation section of this chapter.

Table 8. 1 Deviation of collector temperature values at steady state

| Light Intensity [W/m²] | 1066 | 740 |
|---|-------------|------------|
| Max | 85.45 | 63.15 |
| Min | 72.34 | 57.11 |
| Δ | 13.11 | 6.03 |
| Δ% | 16.61% | 10.03% |
| Eliminating temperature record of thermocouple 9 (Hot spot) * | | |
| Max | 77.04 | 62.74 |
| Min | 72.34 | 57.11 |
| Δ | 4.70 | 5.63 |
| Δ% | 6.29% | 9.39% |

8.1.3 Electrical Performance

The electrical practical performance of the fabricated collector in addition to the conventional PV module is presented in this section. It is evident that the power output from PV cells increase as the radiation intensity striking the surface of the module is increased. The electrical power output of the conventional PV module tested is presented in Fig. 8.6 (a). Although the output power increased due to enhanced illumination, the efficiency exhibits an

adverse correlation due to the elevated temperature of the PV module because of high intensity flux. The efficiency of the conventional PV module tested is presented in Fig 8.6 (b).

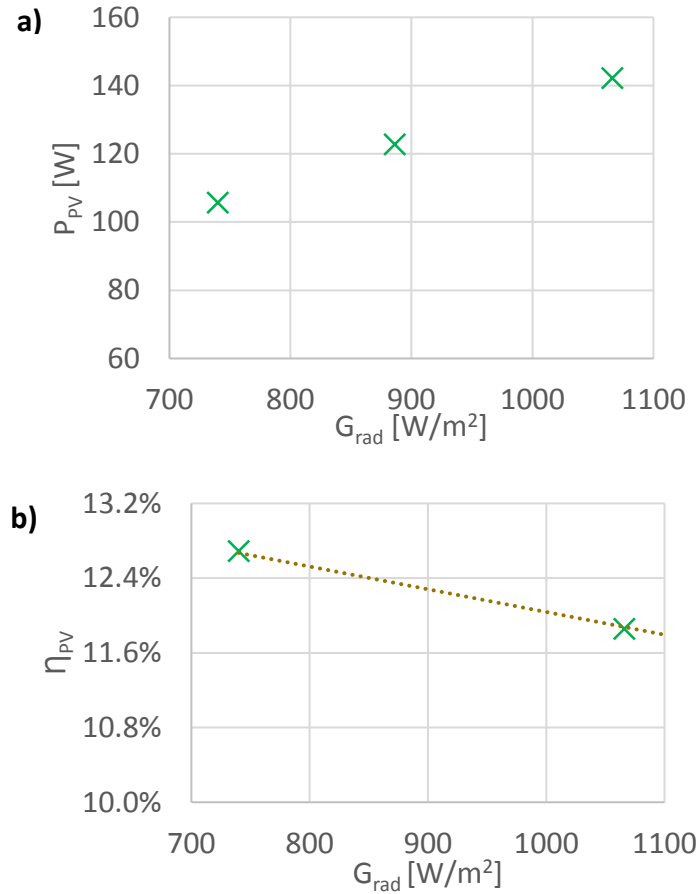


Fig. 8. 6 Recorded power output and estimated efficient of conventional PV module under varying light intensities.

The electrical performance of the PV module in the hybrid PV-TEG collector is displayed in Fig. 8.7 for radiation intensity of $1060 W/m^2$, and ambient temperature of $21^{\circ}C$. The output power available from the collector was

observed to decline as the temperature of the collector increases with time due to continuous illumination on the surface of the collector. The figure below confirms that the voltage at maximum power point decreases as the temperature increase, however, the current is slightly increased by the influence of temperature. Nevertheless, the reduction in the output voltage is of a higher magnitude resulting in degradation in the power output of the module.

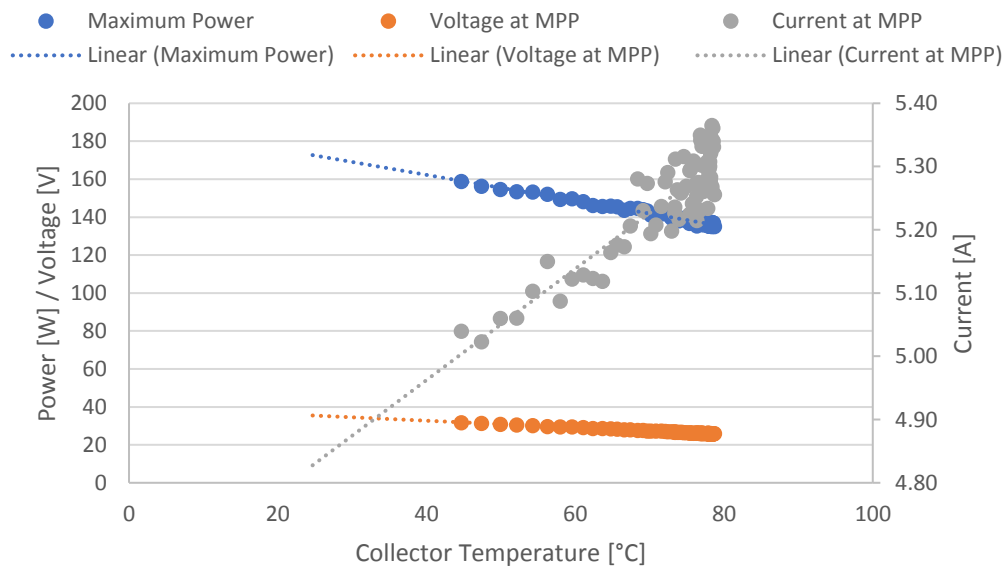


Fig. 8. 7 Electrical performance recorded of integrated PV-TEG collector

Comparison between the conventional PV module and the integrated hybrid PV-TEG collector for the maximum power attained by the collectors is given in Fig. 8.8 for identical conditions. The integrated PV-TEG collector was observed

to have higher power output compared to the conventional PV module throughout the testing period due to the additional power available from the TEG modules. Comparison of the steady state collector's temperature of three collectors considered in this research for varying light intensities is illustrated in Fig. 8.9. Throughout the range of light intensities considered, the integrated collector without insulation displayed improved power output compared to the conventional PV module and the generation capabilities of the integrated collector with insulation. The integrated collector with insulation was considered to assess and additional improvements associated to the direct conversion of recovered heat to electricity via the incorporated TEG modules.

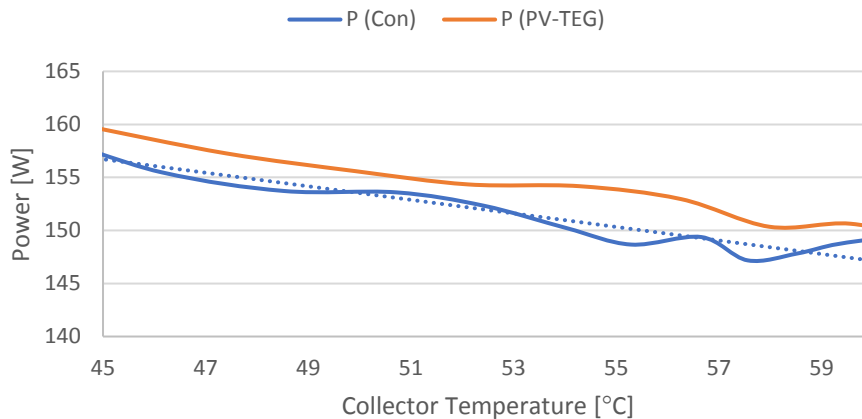


Fig. 8. 8 Comparison between experimental results of conventional PV module and integrated PV-TEG module without insulation

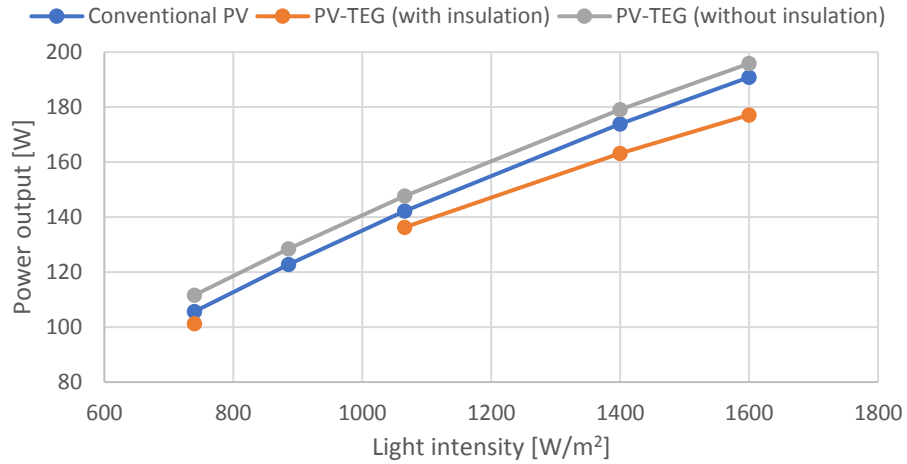


Fig. 8. 9 Power measured for the considered collectors under varying light intensity

8.1.4 TEG Thermal Performance

In this section, the thermal performance of the TEG module incorporated in the waste heat recovery system is illustrated. The conditions applied within the test are of solar light intensity of 1060 W/m^2 , and ambient temperature of 21°C . The temperature response of the condenser and temperature difference across the TEG plates as a function of the recorded collector temperature is shown in Fig. 8.10 (a). An illustration of the condenser section temperature response and the TEG hot plate as well as the difference between the two values as a function of the collector measured temperature is given in Fig. 8.10 (b). From the difference between the condenser temperature and the TEG hot side, it is

suggested that negative difference value confirmed that the TEG is indeed able to absorb some of the thermal energy available from the collector.

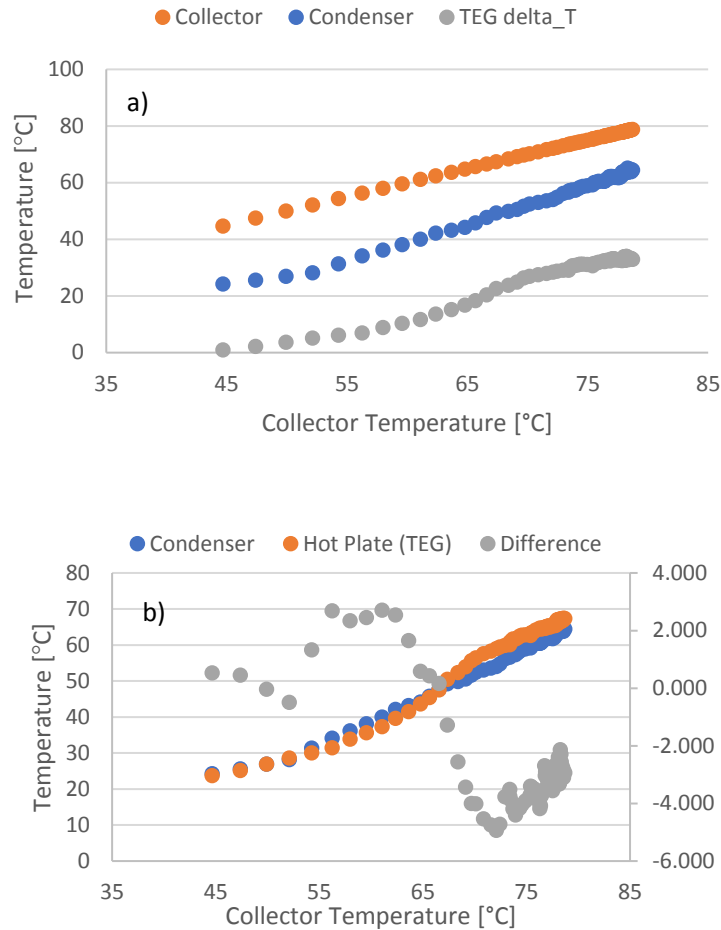


Fig. 8. 10 Thermoelectric generator thermal performance

The corresponding TEG open circuit voltage under identical conditions is given in Fig. 8.11. It is confirmed as the continuous illumination contributes to an elevated temperature, the temperature difference across the TEG plate is enhanced while maintaining the cooling fan in operation. Subsequently, the

open circuit voltage available from the TEG bank attain a value of 8 volts at the maximum temperature difference ($\sim 33^{\circ}\text{C}$) available because of the incoming light intensity of 1060 W/m^2 .

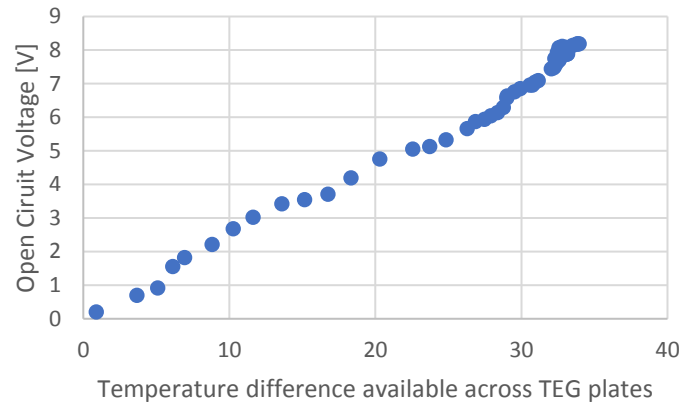


Fig. 8. 11 Open circuit voltage of TEG bank at light intensity of 1060 W/m^2

8.2 Computer Model Validation

8.2.1 Photovoltaic Electrical Characteristics

The electrical characteristics of the PV module operated in this investigation is given in Table 8.2 (Available in Appendix). Given the characteristics of the module satisfy the standard testing conditions of radiation intensity level of 1000 W/m², cell temperature of 25 °C, and air mass of 1.5, the conversion efficiency (η_{pv}) is estimated based on Eq. 8.1

Table 8. 2 PV module characteristics reported in manufacturer's datasheet

| V_{oc} | V_{mp} | I_{sc} | I_{mp} | P_m | η_{pv} |
|----------|----------|----------|----------|-------|-------------|
| [V] | | [A] | | [W] | [%] |
| 44.3 | 35.3 | 5.25 | 4.82 | 170 | 15.2 |

$$\eta_{PV} = \frac{P_{max}}{G A_{PV}} \quad (8.1)$$

In order to validate the computer model, the predicted characteristics of the collector are compared against the manufacturer's reported performance parameters in addition to a set of recorded data at various operating conditions. The input conditions and parameters considered for the validation of the theoretical model are presented in Table 8.3. The cell temperature at the start of the test is close enough to the cells' temperature

requirement of STC, hence validation against the manufacturer's datasheet is performed initially. This allow calibration of the PV module to match the spectral characteristics of the solar simulator used during the experiment. It is crucial to consider such step to confirm the results obtained are in accordance to the PV module employed. Consequently, in attempt to further justify the computer model developed, validation against laboratory tests conducted at various operating conditions is also presented. The electrical power output of the PV module along with the conversion efficiency and module temperature are estimated for range of solar radiation intensities.

Table 8. 3 Conventional PV module validation parameters considered

| Component | Validated against | Input Conditions | Validated Parameters |
|------------------|---|---|--------------------------------------|
| PV Module | Manufacturer's datasheet | $G_{rad}=1000W/m^2$ $T_{amb}=25^{\circ}C$ | T_{PV} P_{mpp} η_{PV} |
| | Laboratory test of conventional PV module | $G_{rad}=740-1060 W/m^2$ $V_{wind}= 0 m/s$ | |

8.2.1.1 Validation Against Manufacturer's Datasheet

The rationale behind validating the PV module against the manufacturer's reported performance is to aid calibrating the spectral response of the solar simulator to that of natural sunlight. As such, the

influence of spectral mismatch between the solar cells spectral response and the light source is eliminated by assuming the solar simulator projected light that resemble natural sunlight. One of the parameters associated with defining the conversion efficiency of PV modules is the *Fill Factor*. Such parameter is defined as the ratio of the maximum power from the solar cell to the product of the open circuit voltage, (V_{oc}), and the open circuit current, (I_{sc}), Eq. 8.2. The voltage at the maximum power point (V_{mpp}) is not affected by the spectral response of the light source, in fact slightly higher value was observed, unlike the current (I_{mpp}) as observed by comparing recorded characteristics at solar intensity of 1000 W/m² and module temperature of 25 °C, Table 8.4. This drastic drop in the current suggests the need to calibrate the solar simulator to estimate the effective solar radiation intensity that matches with the cells spectral characteristics.

$$FF = \frac{V_{mp} I_{mp}}{V_{oc} I_{sc}} \quad (8.2)$$

Table 8. 4 Recorded results and influence of spectral mismatch on PV performance

| Parameter | V_{oc} | V_{mpp} | I_{sc} | I_{mpp} | P_{max} |
|------------------|-----------------------|------------------------|-----------------------|------------------------|------------------------|
| [Unit] | [V] | [V] | [A] | [A] | [W] |
| Measured | 43.2 | 37.3 | 2.32 | 2.15 | 81 |
| Predicted | 44.2 | 35.2 | 5.29 | 4.80 | 169 |
| Var. [%] | 2.5 | -5.67 | 126 | 124 | 110 |

8.2.1.2 Validation Against Experimental Test

Applying the definition of the fill factor at STC after matching the spectral response of both simulator and solar cells allow estimation of the actual IV characteristics of the PV module under investigation. Calculation of efficiency under measured light intensity before correction and with the effective intensity based on satisfying the rule of achieving the performance of STC is essential to the accurate prediction of output power and temperature response of the collector. However, the radiation intensity affecting the thermal performance is applied in the simulation model without any alteration as it influences the temperature response of the module as discussed in following section of the simulation model's validation. Applying the variation factors within Table 8.4 to the current at maximum power point provides a new set of data that is used to compare the performance with the manufacturer's reported ones. It is evident that such simplified yet practical approach permits the validation of the developed computer model with experimentally recorded performance for a set of varying conditions applied to the collector.

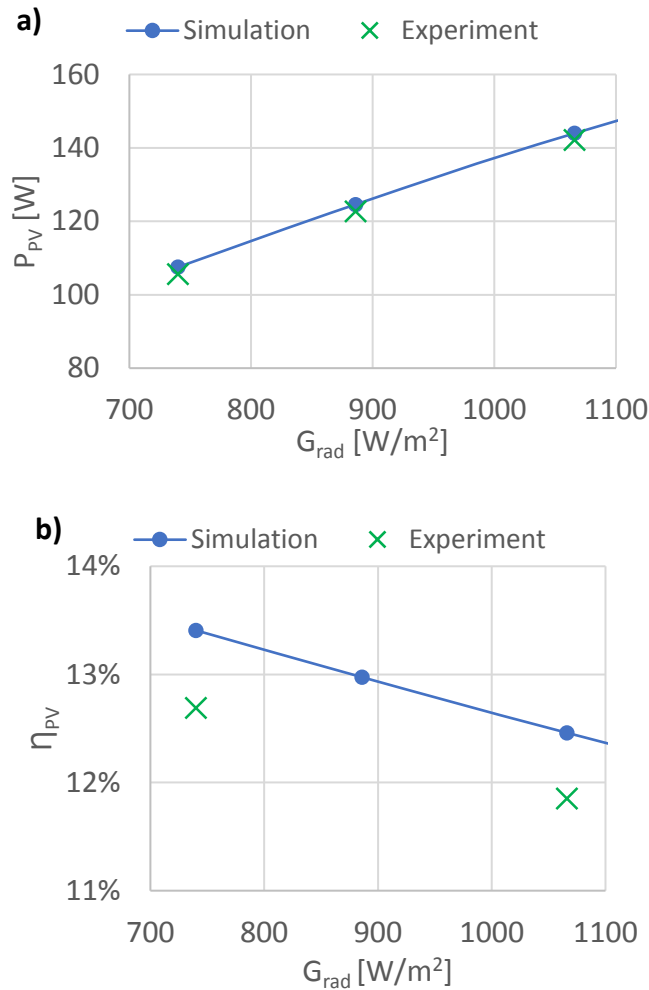


Fig. 8. 12 Comparison of power output and conversion efficiency trends of conventional PV module

The power output of the conventional PV module is validated against the experimentally recorded values for a range of incoming solar radiation as observed in Fig. 8.12 (a). Both curves are in good agreement. On the other hand, the conversion efficiency of the module is compared against the efficiency estimated based on the recorded characteristics, likewise fairly good agreement between both results is identified in Fig. 8.12 (b).

Additionally, the module temperature at steady state condition for both

investigations is compared in Fig. 8.13, and close correlation is noted. A summary of the validated parameters within the simulation model along with variation with experimentally recorded data is presented in Table 8.5.

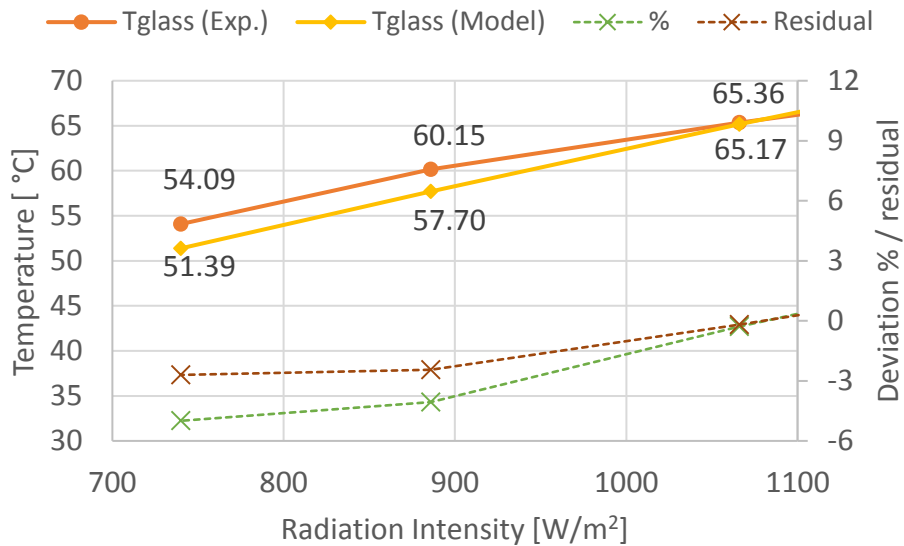


Fig. 8. 13 Temperature response of PV module under varying of light intensities

Table 8. 5 Summary of PV module power output and temperature response validation

| G | T (Exp.) | T (Sim.) | P _{max} (Exp.) | P _{max} (Sim.) | η _{PV} (Exp.) | η _{PV} (Sim.) |
|---------------------|----------|----------|-------------------------|-------------------------|------------------------|------------------------|
| [W/m ²] | [° C] | | [W] | | [%] | |
| 1066 | 65.36 | 64.65 | 142.16 | 143.97 | 11.85 | 12.46 |
| 886 | 60.15 | 57.20 | 122.74 | 124.59 | N/A | 12.97 |
| 740 | 54.09 | 50.92 | 105.65 | 107.54 | 12.69 | 13.41 |

8.2.2 Thermoelectric Electrical Characteristics

The validation of the thermoelectric generator adopted in the hybrid PV collector is presented in this section. Likewise, validation against the performance reported in the manufacturer's datasheet in addition to a laboratory scale experiment performed on a single TEG module is described in this section. Table 8.6 below summarizes the validation for the TEG model developed in chapter 5 earlier along with the conditions applied and parameters validated.

Table 8. 6 TEG module validation parameters considered

| Component | Validated against | Condition | Validated Parameters |
|-------------------|--------------------------------------|----------------------------|--|
| TEG Module | Laboratory test of single TEG module | Data available in Appendix | V_{emf} V_{mpp} I_{mpp} P_{mpp} |

8.2.2.2 Validation of TEG Against Experimental Test of Single Module

To further justify the TEG model developed, validation against a test conducted on a single TEG module in a similar approach applied to the TEG assemblies within the integrated PV-TEG hybrid collector is described here. Integrating the fan-heat sink assembly at the cold plate of the TEG is considered, however, a heating element that resembles the heat pipe

condensers' section is utilised instead. The conditions at which the TEG model was tested against are presented in Fig. 8.18, in which applying these conditions aids the justification of the TEG model. Limitation of the heating element power capabilities add constraints on the range of operating conditions applied to the TEG module, nevertheless, for verifying the theoretical model against the devices' datasheet bridges the gap in the elevated temperature range. The practical performance characteristics obtained from testing a single TEG module with the fan-heat sink attached at the cold side plate is presented in Fig. 8.19. The characteristics presented in are compared against simulation prediction separately, Fig. 8.20.

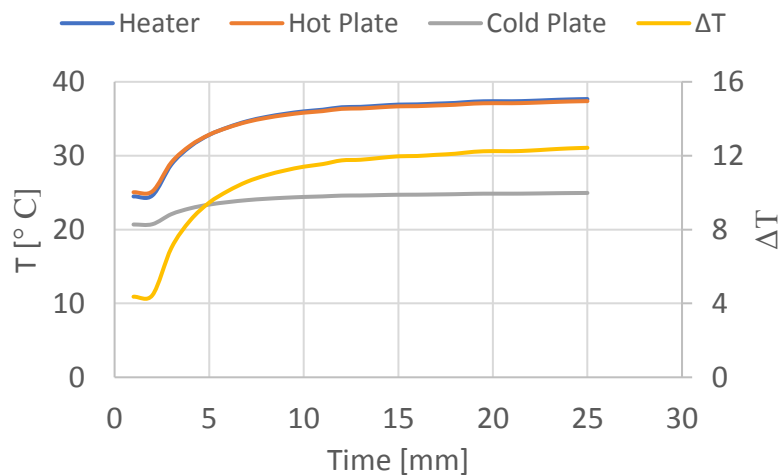


Fig. 8. 14 Experimental testing condition experienced during characterization of single TEG module

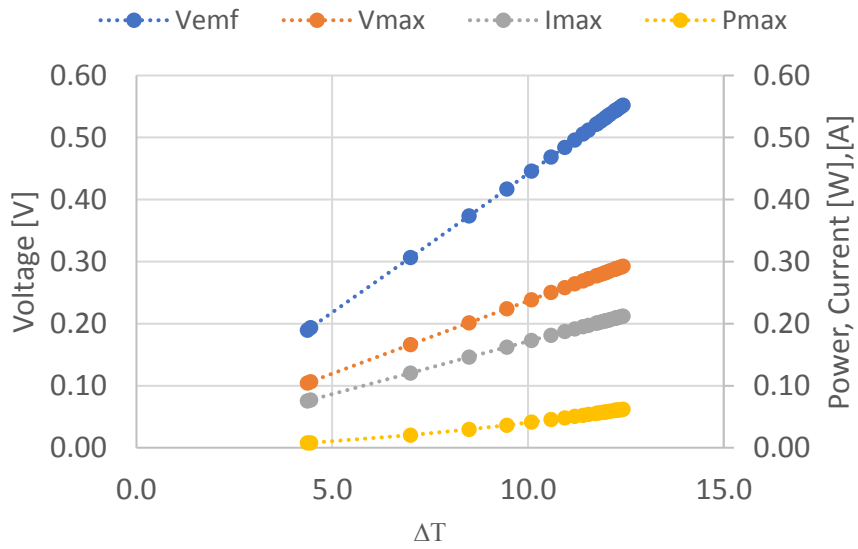
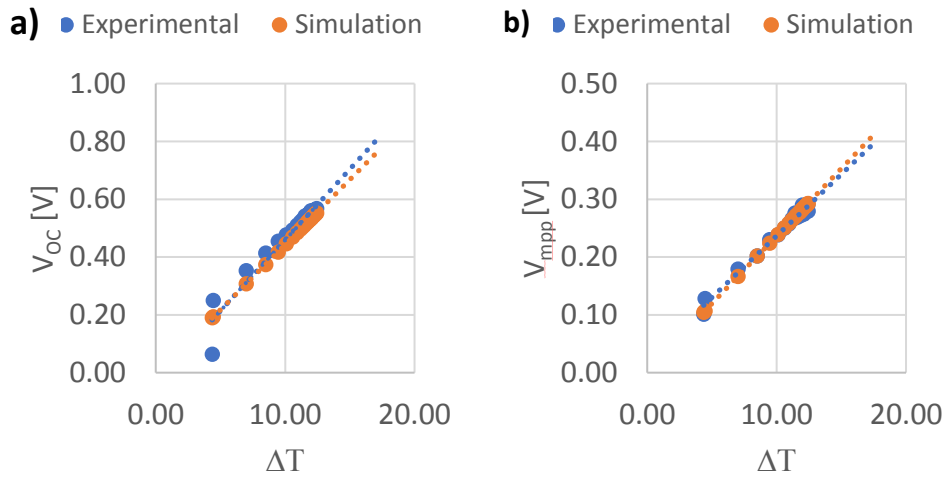


Fig. 8. 15 Simulation results applying conditions experienced during experimental test of a single TEG module



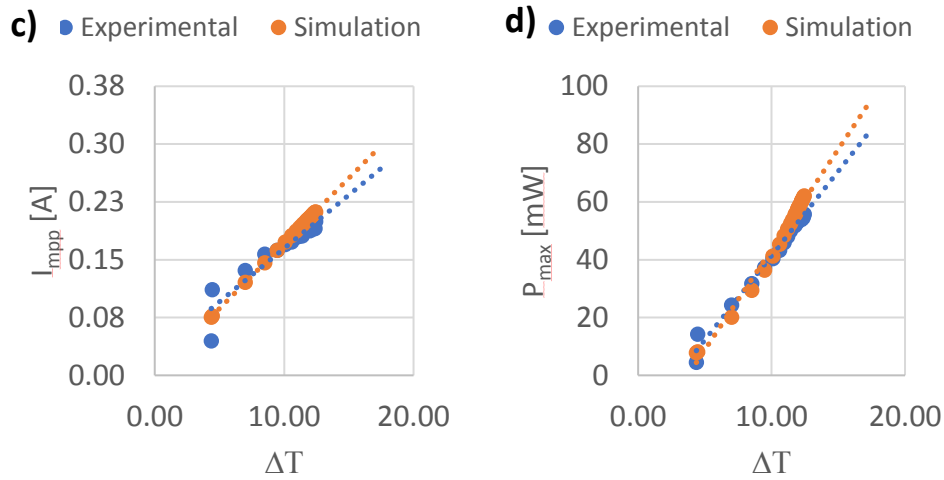


Fig. 8. 16 Comparison between theoretical predictions and experimental results for a single TEG module

To conclude the verification process of the TEG model, a comparison between the time responses of each of the validated parameters is also presented in Fig. 8.21. The variation between predicted results and measured ones are better observed in Fig. 8.22. It can be noted that maximum deviation occurs in the maximum power point ($\sim 12\%$) with an average of ($\sim 7\%$) considering the whole testing period. The variation of the open circuit voltage (V_{emf}), voltage and current at maximum power point (V_{mpp}, I_{mpp}) are ($\sim -4\%$), ($\sim 1\%$), and ($\sim 6\%$) respectively.

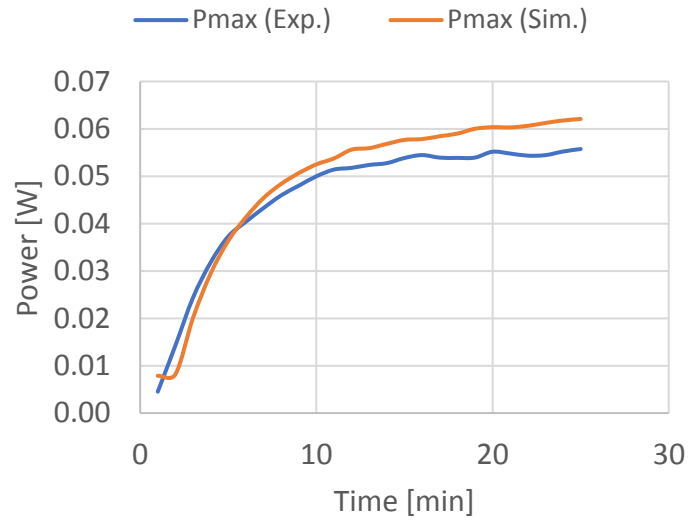


Fig. 8. 17 Comparison between simulated and recorded maximum power output of single TEG module

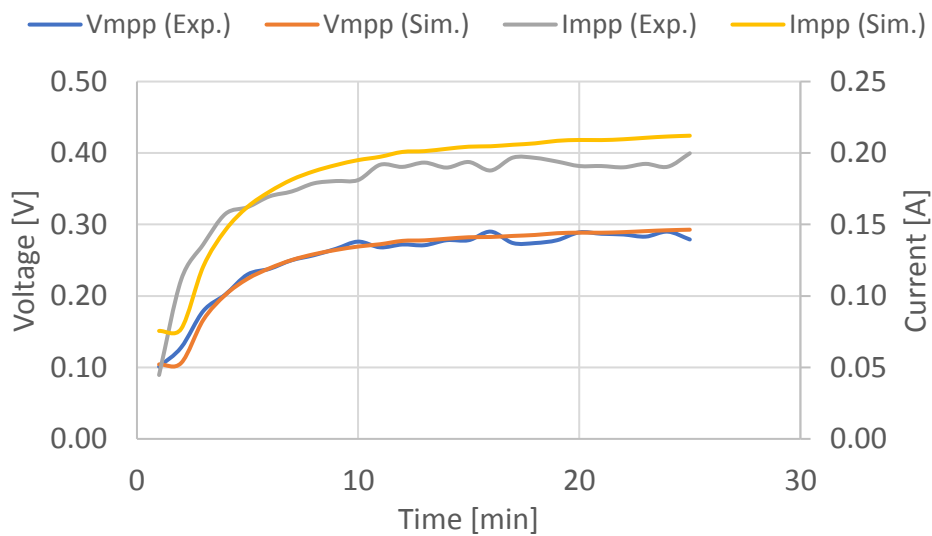


Fig. 8. 18 Comparison between simulated and recorded voltages and currents at maximum power point for single TEG module

Having theoretical predictions in accordance to both manufacturer's and practically measured characteristics at steady state condition, in addition to the transient responses of the identical parameters, it is fair to conclude that the computer model is valid within allowable deviances attributed to

measurement errors and simplifications within the test set-up. The variations between the simulated and recorded results is summarized in Fig. 8.23 below. Average variation in the order of less than 5% is observed in the open circuit voltage of the TEG module, while less than 1% deviation is noted in the voltage at maximum power point. The average deviation of the maximum power point however is recorded at 7%, influenced by the deviation in the current at maximum power point between simulation model and tested TEG module.

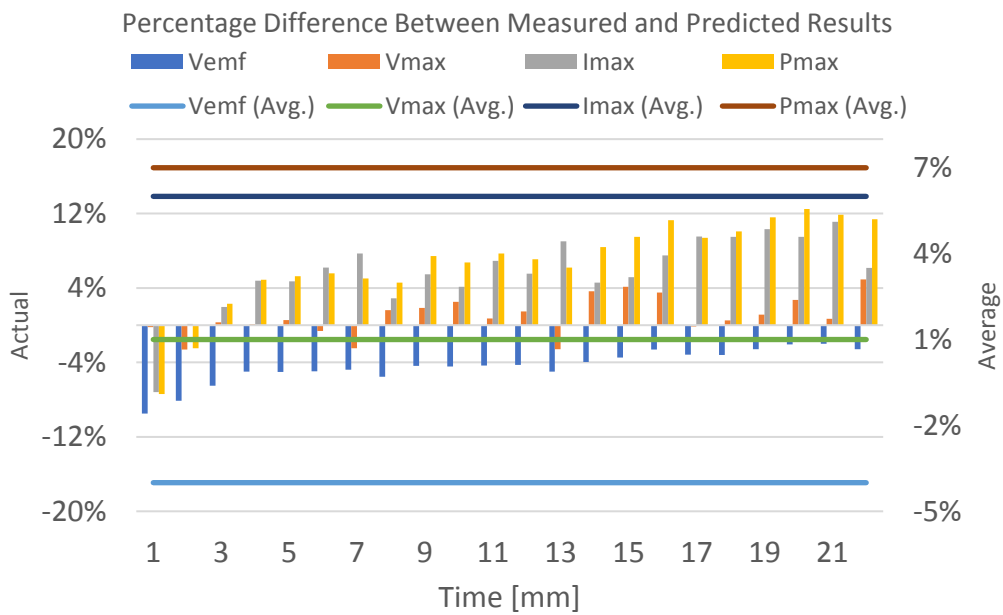


Fig. 8. 19 Actual and averaged deviation of TEG module performance parameters

8.2.3 Heat Pipe Performance Validation

The validation of the heat pipe performance within the integrated PV-TEG collector is compared against a set of recorded data obtained at the experimental investigation stage. Temperature sensors attached at both evaporator and condenser sections of the heat pipe aided comparison of both sets of data. It is important to emphasize that the heat pipe model developed in chapter 5 considers a simplified approach based on the energy balance of both evaporator and condenser sections and the associated thermal resistances. Here, the temperature recorded during the experiment for a range of incoming solar intensities are compared directly with the temperature predictions for both evaporator and condenser sections of the heat pipe.

At the evaporator section of the heat pipe, it was clearly observed that the temperature response of both predicted results and measurements are in perfect agreement, with a maximum deviation of less than (3%), Fig. 8.24. Meanwhile, Fig. 8.25 below presents the correlation between the temperature response of the condenser section for both theoretical model and practically measured ones at steady state. It is evident that the temperature response for both investigation follow a similar trend with an average deviation of ($\approx 13\%$) over the total incoming solar intensity range of

the test, and deviation of ($\approx 3\%$) and ($\approx 20\%$) at the low and high intensity range respectively. Such higher percentage compared to the evaporator section is attributed to the assumption of uniform temperature distribution across the collector addressed earlier. However, the actual temperature recorded within the experiment suggests a non-uniform temperature distribution.

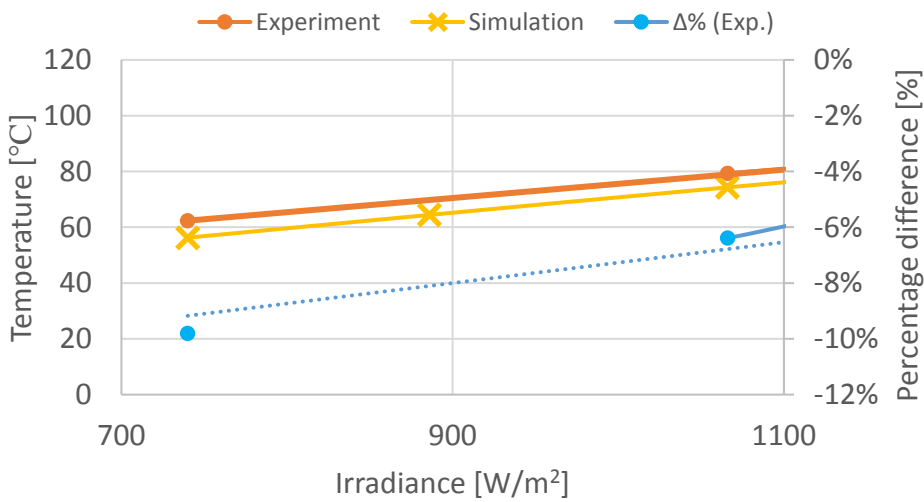


Fig. 8. 20 Evaporator section temperature comparison

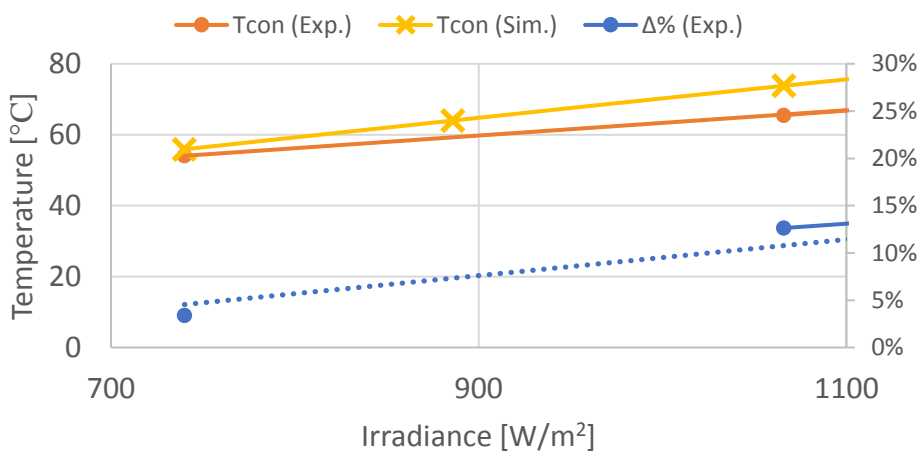
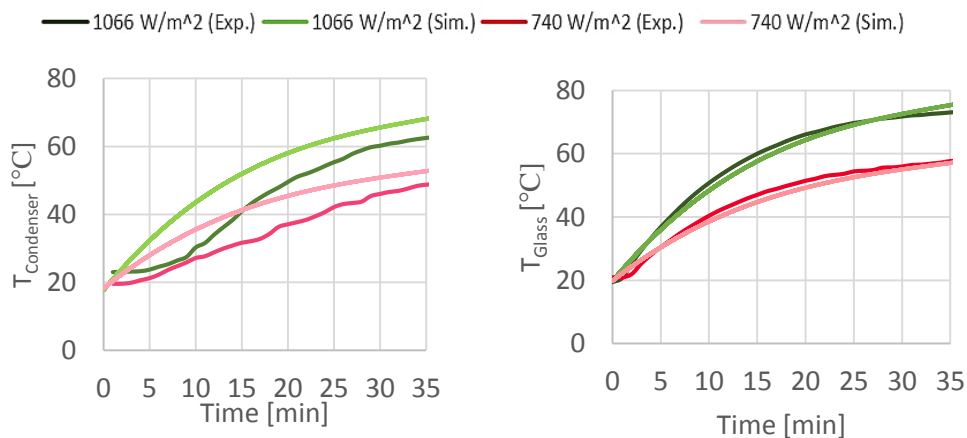


Fig. 8. 21 Evaporator section temperature comparison

In attempt to further justify the heat pipe performance, the transient response of the condenser temperature, power output, and front glazing temperature of the integrated hybrid collector are compared in Fig. 8.26. It can be observed that the time responses match in a similar trend, with a slight delay attributed to the heat accumulating at the rear and absorbed by the evaporator section for the condenser temperature, while a perfect match in the output power and front glazing temperature was identified. The deviation of the output power for the range of incoming light intensities for both simulation results and measurements is further exploited in Fig. 8.27. In conclusion, due to such imperfections within measurements and the way the heat pipe condenser was integrated to the system besides loses within the fan-heat sink assembly through the acrylic material and the aluminium heating block, the deviation between the predicted results and the recorded measurement are justified.



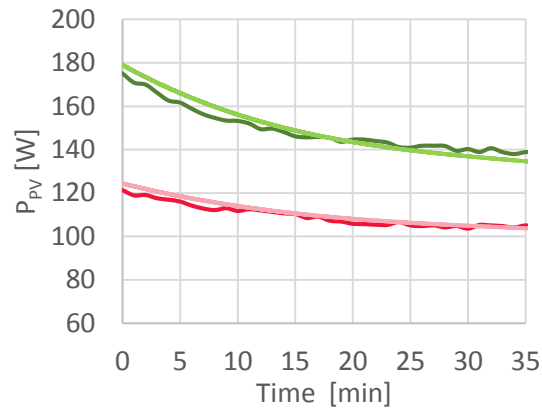


Fig. 8. 22 Transient response of the integrated collector power output, front glazing, and condenser section temperature for validation purpose

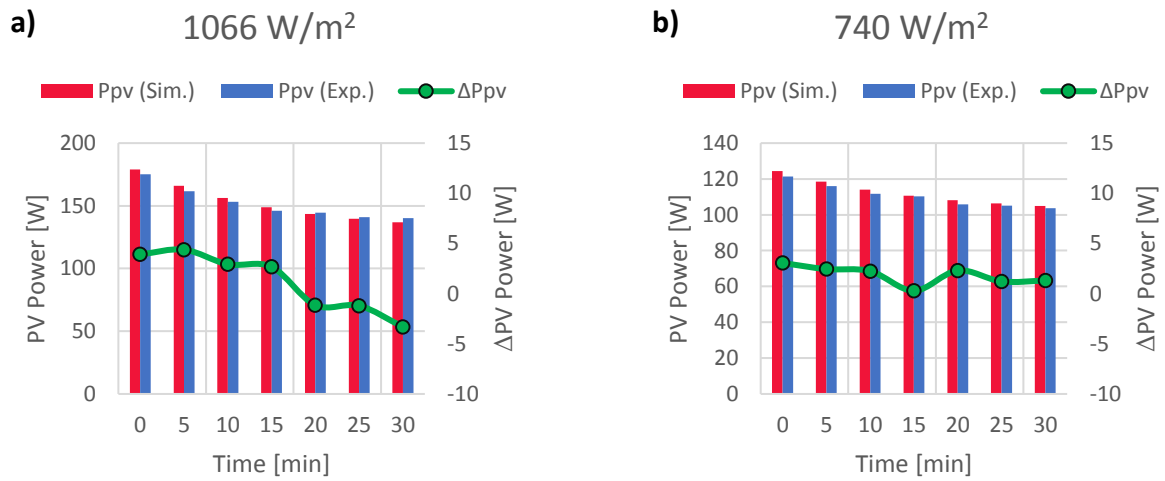


Fig. 8. 23 deviation of the output power for the range of incoming light intensities

8.3 System Optimization

The validated computer model is utilised in this section in order to optimise the integrated collector design assessing any further improvement in the performance associated to the number of heat pipes incorporated in the collector design.

8.3.1 Influence of Pipes Number Attached on System Performance

The theoretical analysis performed for the integrated heat-pipe based PV-TEG collector at the presence of insulation at the rear of the collector predicted further elevated temperature of the PV module, hindering the performance of the cells. The collector however, exhibited improved performance of the TEG modules incorporated in the waste heat recovery assembly's due to higher thermal flux available in the module due to eliminating the losses associated with convection and radiation at the rear of the collector. Therefore, improved power output was attained by the thermoelectric bank. In attempt to further investigate any performance improvements through further reduction in the PV module temperature, the number of heat pipes incorporated in the collector is investigated. In this section, the analysis is illustrated for both PV module temperature and total power output of the hybrid collector.

8.3.1.1 Temperature Response

The integrated collector with insulation exhibits the highest temperature compared to both conventional and integrated PV-TEG module without insulation. Hence, in order to utilize the thermal energy available from the collector efficiently, the number of heat pipes attached to the panel is investigated. The pitch distance between the pipes is varied such that the number of heat pipes attached at the rear is varied for optimized design. Fig 8.28 illustrates the influence of the number of heat pipes attached on the temperature response of the collectors for steady light intensity of 1000 W/m^2 , ambient temperature of $25 \text{ }^\circ\text{C}$, and wind speed of 0 m/s .

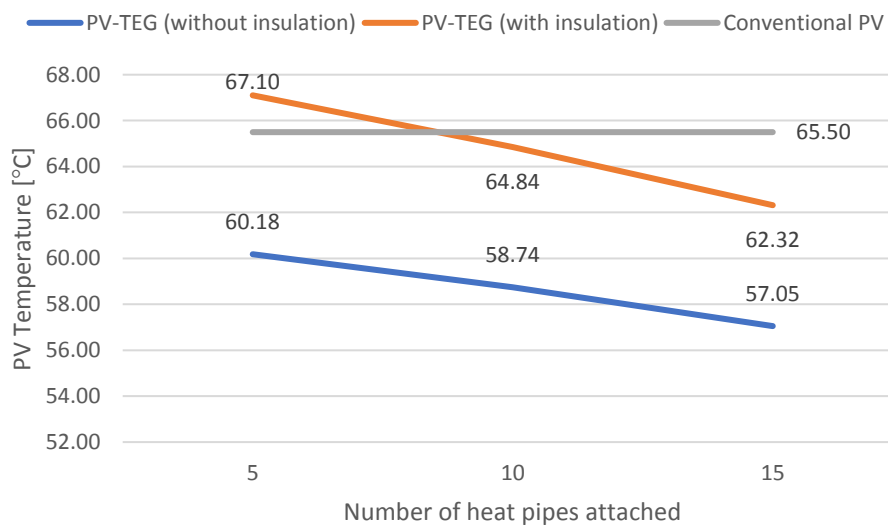


Fig. 8. 24 Influence of number of heat pipes attached on the temperature response of the collectors

The temperature response of both integrated collectors with and without insulation is directly influenced by the number of heat pipes attached, exhibiting improved thermal management of the PV cells as the number of the heat pipes is increased. The temperature response of the insulated collector is improved compared to the conventional PV module as the number of heat pipes is increased to 10. Further temperature reduction is observed as the number is further increased to 15 pipes. The integrated PV-TEG collector without insulation however, maintains an improved operating temperature with an almost constant temperature difference as the ambient temperature is varied, Fig. 8.29.

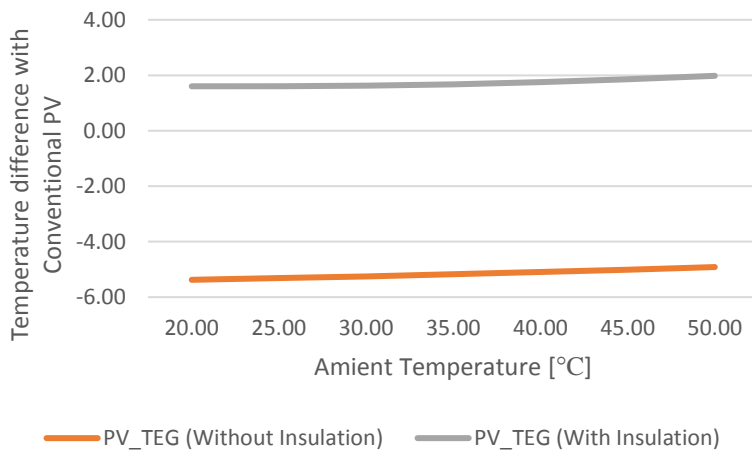


Fig. 8. 25 PV Temperature difference between integrated collector and conventional PV module at wind speed 0 and varying ambient temperature

8.3.1.2 Electrical Performance

The electrical performance of the integrated collector with various number of heat pipes attached relative to the conventional PV module is presented and discussed in this section. Fig 8.30 illustrates the influence of the number of heat pipes attached on the power output of the collectors under steady state condition for light intensity of 1000 W/m^2 , ambient temperature of $25 \text{ }^\circ\text{C}$, and wind speed of 0 m/s .

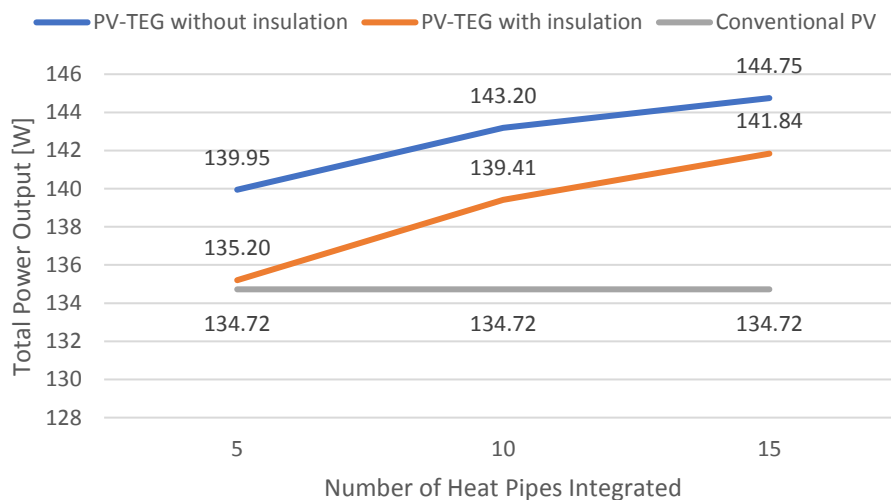


Fig. 8. 26 Influence of number of heat pipes attached on the total power output

The output power response presented is the sum of power output from both PV module in addition to the TEG modules incorporated in the heat recovery system. The power yield of the collector is enhanced as the number of heat pipes is increased as a result of further reduction in the PV cells temperature presented earlier. The integrated collector without insulation

at the rear attained the maximum power output compared to the other investigated collectors confirming the observations discussed earlier in the computer modelling results. The power output of the integrated collector with 5 heat pipes attached at the presence of the insulation exhibited almost identical value compared to the conventional PV module. Increasing the number of heat pipes resulted in improved power output, due to more efficient heat extraction via the heat pipes, as well as increased heat flux absorbed by the TEG bank leading to further electrical power output.

Chapter 9

Conclusion and Future Work

9.1 Summary

Improvements in the energy conversion efficiency of Photovoltaic systems through investigating a strategy to provide effective cooling and permit utilization of waste heat for useful applications is addressed in this research. The system proposed adopts a hybrid design that incorporates Photovoltaic (PV) technology in combination with Thermoelectric Generators (TEGs) and Heat Pipes in a modular integration. In that regard, the incorporation of heat pipes and thermoelectric generation technologies for thermal management of PV cells was investigated theoretically and experimentally.

The absorber of the integrated PV-TEG collector consists of a PV module with surface area of 1.3 m² and rated at 170 W serving as power generator as well as thermal absorber. Five heat pipes were attached to the rear of the to extract excessive heat accumulating on solar cells, each with evaporator section length of 1700 mm and condenser section of 63 mm. The extracted heat is transferred via boiling-condensation process within the heat pipe to five 40 mm x 40 mm TEG modules, each attached to the condenser section of each heat pipe, and waste-heat is recovered via direct conversion of the temperature difference available across the TEG plates to electrical energy.

A theoretical numerical model of the collector proposed was developed through derivation of 2-dimensional partial differential equations governing the energy exchange within the system components based on energy balance concepts while applying explicit finite difference numerical approach for implementation in MATLAB software. Experimental tests were also conducted allowing for practical performance evaluation of the system investigated. The developed numerical model was validated against experimental data and a refined model was utilised for performance predictions of the hybrid collector under various climatic conditions in addition to system design optimization to assess the optimum number of heat pipes required for a given collector area. The proposed collector was evaluated through analysing the electrical and thermal responses, in addition to the total energy conversion efficiency of the collector.

The set of tasks accomplished within this research include:

- ❖ A thorough review of the literature has been conducted assessing different techniques applied to achieve thermal management for PV systems in an attempt to further enhance their power generation capabilities. Techniques vary from the methods heat is extracted by to the product of the thermal heat recovery.

- ❖ A theoretical background research of technologies and components incorporated in the integrated hybrid collector including mainly, Solar Photovoltaics, Heat Pipes, and Thermoelectric Generation technologies.
- ❖ Derivation of differential equations for the energy exchange within the system components based on the energy balance concept, and applying explicit finite difference numerical approaches for solutions.
- ❖ Integration of mathematical models of technologies incorporated in in MATLAB software to evaluate and predict the performance of the proposed hybrid collector under varying operating conditions.
- ❖ Fabrication of the proposed collector prototype to investigate the practical performance and improvement capabilities of the integrated system and various operating conditions.
- ❖ Validation and calibration of the theoretical model against experimental results leading to a refined and improved simulation model.

9.2 Research Findings

The performance analysis considered three collectors to facilitate comparisons and realize the significance of the integrated heat pipe-based PV/TEG collector with and without insulation present at the rear of the module compared against a conventional PV module under identical operating parameters. It is evident that the existence of insulation at the rear of the collector contributes to further rise the temperature of the PV layer in the order of 2-10°C under maximum light intensity of 1000 W/m² and wind speed condition range of 0-5 m/s when compared against the conventional PV module. Although elevated temperature has an adverse effect on the electrical performance of the PV cells, high thermal energy flux is desirable to enhance the generation capacity of the thermal recovery system. Therefore, the presence of mineral wool insulation layer at the rear of the module is desired to minimize thermal losses to the environment. Therefore, the integrated collector at the presence of the insulation layer attained maximum temperature at all conditions when compared with that of no insulation and the conventional PV module. This is due to the fact that the rate of thermal heat dissipation on the absorber surface is far superior to the heat extraction rate of the heat pipes attached. Additionally, the cooling rate of the condenser section of the heat pipes was not sufficient to

further drop the temperature of the PV cell for the integrated collector with insulation.

On the other hand, the temperature response of both conventional PV module and integrated collector without insulation attained lower temperature due to the influence of free convection at the rear of the module. Under light intensity of ($G_{rad}=1000 \text{ W/m}^2$), maximum temperature difference between both collectors of 8°C was observed, contributing to temperature reduction of only 16% when compared with the conventional PV module. In terms of the supplemental power generation via the thermal waste heat recovery system, insignificant additional power of only 2 W was attained. Thermal waste recovery adopting thermoelectric devices require large temperature difference across the hot and cold plates of the device, making improvement in performance limited with the current TE technologies available. Hence, the additional power from the integrated TEG bank was not sufficient to compensate for the deteriorated electrical performance for the integrated collector with insulation.

In terms of the total electrical power generation the integrated collector at the absence of insulation exhibited superior performance compared to the conventional PV module due to reduction in the temperature of the PV cells. Under light intensity of ($G_{rad}=1000 \text{ W/m}^2$), maximum power difference between the two collectors of 5.8 Watts was observed, corresponding to

about 4% improvement. The overall energy conversion efficiency of the integrated collector was observed to be steady at about 11% compared to that of the conventional PV module (9.5%) even at high ambient temperature and low wind speeds.

Optimization of the collector proposed was conducted to evaluate the performance improvements associated to increasing the number for heat pipes attached into the collector. Under steady light intensity of 1000 W/m^2 , ambient temperature of $25 \text{ }^\circ\text{C}$, and wind speed of 0 m/s , the electrical and temperature response of the hybrid collector are presented in Table 9.1. increasing the number of heat pipes from 5 to 15 pipes contributes to further reduction in the PV module temperature of 7.5% and 5% for the hybrid collector with and without insulation respectively. In terms of total power generated improved output of additional 5% and 3.4% is attained.

Table 9. 1 Performance improvements of the hybrid collector as function of heat pipe number attached

| Conventional PV module | PV module temperature [$^\circ\text{C}$] | | | Total power output [W] | | |
|-------------------------------------|--|------|----|------------------------|-----|-----|
| | 5 | 10 | 15 | 5 | 10 | 15 |
| No. of heat pipes attached | | | | | | |
| Hybrid collector with insulation | 67 | 65 | 62 | 135 | 139 | 142 |
| Hybrid collector without insulation | 60 | 58.7 | 57 | 140 | 143 | 145 |

Although the additional power from the thermal waste recovery system was insignificant, the investigation proved the potential integrating heat pipes and TEG module has with PV technology. Due to the low grade of thermal energy available within single junction PV modules as the one considered in this investigation, integration for concentrated PV utilising multijunction PV technology can be attractive, where elevated temperature in the range 150-300°C can be achieved using optical concentrators.

The outcomes of this research can have significant impact on the scientific community, researchers and industries. In terms of new knowledge, an innovative technique for thermal waste heat recovery from PV modules is introduced where efficient utilisation of solar energy available from the sun is permitted. This research has the potential to open door for further enhancement applying various settings and arrangements.

9.3 Limitations

The research conducted is governed by some limitations that can contribute towards measurement uncertainties as well as limitation to performance improvements. The following statements summarise the limitations within this research.

- The use of cylindrical heat pipes has an influence on the heat extraction/transport capability which is limited by the contact point

between the module and the heat pipes attached. The use of aluminium heat spreaders to increase the area of the heat pipe evaporator section introduces further thermal losses.

- The incorporation of TEG modules with the heat pipes is limited to a single TEG per heat pipe based on the system design. Increasing the number of TEG attached has the potential to further lower the temperature of the PV cells.
- The performance of the heat pipes employed within this investigation is limited by the cooling capability of the fan-heat sink assembly attached at the condenser section of the heat pipe.
- The PV technology employed within this investigation does not consider concentrated solar light, which is able to enhance power generation of the thermal waste recovery system due to high thermal dissipation from concentrated irradiance. Thermal waste recovery adopting thermoelectric devices require large temperature difference across the hot and cold plates of the device.
- Artificial solar simulators are governed by limitations, mainly associated to mismatch in the spectral response between artificial light source and natural sunlight, introducing measurement uncertainties.

9.4 Recommendation for Future Work

Although the proposed system exhibited improved performance, further improvements associated with the collector design is required to further enhance the system performance. The recommendations based on the constraints and limitations of the system investigated are listed as follows:

- Dissipation of heat to the surrounding at the cold plate surface of the TEG is limited by convection thermal transfer, which is improved due to the incorporation of the cooling fan. However, as the light intensity is increased the waste heat recovery system is limited by the cooling capability of the attached fan. An alternative to using the cooling fan can be the utilization of liquid cooling at the TEG cold plate.
- Improvements within design can be seen in assessing incorporation of few TEG modules to a single heat pipe. Additional TEG modules can further improve the thermal waste heat recovery as well as the enhancing the rate at which the condenser section is cooled, and hence higher rate of thermal energy extraction.
- The developed computer model can be further improved to consider other climatic parameters that contributes towards degradation of the performance of PV cells, such as humidity and soiling.

- The utilisation of micro flat heat pipes instead of cylindrical ones has the potential to enhance heat extraction associated to the limited contact point between the evaporator section of the heat pipe and the rear of the module. Flat heat pipes can also eliminate the necessity of aluminium heat spreaders to increase the evaporator section area of the pipes, hence reducing thermal losses due to conduction.
- Application of concentrated solar energy can improve the feasibility of the system utilisation multijunction PV technology that are able to operate at elevated temperature (150-300°C) and further promote better thermal waste heat recovery using thermoelectric generators.
- Experimental investigation under artificial sunlight introduce uncertainties and in many cases, does not reflect the practical performance of PV systems. Therefore, experimental testing under natural sunlight can be considered for future work.
- Economic analysis is also recommended to evaluate the feasibility of the collector for practical application. However, the low grade thermal energy available from single junction PV modules, economic study is only valuable for concentrated PV application.

References

A. G. Redpath, D., Singh, H., Tierney, C. and Dalzell, P. (2012) 'An experimental comparison of two solar Photovoltaic- thermal (PVT) energy conversion systems for production of heat and power', *Energy and Power*, 2(4), pp. 46–50. doi: 10.5923/j.ep.20120204.01.

Aavid Thermalloy (2016) *Fan heat sinks - heat sink design*. Available at: <https://www.aavid.com/solutions/fan-heatsink> (Accessed: 21 February 2017).

Abhat, A. (1983) 'Low temperature latent heat thermal energy storage: Heat storage materials', *Solar Energy*, 30(4), pp. 313–332. doi: 10.1016/0038-092x(83)90186-x.

Agrawal, S. and Tiwari, A. (2011) 'Experimental validation of glazed hybrid micro-channel solar cell thermal tile', *Solar Energy*, 85(11), pp. 3046–3056. doi: 10.1016/j.solener.2011.09.003.

Agrawal, S. and Tiwari, G.N. (2011) 'Energy and exergy analysis of hybrid micro-channel photovoltaic thermal module', *Solar Energy*, 85(2), pp. 356–370. doi: 10.1016/j.solener.2010.11.013.

Agrawal, S. and Tiwari, G.N. (2013) 'Overall energy, exergy and carbon credit analysis by different type of hybrid photovoltaic thermal air collectors', *Energy Conversion and Management*, 65, pp. 628–636. doi: 10.1016/j.enconman.2012.09.020.

Agyenim, F., Hewitt, N., Eames, P. and Smyth, M. (2010) 'A review of materials, heat transfer and phase change problem formulation for latent heat thermal energy storage systems (LHTESS)', *Renewable and Sustainable Energy Reviews*, 14(2), pp. 615–628. doi: 10.1016/j.rser.2009.10.015.

Ahiska, R., Dislitas, S. and Omer, G. (2012) 'A new method and computer-controlled system for measuring the time constant of real thermoelectric modules', *Energy Conversion and Management*, 53(1), pp. 314–321. doi: 10.1016/j.enconman.2011.09.003.

Akbarzadeh, A. and Wadowski, T. (1996) 'Heat pipe-based cooling systems for photovoltaic cells under concentrated solar radiation', *Applied Thermal Engineering*, 16(1), pp. 81–87. doi: 10.1016/1359-4311(95)00012-3.

Al-Hawaj, O.M. (2011) 'Theoretical analysis of sliding vane energy recovery device', *Desalination and Water Treatment*, 36(1-3), pp. 354–362. doi: 10.5004/dwt.2011.2639.

References

Al-Amri, F. and Mallick, T.K. (2013) 'Alleviating operating temperature of concentration solar cell by air active cooling and surface radiation', *Applied Thermal Engineering*, 59(1-2), pp. 348–354. doi: 10.1016/j.applthermaleng.2013.05.045.

Al-Mosawi, A. (2011) *Thermal Energy Storage for Building-Integrated Photovoltaic Components*. PhD Thesis thesis. University of Strathclyde Glasgow, Scotland. .

Amori, K.E. and Abd-AlRaheem, M.A. (2014) 'Field study of various air based photovoltaic/thermal hybrid solar collectors', *Renewable Energy*, 63, pp. 402–414. doi: 10.1016/j.renene.2013.09.047.

Amori, K.E. and Taqi Al-Najjar, H.M. (2012) 'Analysis of thermal and electrical performance of a hybrid (PV/T) air based solar collector for Iraq', *Applied Energy*, 98, pp. 384–395. doi: 10.1016/j.apenergy.2012.03.061.

Andreev, V.M., Grilikhes, V.A., Romyantsev, V.D., Romyantev, V.D. and Rumiavtsev, V.D. (1997) *Photovoltaic conversion of concentrated sunlight*. New York: Wiley, John & Sons.

Anderson, W., Dussinger, P., Tamanna, S. and Sarraf, D. (2008) 'Heat Pipe Cooling of Concentrating Photovoltaic Cells', San Diego, CA, USA: Photovoltaic Specialists Conference, 33rd IEEE. pp. 1–6.

Angrist, S.W. (1982) *Direct energy conversion*. 4th edn. United States: Allyn and Bacon.

Ansuini, R., Larghetti, R., Giretti, A. and Lemma, M. (2011) 'Radiant floors integrated with PCM for indoor temperature control', *Energy and Buildings*, 43(11), pp. 3019–3026. doi: 10.1016/j.enbuild.2011.07.018.

Arkar, C. and Medved, S. (2007) 'Free cooling of a building using PCM heat storage integrated into the ventilation system', *Solar Energy*, 81(9), pp. 1078–1087. doi: 10.1016/j.solener.2007.01.010.

Armstrong, S. and Hurley, W.G. (2010) 'A thermal model for photovoltaic panels under varying atmospheric conditions', *Applied Thermal Engineering*, 30(11-12), pp. 1488–1495. doi: 10.1016/j.applthermaleng.2010.03.012.

Azad, E. (2008) 'Theoretical and experimental investigation of heat pipe solar collector', *Experimental Thermal and Fluid Science*, 32(8), pp. 1666–1672. doi: 10.1016/j.expthermflusci.2008.05.011.

Bag, B.P. (2009) *Solar energy: How a PV cell works*. Available at: http://www.solarschools.net/resources/stuff/how_pv_cells_work.aspx (Accessed: 17 February 2011).

References

Bambrook, S.M. and Sproul, A.B. (2012) 'Maximising the energy output of a PVT air system', *Solar Energy*, 86(6), pp. 1857–1871. doi: 10.1016/j.solener.2012.02.038.

Biwole, P.H., Eclache, P. and Kuznik, F. (2013) 'Phase-change materials to improve solar panel's performance', *Energy and Buildings*, 62, pp. 59–67. doi: 10.1016/j.enbuild.2013.02.059.

Brinkworth, B.J., Cross, B.M., Marshall, R.H. and Yang, H. (1997) 'Thermal regulation of photovoltaic cladding', *Solar Energy*, 61(3), pp. 169–178. doi: 10.1016/s0038-092x(97)00044-3.

Brogren, M. and Karlsson, B. (2002) 'Low- Concentrating water-cooled PV-Thermal hybrid systems for high latitudes', *29th Photovoltaic Specialists Conference IEEE*, , pp. 1733–36.

Byon, C. (2016) 'Electronics cooling', . doi: 10.5772/62328.

Bouzoukas, A. (2008) *New Approaches for cooling photovoltaic/thermal systems*. PhD Thesis thesis. University of Nottingham. .

Boyen, J.L. (1980) *Practical thermal energy recovery*. 2nd edn. New York: John Wiley & Sons.

California Institute of Technology (2013) *Thermoelectrics at Caltech*. Available at: <http://thermoelectrics.caltech.edu/thermoelectrics/engineering.html> (Accessed: 17 February 2014).

Cengel, Y.A. (2007) *Heat and mass transfer: A practical approach*. 3rd edn. Dubuque, IA: McGraw-Hill Companies, The.

Cerón, I., Neila, J. and Khayet, M. (2011) 'Experimental tile with phase change materials (PCM) for building use', *Energy and Buildings*, 43(8), pp. 1869–1874. doi: 10.1016/j.enbuild.2011.03.031.

Chatterjee, S. and TamizhMani, G. (2011) 'BAPV arrays: Side-by-side comparison with and without fan cooling', *2012 38th IEEE Photovoltaic Specialists Conference, Austin, TX, 2012*, , pp. 000537–000542.

Chan, A.L.S. (2011) 'Energy and environmental performance of building façades integrated with phase change material in subtropical Hong Kong', *Energy and Buildings*, 43(10), pp. 2947–2955. doi: 10.1016/j.enbuild.2011.07.021.

References

Chaosook, C. (2002) *Single-Phase Grid-Connected Photovoltaic System Using Rectified Sinusoidal Hysteresis Current Control*. Masters Thesis thesis. King Mongkut's University of Technology, Thonburi, .

Charalambous, P.G., Maidment, G.G., Kalogirou, S.A. and Yiakoumetti, K. (2007) 'Photovoltaic thermal (PV/T) collectors: A review', *Applied Thermal Engineering*, 27(2-3), pp. 275–286. doi: 10.1016/j.applthermaleng.2006.06.007.

Chaturvedi, S.K. and Abazeri, M. (1987) 'Transient simulation of a capacity-modulated, direct-expansion, solar-assisted heat pump', *Solar Energy*, 39(5), pp. 421–428. doi: 10.1016/s0038-092x(87)80060-9.

Cheng, C.-H., Huang, S.-Y. and Cheng, T.-C. (2010) 'A three-dimensional theoretical model for predicting transient thermal behavior of thermoelectric coolers', *International Journal of Heat and Mass Transfer*, 53(9-10), pp. 2001–2011. doi: 10.1016/j.ijheatmasstransfer.2009.12.056.

Choi, J.-S., Ko, J.-S. and Chung, D.-H. (2010) 'Development of a thermoelectric cooling system for a high efficiency BIPV module', *Journal of Power Electronics*, 10(2), pp. 187–193. doi: 10.6113/jpe.2010.10.2.187.

Chow, T.T. (2010) 'A review on photovoltaic/thermal hybrid solar technology', *Applied Energy*, 87(2), pp. 365–379. doi: 10.1016/j.apenergy.2009.06.037.

Chow, T.T., Chan, A.L.S., Fong, K.F., Lin, Z., He, W. and Ji, J. (2009) 'Annual performance of building-integrated photovoltaic/water-heating system for warm climate application', *Applied Energy*, 86(5), pp. 689–696. doi: 10.1016/j.apenergy.2008.09.014.

Chow, T.T., He, W. and Ji, J. (2006) 'Hybrid photovoltaic-thermosyphon water heating system for residential application', *Solar Energy*, 80(3), pp. 298–306. doi: 10.1016/j.solener.2005.02.003.

Chow, T.T., He, W., Ji, J. and Chan, A.L.S. (2007) 'Performance evaluation of photovoltaic-thermosyphon system for subtropical climate application', *Solar Energy*, 81(1), pp. 123–130. doi: 10.1016/j.solener.2006.05.005.

Chávez-Urbiola, E.A., Vorobiev, Y.V. and Bulat, L.P. (2012) 'Solar hybrid systems with thermoelectric generators', *Solar Energy*, 86(1), pp. 369–378. doi: 10.1016/j.solener.2011.10.020.

Cook, E. (1971) 'The flow of energy in an industrial society', *Scientific American*, 225(3), pp. 134–144. doi: 10.1038/scientificamerican0971-134.

References

Daghigh, R., Ruslan, M.H. and Sopian, K. (2011) 'Advances in liquid based photovoltaic/thermal (PV/T) collectors', *Renewable and Sustainable Energy Reviews*, 15(8), pp. 4156–4170. doi: 10.1016/j.rser.2011.07.028.

Del Cueto, J. (2002) 'Comparison of energy production and performance from flat-plate photovoltaic module technologies deployed at fixed tilt', *In: Proceeding of the 29th IEEE PV specialists conference*, .

Du, B., Hu, E. and Kolhe, M. (2012) 'Performance analysis of water cooled concentrated photovoltaic (CPV) system', *Renewable and Sustainable Energy Reviews*, 16(9), pp. 6732–6736. doi: 10.1016/j.rser.2012.09.007.

Du, D., Darkwa, J. and Kokogiannakis, G. (2013) 'Thermal management systems for Photovoltaics (PV) installations: A critical review', *Solar Energy*, 97, pp. 238–254. doi: 10.1016/j.solener.2013.08.018.

Deng, Y., Zhu, W., Wang, Y. and Shi, Y. (2013) 'Enhanced performance of solar-driven photovoltaic–thermoelectric hybrid system in an integrated design', *Solar Energy*, 88, pp. 182–191. doi: 10.1016/j.solener.2012.12.002.

Di Vincenzo, M.C. and Infield, D. (2013) 'Detailed PV array model for non-uniform irradiance and its validation against experimental data', *Solar Energy*, 97, pp. 314–331. doi: 10.1016/j.solener.2013.08.030.

Dincer, I., Rosen, M.A. and Dincer, M.R.A. (2002) *Thermal energy storage: Systems and applications*. Chichester, United Kingdom: Wiley, John & Sons.

Domenech-Garret, J.-L. (2011) 'Cell behaviour under different non-uniform temperature and radiation combined profiles using a two dimensional finite element model', *Solar Energy*, 85(2), pp. 256–264. doi: 10.1016/j.solener.2010.12.007.

Dubey, S., Sandhu, G.S. and Tiwari, G.N. (2009) 'Analytical expression for electrical efficiency of PV/T hybrid air collector', *Applied Energy*, 86(5), pp. 697–705. doi: 10.1016/j.apenergy.2008.09.003.

Dubey, S. and Tiwari, G.N. (2009) 'Analysis of PV/T flat plate water collectors connected in series', *Solar Energy*, 83(9), pp. 1485–1498. doi: 10.1016/j.solener.2009.04.002.

Duffie, J.A. and Beckman, W.A. (2013) *Solar engineering of thermal processes, 4th edition*. 4th edn. United States: John Wiley & Sons.

Dunn, P.D., Reay, D.A. and Dunn, P. (1994) *Heat pipes*. 4th edn. Oxford, England: Pergamon.

References

Duran, E., Sidrach-de-Cardona, M., Galan, J. and Andujar, J.M. (2009) 'Measurement method for PV modules based on DC-DC converters with microcontroller', pp. 1–10.

The Eco Experts (2015) *Most efficient solar panels 2017*. Available at: <http://www.theecoexperts.co.uk/which-solar-panels-are-most-efficient> (Accessed: 17 December 2016).

El-Genk, M. and Saber, H. (2002) 'Performance optimization of Segmented Thermoelectric Unicouples.', AIP Conference Proceedings. pp. 980–988.

Emery, K. (1999) 'The rating of photovoltaic performance', *IEEE Transactions on Electron Devices*, 46(10), pp. 1928–1931. doi: 10.1109/16.791980.

Enrique, J.M., Duran, E., Sidrach-de-Cardona, M., Andujar, J.M., Bohorquez, M.A. and Carretero (2005) 'A new Approach to Obtain I-V and P-V Curves of Photovoltaic Modules by Using DC-DC Converters', *IEEE Transaction*, , pp. 1769–1772.

European Centre for Medium-Range Weather Forecasts (no date) *Atmospheric physics*. Available at: <http://www.ecmwf.int/en/research/modelling-and-prediction/atmospheric-physics> (Accessed: 13 February 2017).

George, A. (2011) 'Population expert: There could be 11 billion people on the planet', *New Scientist*, 210(2806), p. 27. doi: 10.1016/s0262-4079(11)60736-7.

Goswami, Y.D., Kreith, F. and Kreider, J.F. (2000) *Principles of solar engineering*. 2nd edn. Philadelphia, PA: Taylor & Francis.

Fadhl, B. (2014) 'Modelling of the thermal behaviour of heat pipes', *Advanced Computational Methods and Experiments in Heat Transfer XIII*, . doi: 10.2495/ht140331.

Fanchi, J.R. (2005) *Energy in the 21st century*. Singapore, Singapore: World Scientific Publishing Company.

Farahat, M. (2004) 'Improvement in the thermal electric performance of a photovoltaic cells by cooling and concentration techniques', New York: Proceeding The 39th International Universities Power Engineering Conference (UPEC) IEEE. pp. 623–28.

Feldman, K., Kenney, D. and Edenburn, M. (1987) 'A passive heat pipe cooled photovoltaic receiver', 15th IEEE PVSC. pp. 165–172.

Gang, P., Huide, F., Huijuan, Z. and Jie, J. (2012) 'Performance study and parametric analysis of a novel heat pipe PV/T system', *Energy*, 37(1), pp. 384–395. doi: 10.1016/j.energy.2011.11.017.

References

Gang, P., Huide, F., Jie, J., Tin-tai, C. and Tao, Z. (2012) 'Annual analysis of heat pipe PV/T systems for domestic hot water and electricity production', *Energy Conversion and Management*, 56, pp. 8–21. doi: 10.1016/j.enconman.2011.11.011.

Garg, H.P. and Adhikari, R.S. (1997) 'Conventional hybrid photovoltaic/thermal (PV/T) air heating collectors: Steady-state simulation', *Renewable Energy*, 11(3), pp. 363–385. doi: 10.1016/s0960-1481(97)00007-4.

Garg, H.P. and Agarwal, R.K. (1995) 'Some aspects of a PV/T collector/forced circulation flat plate solar water heater with solar cells', *Energy Conversion and Management*, 36(2), pp. 87–99. doi: 10.1016/0196-8904(94)00046-3.

Giovannetti, F., Föste, S., Ehrmann, N. and Rockendorf, G. (2014) 'High transmittance, low emissivity glass covers for flat plate collectors: Applications and performance', *Solar Energy*, 104, pp. 52–59. doi: 10.1016/j.solener.2013.10.006.

Hamid Elsheikh, M., Shnawah, D.A., Sabri, M.F.M., Said, S.B.M., Haji Hassan, M., Ali Bashir, M.B. and Mohamad, M. (2014) 'A review on thermoelectric renewable energy: Principle parameters that affect their performance', *Renewable and Sustainable Energy Reviews*, 30, pp. 337–355. doi: 10.1016/j.rser.2013.10.027.

Han, X., Wang, Y. and Zhu, L. (2013) 'The performance and long-term stability of silicon concentrator solar cells immersed in dielectric liquids', *Energy Conversion and Management*, 66, pp. 189–198. doi: 10.1016/j.enconman.2012.10.009.

Harman, T.C. (1958) 'Multiple stage thermoelectric generation of power', *Journal of Applied Physics*, 29(10), pp. 1471–1473. doi: 10.1063/1.1722971.

Hasan, A., McCormack, S.J., Huang, M.J. and Norton, B. (2010) 'Evaluation of phase change materials for thermal regulation enhancement of building integrated photovoltaics', *Solar Energy*, 84(9), pp. 1601–1612. doi: 10.1016/j.solener.2010.06.010.

Hassan, A. (2010) *Phase Change Materials for Thermal Regulation of Building Integrated Photovoltaics*. PhD Thesis thesis. Dublin Institute of Technology, Ireland. .

Hasse, C., Grenet, M., Bontemps, A., Dendievel, R. and Sallée, H. (2011) 'Realization, test and modelling of honeycomb wallboards containing a phase change material', *Energy and Buildings*, 43(1), pp. 232–238. doi: 10.1016/j.enbuild.2010.09.017.

Hawes, D.W., Feldman, D. and Banu, D. (1993) 'Latent heat storage in building materials', *Energy and Buildings*, 20(1), pp. 77–86. doi: 10.1016/0378-7788(93)90040-2.

References

He, W., Chow, T.-T., Ji, J., Lu, J., Pei, G. and Chan, L. (2006) 'Hybrid photovoltaic and thermal solar-collector designed for natural circulation of water', *Applied Energy*, 83(3), pp. 199–210. doi: 10.1016/j.apenergy.2005.02.007.

He, W., Su, Y., Wang, Y.Q., Riffat, S.B. and Ji, J. (2012) 'A study on incorporation of thermoelectric modules with evacuated-tube heat-pipe solar collectors', *Renewable Energy*, 37(1), pp. 142–149. doi: 10.1016/j.renene.2011.06.002.

van Helden, W.G.J., van Zolingen, R.J.C. and Zondag, H.A. (2004) 'PV thermal systems: PV panels supplying renewable electricity and heat', *Progress in Photovoltaics: Research and Applications*, 12(6), pp. 415–426. doi: 10.1002/pip.559.

Ho, C.J., Jou, B.-T., Lai, C.-M. and Huang, C.-Y. (2013) 'Performance assessment of a BIPV integrated with a layer of water-saturated MEPCM', *Energy and Buildings*, 67, pp. 322–333. doi: 10.1016/j.enbuild.2013.08.035.

Ho, C.J., Tanuwijava, A.O. and Lai, C.-M. (2012) 'Thermal and electrical performance of a BIPV integrated with a microencapsulated phase change material layer', *Energy and Buildings*, 50, pp. 331–338. doi: 10.1016/j.enbuild.2012.04.003.

Holman, J.P. (2009) *Heat transfer*. 10th edn. New York, NY, United States: McGraw Hill Higher Education.

Huang, H.-J., Shen, S.-C. and Shaw, H.-J. (2012) 'Design and fabrication of a novel hybrid-structure heat pipe for a Concentrator Photovoltaic', *Energies*, 5(12), pp. 4340–4349. doi: 10.3390/en5114340.

Huang, M.J., Eames, P.C. and Norton, B. (2004) 'Thermal regulation of building-integrated photovoltaics using phase change materials', *International Journal of Heat and Mass Transfer*, 47(12-13), pp. 2715–2733. doi: 10.1016/j.ijheatmasstransfer.2003.11.015.

Huang, M.J., Eames, P.C. and Norton, B. (2006) 'Phase change materials for limiting temperature rise in building integrated photovoltaics', *Solar Energy*, 80(9), pp. 1121–1130. doi: 10.1016/j.solener.2005.10.006.

Huang, M.J., Eames, P.C., Norton, B. and Hewitt, N.J. (2011) 'Natural convection in an internally finned phase change material heat sink for the thermal management of photovoltaics', *Solar Energy Materials and Solar Cells*, 95(7), pp. 1598–1603. doi: 10.1016/j.solmat.2011.01.008.

Huang, B.J., Lin, T.H., Hung, W.C. and Sun, F.S. (2001) 'Performance evaluation of solar photovoltaic/thermal systems', *Solar Energy*, 70(5), pp. 443–448. doi: 10.1016/s0038-092x(00)00153-5.

References

- Huang, B.J., Yang, P.E., Lin, Y.P., Lin, B.Y., Chen, H.J., Lai, R.C. and Cheng, J.S. (2011) 'Solar cell junction temperature measurement of PV module', *Solar Energy*, 85(2), pp. 388–392. doi: 10.1016/j.solener.2010.11.006.
- Hughes, B., Cherisa, N. and Beg, O. (2011) 'Computational Study of Improving the Efficiency of Photovoltaic Panels in the UAE', *Engineering and Technology, World Academy of Science*, 49, pp. 278–87.
- Ibrahim, A. (2009) 'Performance of photovoltaic thermal collector (PVT) with different absorbers design', *WSEAS Transactions on Environment and Development*, , p. ;5(3):321–30.
- Ibrahim, A., Jin, G.L., Daghigh, R., Salleh, M.H.M., Othman, M.Y., Ruslan, M.H., Mat, S. and Sopian, K. (2009) 'Hybrid Photovoltaic thermal (PV/T) air and water based solar collectors suitable for building integrated applications', *American Journal of Environmental Sciences*, 5(5), pp. 618–624. doi: 10.3844/ajessp.2009.618.624.
- Iqbal, M. (1984) *An introduction to solar radiation*. Toronto: Academic Press.
- Janjai, S. and Tung, P. (2005) 'Performance of a solar dryer using hot air from roof-integrated solar collectors for drying herbs and spices', *Renewable Energy*, 30(14), pp. 2085–2095. doi: 10.1016/j.renene.2005.02.006.
- Ji, J., Han, J., Chow, T., Yi, H., Lu, J., He, W. and Sun, W. (2006) 'Effect of fluid flow and packing factor on energy performance of a wall-mounted hybrid photovoltaic/water-heating collector system', *Energy and Buildings*, 38(12), pp. 1380–1387. doi: 10.1016/j.enbuild.2006.02.010.
- Ji, J., He, H., Chow, T., Pei, G., He, W. and Liu, K. (2009) 'Distributed dynamic modeling and experimental study of PV evaporator in a PV/T solar-assisted heat pump', *International Journal of Heat and Mass Transfer*, 52(5-6), pp. 1365–1373. doi: 10.1016/j.ijheatmasstransfer.2008.08.017.
- Ji, J., Liu, K., Chow, T., Pei, G., He, W. and He, H. (2008) 'Performance analysis of a photovoltaic heat pump', *Applied Energy*, 85(8), pp. 680–693. doi: 10.1016/j.apenergy.2008.01.003.
- Ji, J., Pei, G., Chow, T., Liu, K., He, H., Lu, J. and Han, C. (2008) 'Experimental study of photovoltaic solar assisted heat pump system', *Solar Energy*, 82(1), pp. 43–52. doi: 10.1016/j.solener.2007.04.006.
- JONES, A.D. and UNDERWOOD, C.P. (2002) 'A thermal model for photovoltaic systems', *Fuel and Energy Abstracts*, 43(3), p. 199. doi: 10.1016/s0140-6701(02)85831-3.

References

Joshi, A.S., Tiwari, A., Tiwari, G.N., Dincer, I. and Reddy, B.V. (2009) 'Performance evaluation of a hybrid photovoltaic thermal (PV/T) (glass-to-glass) system', *International Journal of Thermal Sciences*, 48(1), pp. 154–164. doi: 10.1016/j.ijthermalsci.2008.05.001.

Jun Huang, M. (2011) 'The effect of using two PCMs on the thermal regulation performance of BIPV systems', *Solar Energy Materials and Solar Cells*, 95(3), pp. 957–963. doi: 10.1016/j.solmat.2010.11.032.

Kandasamy, R., Wang, X.-Q. and Mujumdar, A.S. (2007) 'Application of phase change materials in thermal management of electronics', *Applied Thermal Engineering*, 27(17-18), pp. 2822–2832. doi: 10.1016/j.applthermaleng.2006.12.013.

Kane, A. and Verm, V. (2013) 'Performance Enhancement of Building Integrated Photovoltaic Module using Thermoelectric Cooling', *International Journal of Renewable Energy Research*, 3(2), pp. 320–4.

Kern, E.C. and Russell, M.C. (1978) 'Combined photovoltaic and thermal hybrid collector systems.', *In: Photovoltaic Specialists Conference, 13th, Washington, D.C., .*

Koo, J., So, H., Hong, S.W. and Hong, H. (2011) 'Effects of wallboard design parameters on the thermal storage in buildings', *Energy and Buildings*, 43(8), pp. 1947–1951. doi: 10.1016/j.enbuild.2011.03.038.

Kourvisianos, G. (2013) *Photovoltaic-thermal collectors and phase change material: A literature review with references to the Australian market*. MSc Dissertation thesis. Murdoch University, Perth, Australia. .

Kraemer, D., McEnaney, K., Chiesa, M. and Chen, G. (2012) 'Modeling and optimization of solar thermoelectric generators for terrestrial applications', *Solar Energy*, 86(5), pp. 1338–1350. doi: 10.1016/j.solener.2012.01.025.

kreazone, D. - (no date) *Thermoelectric generators operating on gas fuel*. Available at: <http://kryothermtec.com/thermoelectric-generators-operating-on-gas-fuel.html> (Accessed: 17 February 2015).

Kulish, M.R. and Object, object (2016) 'Luminescent converter of solar light into electrical energy. Review', *Semiconductor Physics Quantum Electronics and Optoelectronics*, 19(3), pp. 229–247. doi: 10.15407/spqeo19.03.229.

Kurtz, S. (2012) 'Opportunities for Development of a Mature Concentrating Photovoltaic Power Industry', *National Renewable Energy Laboratory*, (NREL/TP-5200-43208).

References

King, D. and Eckert, P. (1996) '96/04014 model to estimate performance of photovoltaic pump sets under different operating conditions', *Fuel and Energy Abstracts*, 37(4), p. 280. doi: 10.1016/0140-6701(96)82308-3.

Lai, C., Chen, R.H. and Lin, C.-Y. (2010) 'Heat transfer and thermal storage behaviour of gypsum boards incorporating micro-encapsulated PCM', *Energy and Buildings*, 42(8), pp. 1259–1266. doi: 10.1016/j.enbuild.2010.02.018.

Lee, H.S. (2010) *Thermal design: Heat sinks, Thermoelectrics, heat pipes, compact heat exchangers, and solar cells*. San Francisco, CA, United States: John Wiley & Sons.

Lee, K.H., Kim, H. and Kim, O.J. (2010) 'Effect of thermoelectric and electrical properties on the cooling performance of a micro thermoelectric cooler', *Journal of Electronic Materials*, 39(9), pp. 1566–1571. doi: 10.1007/s11664-010-1285-2.

Leonov, V., Torfs, T., Vullers, R.J.M. and Van Hoof, C. (2010) 'Hybrid Thermoelectric–Photovoltaic generators in wireless Electroencephalography Diadem and Electrocardiography shirt', *Journal of Electronic Materials*, 39(9), pp. 1674–1680. doi: 10.1007/s11664-010-1230-4.

Li, Y., Witharana, S., Cao, H., Lasfargues, M., Huang, Y. and Ding, Y. (2014) 'Wide spectrum solar energy harvesting through an integrated photovoltaic and thermoelectric system', *Particuology*, 15, pp. 39–44. doi: 10.1016/j.partic.2013.08.003.

Liebl, J., Neugebauer, S., Eder, A., Linde, M., Mazar, B. and Stütz, W. (2009) 'The thermoelectric generator from BMW is making use of waste heat', *MTZ worldwide*, 70(4), pp. 4–11. doi: 10.1007/bf03226939.

Lo Brano, V., Ciulla, G., Piacentino, A. and Cardona, F. (2013) 'On the efficacy of PCM to shave peak temperature of crystalline Photovoltaic panels: An FDM model and field validation', *Energies*, 6(12), pp. 6188–6210. doi: 10.3390/en6126188.

Lu, T.J. (2000) 'Thermal management of high power electronics with phase change cooling', *International Journal of Heat and Mass Transfer*, 43(13), pp. 2245–2256. doi: 10.1016/s0017-9310(99)00318-x.

Luque, A. (2010) *Handbook of photovoltaic science and engineering*. Edited by Antonio Luque and Steven Hegedus. 2nd edn. Chichester, United Kingdom: Wiley-Blackwell (an imprint of John Wiley & Sons Ltd).

MacDonald, D.K.C. (2006) *Thermoelectricity: An introduction to the principles*. United States: Dover Publications.

References

Makki, A., Omer, S. and Sabir, H. (2015) 'Advancements in hybrid photovoltaic systems for enhanced solar cells performance', *Renewable and Sustainable Energy Reviews*, 41, pp. 658–684. doi: 10.1016/j.rser.2014.08.069.

Makki, Omar, Su and Riffat (2015) 'Performance analysis of heat pipe-based photovoltaic-thermoelectric generator hybrid system', Nottingham: 14th International Conference on Sustainable Energy Technologies.

Makki, A., Omer, S., Su, Y. and Sabir, H. (2016) 'Numerical investigation of heat pipe-based photovoltaic-thermoelectric generator (HP-PV/TEG) hybrid system', *Energy Conversion and Management*, 112, pp. 274–287. doi: 10.1016/j.enconman.2015.12.069.

Malvi, C.S., Dixon-Hardy, D.W. and Crook, R. (2011) 'Energy balance model of combined photovoltaic solar-thermal system incorporating phase change material', *Solar Energy*, 85(7), pp. 1440–1446. doi: 10.1016/j.solener.2011.03.027.

Markvart, T. (ed.) (2000) *Solar electricity*. 2nd edn. United Kingdom: Wiley, John & Sons.

Maiti, S., Banerjee, S., Vyas, K., Patel, P. and Ghosh, P.K. (2011) 'Self regulation of photovoltaic module temperature in V-trough using a metal-wax composite phase change matrix', *Solar Energy*, 85(9), pp. 1805–1816. doi: 10.1016/j.solener.2011.04.021.

McEnaney, K., Kraemer, D., Ren, Z. and Chen, G. (2011) 'Modeling of concentrating solar thermoelectric generators', *Journal of Applied Physics*, 110(7), p. 074502. doi: 10.1063/1.3642988.

Michael, S. (2009b) *On the evaluation of spectral effects on photovoltaic modules performance parameters and hotspots in solar cells*. PhD thesis. University of Fort Hare.

Miller, T.G., Spoolman, S.E. and Miller, G. (2014) *Living in the environment: Principles, connections, and solutions*. 18th edn. Stamford, CT, United States: South-Western.

Min, C., Nuofu, C., Xiaoli, Y., Yu, W., Yiming, B. and Xingwang, Z. (2009) 'Thermal analysis and test for single concentrator solar cells', *Journal of Semiconductors*, 30(4), p. 044011. doi: 10.1088/1674-4926/30/4/044011.

Moshfegh, B. and Sandberg, M. (1998) 'Flow and heat transfer in the air gap behind photovoltaic panels', *Renewable and Sustainable Energy Reviews*, 2(3), pp. 287–301. doi: 10.1016/s1364-0321(98)00005-7.

Najafi, H. and Woodbury, K.A. (2013) 'Optimization of a cooling system based on Peltier effect for photovoltaic cells', *Solar Energy*, 91, pp. 152–160. doi: 10.1016/j.solener.2013.01.026.

References

Ngo, C. and Natowitz, J.B. (2009) *Our energy future: Resources, alternatives, and the environment*. Chichester, United Kingdom: Wiley-Blackwell (an imprint of John Wiley & Sons Ltd).

Nguyen, N.Q. and Pochiraju, K.V. (2013) 'Behavior of thermoelectric generators exposed to transient heat sources', *Applied Thermal Engineering*, 51(1-2), pp. 1–9. doi: 10.1016/j.applthermaleng.2012.08.050.

Nolas, G.S., Morelli, D.T. and Tritt, T.M. (1999) 'SKUTTERUDITES: A Phonon-Glass-Electron crystal approach to advanced thermoelectric energy conversion applications', *Annual Review of Materials Science*, 29(1), pp. 89–116. doi: 10.1146/annurev.matsci.29.1.89.

Oksengendler, B.L., Turaeva, N.N. and Rashidova, S.S. (2009) 'Statistical theory of multiple exciton generation in quantum dot solar cells', *Applied Solar Energy*, 45(3), pp. 162–165. doi: 10.3103/s0003701x09030074.

Omer, S. (1998) 'Design optimization of thermoelectric devices for solar power generation', *Solar Energy Materials and Solar Cells*, 53(1-2), pp. 67–82. doi: 10.1016/s0927-0248(98)00008-7.

Omer, S.A. and Infield, D.G. (2000) 'Design and thermal analysis of a two stage solar concentrator for combined heat and thermoelectric power generation', *Energy Conversion and Management*, 41(7), pp. 737–756. doi: 10.1016/s0196-8904(99)00134-x.

Othman, M. (2013) 'Performance Study of Air-based Photovoltaic-thermal (PV/T) Collector with Different Designs of Heat Exchanger', *Sains Malaysiana*, , pp. 1319–25.

Paris, J., Villain, F. and Houle, J.-F. (1999) 'Incorporation of PCM in wallboards: a review of recent developments', Reading, UK: Proceedings of the 1st World Renewable Energy Congress. pp. 2397–2401.

Pasupathy, A. and Velraj, R. (2008) 'Effect of double layer phase change material in building roof for year round thermal management', *Energy and Buildings*, 40(3), pp. 193–203. doi: 10.1016/j.enbuild.2007.02.016.

Pei, G., Zhang, T., Yu, Z., Fu, H. and Ji, J. (2011) 'Comparative study of a novel heat pipe photovoltaic/thermal collector and a water thermosiphon photovoltaic/thermal collector', *Proceedings of the Institution of Mechanical Engineers, Part A: Journal of Power and Energy*. pp. 225–271.

Peippo, K., Kauranen, P. and Lund, P.D. (1991) 'A multicomponent PCM wall optimized for passive solar heating', *Energy and Buildings*, 17(4), pp. 259–270. doi: 10.1016/0378-7788(91)90009-r.

References

Petter Jelle, B., Breivik, C. and Drolsum Røkenes, H. (2012) 'Building integrated photovoltaic products: A state-of-the-art review and future research opportunities', *Solar Energy Materials and Solar Cells*, 100, pp. 69–96. doi: 10.1016/j.solmat.2011.12.016.

PPG Industries Inc. (2010) *Solarphire PV PDS FINAL*. Available at: http://www.glassonweb.com/sites/default/files/UserFiles/Solarphire%20PV%20PDS_FINAL.pdf (Accessed: 21 February 2015).

Prudhvi, P. (2012) 'Efficiency improvement of solar panels using active cooling', 11th International Conference on Environment and Electrical Engineering (EEEIC) IEEE: . pp. 1093–97.

Radziemska, E. (2003) 'The effect of temperature on the power drop in crystalline silicon solar cells', *Renewable Energy*, 28(1), pp. 1–12. doi: 10.1016/s0960-1481(02)00015-0.

Rajoria, C.S., Agrawal, S. and Tiwari, G.N. (2012) 'Overall thermal energy and exergy analysis of hybrid photovoltaic thermal array', *Solar Energy*, 86(5), pp. 1531–1538. doi: 10.1016/j.solener.2012.02.014.

Rajoria, C.S., Agrawal, S. and Tiwari, G.N. (2013) 'Exergetic and enviroeconomic analysis of novel hybrid PVT array', *Solar Energy*, 88, pp. 110–119. doi: 10.1016/j.solener.2012.11.018.

Reay, D.A., Kew, P.A. and McGlen, R. (2006) *Heat pipes: Theory, design and applications*. 5th edn. Oxford: Butterworth-Heinemann.

Riffat, S.B., Omer, S.A. and Ma, X. (2001) 'A novel thermoelectric refrigeration system employing heat pipes and a phase change material: An experimental investigation', *Renewable Energy*, 23(2), pp. 313–323. doi: 10.1016/s0960-1481(00)00170-1.

Royne, A. (2005) *Cooling Devices for Densely Packed High Concentration PV Array*. Master of Science Thesis thesis. The University of Sydney, . .

ROYNE, A., DEY, C. and MILLS, D. (2005) 'Cooling of photovoltaic cells under concentrated illumination: A critical review', *Solar Energy Materials and Solar Cells*, 86(4), pp. 451–483. doi: 10.1016/j.solmat.2004.09.003.

Russell, R. (1982) *Uniform temperature heat pipe and method of using the same*. USA patent no. Patent US4320246.

Sark, W.G.J.H.M. van (2011) 'Feasibility of photovoltaic – thermoelectric hybrid modules', *Applied Energy*, 88(8), pp. 2785–2790. doi: 10.1016/j.apenergy.2011.02.008.

References

Shahsavari, A. and Ameri, M. (2010) 'Experimental investigation and modeling of a direct-coupled PV/T air collector', *Solar Energy*, 84(11), pp. 1938–1958. doi: 10.1016/j.solener.2010.07.010.

Shapiro, M., Feldman, D., Hawes, D. and Banu, D. (1987) 'PCM thermal storage in wallboard', Portland, USA: Proceedings of 12th Passive Solar Conference. pp. 38–58.

Sharma, A., Tyagi, V.V., Chen, C.R. and Buddhi, D. (2009) 'Review on thermal energy storage with phase change materials and applications', *Renewable and Sustainable Energy Reviews*, 13(2), pp. 318–345. doi: 10.1016/j.rser.2007.10.005.

Shatat, M., Riffat, S. and Agyenim, F. (2013) 'Experimental testing method for solar light simulator with an attached evacuated solar collector', *International Journal of Energy And Environment*, Volume 4(2), p. pp.219–230.

Solanki, S.C., Dubey, S. and Tiwari, A. (2009) 'Indoor simulation and testing of photovoltaic thermal (PV/T) air collectors', *Applied Energy*, 86(11), pp. 2421–2428. doi: 10.1016/j.apenergy.2009.03.013.

Sukamongkol, Y., Chungpaibulpatana, S., Limmeechokchai, B. and Sripadungtham, P. (2010) 'Condenser heat recovery with a PV/T air heating collector to regenerate desiccant for reducing energy use of an air conditioning room', *Energy and Buildings*, 42(3), pp. 315–325. doi: 10.1016/j.enbuild.2009.09.009.

Sukhatme, S.P., Nayak, J.K., Sukhatme, S. and Nayak, J. (2008) *Solar energy principles of thermal collection and storage 3rd edition*. 3rd edn. New Delhi: McGraw-Hill Professional.

Tan, F. and Fok, S. (2007) 'Thermal management of mobile phones using phase change materials', IEEE 9th Electronics Packaging Technology Conference. pp. 836–842.

Tang, X., Quan, Z. and Zhao, Y. (2010) 'Experimental investigation of solar panel cooling by a novel micro heat pipe array', *Energy and Power Engineering*, 02(03), pp. 171–174. doi: 10.4236/epe.2010.23025.

Theodore, L. (2011) *Heat transfer applications for the practicing engineer*. United States: Wiley, John & Sons.

Thirugnanasambandam, M., Iniyar, S. and Goic, R. (2010) 'A review of solar thermal technologies☆', *Renewable and Sustainable Energy Reviews*, 14(1), pp. 312–322. doi: 10.1016/j.rser.2009.07.014.

Tiwari, A., Dubey, S., Sandhu, G.S., Sodha, M.S. and Anwar, S.I. (2009) 'Exergy analysis of integrated photovoltaic thermal solar water heater under constant flow rate and

References

constant collection temperature modes', *Applied Energy*, 86(12), pp. 2592–2597. doi: 10.1016/j.apenergy.2009.04.004.

Tonui, J.K. and Tripanagnostopoulos, Y. (2008) 'Performance improvement of PV/T solar collectors with natural air flow operation', *Solar Energy*, 82(1), pp. 1–12. doi: 10.1016/j.solener.2007.06.004.

Tseng, S.-F., Hsiao, W.-T., Chiang, D., Huang, K.-C. and Chou, C.-P. (2011) 'Mechanical and optoelectric properties of post-annealed fluorine-doped tin oxide films by ultraviolet laser irradiation', *Applied Surface Science*, 257(16), pp. 7204–7209. doi: 10.1016/j.apsusc.2011.03.091.

Tyagi, V.V., Kaushik, S.C. and Tyagi, S.K. (2012) 'Advancement in solar photovoltaic/thermal (PV/T) hybrid collector technology', *Renewable and Sustainable Energy Reviews*, 16(3), pp. 1383–1398. doi: 10.1016/j.rser.2011.12.013.

US Department of Energy (2009) *Waste heat recovery: Technology and opportunities in U.S. Industry*. Available at: https://www1.eere.energy.gov/manufacturing/intensiveprocesses/pdfs/waste_heat_recovery.pdf.

de Vries, D. (1998) *Design of a PV/Thermal Combi Panel*. Ph.D. Thesis thesis. Eindhoven University of Technology. .

Vorobiev, Y., González-Hernández, J., Vorobiev, P. and Bulat, L. (2006) 'Thermal-photovoltaic solar hybrid system for efficient solar energy conversion', *Solar Energy*, 80(2), pp. 170–176. doi: 10.1016/j.solener.2005.04.022.

Walker, A. (2013) *Solar energy: Technologies and the project delivery process for buildings*. United States: John Wiley & Sons.

Wallace, J.M. and Hobbs, P.V. (2006) *Atmospheric science: An introductory survey*. 2nd edn. Boston: Elsevier Academic Press.

Watt Committee on Energy (1999) *Energy demand and planning*. Edited by J. C. McVeigh and J. G. Mordue. London: Taylor & Francis.

Wang, N., Han, L., He, H., Park, N.-H. and Koumoto, K. (2011) 'A novel high-performance photovoltaic–thermoelectric hybrid device', *Energy & Environmental Science*, 4(9), p. 3676. doi: 10.1039/c1ee01646f.

Wesoff, E. (2016) *SunPower holds world record for most efficient rooftop solar panel, again*. Available at: <https://www.greentechmedia.com/articles/read/SunPower-Again->

References

Holds-Record-For-Worlds-Most-Efficient-Rooftop-Solar-Panel (Accessed: 17 February 2017).

Wirtz, R., Zheng, N. and Chandra, D. (1999) 'Thermal management using "dry" phase change materials', San Diego, CA, USA: Proceedings of Fifteen IEEE Semiconductor Thermal Measurement and Management Symposium. pp. 74–82.

Wu, S.-Y., Zhang, Q.-L., Xiao, L. and Guo, F.-H. (2011) 'A heat pipe photovoltaic/thermal (PV/T) hybrid system and its performance evaluation', *Energy and Buildings*, 43(12), pp. 3558–3567. doi: 10.1016/j.enbuild.2011.09.017.

Xi, H., Luo, L. and Fraise, G. (2007) 'Development and applications of solar-based thermoelectric technologies', *Renewable and Sustainable Energy Reviews*, 11(5), pp. 923–936. doi: 10.1016/j.rser.2005.06.008.

Xu, G., Zhang, X. and Deng, S. (2011) 'Experimental study on the operating characteristics of a novel low-concentrating solar photovoltaic/thermal integrated heat pump water heating system', *Applied Thermal Engineering*, 31(17-18), pp. 3689–3695. doi: 10.1016/j.applthermaleng.2011.01.030.

Xu, X., Meyers, M., Sammakia, B. and Murray, B. (2012) 'Thermal Modeling of Hybrid Concentrating PV/T Collectors with Tree-shaped Channel Networks Cooling System', *In proceeding of 13th IEEE ITherm Conference*, , pp. 1131–39.

Yan, J. (2015) *Handbook of clean energy systems*. Chichester, United Kingdom: Wiley-Blackwell (an imprint of John Wiley & Sons Ltd).

Yang, L., Ye, Q.-H., Ebong, A., Song, W.T., Zhang, G.J., Wang, J.X. and Ma, Y. (2010) 'High efficiency screen printed bifacial solar cells on monocrystalline CZ silicon', *Progress in Photovoltaics: Research and Applications*, 19(3), pp. 275–279. doi: 10.1002/pip.1018.

Yun, G.Y., McEvoy, M. and Steemers, K. (2007) 'Design and overall energy performance of a ventilated photovoltaic façade', *Solar Energy*, 81(3), pp. 383–394. doi: 10.1016/j.solener.2006.06.016.

Zhang, X. and Chau, K.T. (2011) 'An automotive thermoelectric–photovoltaic hybrid energy system using maximum power point tracking', *Energy Conversion and Management*, 52(1), pp. 641–647. doi: 10.1016/j.enconman.2010.07.041.

Zhang, X., Zhao, X., Smith, S., Xu, J. and Yu, X. (2012) 'Review of R&D progress and practical application of the solar photovoltaic/thermal (PV/T) technologies', *Renewable and Sustainable Energy Reviews*, 16(1), pp. 599–617. doi: 10.1016/j.rser.2011.08.026.

References

Zhang, X., Zhao, X., Shen, J., Xu, J. and Yu, X. (2014) 'Dynamic performance of a novel solar photovoltaic/loop-heat-pipe heat pump system', *Applied Energy*, 114, pp. 335–352. doi: 10.1016/j.apenergy.2013.09.063.

Zhang, X., Zhao, X., Xu, J. and Yu, X. (2013) 'Characterization of a solar photovoltaic/loop-heat-pipe heat pump water heating system', *Applied Energy*, 102, pp. 1229–1245. doi: 10.1016/j.apenergy.2012.06.039.

Zhao, X., Zhang, X., Riffat, S.B. and Su, Y. (2011) 'Theoretical study of the performance of a novel PV/e roof module for heat pump operation', *Energy Conversion and Management*, 52(1), pp. 603–614. doi: 10.1016/j.enconman.2010.07.036.

Zhu, L., Boehm, R.F., Wang, Y., Halford, C. and Sun, Y. (2011) 'Water immersion cooling of PV cells in a high concentration system', *Solar Energy Materials and Solar Cells*, 95(2), pp. 538–545. doi: 10.1016/j.solmat.2010.08.037.

Zondag, H., Vries, D. and Van Steenhoven, A. (1999) 'Thermal and electrical yield of a combi-panel', In: Proceedings of ISES Bi-annual Conference

Zondag, H.A., de Vries, D.W., van Helden, W.G.J., van Zolingen, R.J.C. and van Steenhoven, A.A. (2002) 'The thermal and electrical yield of a PV-thermal collector', *Solar Energy*, 72(2), pp. 113–128. doi: 10.1016/s0038-092x(01)00094-9.

Appendix

Thermoelectric Generator Module Validation

Simulation results utilising testing conditions reported in manufacturer's datasheet

| T_{hot} | T_{cold} | V_{emf} | V_{max} | I_{max} | P_{max} | T_{hot} | T_{cold} | V_{emf} | V_{max} | I_{max} | P_{max} |
|-----------|------------|-----------|-----------|-----------|-----------|-----------|------------|-----------|-----------|-----------|-----------|
| 50 | 30 | 0.835 | 0.463 | 0.336 | 0.155 | 50 | 50 | | | | |
| 70 | 30 | 1.705 | 0.895 | 0.648 | 0.580 | 70 | 50 | 0.860 | 0.451 | 0.327 | 0.147 |
| 100 | 30 | 3.036 | 1.478 | 1.071 | 1.583 | 100 | 50 | 2.186 | 1.064 | 0.771 | 0.821 |
| 120 | 30 | 3.914 | 1.829 | 1.326 | 2.425 | 120 | 50 | 3.068 | 1.434 | 1.039 | 1.490 |
| 150 | 30 | 5.171 | 2.318 | 1.680 | 3.894 | 150 | 50 | 4.343 | 1.947 | 1.411 | 2.746 |
| 175 | 30 | 6.127 | 2.712 | 1.965 | 5.328 | 175 | 50 | 5.322 | 2.356 | 1.707 | 4.021 |
| 200 | 30 | 6.961 | 3.110 | 2.254 | 7.009 | 200 | 50 | 6.190 | 2.766 | 2.004 | 5.542 |
| 225 | 30 | 7.638 | 3.520 | 2.551 | 8.979 | 225 | 50 | 6.910 | 3.184 | 2.307 | 7.348 |
| 250 | 30 | 8.126 | 3.933 | 2.850 | 11.212 | 250 | 50 | 7.448 | 3.606 | 2.613 | 9.421 |
| T_{hot} | T_{cold} | V_{emf} | V_{max} | I_{max} | P_{max} | T_{hot} | T_{cold} | V_{emf} | V_{max} | I_{max} | P_{max} |
| 50 | 80 | | | | | 50 | 100 | | | | |
| 70 | 80 | | | | | 70 | 100 | | | | |
| 100 | 80 | 0.884 | 0.431 | 0.312 | 0.134 | 100 | 100 | | | | |
| 120 | 80 | 1.773 | 0.829 | 0.600 | 0.498 | 120 | 100 | 0.893 | 0.417 | 0.302 | 0.126 |
| 150 | 80 | 3.073 | 1.378 | 0.998 | 1.375 | 150 | 100 | 2.210 | 0.991 | 0.718 | 0.712 |
| 175 | 80 | 4.089 | 1.810 | 1.312 | 2.374 | 175 | 100 | 3.251 | 1.439 | 1.043 | 1.500 |
| 200 | 80 | 5.007 | 2.237 | 1.621 | 3.626 | 200 | 100 | 4.201 | 1.877 | 1.360 | 2.553 |
| 225 | 80 | 5.790 | 2.668 | 1.934 | 5.160 | 225 | 100 | 5.027 | 2.317 | 1.679 | 3.890 |
| 250 | 80 | 6.406 | 3.101 | 2.247 | 6.968 | 250 | 100 | 5.694 | 2.757 | 1.997 | 5.506 |

Appendix

Experimental results of testing single TEG module vs simulation predictions for identical operating conditions.

| Testing Conditions | | | | Experimental | | | | | | Simulation | | | | |
|--------------------|-----------|------------|------------|-----------------|-----------------|------------------|------------------|------------------|-------------------|------------------|------------------|------------------|------------------|-------------------|
| Heater | Hot Plate | Cold Plate | ΔT | V_{oc} [V] | I_{sc} [A] | V_{max} [V] | I_{max} [A] | P_{max} [W] | P_{max} [mW] | V_{emf} [V] | V_{max} [V] | I_{max} [A] | P_{max} [W] | P_{max} [mW] |
| 24.49 | 25.05 | 20.69 | 4.36 | 0.064 | 0.045 | 0.101 | 0.045 | 0.005 | 4.515 | 0.190 | 0.104 | 0.076 | 0.008 | 7.873 |
| 24.62 | 25.18 | 20.73 | 4.45 | 0.250 | 0.172 | 0.128 | 0.111 | 0.014 | 14.259 | 0.193 | 0.106 | 0.077 | 0.008 | 8.179 |
| 28.80 | 29.08 | 22.08 | 7.00 | 0.353 | 0.240 | 0.179 | 0.136 | 0.024 | 24.362 | 0.307 | 0.167 | 0.121 | 0.020 | 20.092 |
| 31.24 | 31.37 | 22.88 | 8.50 | 0.413 | 0.281 | 0.202 | 0.157 | 0.032 | 31.795 | 0.374 | 0.202 | 0.146 | 0.029 | 29.443 |
| 32.82 | 32.84 | 23.38 | 9.46 | 0.454 | 0.307 | 0.230 | 0.162 | 0.037 | 37.283 | 0.417 | 0.224 | 0.162 | 0.036 | 36.359 |
| 33.85 | 33.81 | 23.72 | 10.09 | 0.477 | 0.322 | 0.238 | 0.170 | 0.040 | 40.389 | 0.446 | 0.239 | 0.173 | 0.041 | 41.314 |
| 34.67 | 34.57 | 23.98 | 10.59 | 0.493 | 0.333 | 0.250 | 0.173 | 0.043 | 43.275 | 0.468 | 0.250 | 0.181 | 0.045 | 45.396 |
| 35.24 | 35.11 | 24.17 | 10.94 | 0.510 | 0.343 | 0.257 | 0.179 | 0.046 | 45.952 | 0.484 | 0.258 | 0.187 | 0.048 | 48.377 |
| 35.66 | 35.51 | 24.31 | 11.20 | 0.522 | 0.351 | 0.266 | 0.180 | 0.048 | 47.986 | 0.496 | 0.264 | 0.192 | 0.051 | 50.654 |
| 36.00 | 35.82 | 24.42 | 11.41 | 0.531 | 0.357 | 0.276 | 0.181 | 0.050 | 49.984 | 0.506 | 0.269 | 0.195 | 0.053 | 52.500 |
| 36.23 | 36.03 | 24.49 | 11.54 | 0.542 | 0.364 | 0.268 | 0.192 | 0.051 | 51.402 | 0.512 | 0.272 | 0.197 | 0.054 | 53.758 |
| 36.56 | 36.34 | 24.60 | 11.75 | 0.545 | 0.366 | 0.272 | 0.190 | 0.052 | 51.762 | 0.521 | 0.277 | 0.201 | 0.056 | 55.611 |
| 36.61 | 36.39 | 24.61 | 11.78 | 0.547 | 0.367 | 0.271 | 0.193 | 0.052 | 52.384 | 0.523 | 0.278 | 0.201 | 0.056 | 55.923 |
| 36.77 | 36.54 | 24.67 | 11.88 | 0.551 | 0.369 | 0.278 | 0.190 | 0.053 | 52.764 | 0.527 | 0.280 | 0.203 | 0.057 | 56.829 |
| 36.92 | 36.68 | 24.71 | 11.97 | 0.555 | 0.372 | 0.278 | 0.194 | 0.054 | 53.849 | 0.531 | 0.282 | 0.204 | 0.058 | 57.667 |
| 36.95 | 36.71 | 24.72 | 11.98 | 0.560 | 0.375 | 0.290 | 0.188 | 0.054 | 54.462 | 0.532 | 0.283 | 0.205 | 0.058 | 57.840 |
| 37.05 | 36.81 | 24.76 | 12.05 | 0.557 | 0.373 | 0.274 | 0.197 | 0.054 | 53.923 | 0.535 | 0.284 | 0.206 | 0.058 | 58.442 |
| 37.15 | 36.89 | 24.79 | 12.11 | 0.557 | 0.373 | 0.274 | 0.197 | 0.054 | 53.868 | 0.538 | 0.285 | 0.207 | 0.059 | 58.988 |
| 37.32 | 37.06 | 24.84 | 12.21 | 0.557 | 0.373 | 0.278 | 0.194 | 0.054 | 53.932 | 0.543 | 0.288 | 0.209 | 0.060 | 60.011 |
| 37.38 | 37.11 | 24.86 | 12.25 | 0.562 | 0.376 | 0.289 | 0.191 | 0.055 | 55.170 | 0.544 | 0.289 | 0.209 | 0.060 | 60.352 |
| 37.37 | 37.10 | 24.86 | 12.24 | 0.562 | 0.376 | 0.287 | 0.191 | 0.055 | 54.788 | 0.544 | 0.288 | 0.209 | 0.060 | 60.305 |
| 37.43 | 37.16 | 24.88 | 12.28 | 0.560 | 0.375 | 0.286 | 0.190 | 0.054 | 54.340 | 0.546 | 0.289 | 0.210 | 0.061 | 60.640 |
| 37.53 | 37.25 | 24.91 | 12.34 | 0.560 | 0.374 | 0.283 | 0.192 | 0.054 | 54.449 | 0.548 | 0.291 | 0.211 | 0.061 | 61.243 |
| 37.62 | 37.33 | 24.94 | 12.39 | 0.562 | 0.375 | 0.290 | 0.190 | 0.055 | 55.216 | 0.551 | 0.292 | 0.212 | 0.062 | 61.766 |
| 37.67 | 37.38 | 24.96 | 12.43 | 0.567 | 0.379 | 0.279 | 0.200 | 0.056 | 55.744 | 0.552 | 0.293 | 0.212 | 0.062 | 62.088 |

Temperature-dependant thermal properties for heat pipe

| T_{sat} | K_{liquid} | C_{pl} | h_{fg} | ρ_l | ρ_v | v_l |
|-----------|--------------|----------|----------|----------|----------|-----------|
| 20 | 0.598 | 4182 | 2454 | 998 | 0.0173 | 1.002E-03 |
| 25 | 0.607 | 4180 | 2442 | 997 | 0.0231 | 8.910E-04 |
| 30 | 0.615 | 4178 | 2431 | 996 | 0.0304 | 7.980E-04 |
| 35 | 0.623 | 4178 | 2419 | 994 | 0.0397 | 7.200E-04 |
| 40 | 0.631 | 4179 | 2407 | 992.1 | 0.0512 | 6.530E-04 |
| 45 | 0.637 | 4180 | 2395 | 990.1 | 0.0655 | 5.960E-04 |
| 50 | 0.644 | 4181 | 2383 | 988.1 | 0.0831 | 5.470E-04 |
| 55 | 0.649 | 4183 | 2371 | 985.2 | 0.1045 | 5.040E-04 |
| 60 | 0.654 | 4185 | 2359 | 983.3 | 0.1304 | 4.670E-04 |
| 65 | 0.659 | 4187 | 2346 | 980.4 | 0.1614 | 4.330E-04 |
| 70 | 0.663 | 4190 | 2334 | 977.5 | 0.1983 | 4.040E-04 |
| 75 | 0.667 | 4193 | 2321 | 974.7 | 0.2421 | 3.780E-04 |
| 80 | 0.67 | 4197 | 2309 | 971.8 | 0.2935 | 3.550E-04 |
| 85 | 0.673 | 4201 | 2296 | 968.1 | 0.3536 | 3.330E-04 |
| 90 | 0.675 | 4206 | 2283 | 965.3 | 0.4235 | 3.150E-04 |

h_{fg} and ρ_v are evaluated and the saturation temperature ($T_{sat} = 40\text{ °C}$ constant)

All properties of the liquid are to be evaluated at the film temperature

$$T_f = \frac{T_{sat} - T_{con}}{2}$$

Appendix

Computer model result for integrated PV-TEG collector

| 740 [W/m ²] | wind | Temperatures | | | | | | | | | | | | | | | | | |
|-------------------------|------|--------------------|------|-----------------|------|-------------------|------|-------------------------|------|------------------------|------|------------------|------|----------------|------|----------------|------|-------------------|-----|
| | | T _{glass} | | T _{pv} | | T _{base} | | T _{evaporator} | | T _{condenser} | | T _{hot} | | T _p | | T _n | | T _{cold} | |
| | | W | W/O | W | W/O | W | W/O | W | W/O | W | W/O | W | W/O | W | W/O | W | W/O | W | W/O |
| 0 | 55.7 | 48.3 | 56.4 | 48.8 | 56.3 | 48.5 | 56.3 | 48.5 | 55.9 | 48.2 | 55.6 | 48.0 | 36.8 | 33.4 | 40.6 | 35.7 | 22.7 | 21.8 | |
| 1 | 49.5 | 44.1 | 50.2 | 44.7 | 50.1 | 44.4 | 50.1 | 44.4 | 49.8 | 44.2 | 49.5 | 43.9 | 34.1 | 31.6 | 36.7 | 33.2 | 21.9 | 21.4 | |
| 2 | 44.8 | 40.8 | 45.5 | 41.4 | 45.5 | 41.2 | 45.5 | 41.2 | 45.2 | 41.0 | 45.0 | 40.8 | 32.1 | 30.2 | 33.9 | 31.4 | 21.5 | 21.2 | |
| 3 | 41.3 | 38.2 | 42.0 | 38.9 | 41.9 | 38.7 | 41.9 | 38.7 | 41.7 | 38.5 | 41.5 | 38.3 | 30.5 | 29.1 | 31.8 | 30.0 | 21.2 | 21.1 | |
| 4 | 38.5 | 36.2 | 39.3 | 36.8 | 39.2 | 36.7 | 39.2 | 36.7 | 39.0 | 36.5 | 38.8 | 36.4 | 29.3 | 28.3 | 30.3 | 29.0 | 21.1 | 21.1 | |
| 5 | 36.3 | 34.5 | 37.1 | 35.2 | 37.0 | 35.1 | 37.0 | 35.1 | 36.9 | 34.9 | 36.7 | 34.8 | 28.4 | 27.6 | 29.2 | 28.1 | 21.1 | 21.1 | |
| 6 | 34.6 | 33.1 | 35.3 | 33.8 | 35.3 | 33.7 | 35.3 | 33.7 | 35.2 | 33.6 | 35.0 | 33.4 | 27.7 | 27.0 | 28.2 | 27.4 | 21.1 | 21.1 | |
| 7 | 33.2 | 32.0 | 33.9 | 32.7 | 33.9 | 32.6 | 33.9 | 32.6 | 33.7 | 32.5 | 33.6 | 32.3 | 27.1 | 26.5 | 27.5 | 26.9 | 21.1 | 21.1 | |
| 8 | 32.0 | 31.0 | 32.7 | 31.7 | 32.7 | 31.6 | 32.7 | 31.6 | 32.6 | 31.5 | 32.5 | 31.4 | 26.6 | 26.1 | 26.9 | 26.4 | 21.1 | 21.2 | |
| 886 [W/m ²] | wind | Temperatures | | | | | | | | | | | | | | | | | |
| | | T _{glass} | | T _{pv} | | T _{base} | | T _{evaporator} | | T _{condenser} | | T _{hot} | | T _p | | T _n | | T _{cold} | |
| | | W | W/O | W | W/O | W | W/O | W | W/O | W | W/O | W | W/O | W | W/O | W | W/O | W | W/O |
| 0 | 63.8 | 54.2 | 64.6 | 54.9 | 64.4 | 54.5 | 64.4 | 54.5 | 64.0 | 54.2 | 63.6 | 53.8 | 40.5 | 36.0 | 46.4 | 39.5 | 24.2 | 22.5 | |
| 1 | 56.2 | 49.2 | 57.1 | 50.0 | 57.0 | 49.6 | 57.0 | 49.6 | 56.6 | 49.3 | 56.3 | 49.1 | 37.1 | 33.9 | 41.1 | 36.4 | 22.8 | 21.9 | |
| 2 | 50.5 | 45.4 | 51.4 | 46.1 | 51.3 | 45.8 | 51.3 | 45.8 | 51.0 | 45.6 | 50.7 | 45.3 | 34.6 | 32.2 | 37.4 | 34.1 | 22.0 | 21.5 | |
| 3 | 46.2 | 42.3 | 47.1 | 43.0 | 47.0 | 42.8 | 47.0 | 42.8 | 46.8 | 42.6 | 46.5 | 42.4 | 32.7 | 30.9 | 34.8 | 32.3 | 21.6 | 21.3 | |
| 4 | 42.8 | 39.8 | 42.8 | 40.6 | 43.7 | 40.4 | 43.7 | 40.4 | 43.4 | 40.2 | 43.2 | 40.0 | 31.3 | 29.9 | 32.8 | 31.0 | 21.3 | 21.2 | |
| 5 | 40.2 | 37.8 | 41.1 | 38.6 | 41.0 | 38.4 | 41.0 | 38.4 | 40.8 | 38.2 | 40.6 | 38.1 | 30.1 | 29.0 | 31.3 | 29.9 | 21.2 | 21.1 | |
| 6 | 38.0 | 36.1 | 38.9 | 36.9 | 38.9 | 36.8 | 38.9 | 36.8 | 38.7 | 36.6 | 38.5 | 36.5 | 29.2 | 28.3 | 30.1 | 29.0 | 21.1 | 21.1 | |
| 7 | 36.3 | 34.7 | 37.2 | 35.5 | 37.1 | 35.4 | 37.1 | 35.4 | 37.0 | 35.3 | 36.8 | 35.1 | 28.5 | 27.7 | 29.2 | 28.3 | 21.1 | 21.1 | |
| 8 | 34.8 | 33.5 | 35.7 | 34.4 | 35.7 | 34.2 | 35.7 | 34.2 | 35.5 | 34.1 | 35.4 | 34.0 | 27.8 | 27.2 | 28.4 | 27.7 | 21.1 | 21.1 | |

Appendix

| 1066 [W/m ²] | wind | Temperatures | | | | | | | | | | | | | | | | | |
|--------------------------|------|--------------------|------|-----------------|------|-------------------|------|-------------------------|------|------------------------|------|------------------|------|----------------|------|----------------|------|-------------------|-----|
| | | T _{glass} | | T _{pv} | | T _{base} | | T _{evaporator} | | T _{condenser} | | T _{hot} | | T _p | | T _n | | T _{cold} | |
| | | W | W/O | W | W/O | W | W/O | W | W/O | W | W/O | W | W/O | W | W/O | W | W/O | W | W/O |
| 0 | 73.5 | 61.4 | 74.5 | 62.1 | 74.3 | 61.7 | 74.3 | 61.7 | 73.8 | 61.3 | 73.3 | 60.9 | 45.1 | 39.2 | 53.9 | 44.4 | 26.7 | 23.7 | |
| 1 | 64.4 | 55.5 | 65.5 | 56.3 | 65.3 | 55.9 | 65.3 | 55.9 | 64.9 | 55.6 | 64.5 | 55.2 | 40.8 | 36.7 | 47.0 | 40.4 | 24.4 | 22.7 | |
| 2 | 57.6 | 50.9 | 58.6 | 51.7 | 58.5 | 51.4 | 58.5 | 51.4 | 58.1 | 51.1 | 57.8 | 50.8 | 37.7 | 34.6 | 42.1 | 37.5 | 23.0 | 22.0 | |
| 3 | 52.3 | 47.2 | 53.4 | 48.1 | 53.3 | 47.8 | 53.3 | 47.8 | 52.9 | 47.5 | 52.6 | 47.3 | 35.4 | 33.1 | 38.7 | 35.3 | 22.2 | 21.6 | |
| 4 | 48.2 | 44.2 | 49.2 | 45.1 | 49.2 | 44.9 | 49.2 | 44.9 | 48.9 | 44.6 | 48.6 | 44.4 | 33.6 | 31.8 | 36.1 | 33.5 | 21.7 | 21.4 | |
| 5 | 44.9 | 41.8 | 46.0 | 42.7 | 45.9 | 42.5 | 45.9 | 42.5 | 45.7 | 42.3 | 45.4 | 42.1 | 32.2 | 30.8 | 34.1 | 32.1 | 21.5 | 21.3 | |
| 6 | 42.2 | 39.7 | 43.3 | 40.7 | 43.3 | 40.5 | 43.3 | 40.5 | 43.0 | 40.3 | 42.8 | 40.1 | 31.1 | 29.9 | 32.6 | 31.0 | 21.3 | 21.2 | |
| 7 | 40.1 | 38.0 | 41.2 | 39.0 | 41.1 | 38.9 | 41.1 | 38.9 | 40.9 | 38.7 | 40.7 | 38.5 | 30.2 | 29.2 | 31.4 | 30.1 | 21.2 | 21.1 | |
| 8 | 38.3 | 36.6 | 39.4 | 37.6 | 39.3 | 37.5 | 39.3 | 37.5 | 39.2 | 37.3 | 39.0 | 37.1 | 29.4 | 28.6 | 30.4 | 29.4 | 21.1 | 21.1 | |

| 1400 [W/m ²] | wind | Temperatures | | | | | | | | | | | | | | | | | |
|--------------------------|------|--------------------|------|-----------------|------|-------------------|------|-------------------------|------|------------------------|------|------------------|------|----------------|------|----------------|------|-------------------|-----|
| | | T _{glass} | | T _{pv} | | T _{base} | | T _{evaporator} | | T _{condenser} | | T _{hot} | | T _p | | T _n | | T _{cold} | |
| | | W | W/O | W | W/O | W | W/O | W | W/O | W | W/O | W | W/O | W | W/O | W | W/O | W | W/O |
| 0 | 90.9 | 74.1 | 92.3 | 75.1 | 92.1 | 74.4 | 92.0 | 74.4 | 91.4 | 73.9 | 90.8 | 73.4 | 54.2 | 45.2 | 69.3 | 54.1 | 33.1 | 26.9 | |
| 1 | 79.3 | 66.7 | 80.7 | 67.8 | 80.5 | 67.2 | 80.5 | 67.2 | 80.0 | 66.8 | 79.5 | 66.3 | 48.1 | 41.8 | 59.1 | 48.4 | 28.6 | 24.9 | |
| 2 | 70.4 | 60.8 | 71.8 | 61.9 | 71.7 | 61.5 | 71.6 | 61.5 | 71.2 | 61.1 | 70.7 | 60.7 | 43.7 | 39.1 | 51.8 | 44.2 | 25.9 | 23.6 | |
| 3 | 63.4 | 56.1 | 64.9 | 57.3 | 64.8 | 56.9 | 64.7 | 56.9 | 64.3 | 56.5 | 63.9 | 56.2 | 40.5 | 37.0 | 46.5 | 41.0 | 24.2 | 22.8 | |
| 4 | 58.0 | 52.2 | 59.4 | 53.4 | 59.3 | 53.1 | 59.3 | 53.1 | 58.9 | 52.8 | 58.6 | 52.5 | 38.1 | 35.4 | 42.7 | 38.6 | 23.1 | 22.2 | |
| 5 | 53.6 | 49.0 | 55.1 | 50.3 | 55.0 | 50.0 | 55.0 | 50.0 | 54.6 | 49.7 | 54.3 | 49.4 | 36.1 | 34.0 | 39.7 | 36.6 | 22.4 | 21.8 | |
| 6 | 50.1 | 46.4 | 51.5 | 47.7 | 51.5 | 47.4 | 51.5 | 47.4 | 51.1 | 47.1 | 50.8 | 46.9 | 34.6 | 32.9 | 37.5 | 35.0 | 22.0 | 21.6 | |
| 7 | 47.2 | 44.2 | 48.6 | 45.5 | 48.6 | 45.2 | 48.6 | 45.2 | 48.3 | 45.0 | 48.0 | 44.7 | 33.4 | 31.9 | 35.7 | 33.7 | 21.7 | 21.4 | |
| 8 | 44.8 | 42.3 | 46.2 | 43.6 | 46.2 | 43.4 | 46.2 | 43.4 | 45.9 | 43.1 | 45.6 | 42.9 | 32.3 | 31.1 | 34.2 | 32.6 | 21.5 | 21.3 | |

Appendix

| 1600 [W/m ²] | wind | Temperatures | | | | | | | | | | | | | | | | | |
|--------------------------|------|--------------------|------|-----------------|------|-------------------|------|-------------------------|------|------------------------|------|------------------|------|----------------|------|----------------|------|-------------------|------|
| | | T _{glass} | | T _{pv} | | T _{base} | | T _{evaporator} | | T _{condenser} | | T _{hot} | | T _p | | T _n | | T _{cold} | |
| | | W | W/O | W | W/O | W | W/O | W | W/O | W | W/O | W | W/O | W | W/O | W | W/O | W | W/O |
| 0 | | 101.0 | 81.4 | 102.6 | 82.5 | 102.3 | 81.8 | 102.3 | 81.8 | 101.6 | 81.2 | 101.0 | 80.7 | 60.3 | 48.9 | 79.0 | 60.2 | 37.8 | 29.3 |
| 1 | | 88.0 | 73.2 | 89.6 | 74.4 | 89.4 | 73.8 | 89.4 | 73.8 | 88.8 | 73.3 | 88.2 | 72.8 | 52.7 | 44.9 | 66.8 | 53.5 | 31.8 | 26.7 |
| 2 | | 77.9 | 66.6 | 79.6 | 67.9 | 79.4 | 67.4 | 79.4 | 67.4 | 78.8 | 66.9 | 78.3 | 66.5 | 47.4 | 41.8 | 58.1 | 48.5 | 28.1 | 24.9 |
| 3 | | 70.0 | 61.3 | 71.7 | 62.6 | 71.6 | 62.2 | 71.6 | 62.2 | 71.1 | 61.8 | 70.6 | 61.4 | 43.6 | 39.4 | 51.7 | 44.7 | 25.8 | 23.7 |
| 4 | | 63.8 | 56.9 | 65.5 | 58.3 | 65.4 | 57.9 | 65.4 | 57.9 | 64.9 | 57.6 | 64.5 | 57.2 | 40.7 | 37.5 | 47.0 | 41.8 | 24.3 | 22.9 |
| 5 | | 58.8 | 53.3 | 60.5 | 54.8 | 60.4 | 54.4 | 60.4 | 54.4 | 60.0 | 54.1 | 59.6 | 53.8 | 38.5 | 35.9 | 43.4 | 39.4 | 23.3 | 22.4 |
| 6 | | 54.8 | 50.3 | 56.4 | 51.8 | 56.3 | 51.5 | 56.3 | 51.5 | 56.0 | 51.2 | 55.6 | 50.9 | 36.7 | 34.6 | 40.6 | 37.5 | 22.6 | 22.0 |
| 7 | | 51.4 | 47.8 | 53.1 | 49.3 | 53.0 | 49.0 | 53.0 | 49.0 | 52.7 | 48.7 | 52.4 | 48.4 | 35.3 | 33.6 | 38.5 | 36.0 | 22.1 | 21.7 |
| 8 | | 48.6 | 45.6 | 50.3 | 47.1 | 50.2 | 46.9 | 50.2 | 46.9 | 49.9 | 46.6 | 49.6 | 46.4 | 34.1 | 32.6 | 36.7 | 34.7 | 21.8 | 21.5 |

| 740 [W/m ²] | wind | TEG Electrical parameters | | | | | | | | PV electrical parameters | | | |
|-------------------------|------|---------------------------|------|------|------|------|------|------|--------|--------------------------|--------|------------|-----|
| | | Vemf | | Vmax | | Imax | | Pmax | | Power | | efficiency | |
| | | W | W/O | W | W/O | W | W/O | W | W/O | W | W/O | W | W/O |
| 0 | 1.70 | 1.34 | 1.06 | 0.85 | 0.77 | 0.61 | 0.82 | 0.52 | 104.57 | 108.76 | 13.04% | 13.56% | |
| 1 | 1.41 | 1.14 | 0.89 | 0.73 | 0.65 | 0.53 | 0.58 | 0.38 | 108.00 | 111.06 | 13.47% | 13.85% | |
| 2 | 1.19 | 0.99 | 0.76 | 0.63 | 0.55 | 0.46 | 0.42 | 0.29 | 110.57 | 112.84 | 13.79% | 14.07% | |
| 3 | 1.02 | 0.86 | 0.65 | 0.55 | 0.47 | 0.40 | 0.31 | 0.22 | 112.52 | 114.25 | 14.03% | 14.24% | |
| 4 | 0.89 | 0.76 | 0.57 | 0.49 | 0.41 | 0.35 | 0.23 | 0.17 | 114.04 | 115.38 | 14.22% | 14.38% | |
| 5 | 0.78 | 0.68 | 0.50 | 0.44 | 0.36 | 0.32 | 0.18 | 0.14 | 115.24 | 116.29 | 14.37% | 14.50% | |
| 6 | 0.69 | 0.61 | 0.45 | 0.39 | 0.32 | 0.29 | 0.14 | 0.11 | 116.20 | 117.05 | 14.49% | 14.59% | |
| 7 | 0.62 | 0.55 | 0.40 | 0.36 | 0.29 | 0.26 | 0.12 | 0.09 | 116.99 | 117.68 | 14.59% | 14.67% | |
| 8 | 0.56 | 0.51 | 0.36 | 0.33 | 0.26 | 0.24 | 0.09 | 0.08 | 117.64 | 118.21 | 14.67% | 14.74% | |

| 886 [W/m ²] | wind | TEG Electrical parameters | | | | | | | | PV electrical parameters | | | |
|-------------------------|------|---------------------------|------|------|------|------|------|------|--------|--------------------------|--------|------------|-----|
| | | Vemf | | Vmax | | Imax | | Pmax | | Power | | efficiency | |
| | | W | W/O | W | W/O | W | W/O | W | W/O | W | W/O | W | W/O |
| 0 | 2.06 | 1.62 | 1.28 | 1.02 | 0.93 | 0.74 | 1.18 | 0.75 | 119.79 | 126.22 | 12.47% | 13.14% | |
| 1 | 1.73 | 1.39 | 1.08 | 0.88 | 0.79 | 0.64 | 0.85 | 0.56 | 124.76 | 129.48 | 12.99% | 13.48% | |
| 2 | 1.47 | 1.21 | 0.93 | 0.77 | 0.67 | 0.56 | 0.63 | 0.43 | 128.50 | 132.03 | 13.38% | 13.75% | |
| 3 | 1.27 | 1.07 | 0.81 | 0.68 | 0.58 | 0.49 | 0.47 | 0.33 | 131.36 | 134.05 | 13.68% | 13.96% | |
| 4 | 1.11 | 0.95 | 0.71 | 0.61 | 0.51 | 0.44 | 0.36 | 0.27 | 133.58 | 135.67 | 13.91% | 14.13% | |
| 5 | 0.98 | 0.85 | 0.62 | 0.54 | 0.45 | 0.39 | 0.28 | 0.21 | 135.35 | 136.99 | 14.09% | 14.27% | |
| 6 | 0.87 | 0.77 | 0.56 | 0.49 | 0.40 | 0.36 | 0.23 | 0.18 | 136.76 | 138.09 | 14.24% | 14.38% | |
| 7 | 0.78 | 0.70 | 0.50 | 0.45 | 0.36 | 0.33 | 0.18 | 0.15 | 137.92 | 139.00 | 14.36% | 14.47% | |
| 8 | 0.71 | 0.64 | 0.46 | 0.41 | 0.33 | 0.30 | 0.15 | 0.12 | 138.88 | 139.78 | 14.46% | 14.56% | |

| 1066 [W/m ²] | wind | TEG Electrical parameters | | | | | | | | PV electrical parameters | | | |
|--------------------------|------|---------------------------|------|------|------|------|------|------|--------|--------------------------|--------|------------|-----|
| | | Vemf | | Vmax | | Imax | | Pmax | | Power | | efficiency | |
| | | W | W/O | W | W/O | W | W/O | W | W/O | W | W/O | W | W/O |
| 0 | 2.47 | 1.94 | 1.51 | 1.21 | 1.09 | 0.87 | 1.65 | 1.05 | 136.26 | 146.10 | 11.79% | 12.65% | |
| 1 | 2.10 | 1.68 | 1.30 | 1.06 | 0.94 | 0.76 | 1.23 | 0.81 | 143.44 | 150.73 | 12.41% | 13.05% | |
| 2 | 1.80 | 1.48 | 1.13 | 0.93 | 0.82 | 0.67 | 0.92 | 0.63 | 148.89 | 154.37 | 12.89% | 13.36% | |
| 3 | 1.56 | 1.31 | 0.98 | 0.83 | 0.71 | 0.60 | 0.70 | 0.50 | 153.08 | 157.27 | 13.25% | 13.61% | |
| 4 | 1.37 | 1.17 | 0.87 | 0.74 | 0.63 | 0.54 | 0.55 | 0.40 | 156.35 | 159.62 | 13.53% | 13.81% | |
| 5 | 1.22 | 1.05 | 0.77 | 0.67 | 0.56 | 0.49 | 0.43 | 0.33 | 158.95 | 161.54 | 13.76% | 13.98% | |
| 6 | 1.09 | 0.95 | 0.69 | 0.61 | 0.50 | 0.44 | 0.35 | 0.27 | 161.04 | 163.13 | 13.94% | 14.12% | |
| 7 | 0.98 | 0.87 | 0.63 | 0.56 | 0.46 | 0.40 | 0.29 | 0.23 | 162.76 | 164.46 | 14.09% | 14.23% | |
| 8 | 0.89 | 0.80 | 0.57 | 0.51 | 0.42 | 0.37 | 0.24 | 0.19 | 164.18 | 165.60 | 14.21% | 14.33% | |

| 1400 [W/m ²] | wind | TEG Electrical parameters | | | | | | | | PV electrical parameters | | | |
|--------------------------|------|---------------------------|------|------|------|------|------|------|--------|--------------------------|--------|------------|-----|
| | | Vemf | | Vmax | | Imax | | Pmax | | Power | | efficiency | |
| | | W | W/O | W | W/O | W | W/O | W | W/O | W | W/O | W | W/O |
| 0 | 3.12 | 2.47 | 1.86 | 1.51 | 1.35 | 1.09 | 2.50 | 1.65 | 160.43 | 178.41 | 10.57% | 11.76% | |
| 1 | 2.72 | 2.18 | 1.65 | 1.34 | 1.19 | 0.97 | 1.96 | 1.31 | 172.52 | 186.04 | 11.37% | 12.26% | |
| 2 | 2.37 | 1.93 | 1.45 | 1.20 | 1.05 | 0.87 | 1.53 | 1.05 | 181.82 | 192.11 | 11.98% | 12.66% | |
| 3 | 2.08 | 1.73 | 1.29 | 1.08 | 0.93 | 0.78 | 1.20 | 0.85 | 189.05 | 196.99 | 12.46% | 12.98% | |
| 4 | 1.84 | 1.56 | 1.15 | 0.98 | 0.83 | 0.71 | 0.96 | 0.69 | 194.74 | 200.97 | 12.83% | 13.24% | |
| 5 | 1.65 | 1.41 | 1.03 | 0.89 | 0.75 | 0.65 | 0.77 | 0.58 | 199.28 | 204.25 | 13.13% | 13.46% | |
| 6 | 1.48 | 1.29 | 0.93 | 0.82 | 0.68 | 0.59 | 0.63 | 0.48 | 202.96 | 206.98 | 13.38% | 13.64% | |
| 7 | 1.34 | 1.18 | 0.85 | 0.75 | 0.62 | 0.55 | 0.53 | 0.41 | 205.99 | 209.29 | 13.58% | 13.79% | |
| 8 | 1.23 | 1.09 | 0.78 | 0.70 | 0.57 | 0.50 | 0.44 | 0.35 | 208.51 | 211.25 | 13.74% | 13.92% | |

| 1600 [W/m ²] | wind | TEG Electrical parameters | | | | | | | | PV electrical parameters | | | |
|--------------------------|------|---------------------------|------|------|------|------|------|------|------|--------------------------|--------|------------|--------|
| | | Vemf | | Vmax | | Imax | | Pmax | | Power | | efficiency | |
| | | W | W/O | W | W/O | W | W/O | W | W/O | W | W/O | W | W/O |
| 0 | | 3.44 | 2.75 | 2.02 | 1.66 | 1.46 | 1.20 | 2.95 | 2.00 | 171.12 | 195.03 | 9.87% | 11.25% |
| 1 | | 3.04 | 2.45 | 1.82 | 1.50 | 1.32 | 1.08 | 2.39 | 1.62 | 186.57 | 204.70 | 10.76% | 11.80% |
| 2 | | 2.68 | 2.19 | 1.63 | 1.35 | 1.18 | 0.98 | 1.91 | 1.32 | 198.55 | 212.45 | 11.45% | 12.25% |
| 3 | | 2.37 | 1.97 | 1.45 | 1.22 | 1.05 | 0.89 | 1.53 | 1.08 | 207.93 | 218.72 | 11.99% | 12.61% |
| 4 | | 2.11 | 1.78 | 1.31 | 1.11 | 0.95 | 0.81 | 1.24 | 0.90 | 215.35 | 223.85 | 12.42% | 12.91% |
| 5 | | 1.89 | 1.62 | 1.18 | 1.02 | 0.85 | 0.74 | 1.01 | 0.75 | 221.30 | 228.09 | 12.76% | 13.15% |
| 6 | | 1.71 | 1.48 | 1.07 | 0.93 | 0.78 | 0.68 | 0.83 | 0.63 | 226.13 | 231.64 | 13.04% | 13.36% |
| 7 | | 1.56 | 1.36 | 0.98 | 0.86 | 0.71 | 0.63 | 0.69 | 0.54 | 230.10 | 234.64 | 13.27% | 13.53% |
| 8 | | 1.43 | 1.26 | 0.90 | 0.80 | 0.65 | 0.58 | 0.59 | 0.47 | 233.42 | 237.20 | 13.46% | 13.68% |

PV Module Datasheet

Thermoelectric Generator Datasheet